SOME PROPERTIES OF MAGNETIC IONS AND THEIR INTERACTIONS

A THESIS

SUBMITTED FOR THE DEGREE OF

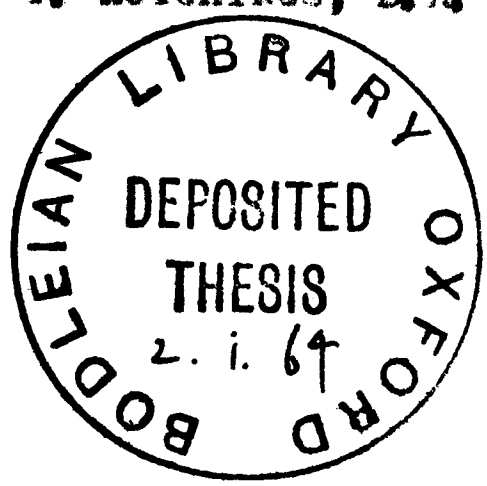
DOCTOR OF PHILOSOPHY

AT THE

UNIVERSITY OF OXFORD

by

M. T. HUTCHINGS, B.A.



The Queen's College,

Trinity Term, 1963.

ACKNOWLEDGEMENTS

The work described in this thesis has been carried out using the full facilities of the Clarendon Laboratory, and I am extremely grateful to Professor B. Bleaney, F.R.S., for allowing me this privilege.

I would like to thank my supervisor, Dr. W. P. Wolf, for his constant advice and encouragement, and for suggesting most of the topics of investigation.

There are many other people I would like to thank, especially:

The Department of Scientific and Industrial Research, for a Research Studentship.

Dr. G. Garton, Mr. M. Ball, Mr. S. Itzcovitz, and Mr. R. Shore, for providing the crystals for investigation, and for assistance with some of the experiments and crystal orientation.

Dr. L. Fox, for extending to me the facilities of the Oxford University Computing Laboratory. Mr. C. D. Marquard for advice on the programming, and Miss A. Robson for her cheerful willingness to operate the computer at all hours.

Mr. M. J. D. Powell, for the generous loan of his fitting programme.

Dr. D. K. Ray, for his very major part in the testing of the ionic model for $PrCl_3$.

Dr. M. C. M. O'Brien, for several discussions on the signs of g values.

Mr. A. Harris, Mr. J. Hurrell, Dr. K. Lea, Dr. M. J. M. Leask, Dr. P. Levy, Dr. M. Linse, Dr. J. Owen, Dr. H. Watanabe, Mr. C. Windsor and Mr. A. F. G. Wyatt for useful discussion.

Mr. B. Anson, for his help with the rehabilitation of the X Band apparatus and with the construction of the pumping manifold.

Dr. F. M. H. Robinson, Mr. J. Pilbrow, and Mr. G. J. Jenkinson for extremely helpful discussions on spectrometer design.

Mr. E. Tilbury, Mr. K. Robinson, Mr. D. Temple, and other staff of the Low Temperature Workshop for constructing the new apparatus.

Mr. D. T. Smith, and the staff of the electronics workshop, for building most of the electronic units used.

Mr. D. Saxton and Mr. S. Giles, for their expert glass blowing.

Mr. T. Carr, Mr. C. Bond, Mr. J. Day, Mr. A. Hazel, Mr. H. Locke, and Mr. S. Merry, for their assistance in many ways.

And finally, but by no means least, my parents and my wife for their support and encouragement.

ABSTRACT

Some properties of magnetic ions and their interactions

Introduction

The techniques of electron paramagnetic resonance (E.P.R.) have been used to investigate the interaction of rare earth ions with

(a) their crystalline environment, by measuring their effective g tensor,

and, (b) each other, by observing their pair spectra.

The experiments have been carried out in host lattices which, when magnetically concentrated, show interesting ordering properties.

The Apparatus

Measurements have been made at both X and K Band frequencies. The X Band spectrometer, originally constructed by Drs. A. H. Cooke and J. G. Park, was modified by the addition of a 115 Kc/s, and 50 c/s, phase sensitive detection system to give greater sensitivity. The K Band spectrometer was designed with a tuneable cylindrical H_{011} transmission cavity, and incorporated an improved system of cryogenics.

E.P.R. of rare earth ions in diamagnetic garnets

The investigation of the properties of rare earth ions in diamagnetic garnets is of importance in connection with their

profound influence on the ferrimagnetism of the iron garnets (for example see Dillon et al. 1960). The results of Ryan (1960) on the E.P.R. of rare earth ions in yttrium aluminium garnet (YAG) and yttrium gallium garnet (YGG) have shown a considerable difference of their g tensors in the two lattices, particularly for the case of Er^{3+}. In order to investigate further this variation, in particular the dependence on the host ion in the rare earth site, measurements have been made of the g tensors in the lutetium garnets LAG and LGG. The results, obtained mainly at X Band and $4.2^{\circ}K$, are given in Table 1 together with that for Dy^{3+} in YAG where no resonance had previously been observed. They indicate that the variation between lutetium and yttrium lattices is not so great as that between the aluminium and gallium lattices.

Table 1

Principal g values of four rare earth ions in diamagnetic garnet lattices.

Ion (1%)	Lattice	g_x	g_y	g_z
Nd^{3+}	LGG	2.083(±0.007)	1.323(±0.007)	3.550(±0.007)
	LAG	1.789(±0.005)	1.237(±0.006)	3.834(±0.005)
Dy^{3+}	LGG	13.45(±0.10)	0.57 (±0.10)	3.41 (±0.03)
	LAG	2.29 (±0.03)	0.91 (±0.05)	16.6 (±0.3)
	YAG	0.73 (±0.15)	0.40 (±0.20)	18.2 (±0.4)
Er^{3+}	LGG	3.183(±0.015)	3.183(±0.015)	12.62(±0.10)
	LAG	6.93 (±0.02)	4.12 (±0.03)	8.43 (±0.04)
Yb^{3+}	LGG	3.653(±0.013)	3.559(±0.013)	2.994(±0.011)
	LAG	3.842(±0.006)	3.738(±0.007)	2.594(±0.004)

Direct use of the g values

In general the above dependence of the g tensor on the exact garnet environment precludes their direct use for the explanation of the magnetically concentrated compounds. However, in two cases they have been used successfully.

Dysprosium aluminium garnet orders antiferromagnetically at 2.5°K (Ball et al. 1962). The highly anisotropic g values found for Dy^{3+} in YAG suggest that the ions in DyAG, which has a similar lattice constant, may be treated to a first approximation as Ising spins with $g_z = 18.0$, $g_x = g_y = 0$. Assuming only dipolar interaction a possible ordered state for such ions has been proposed, and this model allows an explanation of the main features of the susceptibility curve to be made.

As the g values of Yb^{3+} show relatively little variation with lattice, it is possible to use those found in the gallium garnets with some confidence for a discussion of YbIG. From the theory of Wolf (1962), canting of the rare earth sublattices at 20° to the Fe^{3+} sublattice has been predicted, and the order of magnitude of the spontaneous moment at 0°K accounted for.

Discussion of the garnet g values, cubic approximation

In order to make theoretical predictions of the g values in other magnetically concentrated garnets a thorough understanding of the resonance results in terms of the local crystal field is required.

As a first approximation this crystal field has been considered to arise mainly from the nearest eight oxygen neighbours, which are arranged in the form of a distorted cube about the rare earth site. Using the general cubic field calculations of Lea et al. (1962) it has been found that the gross features of the g values can be accounted for on such a model. But only in the case of Yb^{3+} can the values be quantitatively explained to within a few percent.

The trends in the observed g values for Nd^{3+} and Yb^{3+} have been found to follow closely those in the structure parameters describing the positions of the oxygen neighbours. From the Er^{3+} results an estimate has been made of the ratio of the parameters describing the crystal field, A_4^0/A_6^0, and this has been compared with other estimates. The extremely anisotropic g values found for Dy^{3+} in YAG suggest a ground state wavefunction of nearly pure $|J_z = 15/2\rangle$. (Where z is the [001] crystal direction).

Point charge calculations of the garnet crystal field

A general account of the method of derivation of the crystal field parameters from a point charge model of the crystal lattice has been written. In conjunction with Dr. D. K. Ray, the validity of an ionic model of the crystal lattice has been tested by considering the case of $PrCl_3$. This indicated the inadequacies of the model, even when

induced moments on neighbouring ions were considered, but suggested that calculated ratios of parameters may be a good approximation to the true values.

Assuming a model of point charges only, a computer has been used to calculate the contributions from (a) nearest neighbours only, and (b) all the ions in the lattice, to the crystal field parameters A_n^m at the rare earth site in YAG, YGG, LAG, LGG and YIG. The results of these calculations have been discussed. They indicate quite large distortions from a cubic field, and that the parameters for YGG are likely to lie closest to those in YIG.

A possible set of crystal field parameters for Yb^{3+} in YGG

The case of Yb^{3+} in the garnets is best suited to a more detailed theoretical analysis. As there are insufficient experimental data available to enable all the parameters to be found from experiment alone, ratios calculated on the point charge model have been used to reduce the number of parameters to be fitted. Treating first the $J = 5/2$ multiplet by itself, and then the whole ^2F term, a set of parameters which give a fair agreement with experiment have been found using a computer programme. The discrepancies, which should be small, indicate the inadequacies of the approximations made. The wavefunction found for the lowest $J = 5/2$ doublet is similar to that found from perturbation theory, and in general the fit to the data for the $J = 5/2$ state alone is better than that

to the whole ^2F term.

<u>E.P.R. of rare earth ions in weakly paramagnetic garnets. Interaction shift</u>

It has been shown that the resonance from Kramers ions in a lattice containing host ions in a singlet ground state should be shifted but not broadened by the interactions. This shift may be expressed in the same form as the magnetic g tensor. The effective principal g values of Yb^{3+} and Er^{3+} have been measured at X Band frequencies and 4.2°K in such lattices, and the results are given in Table 2. The case of Yb^{3+} in TmAG is believed to show unambiguously such an interaction shift.

<u>Table 2</u>

Effective principal g values of Er^{3+} and Yb^{3+} in weakly paramagnetic garnets.

Ion (~0.005%)	Lattice	g_x	g_y	g_z
Er^{3+}	TmGG	3.76 (±0.02)	3.48 (±0.02)	11.9 (±0.1)
	TmAG	7.69 (±0.03)	4.25 (±0.02)	7.65 (±0.03)
Yb^{3+}	EuGG	3.805 (±0.003)	3.664 (±0.003)	2.670 (±0.007)
	TmGG	3.724 (±0.008)	3.557 (±0.007)	2.944 (±0.010)
	TmAG	4.020 (±0.007)	3.763 (±0.008)	2.554 (±0.009)

E.P.R. of Gd^{3+} in hexagonal lattices

Measurements have been made at X Band frequencies of the crystal field parameters b_n^m for Gd^{3+} in $LaCl_3$ and $LaBr_3$.

Table 3

	$b_2^0 \times 10^4 cm^{-1}$	$b_4^0 \times 10^4 cm^{-1}$	$b_6^0 \times 10^4 cm^{-1}$	$\lvert b_6^6 \rvert \times 10^4 cm^{-1}$	g
$LaCl_3$ (20°K)	18.0 (±0.2)	2.14 (±0.05)	0.23 (±0.05)	0.13 (±0.07)	1.992 (±0.001)
$LaBr_3$ (20°K)	67.6 (±0.3)	11.11 (±0.06)	3.46 (±0.06)	-	1.991 (±0.001)

The results, tabulated above, emphasize their dependence on the lattice spacing in this structure found by Hutchison et al. (1957).

E.P.R. from pairs of Gd^{3+} ions in $LaCl_3$

In order to obtain information on the interactions of a pair of Gd^{3+} ions in $LaCl_3$, which is of interest in connection with the properties of the isostructural ionic ferromagnet $GdCl_3$, their pair spectrum has been investigated at X and K Band frequencies and at 20°K. In such a case of weak isotropic exchange interaction it is possible to obtain measurements of the exchange constants directly from the resonance line position.

The nearest neighbour (n.n.) pair spectrum, with the magnetic field H parallel to the c axis, is symmetric about

the central main line and extends over ~ ± 2,600 gauss. It consists of four outer groups of lines, of overall width ~130 gauss and separation ~370 gauss, and three apparently well resolved inner lines. The spectrum due to next nearest neighbour (n.n.n.) pairs, with H along their symmetry axis, shows no such grouping. There are very many lines within 600 gauss of the central main line, due to more distant neighbours.

The theoretical analysis of the spectrum has been undertaken from the start using a computer. It has not been possible to identify any of the pair transitions with certainty, and because of the large variation of line position with the values of all five parameters in the pair Hamiltonian the interpretation has proved difficult. However if the crystal field parameters for a member of the n.n. pair are assumed not to differ considerably from those of the isolated ions, the grouping of the outer n.n. lines can be explained. It indicates a value of $J_{ex} = +0.011\ (\pm 0.005)\ cm^{-1}$ and $\nu = g^2\mu_B^2/r_{nn}^3 = 0.022\ (\pm 0.002)\ cm^{-1}$ (where $\mathcal{H}_{ex} = J_{ex}\underline{S}^{(1)}.\underline{S}^{(2)}$).

E.P.R. of rare earth ions in YCl_3 and $LuCl_3$

The principal g values of rare earth ions in YCl_3 and $LuCl_3$ have been measured at X Band frequencies and 4.2°K. The results are listed in Table 4. The cases of Dy^{3+}, Er^{3+} and Yb^{3+} show little relative variation with host lattice, and it should be possible to use the values directly for the inter-

pretation of the bulk magnetic properties of the isostructural concentrated compounds. It has been shown that as a first approximation, the crystal field at the rare earth site may be considered to be sixfold cubic, as expected from the location of the nearest Cl^- ions.

Table 4

Principal g values of rare earth ions in monochinic YCl_3 and $LuCl_3$; g_b is measured along the b [010] axis, and g_1 and g_2 lie in the (010) plane, g_1 is at an angle α to the a [100] axis.

Ion (1%)	Lattice	g_1	g_2	g_b	α
Dy^{3+}	YCl_3	6.86 (±0.03)	3.02 (±0.06)	9.34 (±0.03)	±9° (± 5°)
	$LuCl_3$	7.21 (±0.02)	3.16 (±0.05)	8.84 (±0.02)	±7° (± 6°)
Er^{3+}	YCl_3	8.27 (±0.05)	3.78 (±0.05)	7.70 (±0.03)	0 (±8°)
	$LuCl_3$	8.34 (±0.02)	3.51 (±0.03)	7.92 (±0.02)	0 (± 5°)
Yb^{3+}	YCl_3	2.99 (±0.02)	1.53 (±0.02)	2.957 (±0.006)	0 (± 9°)
	$LuCl_3$	2.95 (±0.01)	1.58 (±0.01)	2.96 (±0.01)	0 (± 5°)
Ce^{3+}	YCl_3	1.60 (±0.01)	0.66 (±0.02)	1.708 (±0.003)	0 (±10°)
Nd^{3+}	YCl_3	1.16 (±0.03)	2.63 (±0.02)	1.653 (±0.005)	0 (± 8°)

Miscellaneous E.P.R. experiments

Experiments which have given inconclusive or ambiguous results include measurements on Ce^{3+} pairs in $LaCl_3$, and U^{4+} in ThO_2.

CONTENTS

		Page
ABSTRACT		(i)
CHAPTER 1	**Introduction**	
1.1	Electron paramagnetic resonance	1.1
1.2	The general nature and purpose of the experimental investigation.	1.1
1.3	The interaction of rare earth ions with their crystalline environment.	1.3
1.4	The interaction between rare earth ions.	1.7
CHAPTER 2	**The apparatus**	
2.1	Introduction	2.1
2.2	The X Band spectrometer	2.1
2.3	The K Band spectrometer	2.3
2.4	The magnetic field	2.7
2.5	Measurement of the magnetic field	2.8
2.6	The pumping system	2.9
CHAPTER 3	**Experimental results of paramagnetic resonance of rare earth ions in the garnet crystal structure**	
3.1	Introduction	3.1
3.2	Crystal structure of the garnets	3.3
3.3	The spectrum of rare earth ions in garnets	3.5
3.4	Experimental procedure	3.7
3.5	Experimental results	3.10
CHAPTER 4	**General discussion of the ground state g tensors of rare earth ions in the diamagnetic garnet lattices, with particular reference to a cubic field approximation**	
4.1	Introduction	4.1
4.2	General observations on the ground state g values	4.4
4.2.1	Comparison of the ground state g values and susceptibility measurements	4.7
4.3	The energy levels of rare earth ions in a cubic crystal field	4.9
4.4	Erbium in the cubic approximation	4.11
4.5	Dysprosium in the cubic approximation	4.12

			Page
CHAPTER 4	(Continued)		
	4.6	Neodymium in the cubic approximation	4.16
	4.7	Ytterbium in the cubic approximation	4.20
		4.7.1 Admixture from the J = 5/2 Γ_7 state.	4.27
		4.7.2 Ratio of fourth to sixth order potential	4.30
	4.8	Consideration of the J = 5/2 ytterbium state in the cubic approximation	4.31
	4.9	Conclusion	4.34
CHAPTER 5		Direct application of the experimental A values to magnetically concentrated garnets	
	5.1	Introduction	5.1
	5.2	Antiferromagnetic ordering of dysprosium aluminium garnet	5.1
	5.3	Canting effects in the rare earth iron garnets	5.4
		5.3.1 Spontaneous moment at 0°K of YbIG	5.8
CHAPTER 6		The calculation of the crystal field Hamiltonian from a point charge model of the crystal lattice, and a discussion of the validity of the model.	
	6.1	Introduction	6.1
	6.2	Discussion of the validity of an ionic model of the crystal lattice	6.2
		6.2.1 Conclusion	6.5
CHAPTER 7		Point charge calculations of the garnet crystal field	
	7.1	Introduction	7.1
	7.2	Crystallography and co-ordinate systems used	7.2
	7.3	The calculations	7.4
		7.3.1 The calculation of the crystalline potential due to nearest neighbours only.	7.5
		7.3.2 The calculation of the contribution of all ions in the lattice to the crystal field parameters	7.7
	7.4	Discussion of the results	7.12
	7.5	Summary	7.16

			Page
CHAPTER 8		The determination of a possible set of crystal field parameters for Yb^{3+} in YGG	
	8.1	Introduction	8.1
	8.2	Experimental data for Yb^{3+} in YGG	8.3
	8.3	The fitting procedure	8.5
		8.3.1 Fitting to the J = 5/2 state data alone	8.9
		8.3.2 Fitting to the data for the full ^2F term	8.11
		8.3.3 Sequence of fitting	8.14
	8.4	Discussion of results and conclusions	8.19
CHAPTER 9		Interaction shifts observed in the weakly paramagnetic garnet lattices	
	9.1	Introduction	9.1
	9.2	Theory of the g tensor shift produced by singlet state neighbours	9.2
	9.3	Discussion of the measured g tensors in weakly paramagnetic lattices	9.6
	9.4	Conclusion	9.10
CHAPTER 10		Paramagnetic resonance from pairs of Gd^{3+} ions in lanthanum trichloride: Experimental results	
	10.1	Introduction	10.1
	10.2	Crystallography and orientation of samples	10.2
	10.3	The single ion resonance of Gd^{3+} in $LaCl_3$ and $LaBr_3$	10.5
		10.3.1 Gd^{3+} in $LaCl_3$	10.5
		10.3.2 Gd^{3+} in $LaBr_3$	10.8
	10.4	The spectrum from pairs of Gd^{3+} ions in $LaCl_3$	10.9
		10.4.1 The general nature of the spectrum	10.9
		10.4.2 The nearest neighbour pair spectrum	10.13
		10.4.3 The next nearest neighbour pair spectrum	10.18
		10.4.4 Further relevant experiments	10.20
	10.5	Conclusion	10.21

			Page
CHAPTER 11		Paramagnetic resonance from pairs of Gd^{3+} ions in lanthanum trichloride: Theoretical discussion	
	11.1	Introduction	11.1
	11.2	The pair Hamiltonian	11.1
		11.2.1 Approximate values of the parameters in the Hamiltonian	11.2
	11.3	The calculation of the resonance line positions	11.6
		11.3.1 The computer programme	11.7
	11.4	The results of the calculations	11.12
		11.4.1 The nearest neighbour pair spectrum	11.12
		11.4.2 The next nearest neighbour pair spectrum	11.16
	11.5	Conclusion	11.17
CHAPTER 12		Electron paramagnetic resonance of rare earth ions in the monoclinic yttrium trichloride structure	
	12.1	Introduction	12.1
	12.2	Crystal structure of YCl_3, and the directions of the principal axes of the g tensors.	12.2
	12.3	Crystal orientation and experimental procedure	12.4
	12.4	Experimental results	12.7
	12.5	Discussion	12.10
	12.6	Conclusion	12.15
CHAPTER 13		Miscellaneous E.P.R. experiments on systems of possible interest	
	13.1	Introduction	13.1
	13.2	Resonance from pairs of Ce^{3+} ions in $LaCl_3$	13.1
		13.2.1 Nearest neighbour pairs-theory	13.2
		13.2.2 Nearest neighbour pairs - experiments	13.3
	13.3	E.P.R. of magnetic ions in ThO_2	13.6
		13.3.1 Tb^{4+} in ThO_2	13.6
		13.3.2 U^{4+} in ThO_2, Gd^{3+} in ThO_2	13.7
		13.3.3 Pr^{4+} in ThO_2	13.9
	13.4	Measurements on Er^{3+} in dysprosium ethyl sulphate	13.10
	13.5	The investigation by E.P.R. of rare earth ions in yttrium nitride	13.11

APPENDICES

APPENDIX I — The theoretical determination of the principal g values and a discussion of their sign

APPENDIX II — The calculation of the perturbing crystal field Hamiltonian from a point charge ionic model of the crystal lattice, and the determination of its matrix elements

APPENDIX III — Tables of commonly occurring functions

APPENDIX IV — Computer Programmes

APPENDIX V — Matrices of the n.n. pair Hamiltonian for Gd^{3+} ions in $LaCl_3$.

CHAPTER 1

Introduction

1.1 Electron paramagnetic resonance

Electron paramagnetic resonance (E.P.R.) is the phenomenon of the absorption of electromagnetic radiation by a crystal containing paramagnetic centres when the crystal is placed in a magnetic field, the absorption being due to transitions between the Zeeman levels of the centre. Usually these are observed in the microwave region of the electromagnetic spectrum. The paramagnetic centres concerned in this thesis are ions of the rare earth transition elements, whose paramagnetism arises from a partly filled 4f electron shell.

Since its first observation in 1945 paramagnetic resonance has become an extremely powerful tool for the investigation of many aspects of problems in solid state physics, and the basic experimental techniques are now well established. The theoretical principles of E.P.R. and many experimental results have been summarized in three review articles by Bleaney and Stevens (1953), Bowers and Owen (1955), and Orton (1959), and in three books by Ingram (1955), Low (1960), and Pake (1962).

1.2 The general nature and purpose of the experimental investigation

The work described in this thesis forms a part of a general investigation into the properties of new magnetic materials using susceptibility, magnetic moment, and specific

heat measurements, as well as paramagnetic resonance. The general aim of the group undertaking this research was to investigate rare earth compounds which are as near the "ideal" magnetic material as possible, in order to obtain information on the various interactions between ions in the compounds, and to test existing theories in cases with as few unnecessary complications as possible. For this purpose the "ideal" magnetic material may be said to have the following properties:-

(a) Simple method of growth in the form of good pure single crystals.

(b) A single, well defined, and preferably simple crystal structure.

(c) A large range of chemical composition.

(d) Unique valency for each type of ion present.

(e) 1:1 relation between crystal site and the type of ion occupying it.

(f) Well defined interactions between neighbouring magnetic ions.

The paramagnetic resonance experiments carried out may be divided into two categories. They concern the investigation of the interaction of rare earth ions with either (a) their crystalline environment, or (b) each other, in diamagnetic lattices which when magnetically concentrated exhibit interesting ordering properties. In the next two sections a brief discussion of the principles involved in the two types

of investigation will be given.

1.3 The interaction of rare earth ions with their crystalline environment

The theory of the magnetic properties of rare earth ions in crystalline electric fields has been developed in considerable detail by Elliott and Stevens in four important papers, Stevens (1952), Elliott and Stevens (1952),(1953a), (1953b).

In ionic crystals the effect of the crystalline field is smaller than most interactions occurring within the free rare earth ions and one can treat it as a perturbation on the free ion wavefunctions. Although the basic mechanism of the interaction is well understood (Stevens 1952), it has not yet been possible to account theoretically for the crystal field parameters occurring in the perturbing Hamiltonian in any detail, and they are usually determined from experiment. An elementary discussion of crystal field theory is given in §6.1 and Appendix II. The crystal field effects are generally smaller than the spin orbit coupling in the rare earths and for a first approximation the wavefunctions $|(4f)^n, L, S, J, J_z\rangle$ based on Russell-Saunders coupling (see e.g. Heine 1960) are usually taken. However it is often necessary to include the admixture by the crystal field of at least the first excited J multiplet. Configurational interaction and intermediate coupling effects are generally neglected in the free ion

wavefunctions used (for non S state ions), as errors due to their omission are less than those from the usual uncertainty in the crystal field parameters (Elliott and Stevens 1953a). Except in a few special cases conventional theory cannot explain the magnetic properties of ions in crystals to better than a few per cent.

The splitting of a rare earth configuration under the various interactions is shown diagramatically in Figure 1.1. The crystal field removes some of the degeneracy of the free ion, but in the case of ions with an odd number of magnetic electrons, a general theorem of Kramers (1930) applies. This states that under a purely electrostatic interaction these ions will have evenly degenerate energy levels. The term "Kramers ion" is often used for odd electron ions, and their doubly degenerate energy levels are known as "Kramers doublets".

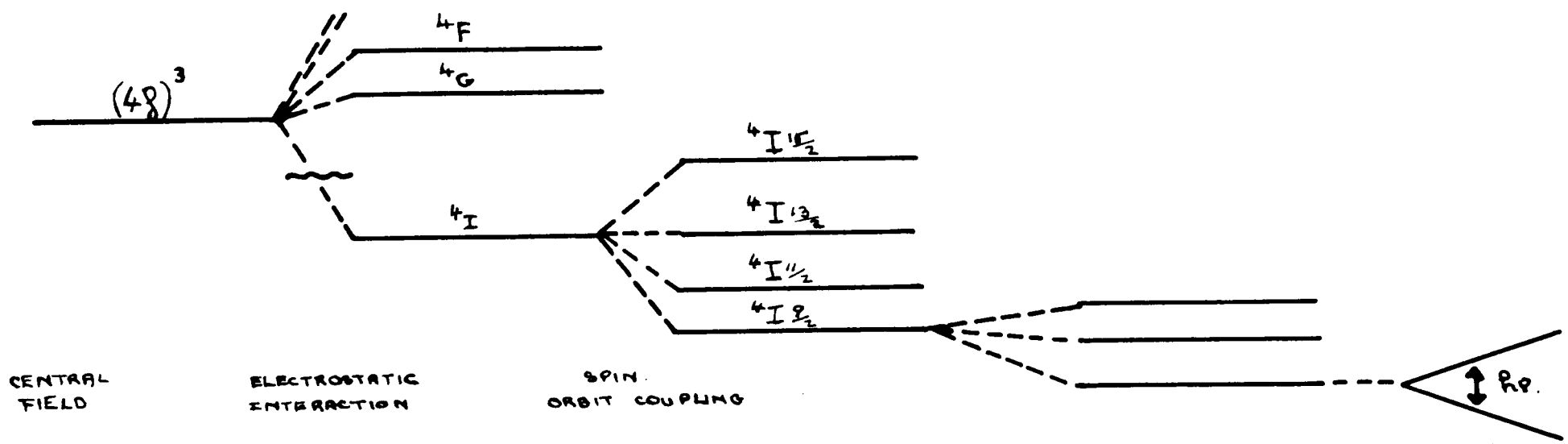
If a magnetic field is now applied to the ion, the Kramers degeneracy is removed, and it is between the resulting energy levels that transitions in the microwave region may be induced. The Hamiltonian representing the interaction with the magnetic field is

$$\mathcal{H}_M = \mu_B \mathbf{H}\cdot(\mathbf{L} + 2\mathbf{S}) \left(= \mu_B g_J \mathbf{H}\cdot\mathbf{J}, \text{ within a manifold of one } J \text{ multiplet}\right) \quad (1.1)$$

As this interaction is usually smaller than the crystal field interaction it may be treated as a perturbation on the crystal field levels (S state ions are an exception).

Paramagnetic resonance from rare earth ions, other than

SCHEMATIC DIAGRAM OF THE ENERGY LEVELS OF Nd^{3+} IN A CRYSTAL FIELD



CONFIGURATION — TERMS — J-MULTIPLETS — EVENLY DEGENERATE LEVELS

FREE ION — C.E.F. — SPLIT BY MAGNETIC FIELD

FIGURE 1-1

those in an S state, is usually only observed at low temperatures ($20^{\circ}K$ or $4.2^{\circ}K$) when the spin lattice relaxation time has become long enough for natural broadening not to contribute to the resonance line width. In most cases only the ground doublet is populated at these temperatures so that just one main line is seen. Pryce (1950) has shown that the doublet can be considered to arise from an effective spin $S' = \frac{1}{2}$, and its interaction with the magnetic field described by a spin Hamiltonian,

$$\mathcal{H}' = \mu_B \mathbf{H} \cdot \mathbf{g} \cdot \mathbf{S}' \qquad (1.2)$$

(In the special case of S state ions, the crystal field only affects the ion in a high order of perturbation theory, its interaction effects are of the same order as those of the magnetic field and both are considered simultaneously in the spin Hamiltonian with $S' = S$, the true spin).

The g tensor thus defined is considered in Appendix I where it is shown that its principle values may be found from the true angular momentum Kramers states $|+\rangle$ and $|-\rangle$ using the relation,

$$\begin{aligned} g_x &= 2 \langle + | L_x + 2S_x | - \rangle \\ g_y &= \frac{-2}{i} \langle + | L_y + 2S_y | - \rangle \\ g_z &= 2 \langle + | L_z + 2S_z | + \rangle \end{aligned} \qquad (1.3)$$

Experimentally, the splitting between the levels in a magnetic field may be used to define an effective g value,

g_{eff}, and the resonance condition $h\nu = g_{eff} \mu_B H$, where $h\nu$ = microwave quantum, leads to the formula for g_{eff}:-

$$g_{eff} = \frac{21.4180 \ (\pm\ 0.0005)}{\lambda_{cm} H_{Kg}} \qquad (1.4)$$

Thus defined, g_{eff} will be equal in magnitude to the principal g values of Equation (1.3) when the field is along these directions, and will have an angular variation between these directions given by Equation (3.2).

It may also be possible to induce transitions between the levels of "non-Kramers" ions, but only in special circumstances can these be observed in the microwave region.

The g tensor of Equation (1.2) describes the magnetic properties of the ion at low temperatures and it may be used to interpret bulk magnetic measurements, of susceptibility for example. However magnetic interactions prohibit, through line broadening, its determination in the concentrated salt, and it is usual to measure its principal values in an isostructural diamagnetic crystal. In this case the crystal field seen by the ion is not necessarily the same, and it is necessary to establish the variation of $\underline{g}$ with host lattice in order to be certain of its correct value in the concentrated salt.

The g tensor also describes the interaction of the magnetic ion with the crystalline field and it provides a source of information on the general problem of crystal field

theory. In this respect it is of special interest to investigate its value for a number of ions in the same crystal field. Supplementary data from optical spectroscopy, and bulk magnetic measurements are usually required in order to determine the crystal field parameters, (if some of these data are determined in concentrated salts allowance must again be made for the variations with lattice). In certain circumstances the g values may be used to derive the wavefunctions of the Kramers doublet without further knowledge, and these are of importance when considering interactions between magnetic ions, or between the magnetic electrons of an ion and its nucleus.

1.4 The interaction between rare earth ions

One of the most direct methods of investigating the interactions between paramagnetic ions in ionic crystals is to observe microwave transitions between the energy levels of a pair of ions, on neighbouring lattice sites, in a diamagnetic host lattice. For small concentrations of magnetic ions there occur isolated groups of two or three ions in the crystal as well as single ions. The intensity of the spectrum, from such pairs of ions for example, will be lower than that from the single ions by an amount roughly proportional to the concentration.

Although a very great deal of work has been carried out on paramagnetic resonance from single ions, the resonance from pairs of ions has only been investigated in a dozen or so

cases mainly on ions from the 3d and 5d transition groups. Probably the best example is the work on the potassium and ammonium chloiridates, (Griffiths et al, 1959). Reviews of the basic theory and results of these investigations have been given by Baker and Bleaney (1955), Bagguley and Owen (1957) and Owen (1961) and (1962). In only one case, that of Nd^{3+} in the ethyl sulphate lattice, has resonance from pairs of rare earth ions been reported (Baker and Bleaney (1955), Bleaney et al. 1951).

The spin Hamiltonian for a pair of ions with spins (or effective spins) $S^{(1)}$ and $S^{(2)}$ may be written

$$\mathcal{H}_p = \mathcal{H}(1) + \mathcal{H}(2) + \mathcal{H}_i(1,2) \qquad (1.5)$$

where $\mathcal{H}(1)$ and $\mathcal{H}(2)$ are the isolated ion spin Hamiltonians, and $\mathcal{H}_i(1,2)$ represents the interaction between the ions. This may include several terms:

(a) A dipolar interaction term.

(b) An isotropic exchange term (i.e. of the form $J_{ex}\, S^{(1)}.\, S^{(2)}$).

(c) An anisotropic exchange term.

(d) Other exchange terms of high order, of forms such as $J'_{ex}\,(S^{(1)}.S^{(2)})^2$ - (these are usually neglected). There may be other forms of interaction in certain special cases.

In general all these interactions will affect the position of the pair resonance lines. But if the isotropic exchange is larger than the other terms in the Hamiltonian (as has been the case in most of the pair spectra investigated) it will only

affect the main pair line positions very slightly, and intensity measurements must be used to find its value (see Owen 1961 e.g.). There is therefore a considerable advantage in investigating the pair spectrum of ions coupled by a small isotropic exchange as is expected in the case of the rare earths. However in the simplest case of two identical ions with $S^{(1)} = S^{(2)} = S' = \frac{1}{2}$, that of most rare earths, the line position is completely independent of the isotropic exchange, whatever its size. An example in which it should be possible to obtain the isotropic exchange constant from the line positions is Gd^{3+} in $LaCl_3$. This interaction is of particular interest since the isostructural compound $GdCl_3$ is one of the few known ionic ferromagnets, ordering at $2.2^{o}K$ (Wolf et al 1962).

In general, care must be taken in using the interaction constants determined from resonance for the explanation of bulk magnetic properties of an isostructural concentrated compound. The exchange constant is usually very dependent on the exact separation of the ions, which will be different in the two lattices, and may also depend on the concentration on account of the superexchange mechanism of the interaction. (Although in the case of the chloroiridates it has been found to be independent of concentration, A. Harris, private communication). Until these effects are established, it is

probably better to treat the two types of measurement as contributing separate information to the general problem of the interaction of magnetic ions. The resonance method has the advantage over bulk measurements, which require a simplified model for analysis and can only measure average effects, in that a particular type of pair of ions can be singled out for investigation, and that by using different host lattices the separation of the ions can be varied.

Information on the interaction between ions may also be obtained by investigating the resonance line width in concentrated salts (see Bleaney and Stevens, 1953 e.g.). However this has the disadvantage of the bulk measurements in that it is an average effect which is observed. A special case where the resonance is shifted in position by the interactions, but not broadened, is that of a Kramers probe ion in a host lattice of paramagnetic ions in a singlet state, and is considered in Chapter 9.

CHAPTER 2

The Apparatus

2.1 Introduction

As the basic techniques of paramagnetic resonance are now well established, and are discussed in most of the general references given in §1.1, only the main features of the apparatus used for the measurements given in Chapters 3, 10, 12 and 13, will be described here. This apparatus consisted of an X Band spectrometer, originally constructed by Dr. A. H. Cooke and Dr. J. G. Park, which was modified to give greater sensitivity, and a new K Band spectrometer. The latter will be described in some detail as it is not of purely conventional design. (A new X Band spectrometer of similar cryogenic design to the K Band apparatus was constructed but not used for any of the work described in this thesis).

2.2 The X Band spectrometer

The basic features of the X Band spectrometer have been described in some detail by Park (1957) and Ryan (1960). The cylindrical transmission cavity was made of german silver and gold plated on the inside, it was operated in the H_{mn} mode. The sample, attached to a perspex holder which screwed into the specimen rod, was positioned near the centre of the top of the cavity. The use of a specimen rod enabled samples to be changed whilst the cavity was at low temperatures.

The microwave circuit was of standard design and is shown

in Figure 2.1 where a schematic block diagram of the complete spectrometer is given. The microwave source used for the experiments described in Chapter 3 was a reflex klystron type C.V.129, and the wavelength was measured using a cavity wavemeter of known dimensions. For all other experiments an L.F.E. "Ultra-stable Microwave Oscillator" type 814A - X-21 was used, the frequency being read off a dial attached to the stabilisation cavity. This dial was calibrated against a Sivers direct reading wavemeter to ± 2 mc/s.

In order to improve the sensitivity so that pair spectra could be observed, a 115 Kc/s field modulation and phase sensitive detection system (Llewellyn 1957) was added. The electronic units, shown in Figure 2.1, were constructed in the Electronics Workshop, (whose reference numbers are given in the figure), from circuits similar to those described by Coles (1959). To enable the 115 Kc/s field modulation to enter the cavity a new specimen rod was constructed, and is shown in the diagram of Figure 2.2. A single loop of stout copper wire carrying the r.f. current encircled the sample and protruded about 5 mm. into the cavity, in a plane parallel to the H vector of the microwave field. The sample and loop were attached to a perspex holder which also carried the nuclear magnetic resonance (N.M.R.) probe coil (see § 2.5). Three leads, which passed down the centre of the rod, supplied the r.f. loop and N.M.R. coil, the latter having an earth return. The 115 Kc/s

SCHEMATIC BLOCK DIAGRAM OF X BAND SPECTROMETER

(POWER SUPPLIES NOT SHOWN)

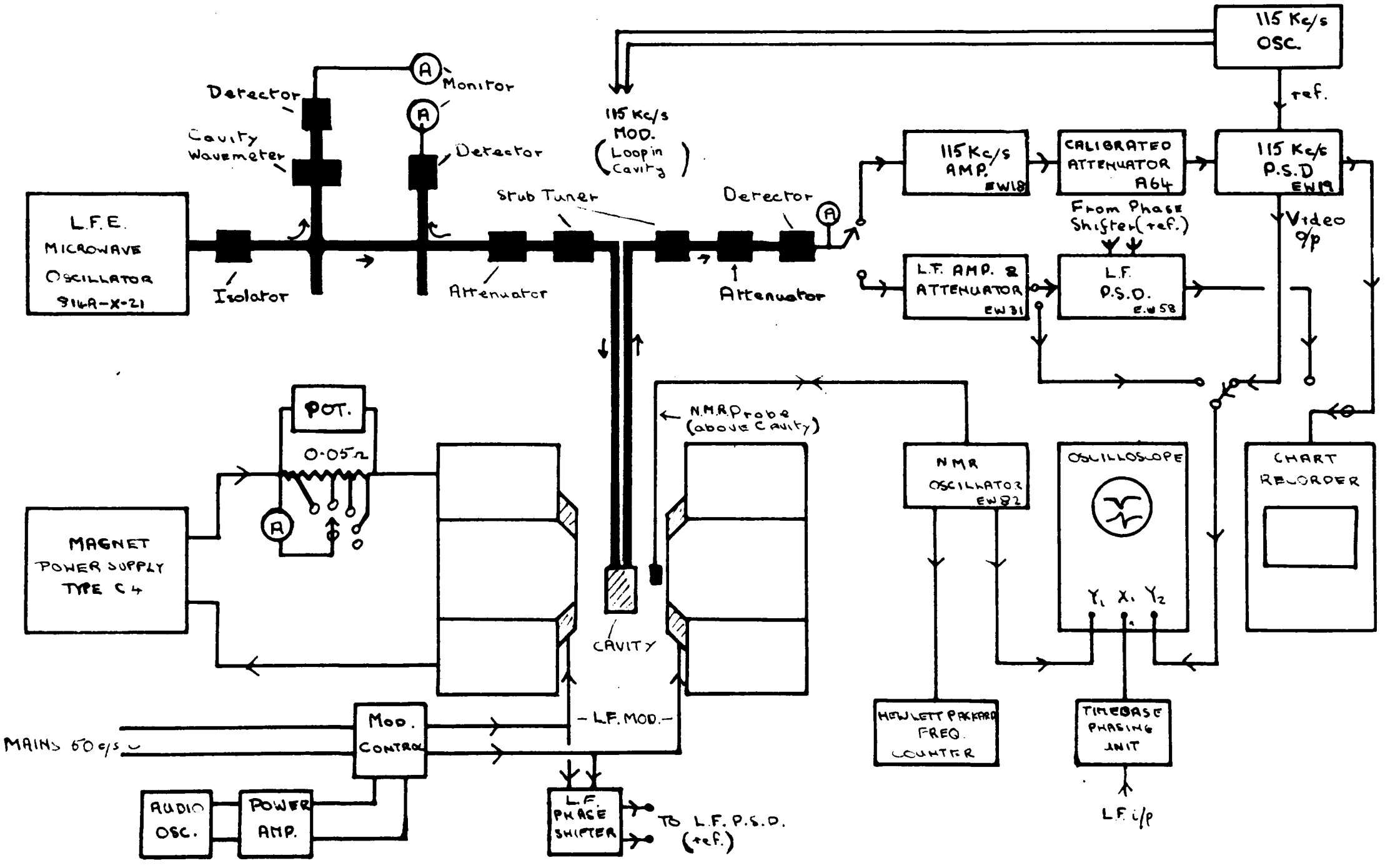


FIGURE 2·1

X BAND SPECIMEN ROD

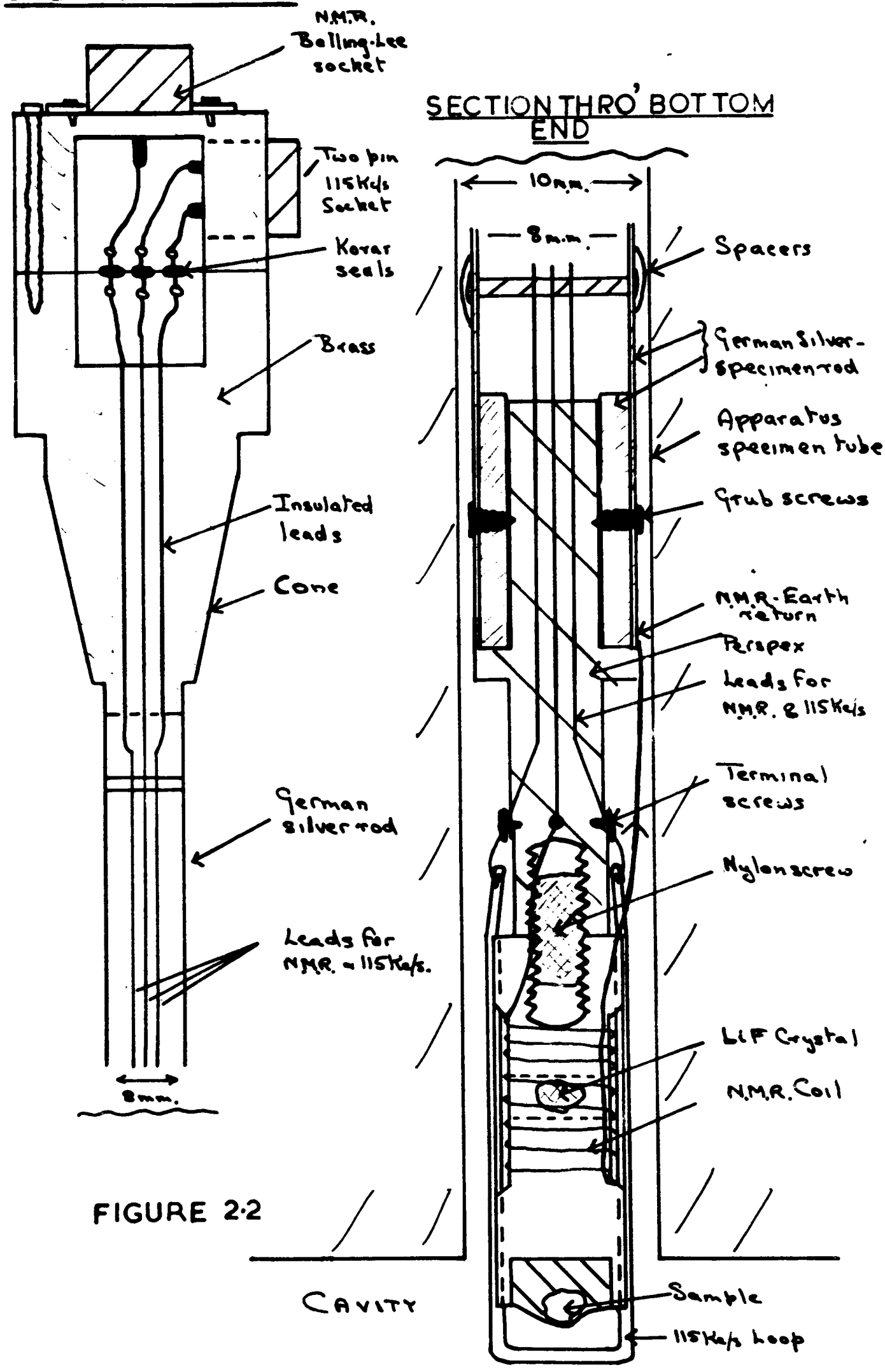


FIGURE 2·2

leads were entirely insulated from earth, being coupled to the oscillator by a transformer; and throughout the signal path, earth loops were eliminated to reduce pickup. It was found that both the N.M.R. and 115 Kc/s video E.P.R. signals could be observed simultaneously in spite of the proximity of the leads in the rod. It was essential that the loop was attached rigidly, as any vibration in the magnetic field caused prohibitive 115 Kc/s modulation of the microwaves.

A low frequency phase sensitive detection system was also added, the external field modulation at frequencies other than 50 c/s being supplied by an audio oscillator and Williamson power amplifier. Full precautions were taken in the construction of the low frequency signal amplifier, which had a gain of 100 db, to reduce noise and pickup. The signal from a phase sensitive detection system has maximum value when the field modulation amplitude is of the order of the line width, the low frequency system was therefore used to detect broad lines since it was possible to obtain up to 200 gauss modulation amplitude at 50 c/s, compared with about 20 gauss at 115 Kc/s.

2.3 The K Band spectrometer

The K Band spectrometer may also be represented by the block diagram of Figure 2.1 as the microwave circuit was similar to that of the X Band system and the same electronic units were used. The microwave source was an A.M.I. klystron type R9602, with power supplied from a standard unit used

extensively in the laboratory and designed by L. J. Arundel. Because of its greater instability, this klystron was stabilised in frequency on to the resonant frequency of the cavity, using a Stabiliser Unit type EW62 built by the Electronics Workshop (not shown in Figure 2.1). This operated by automatically adjusting the mean reflector voltage to minimise the transmitted 500 Kc/s signal when a small 500 Kc/s modulation voltage was fed to the reflector; the signal being least when the klystron frequency was centred at the peak of the cavity mode. A filter circuit placed immediately after the detecting crystal separated the 500 Kc/s stabilisation signal from the E.P.R. signal. The wavelength of the microwaves was measured with a calibrated cavity wavemeter.

The cylindrical transmission cavity, a diagram of which is shown in Figure 2.3, was operated in the H_{011} mode, the sample being placed at its centre. The cavity was of 1.634 cm. diameter and by adjusting the length between ~1.9 and ~1.5 cm. its resonant frequency could be varied between ~25 and ~26 Kmc/s. The 115 Kc/s modulation leads entered the cavity through a choke system designed to present to the microwaves a dead short across the cavity top. They passed vertically through the cavity, and their radial position was chosen so that the degenerate E_{111} mode was damped. In order to enable its position to be varied, the bottom end of the cavity was made in two halves, and was assembled as follows. A positioning ring

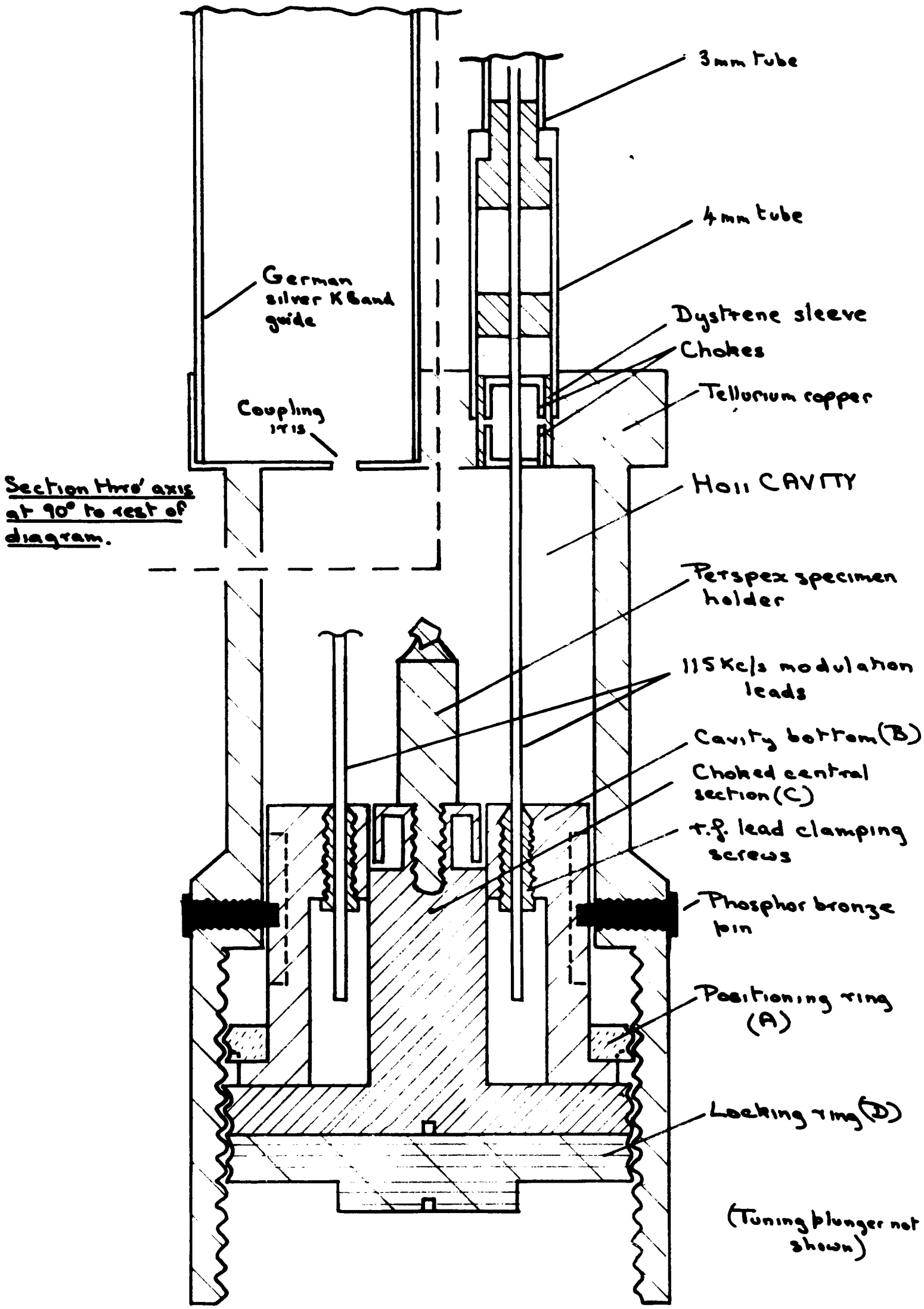


FIGURE 2·3

K BAND CAVITY

(A) was first screwed in to roughly the correct position, and then the outer section (B) inserted, threading the r.f. leads through holes and down the centre of the drilled clamping screws. Two phosphor bronze grub screws, which prevented the section from rotating whilst allowing it to move vertically, were then inserted. Indentations in the lower outer diameter of section (B) made it possible to rotate the ring (A) with (B) in position, if necessary. The r.f. lead clamping screws were then tightened, and the inner section (C) of the cavity bottom, to which the specimen holder and sample were attached, was screwed in. Finally a locking ring (D) was screwed in to clamp the system tight. To change samples only the sections (C) and (D) had to be removed. A P.T.F.E. tuning plunger, (not shown in Figure 2.3), enabled fine tuning of the cavity to be accomplished from the top of the cryostat. The microwaves were coupled into the cavity by irises. These were enlarged in size until the power reflected from the cavity on resonance was just half that reflected off resonance, as judged by monitoring the power reflected from the cavity when the klystron frequency was modulated at 50 c/s. The cavity was made out of tellurium copper and had a Q ~ 3,500 at room temperature. One drawback of this material was that 4.2°K the resistance of the copper became so low that only ~ 10 gauss amplitude low frequency modulation penetrated the cavity from external coils.

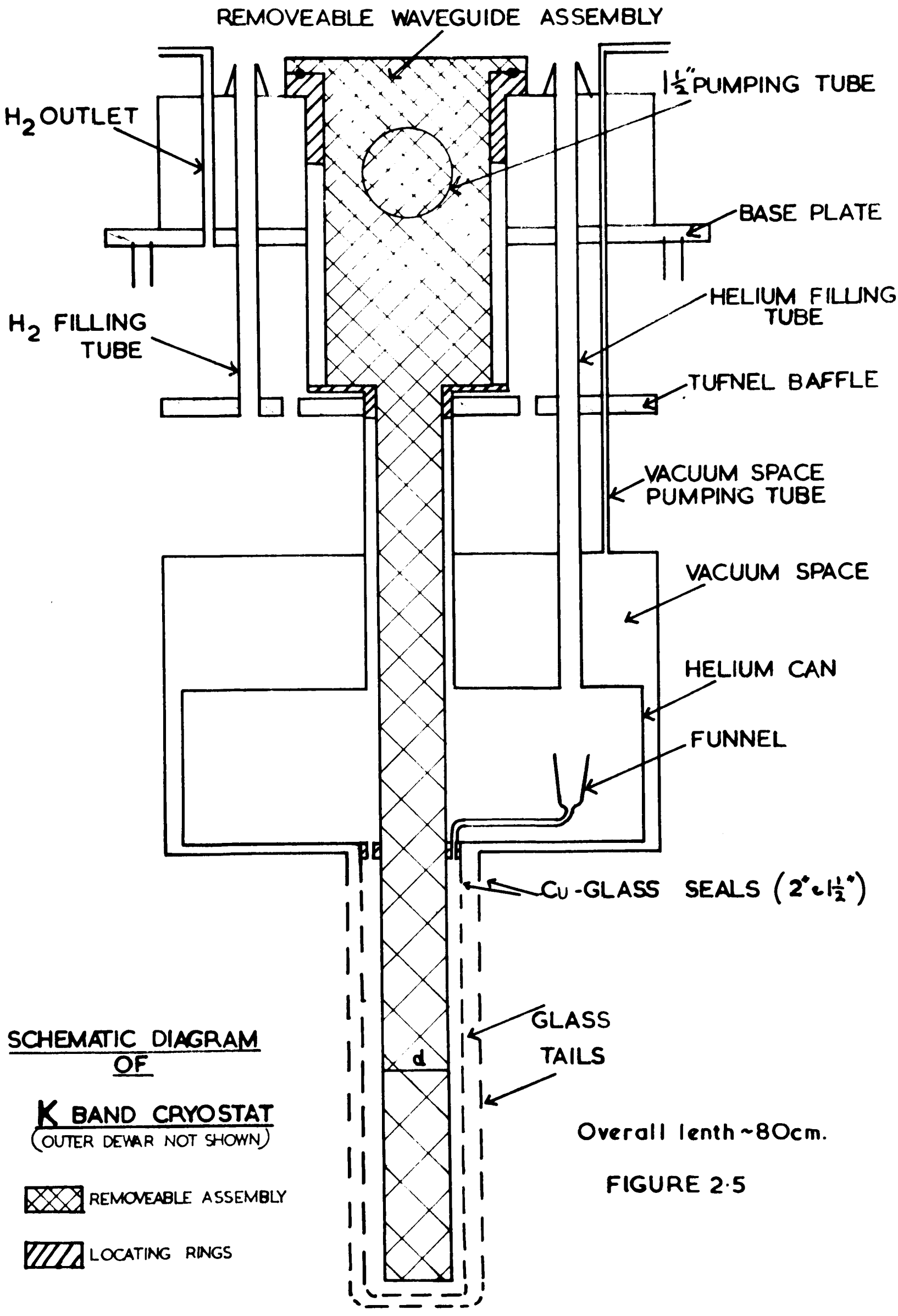
Figure 2.4 shows a photograph of the cavity and waveguide



FIGURE 2·4

assembly. This could be withdrawn from the cryostat which is shown diagrammatically in Figure 2.5 and in the photograph of Figure 2.6. The cavity was vacuum sealed by a surrounding german silver can Woods-metalled to a copper section "d". Kovar seals enabled the r.f. and N.M.R. leads to pass through this section. The waveguides leading from the cavity were made of german silver by Johnson Matthey, and were of standard K Band size (W.G.20). They were joined to a copper bend at the top, and were sealed with mica windows, held by "O" rings, at the couplings to the rest of the microwave circuit. The tuning plunger was also sealed with "O" rings at the top. All joints below the section "d" were made of non-superconducting solder in order not to affect the magnetic field at the cavity. Cd - Bi(M.Pt.140°c) and Cd - Zn(M.Pt.240°c) solders were used, the preparation of which has been described by Wyatt (1963). The removable waveguide assembly (Figure 2.4) was held rigid by a surrounding german silver tube, and it was sealed by an "O" ring at the top of the cryostat.

The diagram of the cryostat, Figure 2.5, is self explanatory. All vertical tubes were made of german silver or stainless steel, and the helium and vacuum cans of brass. Either glass or metal tails could be used, and a 5¼" i.d. glass outer dewar (not shown) surrounded the whole assembly. The diameters of the tails were not kept to a minimum as the magnet also served the X Band apparatus where the pole gap required was at least 2.2".



SCHEMATIC DIAGRAM OF

K BAND CRYOSTAT

(OUTER DEWAR NOT SHOWN)

REMOVEABLE ASSEMBLY

LOCATING RINGS

Overall lenth ~80cm.

FIGURE 2·5

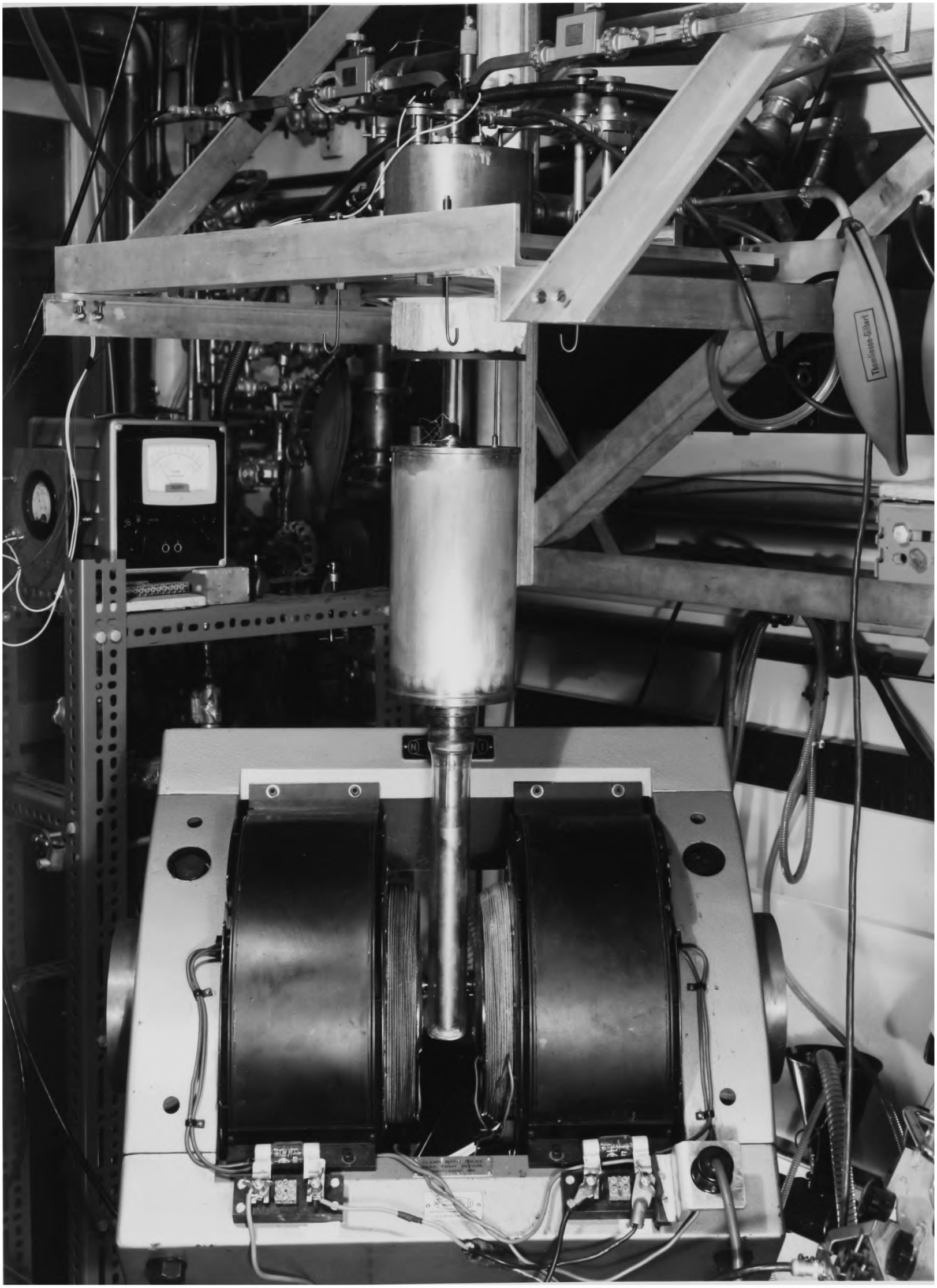


FIGURE 2·6

Resistance thermometers at section "d", and on top of the vacuum can, acted as refrigerant level indicators. The refrigerant could be pumped via a 1½" diameter tube leading out of the central space just above the base plate.

The inner refrigerant space held up to 1,500 c.c. liquid. With no r.f. current passing, hydrogen lasted for 24 hours when surrounded by nitrogen, and helium about 10 hours, when shielded by hydrogen. If small (~ ½ amp.) r.f. currents were used these times were not substantially altered. By pumping on the helium the temperature could be reduced to about 1.2°K. Precooling was accomplished by softening the dewar space with a little helium gas.

2.4 The magnetic field

For most of the experiments discussed in Chapter 3, a 4" pole diameter Tickfords magnet was used, and this has been described by Ryan (1960). The X Band apparatus was then re-mounted, and used for all the other experiments in conjunction with a 7" Newport Type E magnet, which also served the K Band spectrometer. This magnet was powered by a 9 Kw motor generator which supplied up to 26 amps exciting current, stabilised to 1 part in 10^4. Pole pieces tapering to 4" diameter and a pole gap of 2.2" were used, giving a maximum field of 12 Kg for short periods, and of 10 Kg for continuous use. The field could be swept at various speeds by a Newport Electronic Sweep Unit type A. Low frequency modulation coils were wound out of

0.064" diameter copper wire on special fibre glass formers. These were designed to fit the tapered pole pieces, and to allow the existing X Band cryostat dewars to be used. The coils provided up to 500 gauss peak to peak modulation at 50 c/s inside the X Band cavity. The magnet was capable of being raised, and levelled, and its angle of rotation could be read to 0.2°.

2.5 Measurement of the magnetic field

The magnetic field was measured either by simultaneous video display of N.M.R. and E.P.R. signals or by means of a calibration of the magnet exciting current.

For the first method the N.M.R. probe was situated just above the sample, as shown in Figure 2.2, since the field inhomogeneity precluded the use of an external probe. Resonance was observed from protons in perspex, or from Li^7 and F^{19} nuclei in X-irradiated lithium fluoride. Two N.M.R. oscillators were used, both of which were constructed from basic circuits designed by Dr. F. N. H. Robinson. Their principle of operation is discussed by Robinson (1959). The first of these units has been described by Ryan (1960) and was used in conjunction with a frequency meter Type BC221. This unit was used for the measurements described in Chapter 3, but was inconvenient as it had only a relatively small frequency range with a given probe coil. A second oscillator was therefore built and used for most of the other experiments. The circuit diagram is given in

Figure 2.7. It gave sufficient r.f. output to drive a Hewlett-Packard frequency counter which measured the frequency directly. With the main probe coil used, it had a frequency range of ~1.6 - 10.5 mc/s, and enabled fields between ~ 380 g and ~6.3 Kg to be measured very easily.

In the second method, the magnet exciting current was calibrated against the field using a Numar Precision Gaussmeter. This was modified to enable its frequency to be measured directly by the Hewlett-Packard frequency counter. The current was measured accurately by measuring the voltage developed across an oil-immersed eureka coil, of resistance 0.05Ω, placed in series with the magnet (See Figure 2.1). This voltage was measured with a Tinsley portable potentiometer Type 3184 D. The eureka resistance was also tapped to shunt a Turner sub-standard ammeter, and this was used for less accurate measurements. Careful cycling of the current was necessary and if several readings were taken accuracies of ± 5g could be obtained at most fields. This calibration was used for rough measurements and when the chart recorder was used, the chart being marked with a marker pen at regular intervals of field in the usual manner.

2.6 The pumping system

An extensive pumping system was constructed to enable all the necessary pumping operations to be carried out on

NMR OSCILLATOR E.W.82

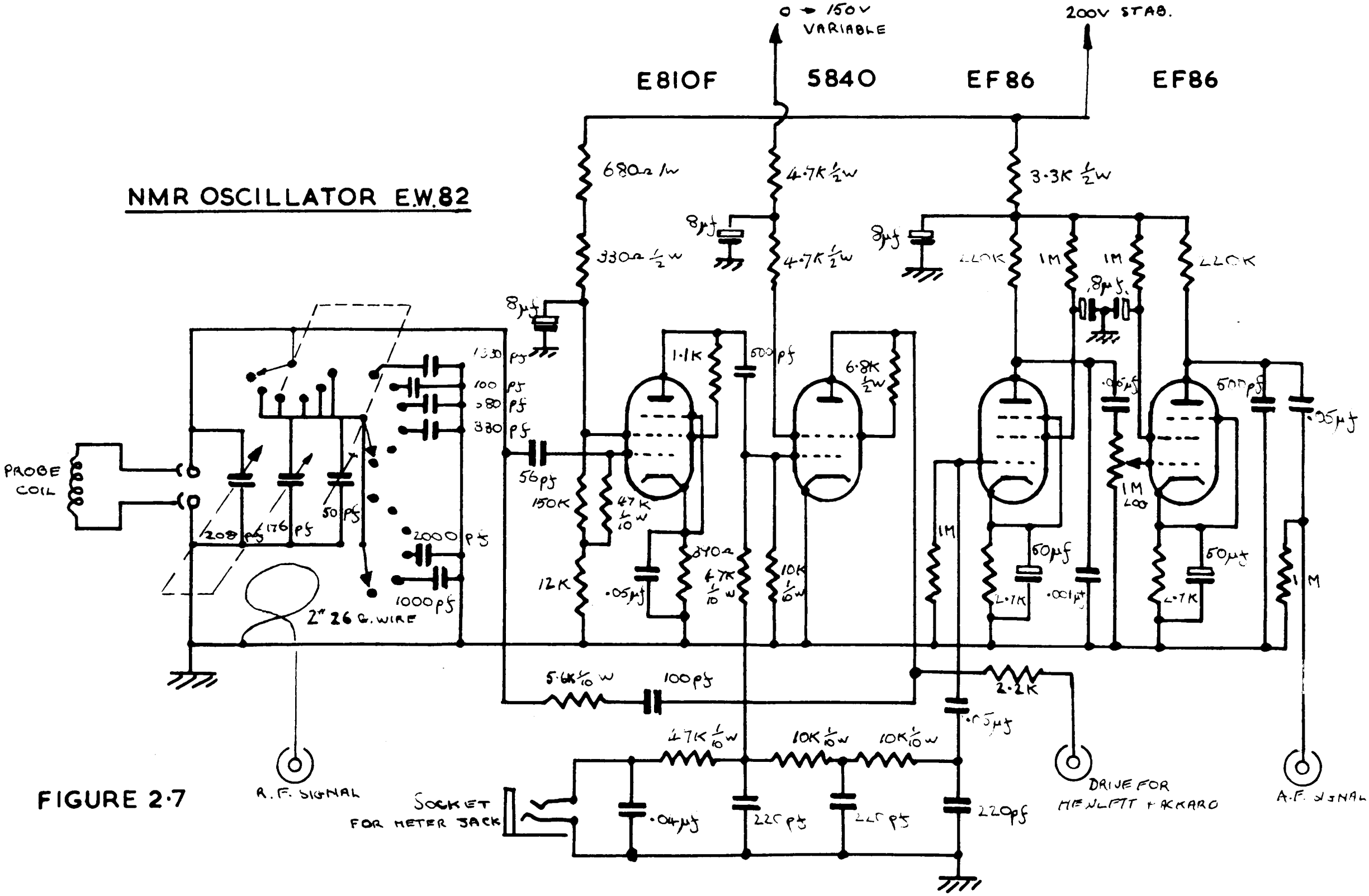


FIGURE 2·7

either the K Band, or the new X Band, apparatus. It enabled the helium space to be pumped through 2" and 1½" tubes by an Edwards 1 cc 450B rotary pump. A separate mobile high vacuum unit enabled the vacuum space to be pumped to $\sim 10^{-4}$ mm.

CHAPTER 3

Experimental results of the paramagnetic resonance of rare earth ions in the garnet crystal structure

3.1 Introduction

In this chapter the experimental results on the paramagnetic resonance of four rare earth ions in diamagnetic, and weakly paramagnetic, garnet lattices are given.

The garnets form what is undoubtedly the best system available in which to investigate the phenomena of ferrimagnetism that is, the exhibition of a spontaneous magnetic moment in a non conducting material due to non parallel alignment of atomic moments, (see for example Wolf 1961). They have many of the ideal properties described in § 1.2. The usual synthetic garnets have the formula $R_3^{3+} X_5^{3+} O_{12}^{2-}$, where R is yttrium, lutetium, or a rare earth ion; and X is iron (Fe^{3+}) in the ferrimagnetic garnets, or aluminium, or gallium, in the paramagnetic and diamagnetic garnets. The largest rare earth ion which can be accommodated varies from gadolinium to praseodymium according to X, but all except cerium can be used to dope the diamagnetic crystals. It is now well known that the incorporation of rare earth ions in place of yttrium in, for example, yttrium iron garnet (YIG) can have profound effects on its spontaneous moment and anisotropy, (see Wolf 1961). A striking instance of such an effect is the occurrence of sharp peaks in the normally smooth angular variation of the ferrimagnetic resonance field of YIG, when

only a small percentage of rare earth ions is added (Dillon and Nielsen 1960). In order to explain such effects in terms of the conventional "single ion" models of ferrimagnetism (as described in Wolf 1957, Wolf 1959, Kittel 1960, and Van Vleck 1962), one must first have a knowledge of the properties of each individual ion in a diamagnetic environment which is as close as possible to that surrounding it in the magnetically concentrated salt, and thus obtain the effect on the ion of its crystalline surroundings alone. It is usual to assume that this is the same in the diamagnetic and concentrated salts, but in the case of the garnets, as will be seen, it is found that this is not necessarily so, and there is a very large dependence on the diamagnetic host lattice used for some rare earth ions.

§ For this reason an extensive programme of research into the properties of rare earth ions in different paramagnetic and diamagnetic garnet lattices was carried out by the group, using bulk magnetic measurements as well as paramagnetic resonance. The work described in this chapter concerns the paramagnetic resonance of Nd^{3+}, Dy^{3+}, Er^{3+} and Yb^{3+} in the two diamagnetic lattices, lutetium aluminium garnet (LAG) and lutetium gallium garnet (LGG), and of Er^{3+} and Yb^{3+} in several weakly paramagnetic lattices. It represents an extension to the work of Ryan (1960) on the resonance of some of these ions in yttrium aluminium garnet (YAG) and yttrium gallium garnet (YGG), which indicated in at least one case a very strong dependence of the magnetic

properties lens on the nature of X. The results of the experiments on the lutetium lattices indicate that the magnetic properties are also quite sensitive to the nature of R, but not to the same extent as to the nature of X. A discussion and interpretation of these results will be given in Chapters 4-8.

Although diamagnetic host lattices are usually used, in certain cases, discussed in §9.1, one can observe resonance from rare earth ions in paramagnetic host lattices without prohibitive interaction broadening of the lines. In §9.2 it is shown that when the host ions are in a singlet state the resonance is shifted but not broadened, and the measurements in weakly paramagnetic garnet lattices were made to investigate such an interaction effect. These measurements are discussed in §9.3. When the interactions between the host and probe ions are very weak, one can use these paramagnetic host lattices to investigate further the variation of the rare earth ions' magnetic properties with lattice alone.

3.2 Crystal structure of the garnets

The major drawback of the garnets from a theoretical point of view is their extremely complex crystal structure, though no doubt if the structure were more simple they would not exhibit so many interesting properties. A model of a unit cell is shown in Figure 3.1. The crystal structure, and range of composition, is now very well established. The structure parameters have been determined by a number of workers (Bertaut and Forrat 1956,



FIGURE 3·1

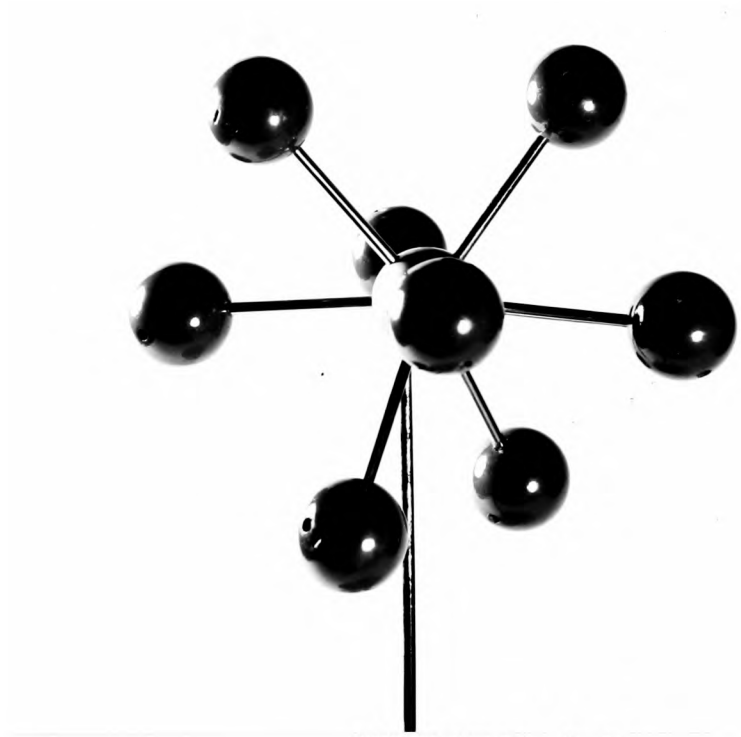


FIGURE 3·2

Geller and Gilleo 1957, Euler and Bruce 1962). Only the immediately relevant details will be given here, further discussion of the symmetry properties can be found in the above references, and in Ryan (1960). This section will be referred to again in Chapter 7.

The unit cell of the garnets is cubic, with space group O_h^{10} - Ia, 3d. There are eight formula units $R_3X_5O_{12}$ per unit cell, a total of 160 ions. The rare earth ions, R, occupy the 24 {c} sites, which have eight nearest neighbour oxygen ions arranged roughly in the form of a distorted cube with the rare earth ion at its centre. Figure 3.2 shows a photograph of this distorted cube of ions. The ions X occupy the 16 [a] and 24 (d) sites, which have six, and four, nearest neighbour oxygen ions, arranged roughly in the form of an octahedron, and tetrahedron, respectively. The oxygen ions occupy the 96 h sites, and their positions are specified in terms of three structure parameters x, y, and z as well as a_o the lattice constant. The {c}, [a] and (d) sites all lie at positions specified in terms of fractions of a_o alone. The point symmetry at the {c} site is D_2, that is it has three mutually perpendicular twofold axes of symmetry. There are six inequivalent {c} sites per unit cell, each of which has an identical surrounding oxygen "cube", apart from its orientation. There is a one to one relation at each site between the twofold axes and the directions of the principal g values described in the next section. <O.

3.3 The spectrum of rare earth ions in garnets

As discussed in §1.3, the interaction with an external magnetic field, of a rare earth ion having an odd number of 4f electrons in a crystalline environment, can usually be represented by the spin Hamiltonian of Equation (1.1) (excluding the case of Gd^{3+}). This Hamiltonian only applies to the main isotopes, with no nuclear spin. At low temperatures, when only the ground doublet is populated, each ion gives rise to one E.P.R. line. Diagonalising the matrix of this spin Hamiltonian, given in Appendix I, it is easily shown that the resonance condition is,

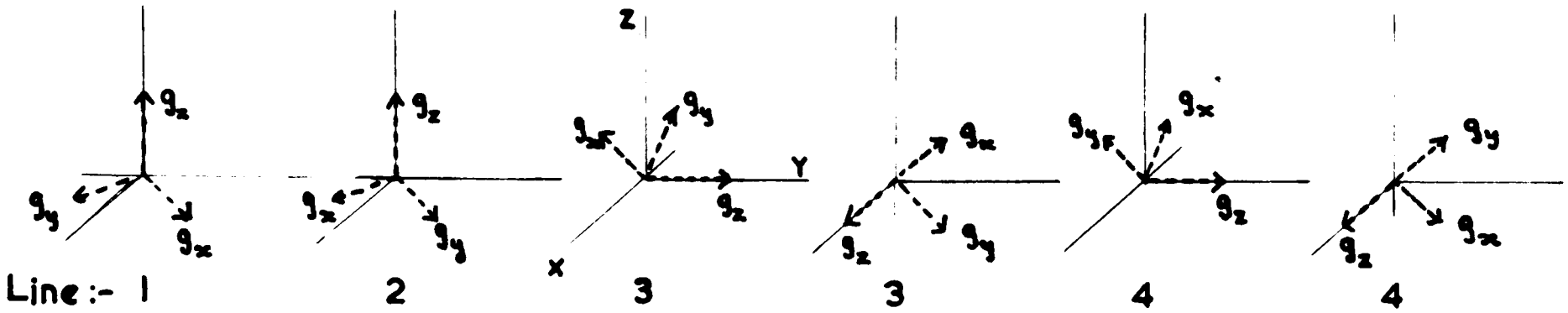
$$h\nu = g_{eff}\mu_B H \qquad (3.1)$$

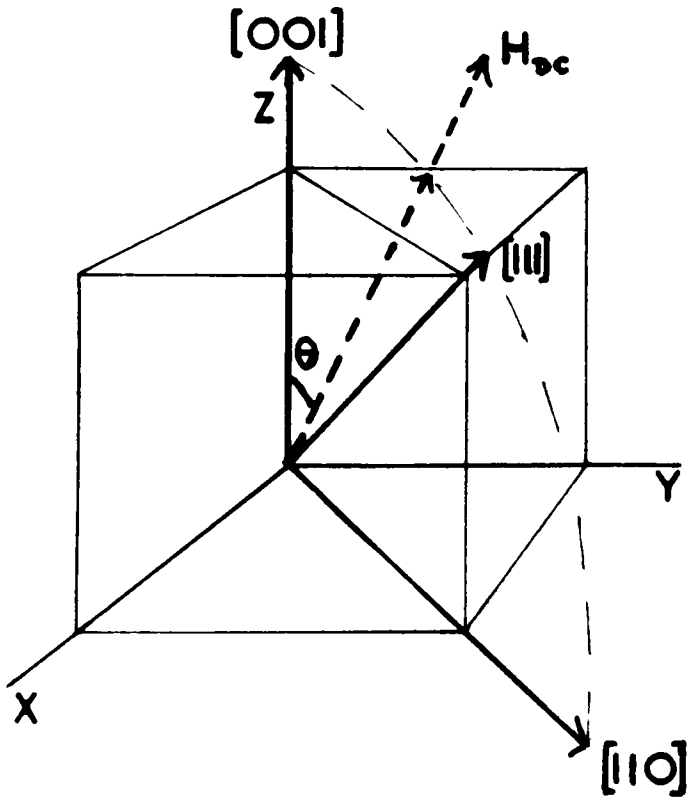
where $$g_{eff}^2 = \sum_{\substack{i= \\ x,y,z}} g_i^2(l_i l_f + m_i m_f + n_i n_f)^2 \qquad (3.2)$$

and, referred to the crystal unit cell axes (X,Y,Z), H has direction cosines (l_f, m_f, n_f) and the ion has principal g values g_i with direction cosines (l_i, m_i, n_i).

In contrast to the complicated crystal structure of the garnets, the resonance spectrum is comparatively simple. The rare earth ions situated at the six inequivalent {c} sites have identical g tensors, but the orientation of the principal axes of this tensor with respect to the cubic unit cell axes differs at each of the six sites. The six different orientations are shown in Figure 3.3 where, for each ion, g_z is chosen to be along an $\langle 001 \rangle$ direction. The photograph in Figure 3.4 shows

SIX INEQUIVALENT IONS IN GARNET





1 $$g_e^2 = g_x^2 + \left[g_z^2 - g_x^2\right]\cos^2\theta$$

2 $$g_e^2 = g_y^2 + \left[g_z^2 - g_y^2\right]\cos^2\theta$$

3 $$g_e^2 = g_x^2\left[\frac{\sin\theta}{2} + \frac{\cos\theta}{\sqrt{2}}\right]^2 + g_y^2\left[-\frac{\sin\theta}{2} + \frac{\cos\theta}{\sqrt{2}}\right]^2 + g_z^2\frac{\sin^2\theta}{2}$$

4 $$g_e^2 = g_x^2\left[-\frac{\sin\theta}{2} + \frac{\cos\theta}{\sqrt{2}}\right]^2 + g_y^2\left[\frac{\sin\theta}{2} + \frac{\cos\theta}{\sqrt{2}}\right]^2 + g_z^2\frac{\sin^2\theta}{2}$$

FIGURE 3·3

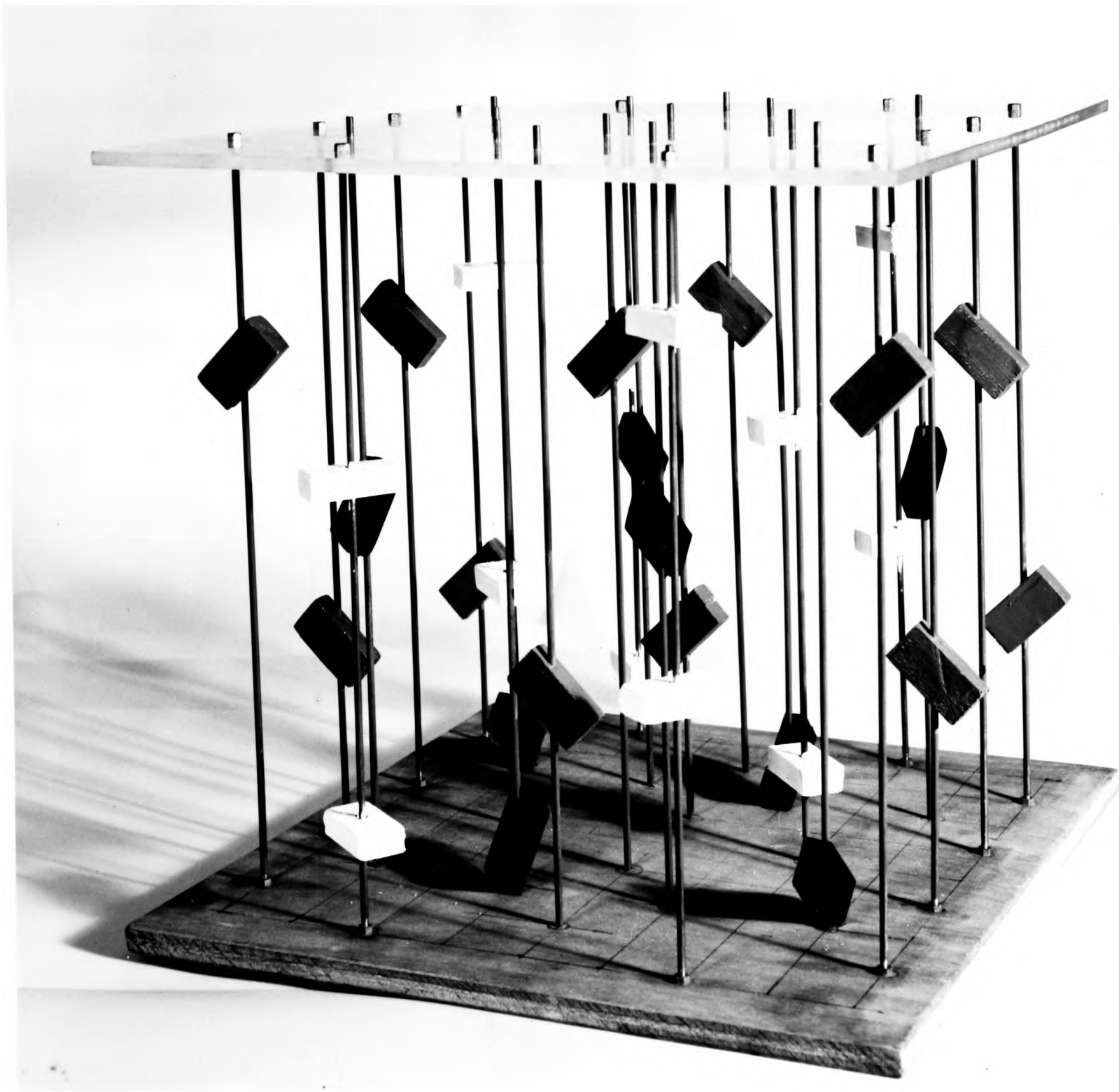


FIGURE 3·4

the {c} sites only, in one unit cell. The blocks of wood have edges parallel to the principal axes of the g tensors. (This model was constructed by Mr. M. Ball). For an arbitrary direction of the magnetic field there will, therefore, be a spectrum of six lines. If, however, the magnetic field is confined to a {110} plane it is easily shown from Equation (3.2) that there are only four magnetically unequivalent ions, and that the resulting four lines will be reduced to two when the field is in the <001> and <111> directions. The equivalent ions are labelled in Figure 3.3, and the value g_{eff} for the four lines seen when the field is in the (110) plane, varies with θ (the angle the field makes with the [001] direction) according to the equations,

1. $g_{eff}^2 = g_x^2 \sin^2\theta + g_z^2 \cos^2\theta$

2. $g_{eff}^2 = g_y^2 \sin^2\theta + g_z^2 \cos^2\theta$

3. $g_{eff}^2 = g_x^2 \left(\frac{\sin\theta}{2} + \frac{\cos\theta}{\sqrt{2}}\right)^2 + g_y^2 \left(\frac{-\sin\theta}{2} + \frac{\cos\theta}{\sqrt{2}}\right)^2 + g_z^2 \frac{\sin^2\theta}{2}$

4. $g_{eff}^2 = g_x^2 \left(\frac{-\sin\theta}{2} + \frac{\cos\theta}{\sqrt{2}}\right)^2 + g_y^2 \left(\frac{\sin\theta}{2} + \frac{\cos\theta}{\sqrt{2}}\right)^2 + g_z^2 \frac{\sin^2\theta}{2}$

..... (3.3)

These equations follow directly from Equation (3.2). The maximum value of g_{eff} for lines 3, and 4, occurs at an angle θ_0 given by

$$\tan 2\theta_0 = \pm \frac{(g_y^2 - g_x^2)\sqrt{8}}{\{2g_z^2 - (g_x^2 + g_y^2)\}} \qquad (3.4)$$

Lines 3 and 4 are identical, but displaced by $2\theta_0$.

A typical spectrum in the (110) plane, that of Yb^{3+} in LAG is shown in Figure 3.5, where the formulae for g_{eff} in the special directions is given. It is evident from Figure 3.3 that g_x and g_y are experimentally indistinguishable, usually the larger of the two has been arbitrarily denoted as g_x. This ambiguity could only be resolved by relating the g values to the immediate surroundings of the ion, by transfer hyperfine structure for example, or by a theoretical correlation via the crystal field.

3.4 Experimental procedure

The crystals used in the experiments were grown by Dr. G. Garton and Mr. M. Ball from a lead oxide-lead fluoride flux, using the method of Nielsen (1960). They were of excellent quality, but in some cases contained up to ~ 0.01% impurities due to their method of growth.

X Band frequencies (~ 9.5 Gc/s) were used for most of the experiments. After preliminary investigations the crystals were oriented so that a {110} plane was horizontal. Because of the highly anisotropic spectra observed in most cases accurate orientation was necessary. This was accomplished by attaching the crystal to a goniometer head with black wax, and orienting it, taking full precautions, firstly on an optical goniometer (to $\pm 2^{\circ}$) and then using Laue back reflection of white X rays (to $\pm 20'$). The crystal was then transferred to a perspex

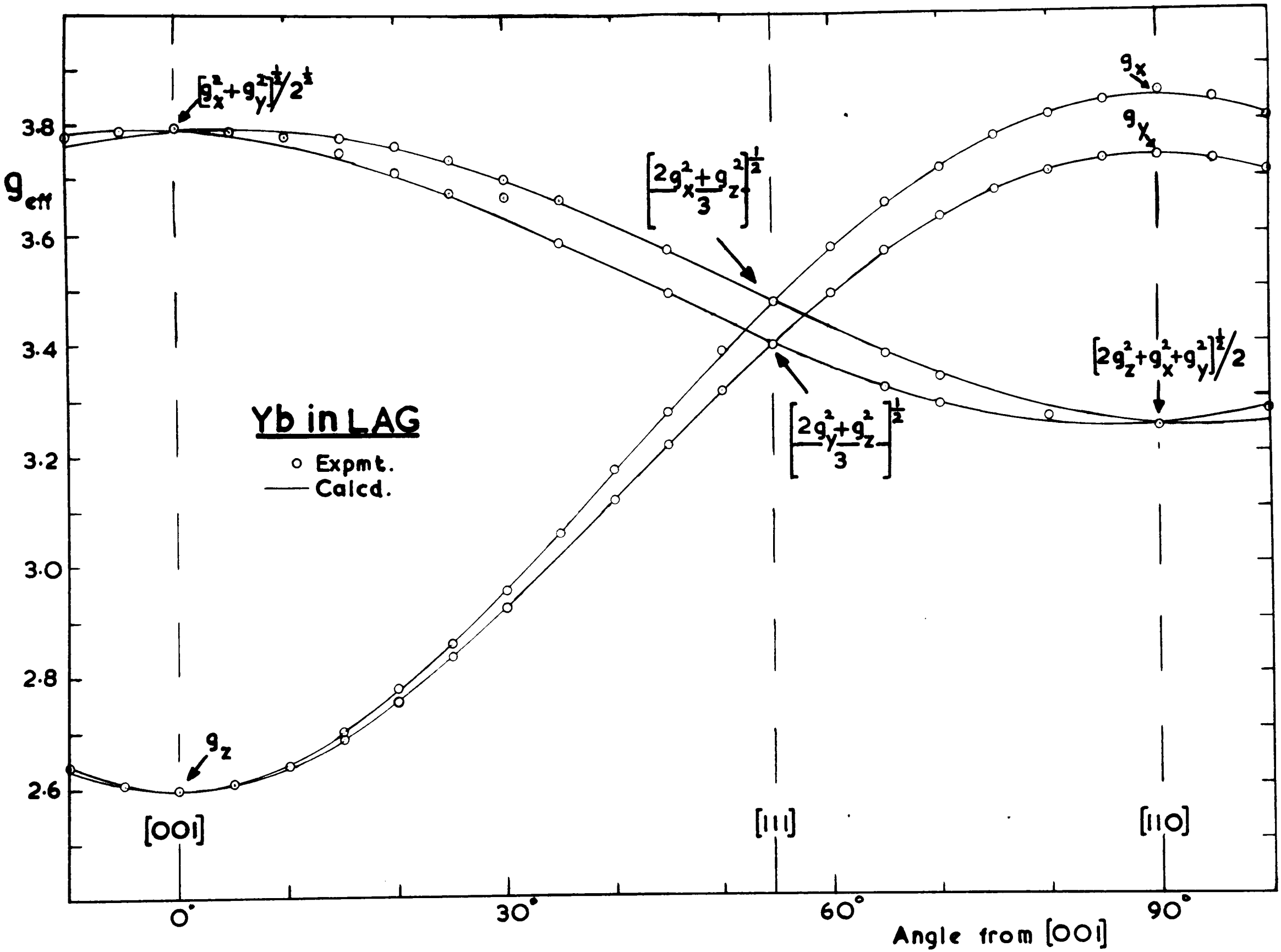

g_{eff}
3.8
3.6
3.4
3.2
3.0
2.8
2.6
$[g_x^2+g_y^2]^{\frac{1}{2}}/2^{\frac{1}{2}}$
$\left[\frac{2g_x^2+g_z^2}{3}\right]^{\frac{1}{2}}$
$\left[\frac{2g_y^2+g_z^2}{3}\right]^{\frac{1}{2}}$
g_x
g_y
$[2g_z^2+g_x^2+g_y^2]^{\frac{1}{2}}/2$
g_z
Yb in LAG
o Expmt.
—— Calcd.
[001]
[111]
[110]
0°
30°
60°
90°
Angle from [001]

FIGURE 3·5

specimen holder which screwed into the specimen rod. Both holder and goniometer head were mounted in a lathe, or the crystal transfer device shown in Figure 10.3 , and the crystal embedded in Araldite (X 83/11 or Z 107 with silica powder filler) in the holder. The black wax was finally dissolved away with benzene. In some cases it was possible to check the orientation in the holder on the optical goniometer. This method is similar to that described by Ryan (1960) where further details may be found. The apparatus specimen tube was made as vertical as possible using a plumb line, and the magnet levelled, and adjusted, so that its axis bisected the line joining the specimen and N.M.R. coil. Final slight adjustment, if necessary, was made by altering the magnet levelling until lines 3, and 4, were unsplit.

Simple video detection was sufficient for all the experiments carried out at X Band. The magnetic field was measured by simultaneous display of N.M.R., the resonance frequency being measured on a B.C.221 frequency meter. The microwave frequency was measured with a cavity wavemeter of known dimensions, accurate to about 1 in 3,000. In most experiments the measured values of g_{eff} were corrected by a factor, determined so that a sample of d.p.p.h., attached to the specimen, gave $g_{corr.} = 2.0036$. This in effect corrected for the microwave frequency errors, and errors arising from there being slightly different fields at the sample and N.M.R. coil.

In the cases of Dy^{3+} in LAG and YAG, the anisotropy was so great, and line widths so large, that the main errors arose from misorientation of the sample, and in estimating the centre of the resonance line. For these cases it was sufficient to measure the magnetic field from the magnet exciting current calibration curve. All measurements were carried out at $4.2^{\circ}K$ except for those on Yb^{3+} in LAG and LGO, which were made at $20^{\circ}K$.

The [001] and [110] directions were found from turning and crossing points of the spectrum, often the [111] crossing points could be located most accurately. Lines 1 and 2 were measured at 5° intervals, and lines 3 and 4 at 10° intervals, over a range of $\theta = -10^{\circ}$ to 100°. The principal g values were found in the usual manner by plotting g_{eff}^2 v $\cos^2\theta$ for lines 1 and 2 as in Figure 3.6. If the range of g_{θ}^2 was too large a residuals method was used, this was also used in the case of Yb^{3+} in LAG to give greater accuracy. From the three principal g values and Equations (3.3) the theoretical lines were computed on the Oxford University Mercury computer (see Appendix IVA), and compared with those found experimentally.

Errors were estimated from the following contributing factors.

(a) Random errors estimated from scatter of points.

(b) Systematic apparatus errors.

(c) Possible error in the "g marker" correction.

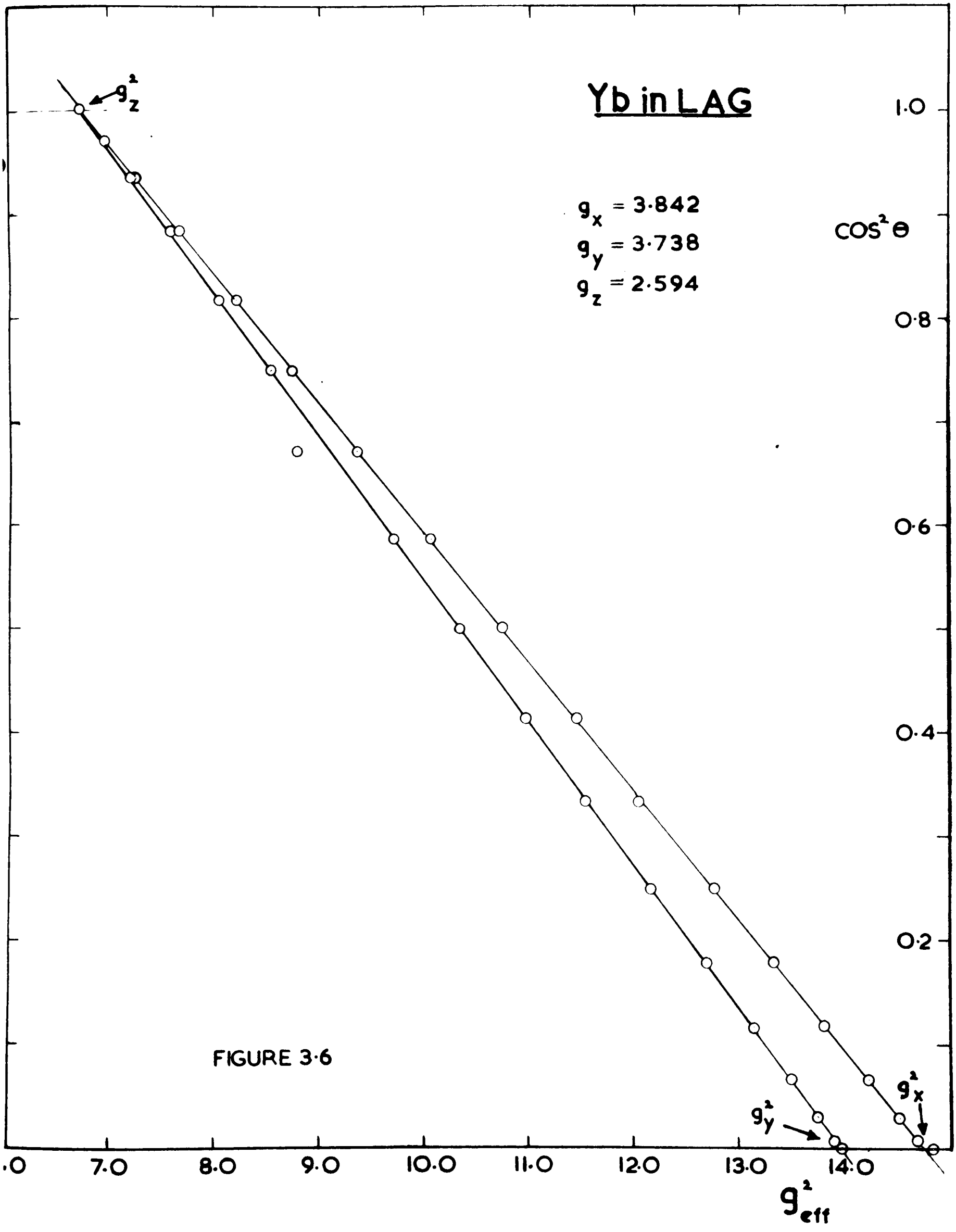

Yb in LAG
$g_x = 3.842$
$g_y = 3.738$
$g_z = 2.594$
g_z^2
$\cos^2\theta$
1.0
0.8
0.6
0.4
0.2
7.0
8.0
9.0
10.0
11.0
12.0
13.0
14.0
g_y^2
g_x^2
g_{eff}^2

FIGURE 3·6

(d) A misalignment error, which due to the anisotropy of the spectra became the main error in some cases. The angle of misalignment could be estimated from the splitting, or maximum possible undetected splitting, of lines 3 and 4 at $\theta = 0^\circ$, or 90°, and this angle used to estimate the possible error in the g values found at $\theta = 0^\circ$, or 90° respectively. Formulae giving these angles and errors are readily obtained from Equation (3.2) and have been given by Ryan (1960).

Readings below about 500 gauss at helium temperature proved to be unreliable because of superconductivity effects of solder on the cavity which affected the magnetic field at the specimen. Principal g values occurring at lower fields than this were found by extrapolation.

3.5 Experimental Results

Measurements were made of the ground doublet g tensor of "Kramers" rare earth ions Nd^{3+}, Dy^{3+}, Er^{3+} and Yb^{3+} in the diamagnetic lattices LAG and LGG. The principal g values of Dy^{3+} in LAG suggested likely values for Dy^{3+} in YAG, where previously no resonance had been detected (Ryan 1960, Carson, J. W. and White, R.L., private communication). A very anisotropic spectrum was observed, and its principal g values determined. The effective principal g tensor of Er^{3+} and Yb^{3+} impurity traces in the weakly paramagnetic lattices thulium aluminium garnet (TmAG), and thulium gallium garnet (TmGG), and that of 1% Yb^{3+} in europium gallium garnet (EuGG), were also

determined. These results are summarized in Tables 3.1 and 3.2 together with previous results for the YAG and YGG lattices. The measured angular variation of g_{eff} is compared with that calculated from the principal g values in Figures 3.7 to 3.16.

Individual comment will not be made on each measurement, but the general features and some relevant points in special cases will be given below.

The line widths (half intensity full width) of the 1% Nd^{3+} and 1% Yb^{3+} resonances were of the order of 30-40 gauss. The Er^{3+} widths were greater, and measurements were made on concentrations of about 0.1%, when they were ~30 gauss. The widths were anisotropic and mainly due to inhomogenous dipolar broadening. In general the Dy^{3+} lines were broader than for other ions, ~ 120 gauss for example in LGG, and consequently the errors were larger. The case of Dy^{3+} in YAG will be discussed briefly below.

Several experiments were carried out on different batches of 1% and 0.1% Dy^{3+} in YAG, but no improvement could be made on the large errors in the principal g values given in Table 1. These arise from several unusual difficulties due to the extreme anisotropy of the spectrum, namely:-

(a) A variation in intensity with orientation of a factor of about 1,000.

(b) The very low resonance field (~ 400 gauss) and small signal, corresponding to the large value of g_z made this

Table 3.1

Principal g values of four rare earth ions in each of four diamagnetic garnet lattices.

Ion	Host Lattice	Concentration	g_x	g_y	g_z
Nd^{3+}	LGG	1%	2.083 (±0.007)	1.323 (±0.007)	3.550 (±0.007)
	YGG†	-	2.027 (±0.008)	1.251 (±0.007)	3.667 (±0.018)
	LAG	1%	1.789 (±0.005)	1.237 (±0.006)	3.634 (±0.005)
	YAG†	-	1.733 (±0.004)	1.179 (±0.002)	3.915 (±0.026)
Dy^{3+}	LGG	1%	13.45 (±0.10)	0.57 (±0.10)	3.41 (±0.03)
	YGG†	-	11.07 (±0.20)	1.07 (±0.14)	7.85 (±0.10)
	LAG	1%	2.29 (±0.03)	0.91 (±0.05)	16.6 (±0.3)
	YAG	1%	0.73 (±0.15)	0.40 (±0.20)	18.2 (±0.4)
Er^{3+}	LGG	0.1%	3.183 (±0.015)	3.183 (±0.015)	12.62 (±0.10)
	YGG†	-	4.69 (±0.03)	4.03 (±0.02)	10.73 (±0.05)
	LAG	0.05%	6.93 (±0.02)	4.12 (±0.03)	8.43 (±0.04)
	YAG†	-	7.75 (±0.09)	3.71 (±0.02)	7.35 (±0.08)
Yb^{3+}	LGG	1%	3.653 (±0.013)	3.559 (±0.013)	2.994 (±0.011)
	YGG†	-	3.73 (±0.02)	3.60 (±0.02)	2.85 (±0.02)
	LAG	1%	3.842 (±0.006)	3.738 (±0.007)	2.594 (±0.004)
	YAG×	-	3.87	3.78	2.47

† Ryan (1960)

× Carson and White (1960)

Table 3.2

Values of the principal g tensors of Yb^{3+} and Er^{3+} in weakly paramagnetic garnet lattices.

Ion	Host Lattice	Concentration	g_x	g_y	g_z
Yb^{3+}	TmAG	Impurity Free	4.020 (±0.007)	3.763 (±0.008)	2.554 (±0.009)
	TmGG	Impurity Free	3.724 (±0.008)	3.557 (±0.007)	2.944 (±0.010)
	GdGG	1%	3.805 (±0.003)	3.664 (±0.003)	2.670 (±0.007)
Er^{3+}	TmAG	Impurity Free	7.89 (±0.03)	4.25 (±0.02)	7.65 (±0.03)
	TmGG	Impurity Free	3.76 (±0.02)	3.48 (±0.02)	11.9 (±0.1)

difficult to measure at X Band. The smallest g value, g_y, was above the limit of the magnetic field available.

(c) Large variations of line width, ranging from 50 to 1000 gauss. These were not appreciably reduced in the 0.1% sample, and were possibly due in part to crystal imperfections.

(d) Extreme sensitivity to misorientation of the crystal. The X Band measurements shown in Figure 3.9 gave $g_x = 0.73 \pm 0.15$, $g_y = 0.40 \pm 0.20$, and $g_z = 17.7 \pm 0.7$, where the large error in g_z was due to the superconductivity effects, and the difficulties mentioned in (b) above. As an accurate value of g_z is of importance in connection with the explanation of the anti-ferromagnetic ordering of DyAG, discussed in § 5.2, its measurement was repeated at K Band frequencies where it occurs at a resonance field of ~1 Kg. The sample was oriented optically and measurements made using 115 Kc/s phase sensitive detection, these gave $g_z = 18.3 \pm 0.4$. The value of $g_z = 18.2 \pm 0.4$ given in Table 3.1 was taken as an average of both measurements.

In all cases of resonance in diamagnetic host lattices there was no apparent indication that the simple Hamiltonian, Equation (1.2), was insufficient to describe the spectrum. Measurements of the hyperfine structure, observed in most cases, were not made as they were irrelevant to the immediate problem in hand.

From the measurements of the resonance of Er^{3+} and Yb^{3+} in the weakly paramagnetic lattices, shown in Figures 3.13 to 3.16,

it is seen that a g tensor variation is also obeyed in these lattices, in accordance with the theory developed in § 9.2. Line widths were ~15-25 gauss in these samples. The principal g values of Er^{3+} in TmGG were found from readings taken along the high symmetry directions only.

A weak resonance of Sm^{3+} in YAG was observed, but found to occur at the extreme limit of the magnetic field available and was not investigated further. No definite resonance was detected in samples of HoAG, HoGG, TbAG, or TbGG; nor from 5% Ho in YAG.

For the sake of completion it might be mentioned here that the paramagnetic resonance of Gd^{3+} has been investigated in YGG, LAG, and LGG, by Overmeyer et al. (1962), and in YAG, and YGG, by Rimai and De Mars, (1962). Geschwind (1961) has investigated the resonance of Fe^{3+} in YGG.

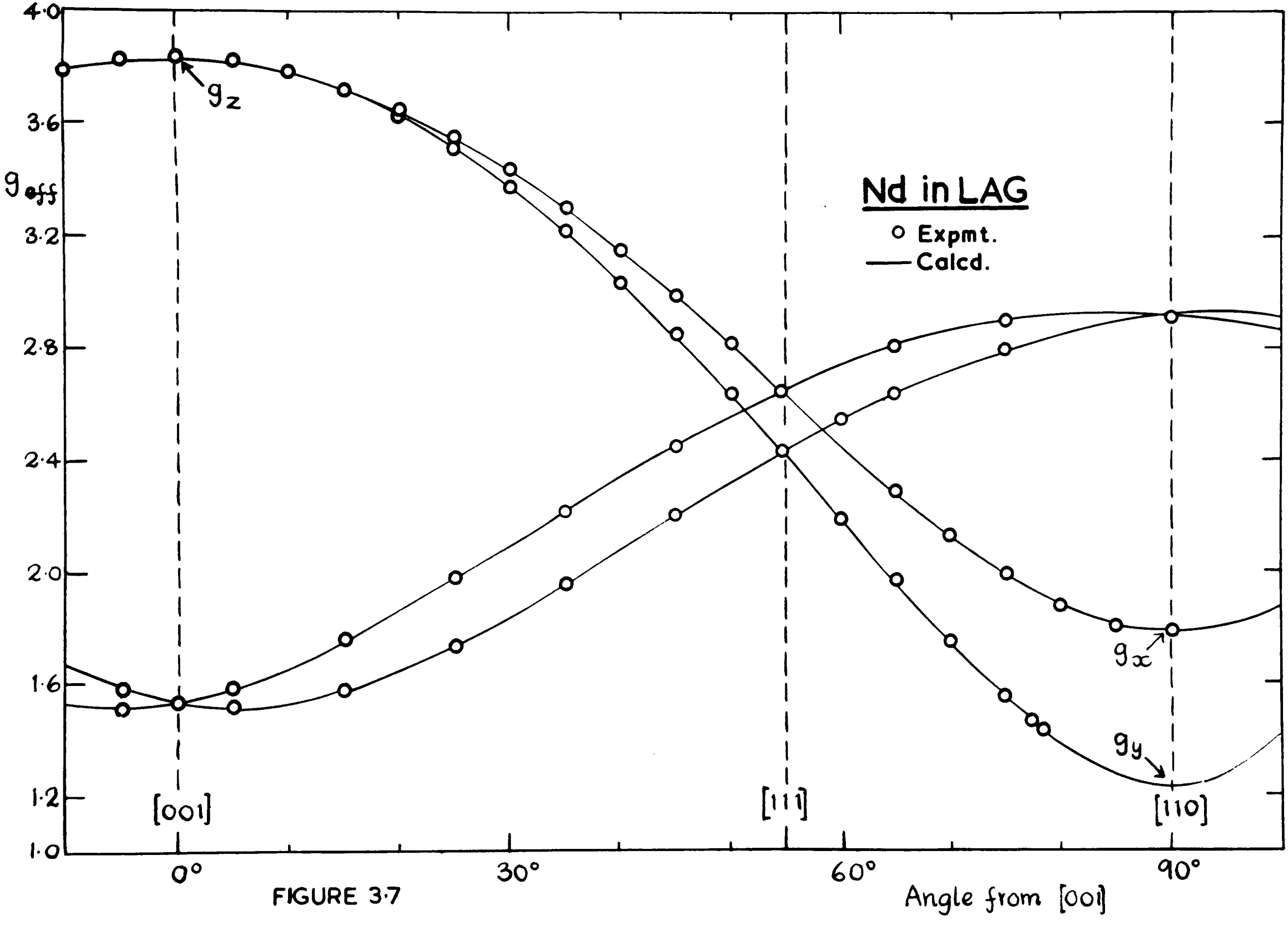

4·0
3·6
3·2
2·8
2·4
2·0
1·6
1·2
1·0
g eff
g z
Nd in LAG
o Expmt.
— Calcd.
g x
g y
[001]
[111]
[110]
0°
30°
60°
90°
Angle from [001]

FIGURE 3·7

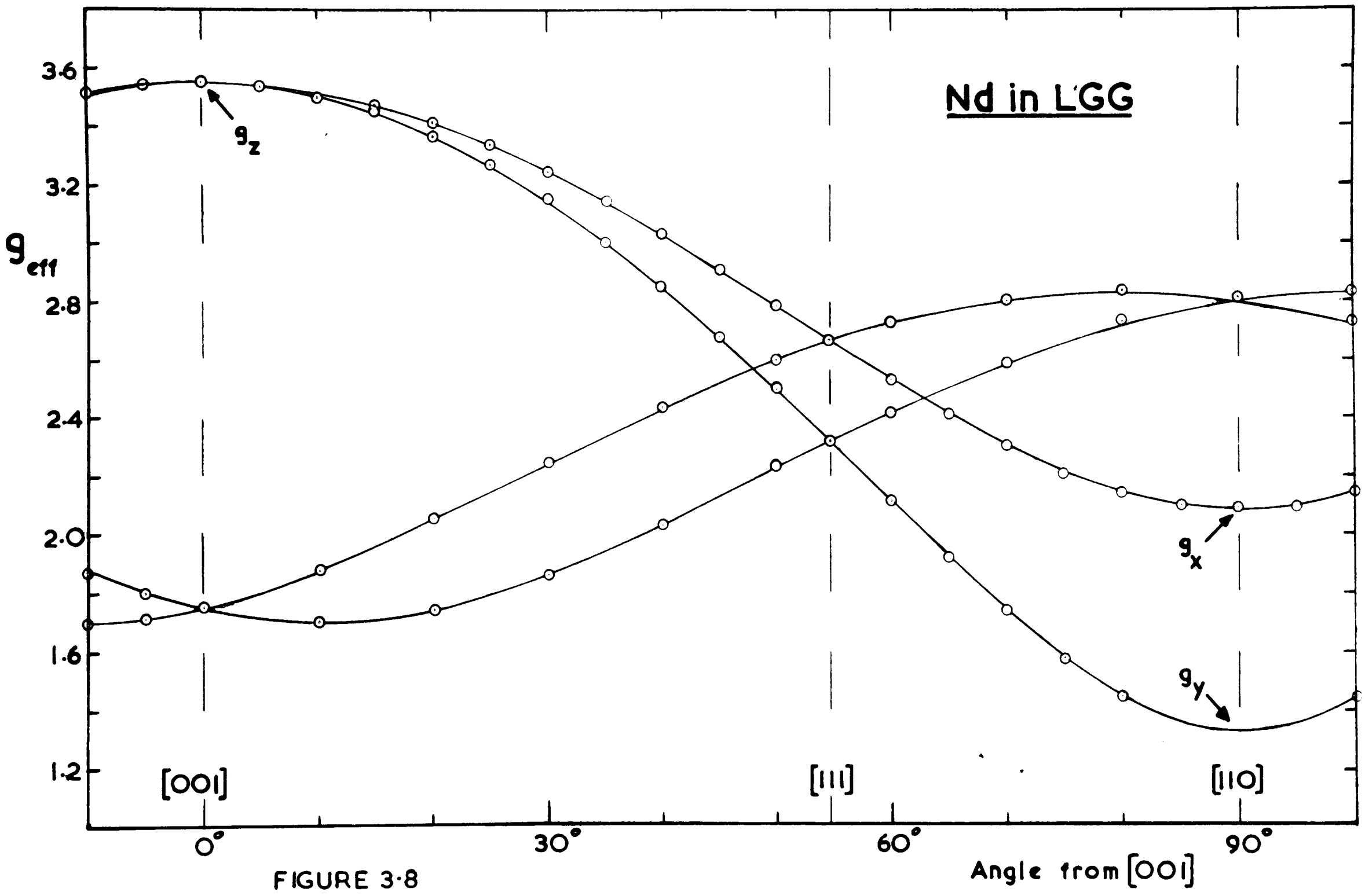

Nd in LGG
g_{eff}
3.6
3.2
2.8
2.4
2.0
1.6
1.2
g_z
g_x
g_y
[001]
[111]
[110]
0°
30°
60°
90°
Angle from [001]

FIGURE 3·8

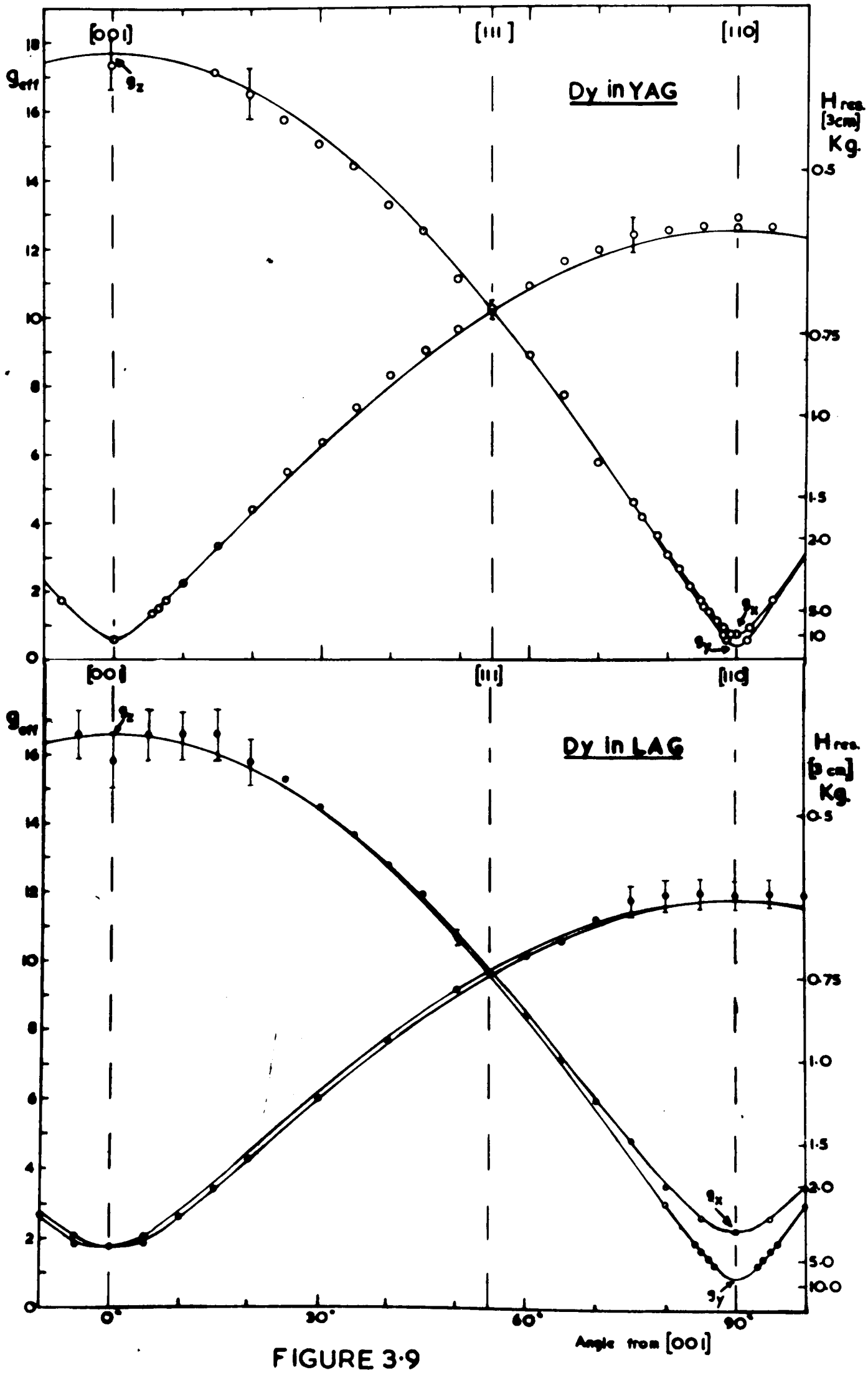

[001]
[111]
[110]
Dy in YAG
g_{eff}
$H_{res.}$ [3cm] Kg.
g_z
g_x
g_y
0
2
4
6
8
10
12
14
16
18
0.5
0.75
1.0
1.5
2.0
5.0
10.0
[001]
[111]
[110]
Dy in LAG
g_{eff}
$H_{res.}$ [3 cm] Kg.
g_z
g_x
g_y
0°
30°
60°
90°
Angle from [001]

FIGURE 3·9

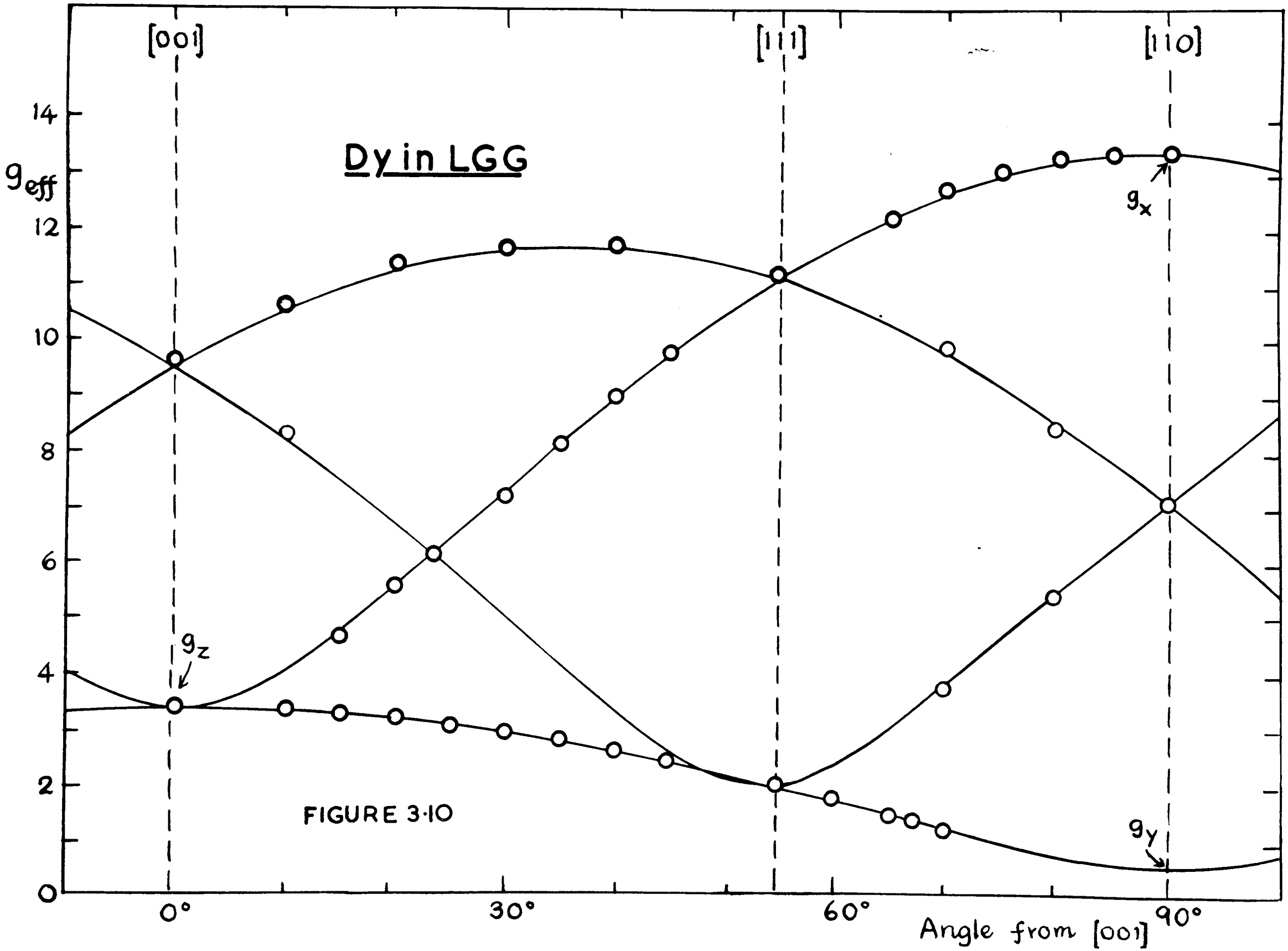

[001]
[111]
[110]
Dy in LGG
g_{eff}
14
12
10
8
6
4
2
0
g_x
g_z
g_y
0°
30°
60°
90°
Angle from [001]

FIGURE 3·10

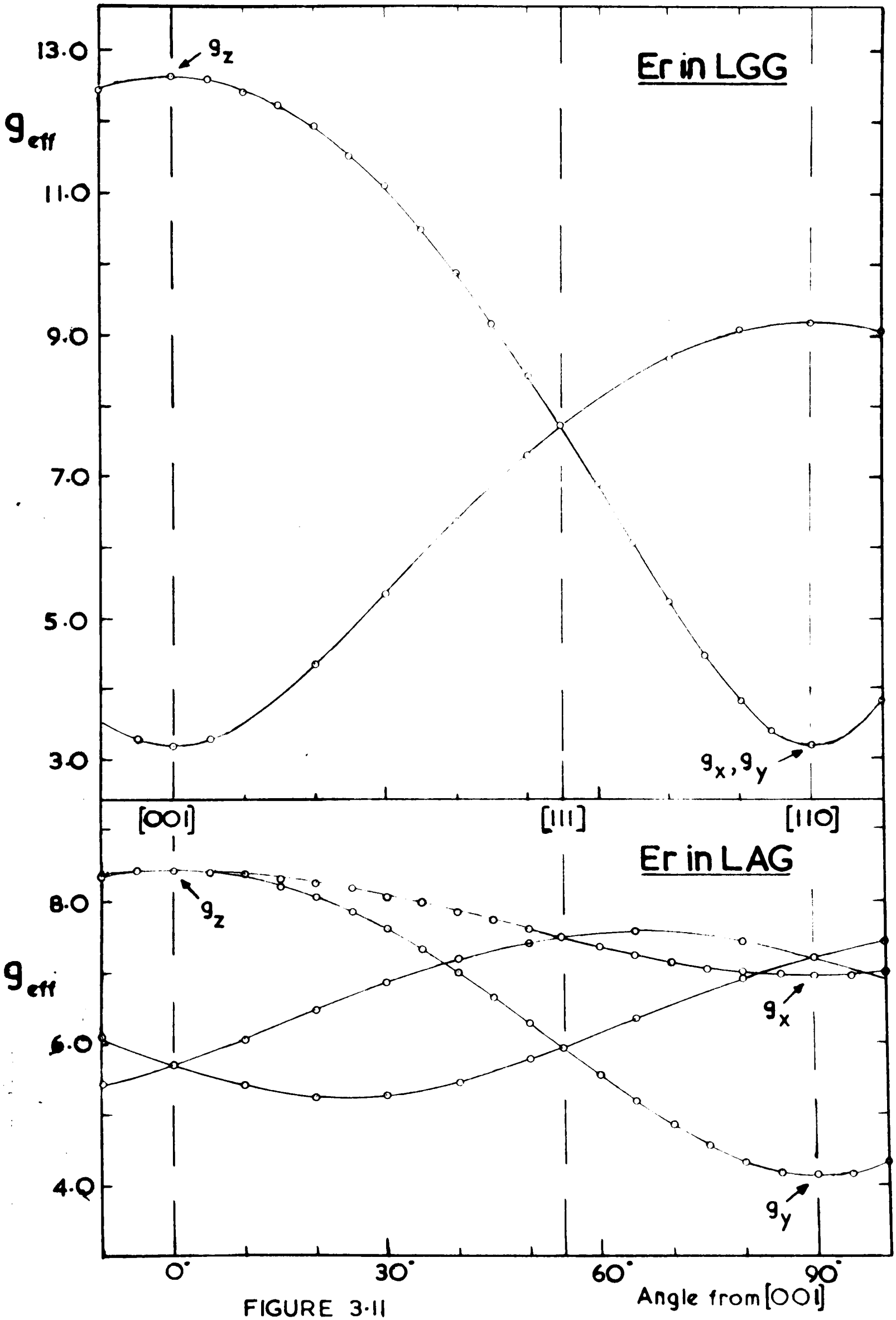

Er in LGG
g_{eff}
13.0
11.0
9.0
7.0
5.0
3.0
g_z
g_x, g_y
[001]
[111]
[110]
Er in LAG
8.0
6.0
4.0
g_z
g_x
g_y
0°
30°
60°
90°
Angle from [001]

FIGURE 3-11

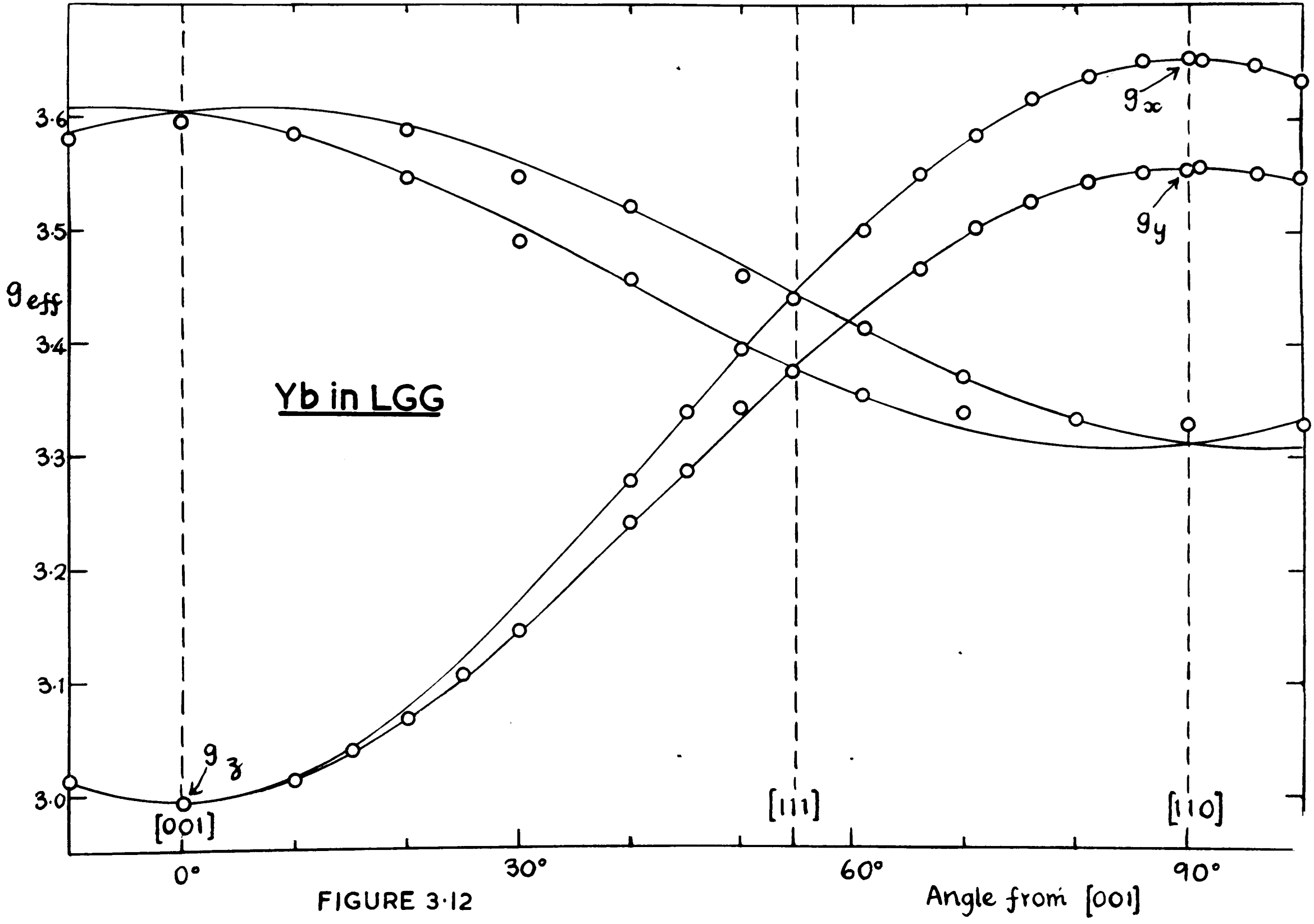

Yb in LGG
g_{eff}
3·6
3·5
3·4
3·3
3·2
3·1
3·0
g_x
g_y
g_z
[001]
[111]
[110]
0°
30°
60°
90°
Angle from [001]

FIGURE 3·12

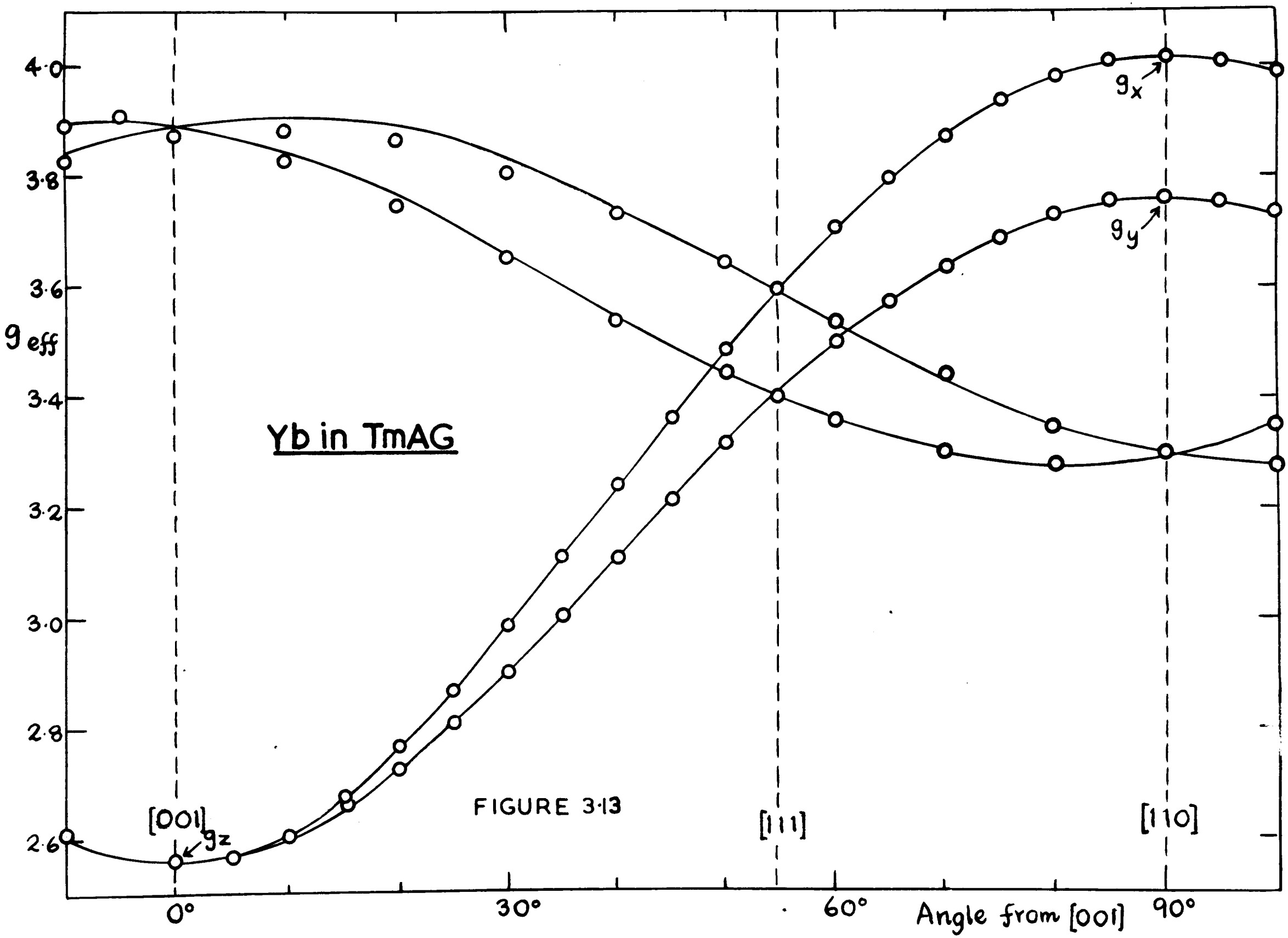

4·0
3·8
3·6
3·4
3·2
3·0
2·8
2·6
g_{eff}
Yb in TmAG
g_x
g_y
g_z
[001]
[111]
[110]
0°
30°
60°
90°
Angle from [001]

FIGURE 3·13

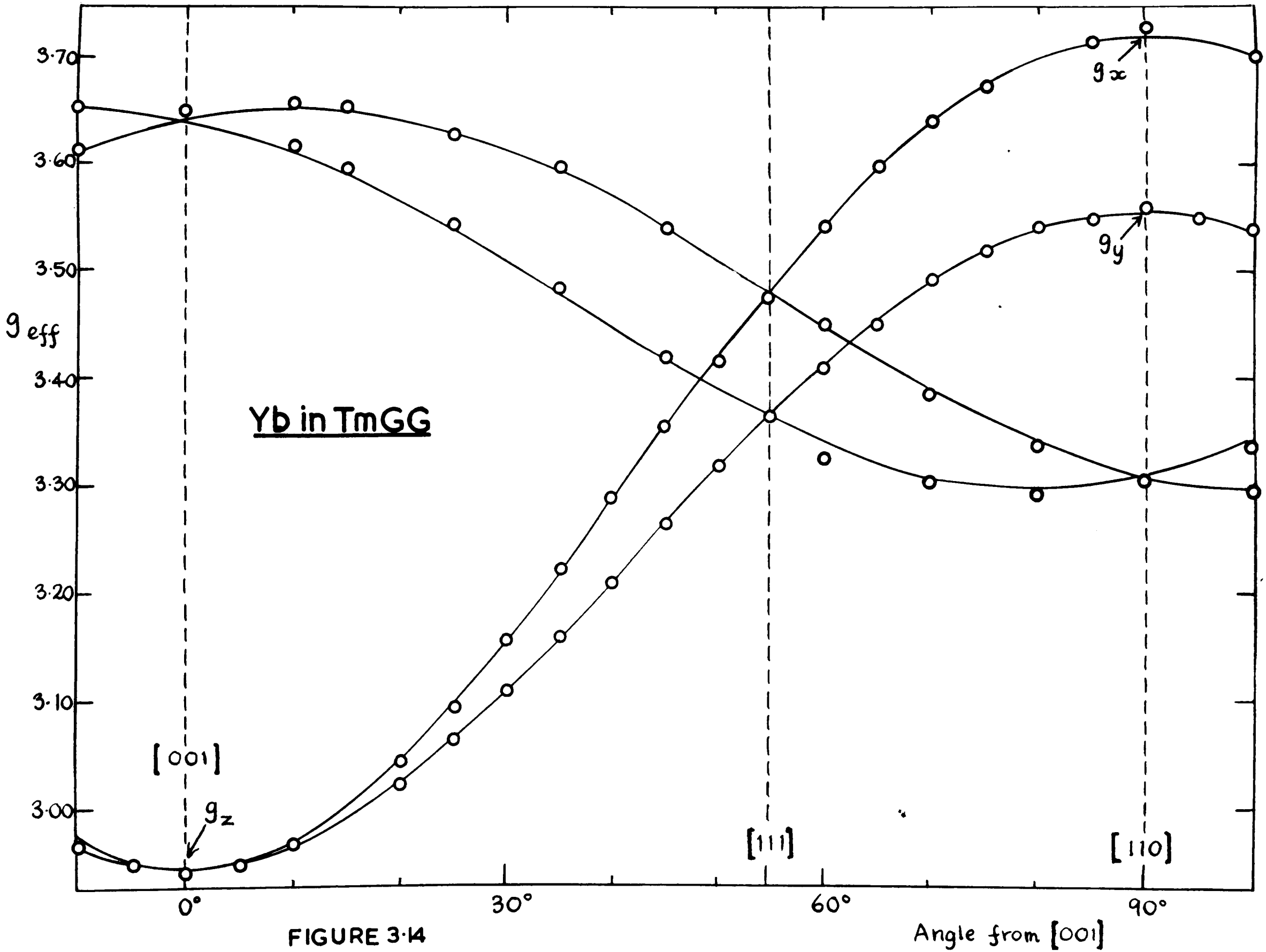

Yb in TmGG
g_{eff}
3·70
3·60
3·50
3·40
3·30
3·20
3·10
3·00
g_x
g_y
g_z
[001]
[111]
[110]
0°
30°
60°
90°
Angle from [001]

FIGURE 3·14

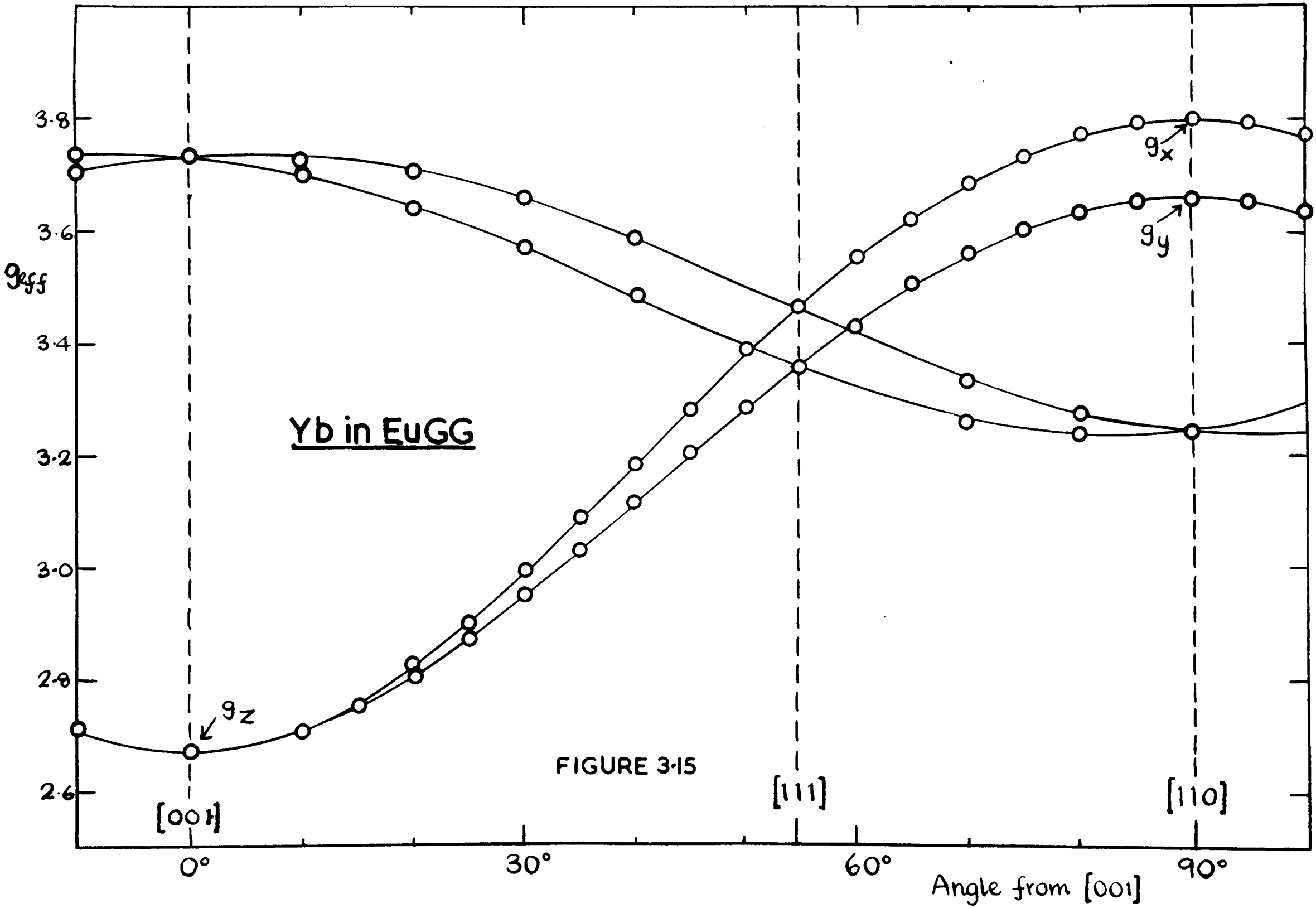

Yb in EuGG
g_{eff}
3·8
3·6
3·4
3·2
3·0
2·8
2·6
g_x
g_y
g_z
[001]
[111]
[110]
0°
30°
60°
90°
Angle from [001]

FIGURE 3·15

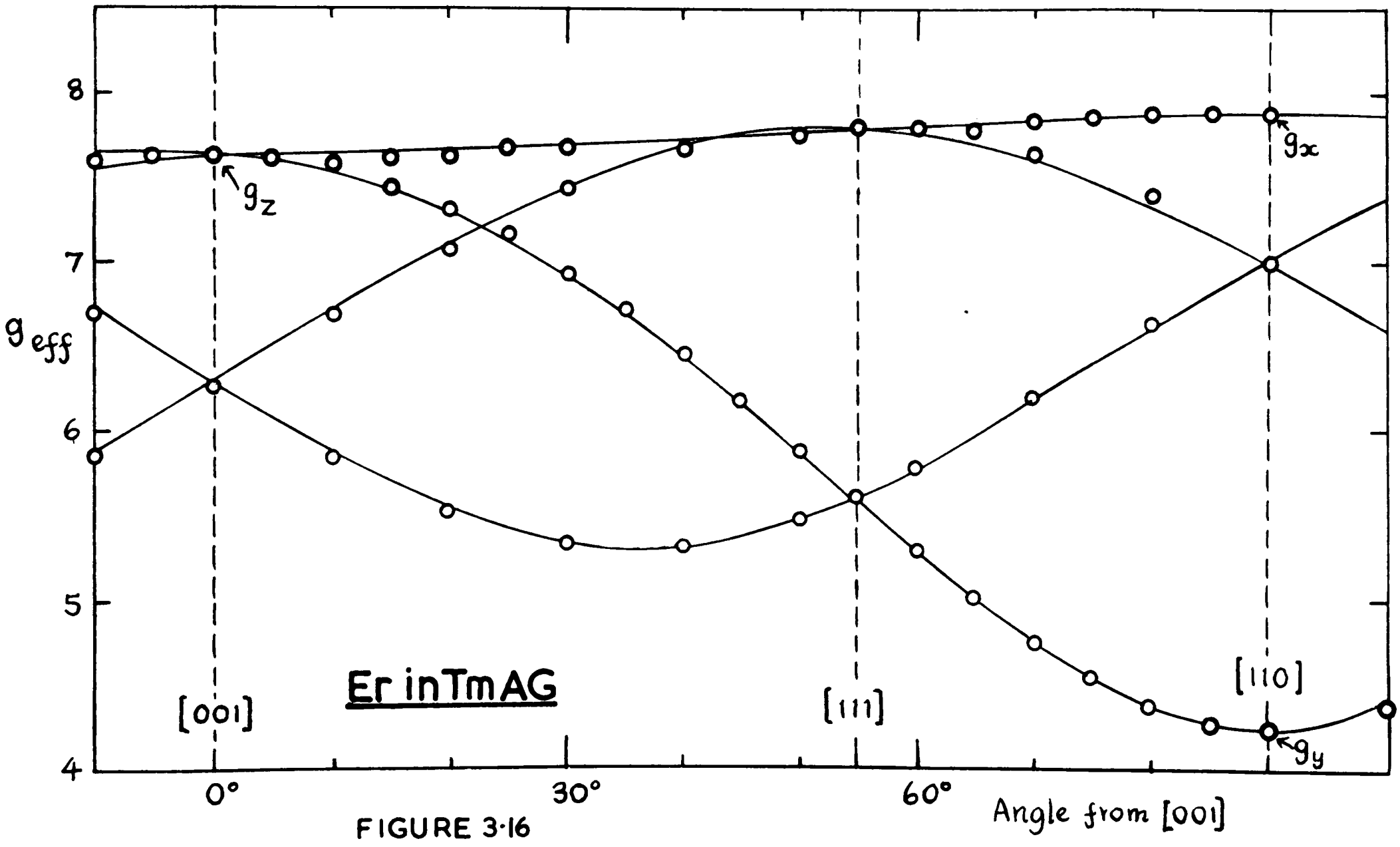


FIGURE 3·16

CHAPTER 4

General discussion of the ground state g tensors of rare earth ions in the diamagnetic garnet lattices, with particular reference to a cubic field approximation

4.1 Introduction

In this chapter, the results of the measurements described in Chapter 3, on rare earth ions in the diamagnetic garnet lattices, will be discussed in a general manner in §4.2, and in terms of a crystal field of near cubic symmetry in the remaining sections. In this section, the difficulties of using these results for the explanation of the concentrated magnetic garnets are outlined, and an introduction is given to the theoretical discussions of Chapters 5 to 8.

The original aim of the investigation was to enable predictions to be made of the g tensors, and possibly the ground state wavefunctions, of rare earth ions in the iron garnet lattices. However, it is immediately seen from Table 3.1 that the g values vary considerably with host lattice, and since the greatest variation occurs when X is changed, as was mentioned in §3.1, the values in YIG will probably be different from the values in any of the diamagnetic lattices. It therefore appears that no direct exact predictions for the properties of rare earth ions in the iron garnets can be made, and that some theoretical estimation must be attempted. One can proceed in two ways:-

(a) One could make some sort of semi-quantitative extrapolation

of the g values in the diamagnetic lattices using the known structure parameters.

(b) If one knew all the crystalline electric field (C.F.) parameters, $A_n^m \langle r^n \rangle$, for each of the diamagnetic lattices, it might be possible to relate them to the structure parameters in such a way that accurate parameters could be predicted for YIG, from which the rare earth ions' magnetic properties could be calculated.

In practice this second method involves a very great deal of work, both experimental and theoretical, and before any accurate predictions are possible, a complete knowledge and understanding of the magnetic properties of the ions in the diamagnetic lattices is necessary. This in itself presents a challenge to conventional crystal field theory, and is the main problem concerned in the next few chapters, which contain what can only be considered to be a start on the full problem. Method (b) is the only one which can be used for the cases of "non-Kramers" rare earth ions. Because of the low symmetry at the rare earth site there are nine parameters $V_n^m = A_n^m \langle r^n \rangle$, $(V_2^0, V_2^2, V_4^0, V_4^2, V_4^4, V_6^0, V_6^2, V_6^4, V_6^6)$, needed to describe the crystal field. (V_n^m is defined in §A2.3.3). In order to determine these experimentally, further data on each lattice from optical spectroscopy, susceptibility, relaxation, or specific heat measurements, must be used to supplement the three ground state g values. Unfortunately sufficient additional

data are not yet available, though optical work by Dieke and Crosswhite (private communication) has been in progress for some time.

The qualitative approach of method (a) is considered in §4.2, where it is seen that there are immediate difficulties in most cases. However it indicates possible g values for Yb^{3+} in YbIG, and the magnetic properties of this compound are considered in §5.3 and §5.3.1.

A consequence of the smaller dependence of the g values on the diluent R is that qualitative predictions of their values in the concentrated paramagnetic garnets should be possible. The susceptibility measurements on these compounds (Lesak 1960) are discussed briefly in §4.2.1, and the special case of DyAG is considered in §5.2.

In an attempt to obtain a more detailed description of the crystal field in the garnets, calculations of the parameters A_n^m have been made from a point charge model of the crystal lattice. These calculations are described in Chapters 6 and 7, and are used in Chapter 8 to reduce the number of experimental data needed to provide a possible set of crystal field parameters for Yb^{3+} in YGG.

It might be mentioned at this point that Ayant and Thomas (1960, 1962a, 1962b) have made attempts to explain the properties of rare earth ions in the diamagnetic and paramagnetic garnets. However, although they claim several "explanations", they make

some severe approximations and only consider the actual g values in the case of ytterbium. Their treatment of this case will be discussed in Chapter 8.

4.2 General observations on the ground state g values

The major conclusion regarding the experimental g values have been pointed out in §4.1. The general trends, and the difficulties in making a semi-quantitative extrapolation of these values to the case of the iron garnets, will now be discussed, with reference to the available structure parameters listed in Table 4.1.

It is seen from Table 3.1 that for both Nd^{3+} and Yt^{3+} there is an increase in anisotropy of the g values in following the sequence LOG, YOG, LAG, YAG. Comparison with the structure parameters listed in Table 4.1, shows that although there is no correlation with a_o, this sequence does follow the trend of the parameters x and y, whilst z is practically constant. It therefore appears that the distortions of the oxygen "cube", which depend on x, y, and z, are closely related to the g values. In the case of Yb^{3+} a graph of g value against x or y gives a smooth curve, as shown in Figures 4.1 and 4.2, (this is only true in the case of g_z for Nd^{3+}). Although it must be emphasised that these curves have no definite theoretical basis they do appear to represent adequately the empirical variation of the g values, at least for the small changes produced by varying the ion on the {c} site. These curves will be used in Chapter 5,

Table 4.1

Structure parameters for the various garnet lattices considered (Euler and Bruce 1962).

Lattice	a_o (Å)	x	y	z
LAG	11.906	-0.0297 (± 0.0005)	0.0536 (±0.0005)	0.1512 (±0.0006)
TmAG	11.957			
YAG	12.000	-0.0307 (± 0.0003)	0.0512 (±0.0003)	0.1504 (±0.0005)
LGG	12.188	-0.0249 (± 0.0005)	0.0566 (±0.0008)	0.1501 (±0.0008)
TmGG	12.225			
YGG	12.280	-0.0271 (± 0.0003)	0.0562 (±0.0004)	0.1494 (±0.0004)
EuGG	12.407			
LIG	12.278	-0.0260 (± 0.0006)	0.0586 (±0.0008)	0.1518 (±0.0007)
YIG	12.376	-0.0279 (± 0.0004)	0.0574 (±0.0005)	0.1510 (±0.0007)

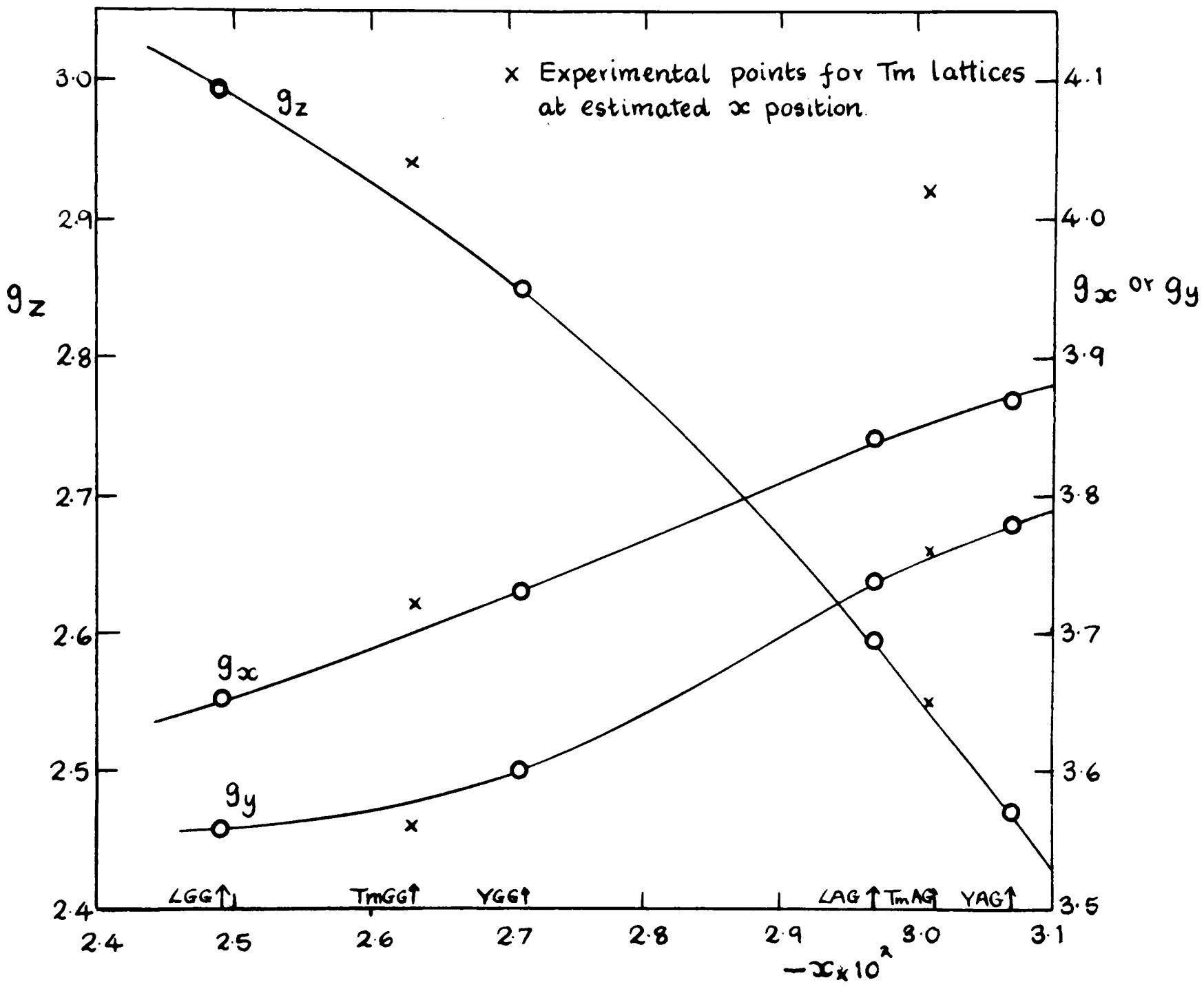
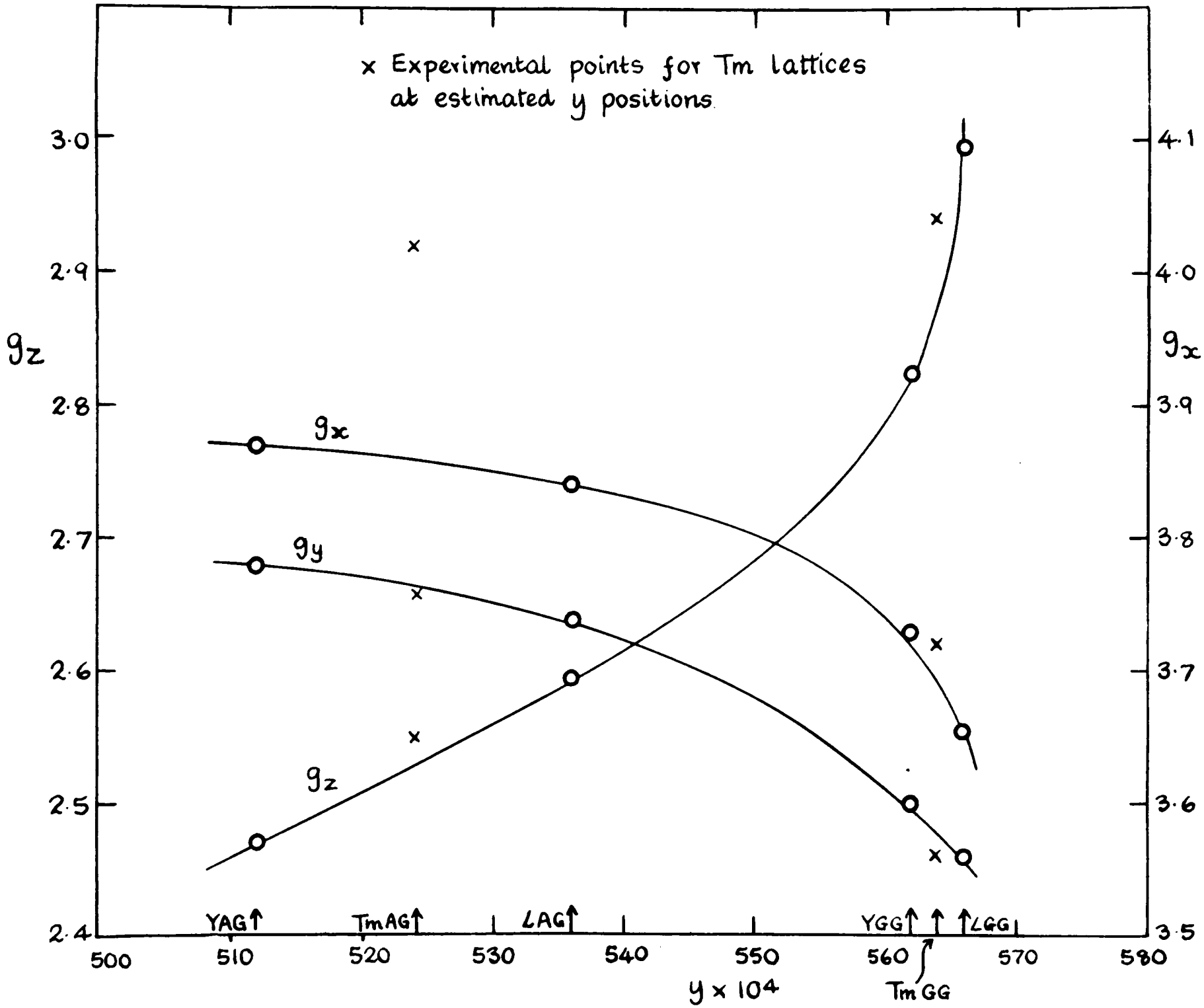


FIGURE 4·1

VARIATION OF g_i WITH STRUCTURE PARAMETER x.



VARIATION OF g_i WITH STRUCTURE PARAMETER y.

FIGURE 4·2

with some success, to interpolate the g values of Yb^{3+} in TmAG, and TmGG, expected on a purely crystalline interaction, with a view to deciding whether there is any observable deviation due to magnetic and exchange interactions in these lattices. Such effects would be expected to be very small for EuGG, but no values of the structure parameters are at present available for this lattice. If one attempts to extrapolate Figures 4.1 and 4.2 to the iron garnets one immediately finds considerable uncertainties, reflecting the fact that the distortion parameters x, and y, do not vary in the same way along the sequence Al→ Ga →Fe garnets. There is thus no obvious simple way of estimating with accuracy the magnetic properties of even Yb^{3+} (the most well behaved ion) in an iron garnet lattice, although the variations are small enough for the values corresponding to LGG (assuming the overall trend is maintained) to be used without very much error. This probably applies equally to Nd^{3+} although here the uncertainty may be more.

An interesting point emerges from the similarity of the trends of Nd^{3+} and Yb^{3+} in that these are ions of very different size, in fact the ionic radii of Nd > of Y > of Yb > of Lu. As both Nd^{3+} and Yb^{3+} show the same trends, it seems that the rare earth does not greatly distort its surroundings, so that the g values are mainly determined by the host lattice.

For the case of erbium there is a profound difference between the g tensors in the gallium and aluminium lattices.

Whereas in the former there is approximate axial symmetry about g_z, in the latter there is approximate axial symmetry about g_y. As only g_x and g_y are experimentally indistinguishable this is a genuine effect. This variation is maintained in the thulium lattices as well (Table 3.2), where the effects of the magnetic interactions are expected to be of only a few per cent. There is also quite a significant dependence of g value on the diluent in the {c} sites, and it is clearly impossible to make any simple extrapolation for YIG in this case.

Similarly in the case of dysprosium there are very profound differences between the results in the gallium and aluminium lattices, these again show approximately axial symmetry about two distinct axes, and there is also a strong dependence on the diluent in the {c} sites.

4.2.1. Comparison of the ground state g values and susceptibility measurements

Table 4.2 gives a comparison between the experimentally determined low temperature Curie constants, and values calculated from the results given in Table 3.1. The R.M.S. g values are also given. This comparison should provide a test of the validity of extrapolating the g values to the concentrated rare earth lattices (though the oxygen structure parameters x, y, z, have only been determined in a few cases). However, although the value for YbGG agrees well with the Yb in LGG results as expected, and that for NdGG is consistent with the resonance

Table 4.2

The Curie constant (C) found from susceptibility measurements (Leask 1960) are compared with those calculated from the principal g values in Table 3.1, ($C = 0.09383\ \overline{g_1^2}$). R.M.S. g values are also given.

Ion	Lattice	$g_{R.M.S.}$	$C_{calcd.}$	(Conc. Compnds.) $C_{expmt.}$
Nd^{3+}	LGG	2.496 (±0.006)	0.585 (±0.003)	0.667
	YGG	2.525 (±0.012)	0.598 (±0.006)	
	LAG	2.545 (±0.005)	0.608 (±0.003)	
	YAG	2.564 (±0.014)	0.617 (±0.007)	
Dy^{3+}	LGG	8.02 (±0.06)	6.03 (±0.10)	7.80
	YGG	7.86 (0.13)	5.80 (±0.20)	
	LAG	9.69 (±0.17)	8.81 (±0.33)	≈12.7
	YAG	10.5 (±0.2)	10.4 (±0.4)	
Er^{3+}	LGG	7.74 (±0.05)	5.62 (±0.08)	6.42
	YGG	7.15 (±0.03)	4.80 (0.04)	
	LAG	6.73 (±0.03)	4.26 (±0.03)	4.3
	YAG	6.53 (±0.07)	4.00 (±0.08)	
Yb^{3+}	LGG	3.414 (±0.010)	1.094 (±0.007)	1.116
	YGG	3.415 (±0.020)	1.095 (±0.013)	
	LAG	3.438 (±0.005)	1.109 (±0.003)	1.111
	YAG	3.433	1.106	

results in view of its larger lattice constant, the cases of Er^{3+} and Dy^{3+} show discrepancies. These latter Curie constants might be expected to lie close to the yttrium resonance results because of their similar lattice size. A possible reason for the disagreement may be an error in the analysis of the susceptibility, in terms of a Curie-Weiss law plus a temperature independent term, due to cross terms between the magnetic or exchange interactions and matrix elements to the next excited doublet. These would in effect alter C (Wolf, W. P., private communication). However such effects do not appear to be important in DyAG, whose ordering properties may be explained very well by the resonance results, as discussed in §5.2.

4.3 The energy levels of rare earth ions in a cubic crystal field.

It was mentioned in §3.2 that the nearest neighbour oxygen co-ordination about the rare earth {c} site is very approximately 8-fold cubic. As the initial step in a more detailed discussion of the resonance results it seems reasonable to consider, as a first approximation, the rare earth ion to be situated in a cubic field, and consider distortions as a perturbation on the cubic wavefunctions. The result of considering the cases of Nd^{3+} and particularly of Yb^{3+} in this way suggests the validity of such an approximation. However, there is evidence, in particular the results of the point

charge calculations described in Chapter 7, that the distortions are quite large.

In this section the general cubic crystal field Hamiltonian will be considered, using the conventional notation described in Appendix II, with particular reference to the work of Lea, Leask and Wolf (L.L.W.), (1962).

As is shown in Appendix II, if axes are correctly chosen, the general cubic crystal field Hamiltonian may be written as

$$\mathcal{H} = B_4^0 (O_4^0 + 5O_4^4) + B_6^0 (O_6^0 - 21O_6^4)$$

where $B_4^0 = A_4^0 \langle r^4 \rangle \beta_J$ and $B_6^0 = A_6^0 \langle r^6 \rangle \gamma_J$ (4.2)

The A_n^m depend on the crystal structure, and $\langle r^n \rangle$, β_J and γ_J on the rare earth ion considered. Lea, Leask and Wolf have rewritten Equation (4.2) as

$$\mathcal{H} = W \left[x \frac{(O_4^0 + 5O_4^4)}{F(4)} + (1 - |x|) \frac{(O_6^0 - 21O_6^4)}{F(6)} \right] \quad (4.3)$$

where W, and x, are defined from the equations

$$B_4^0 \; F(4) = Wx$$

$$B_6^0 \; F(6) = W(1 - |x|) \qquad -1 < x < +1 \qquad (4.4)$$

and F(4) and F(6) are tabulated constants for each rare earth ion. We therefore have that

$$\frac{x}{1 - |x|} = \frac{B_4^0 \, F(4)}{B_6^0 \, F(6)} \quad (4.5)$$

i.e. $x = 0$ when $B_4^0 = 0$, and $x = \pm 1$ when $B_6^0 = 0$.

Using a computer they have diagonalised $\mathcal{H}$ (Equation (4.3)) with W = 1, for values of x between -1 and +1, and tabulated the eigenfunctions and eigenvalues for different values of J. Figures 4.3 - 4.6 show the eigenvalues of four ions as a function of x. They have been reproduced from L.L.W., but only the relevant quadrant (appropriate to an 8-fold cubic field) is given. The eigenvalues are therefore found by multiplying by $|W|$. In order to determine the parameter x, values of B_4^0 and B_6^0 are necessary, and these may be estimated from point charge calculations, or from energy level positions known from optical work.

Each of the four ions investigated will now be discussed in terms of a perturbed cubic field.

4.4 Erbium in the cubic approximation

The completely different symmetries of the principal g values observed in the gallium and aluminium garnets could possibly arise from covalency effects (the aluminium garnets are likely to be more covalent than the gallium garnets), but we would then expect these to affect all the rare earth ions. A more probable explanation is that slight changes in the D_2 symmetry crystal field bring a different state lowest in the two cases, each state giving rise to g values with different symmetry. The appropriate L.L.W. diagram, shown in Figure 4.3, indicates that in the cubic approximation this is in fact possible, and there is a grouping and crossing of states for

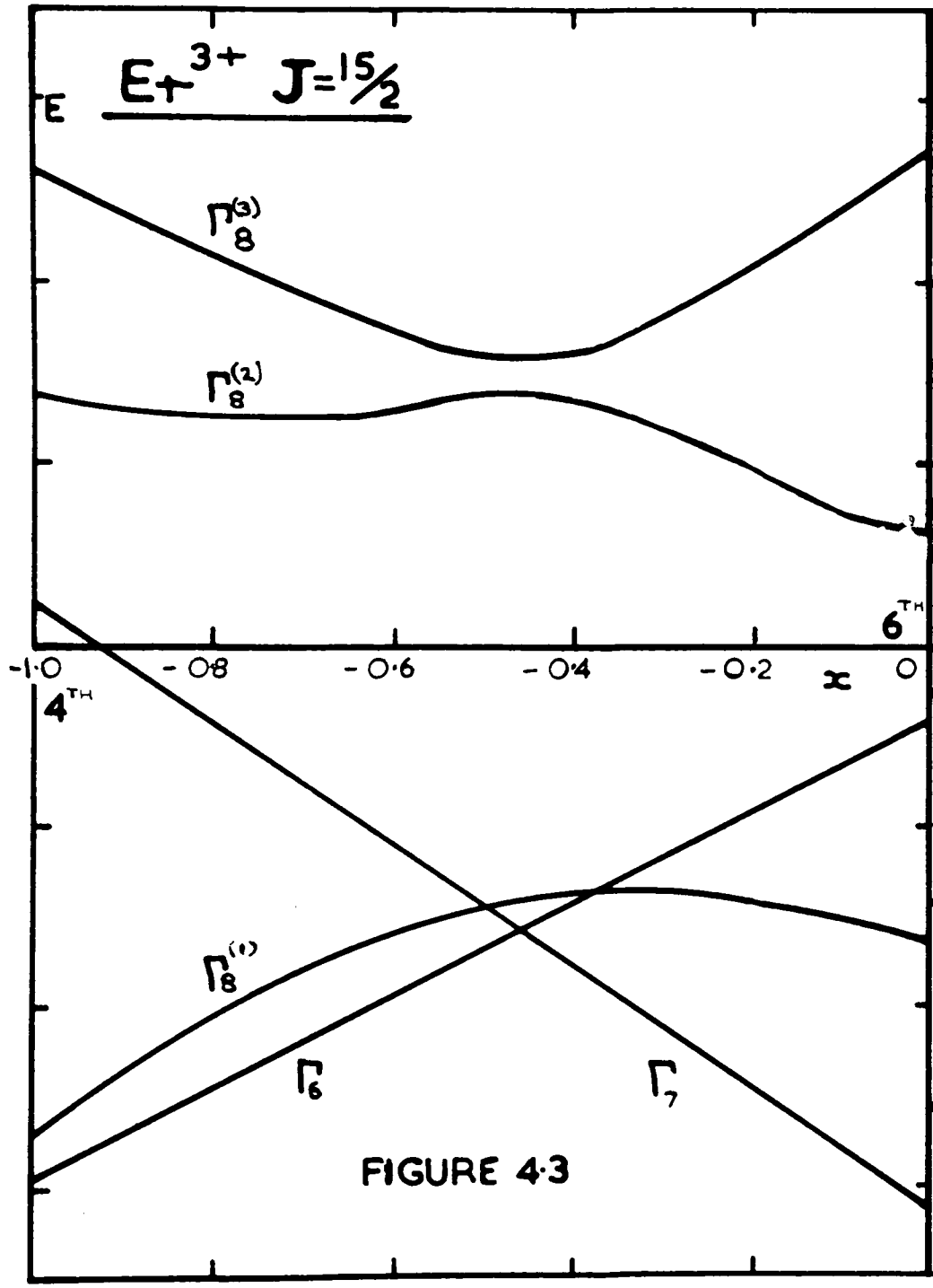


FIGURE 4·3

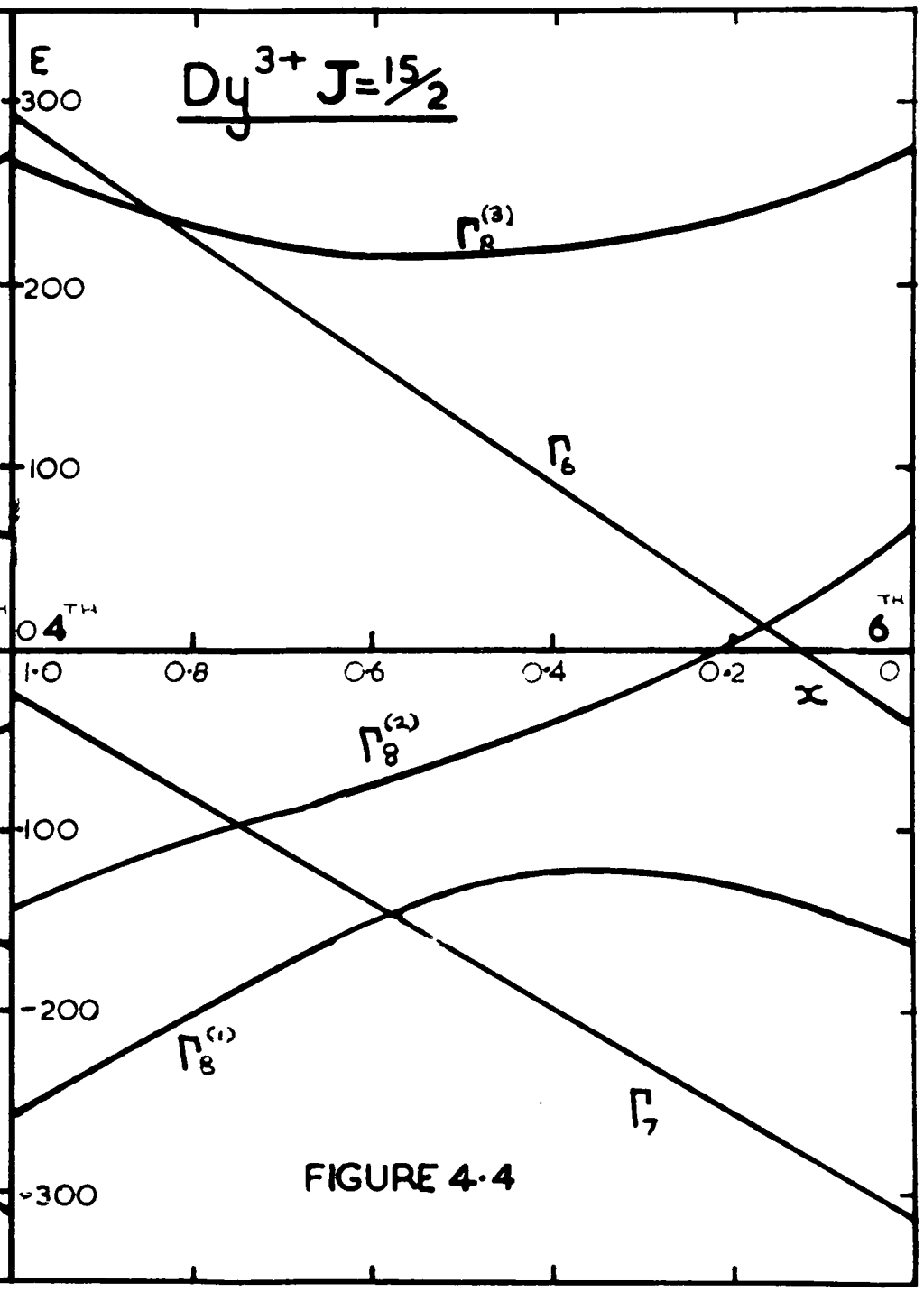


FIGURE 4·4

ENERGY LEVELS IN AN EIGHT-FOLD CUBIC CRYSTAL FIELD

$x \approx -0.46$. The proximity of the $\Gamma_8^{(1)}$ quartet could cause large admixtures of this state, as well as of the Γ_6 and Γ_7, giving very anisotropic g values. This is clearly a case requiring an analysis in terms of the crystal field parameters for a detailed explanation. The E.M.R. experimental g values (Table 4.2) are of the same approximate values as those expected from the Γ_6 ($g = 6.00$) and Γ_7 ($g = 6.80$), states. Dieke (1962) has found from optical work that there are four close low lying doublets in the erbium garnets, separated by a large gap from higher states, which would correspond well with the value of $x \approx -0.46$. This value gives, from Equation (4.5) a value of

$$\frac{V_4^0}{V_6^0} = \frac{A_4^0 \langle r^4 \rangle}{A_6^0 \langle r^6 \rangle} = -9.15 \qquad \text{for erbium.}$$

4.5 Dysprosium in the cubic approximation

As in the case of erbium, it is extremely difficult to infer any precise data from the g values alone. The different symmetry of the g values in the cases of Al^{3+} and Ga^{3+} garnets suggests that there are again different states lowest in the two cases. Figure 4.4 shows the L.L.W. diagram for Dy^{3+}, and it is seen that there is a crossing at $x = +0.56$, the lowest state being either a Γ_6 quartet, or Γ_7 doublet with cubic g value of 7.55. The E.M.R. g value for Dy in the gallium garnets (Table 4.2) is near to 7.55, suggesting that in the cubic approximation $x < 0.56$ in this case.

The crystal field seen by one rare earth ion in each host

lattice should be very much the same, so that having once established the ratio $\frac{A_4^0}{A_6^0}$ in one lattice, it should be possible to determine x for each ion using the known values of β_J and γ_J, and estimated values of $\langle r^n \rangle$ for each ion. For example,

$$\frac{x_{Dy}}{1 - |x_{Dy}|} = \left\{ \frac{F(4)\ B_4^0}{F(6)\ B_6^0} \right\}_{Dy}$$

$$= \frac{x_{Er}}{1 - |x_{Er}|} \times \frac{F(4)_{Dy}\ B_4^0(Dy)}{F(4)_{Er}\ B_4^0(Er)} \times \frac{F(6)_{Er}\ B_6^0(Er)}{F(6)_{Dy}\ B_6^0(Dy)} \quad \ldots (4.6)$$

and $$\frac{B_4^0(Dy)\ B_6^0(Er)}{B_4^0(Er)\ B_6^0(Dy)} = \frac{\beta_{Dy}\,\gamma_{Er}}{\beta_{Er}\,\gamma_{Dy}} \times \frac{\langle r^4 \rangle_{Dy}\ \langle r^6 \rangle_{Er}}{\langle r^4 \rangle_{Er}\ \langle r^6 \rangle_{Dy}} \qquad (4.7)$$

Values of $\langle r^n \rangle$ calculated from Hartree-Fock wave functions, have been given by Freeman and Watson (1962), and the relevant mean radii are listed in Table 4.3.

Table 4.3

Values of $\langle r^n \rangle$, in A.U., calculated from Hartree-Fock wavefunctions (From Freeman and Watson, 1962).

Ion	$\langle r^2 \rangle$	$\langle r^4 \rangle$	$\langle r^6 \rangle$
Ce^{3+}	1.200	3.455	21.226
Nd^{3+}	1.001	2.401	12.396
Gd^{3+}	0.785	1.515	6.281
Dy^{3+}	0.726	1.322	5.102
Er^{3+}	0.666	1.126	3.978
Yb^{3+}	0.613	0.960	3.104

Using Equation (4.6), we can find likely values of x_{Dy} from x_{Er} in the cubic approximation:-

$x_{Er} = -0.46$ gives $x_{Dy} = 0.67$

$x_{Er} = -0.5$ gives $x_{Dy} = 0.71$

$x_{Er} = -0.4$ gives $x_{Dy} = 0.61$

These values for x_{Dy} lie fairly close to the crossing, suggesting that the above explanation for the different symmetries is not incompatible with the cubic approximation.

Although the general situation is again very complex, because of the very unusual experimental g values for Dy^{3+} in YAG, it is possible to deduce the nature of the ground wave-function in this case. If we define the z axis of quantisation as lying along the crystallographic [001] direction, then the most general state of a $J = \frac{15}{2}$ manifold, in a crystal field of D_2 symmetry, may be written as

$$|+\rangle = a\left|\tfrac{15}{2}\right\rangle + b\left|\tfrac{11}{2}\right\rangle + c\left|\tfrac{7}{2}\right\rangle + d\left|\tfrac{3}{2}\right\rangle + e\left|-\tfrac{1}{2}\right\rangle + f\left|-\tfrac{5}{2}\right\rangle + g\left|-\tfrac{9}{2}\right\rangle + h\left|-\tfrac{13}{2}\right\rangle$$

$$|-\rangle = a\left|-\tfrac{15}{2}\right\rangle + b\left|-\tfrac{11}{2}\right\rangle + c\left|-\tfrac{7}{2}\right\rangle + d\left|-\tfrac{3}{2}\right\rangle + e\left|\tfrac{1}{2}\right\rangle + f\left|\tfrac{5}{2}\right\rangle + g\left|\tfrac{9}{2}\right\rangle + h\left|\tfrac{13}{2}\right\rangle$$

where the states are expressed in terms of $|J_z\rangle$. (4.8)

The values of g_z is given by Equation (1.5) with $g_J\underline{J} = \underline{L} + 2\underline{S}$ i.e. $|g_z| = 2g_J\,|\langle +|J_z|+\rangle|$ where $g_J = \frac{4}{3}$ ...(4.19)

Its maximum value occurs when a = 1, and all other coefficients are zero, and is $|g_z| = 20$. The next largest value of $|g_z|$

when there is only one non-zero coefficient, is 17.5, this occurs where h = 1 and all the other coefficients are zero.

As experimentally $g_z = 18.2 \pm 0.4$, it is extremely likely that a ≈ 1 is the correct wave function, and it is shown below that the state must be nearly pure $|\frac{15}{2}\rangle$.

Putting $g_z = 18.2$ in Equation (4.9), we find

$$18.2 = 2 \times \tfrac{4}{3} \times \left[\tfrac{15}{2}a^2 + \tfrac{11}{2}b^2 + \tfrac{7}{2}c^2 + \tfrac{3}{2}d^2 - \tfrac{1}{2}e^2 - \tfrac{5}{2}f^2 - \tfrac{3}{2}g^2 - \tfrac{13}{2}h^2\right] \quad \ldots\ (4.10)$$

where $a^2 + b^2 + c^2 + \ldots + h^2 = 1$, and using this to substitute for a^2

$$b^2 + 2c^2 + 3d^2 + 4e^2 + 5f^2 + 6g^2 + 7h^2 = \frac{3 \times 13.8}{16} = 0.3375 \quad (4.11)$$

It is clear that the smallest value of a would arise when $b \neq 0$, but all other coefficients = 0. This would lead to a wave function

$$|+\rangle = 0.814\,|\tfrac{15}{2}\rangle + 0.581\,|\tfrac{11}{2}\rangle$$

which gives $g_z = 18.2$, but $g_x = g_y = 0$, whereas experimentally they are finite. Using the relations of Equation (1.3), $|g_x|$, and $|g_y|$ = Mod $\Big\{2g_J\Big[\pm ah\sqrt{15} \pm bg\sqrt{39} \pm cf\sqrt{55} \pm de\,3\sqrt{7} + bh\,2\sqrt{7} + gc\,4\sqrt{3} + df\,2\sqrt{15} + 4e^2\Big]\Big\}$ .... (4.12)

where g_x is given by the upper, and g_y by the lower, sign. Clearly it is impossible to determine all the coefficients, but we may note that if only a and h are non zero, the wavefunction is $|+\rangle = 0.976\,|\tfrac{15}{2}\rangle + 0.220\,|-\tfrac{13}{2}\rangle$ giving $g_z = 18.2$, but

$|g_x| = |g_y| = 2.22$. It therefore appears that several of the coefficients are non zero, in which case the ground state of Dy^{3+} in YAG will be mainly $|+\rangle = |\frac{15}{2}\rangle$.

4.6 Neodymium in the cubic approximation

In a purely cubic field of 8-fold co-ordination the lowest state of neodymium is a Γ_8 quartet. This is shown in the L.L.W. diagram, Figure 4.5. The experimental g values (Table 3.1) show a somewhat larger difference between aluminium and gallium garnets than between lutetium and yttrium, but all have the same symmetry. If we consider only the $J = \frac{9}{2}$ manifold and treat the distortions as a perturbation on a pure cubic field we may show that it is possible to account for the observed g values, though not exactly, and derive a possible wavefunction for the ground doublet.

In order to relate theory and experiment we consider an ion with principal g value axes as shown in Figure 4.7a. Figure 4.7b shows, with respect to an origin at this rare earth ion's site, axes (x",y",z") parallel to the surrounding local cube's fourfold axes. The axes (x',y',z'), which will be used for subsequent calculations in this chapter, are (x",y",z") rotated through 45^0 about z". (X,Y,Z) are the cubic unit cell's $\langle 001 \rangle$ axes. L.L.W. give the wavefunctions of the $\Gamma_8^{(2)}$ states, for different values of the parameter x, with respect to the axes (x",y",z"). These states are (in terms of $|J_{z"}\rangle$)

ENERGY LEVELS IN AN EIGHTFOLD CUBIC CRYSTAL FIELD

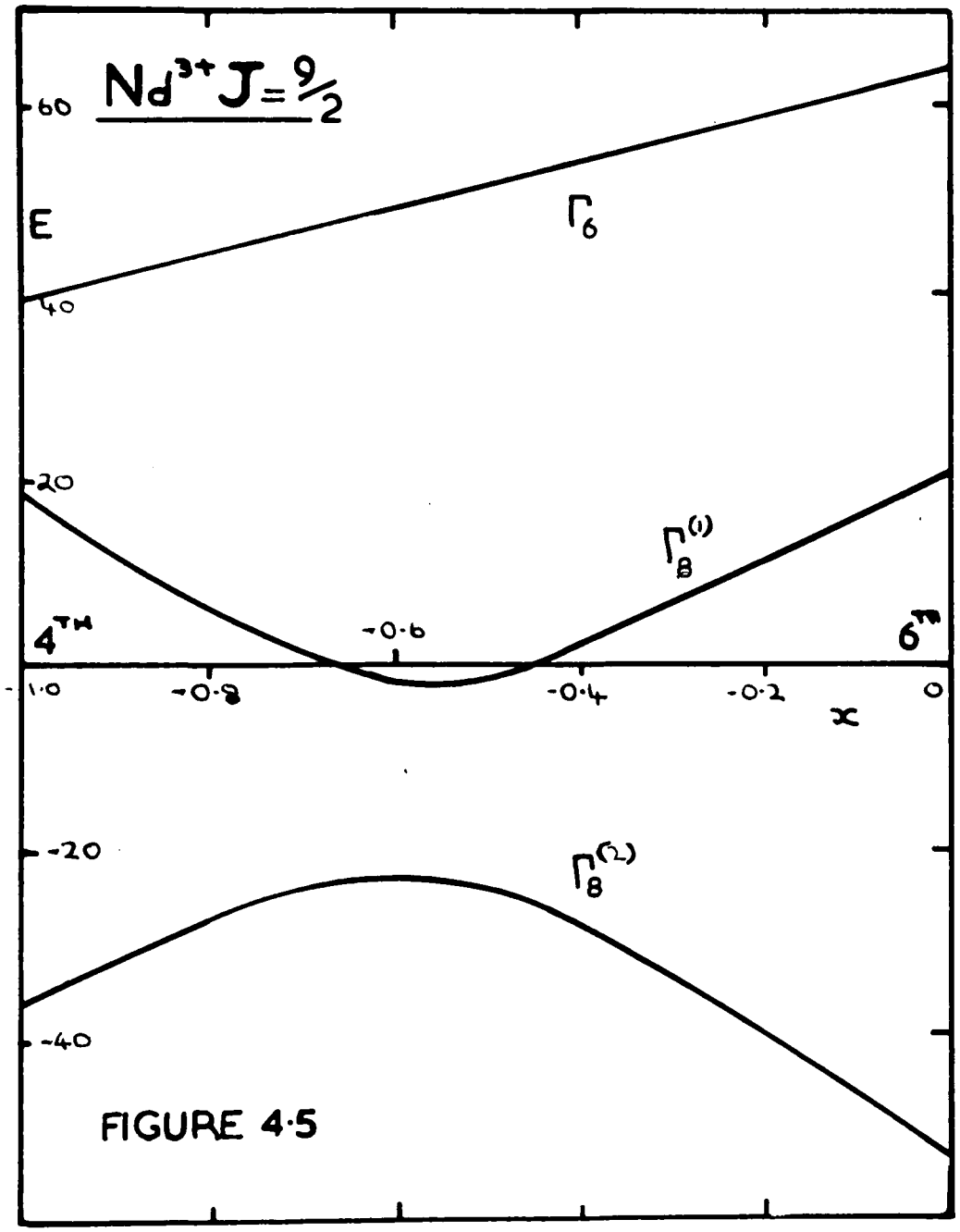


FIGURE 4·5

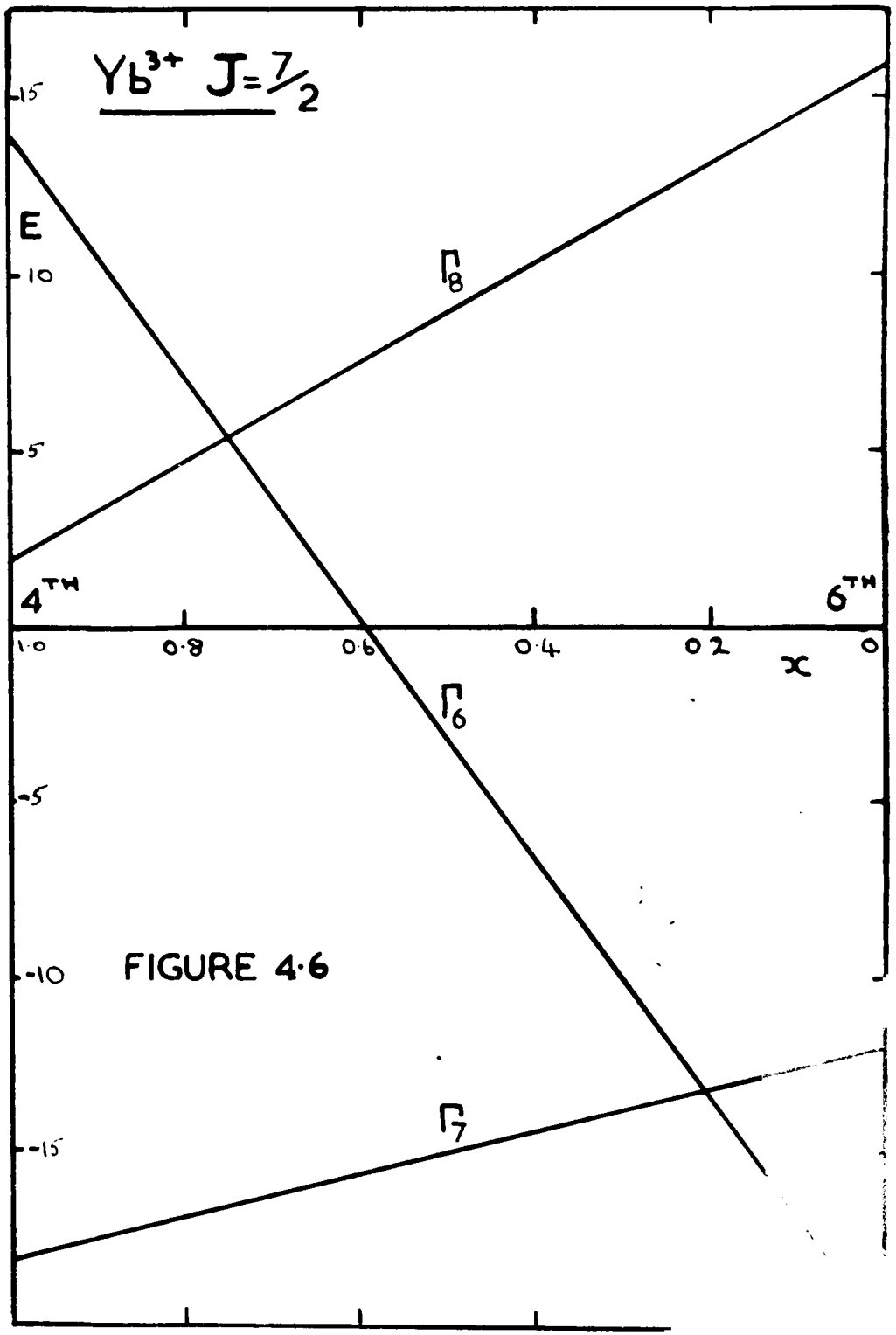


FIGURE 4·6

LOCAL AXES AT {C} SITE

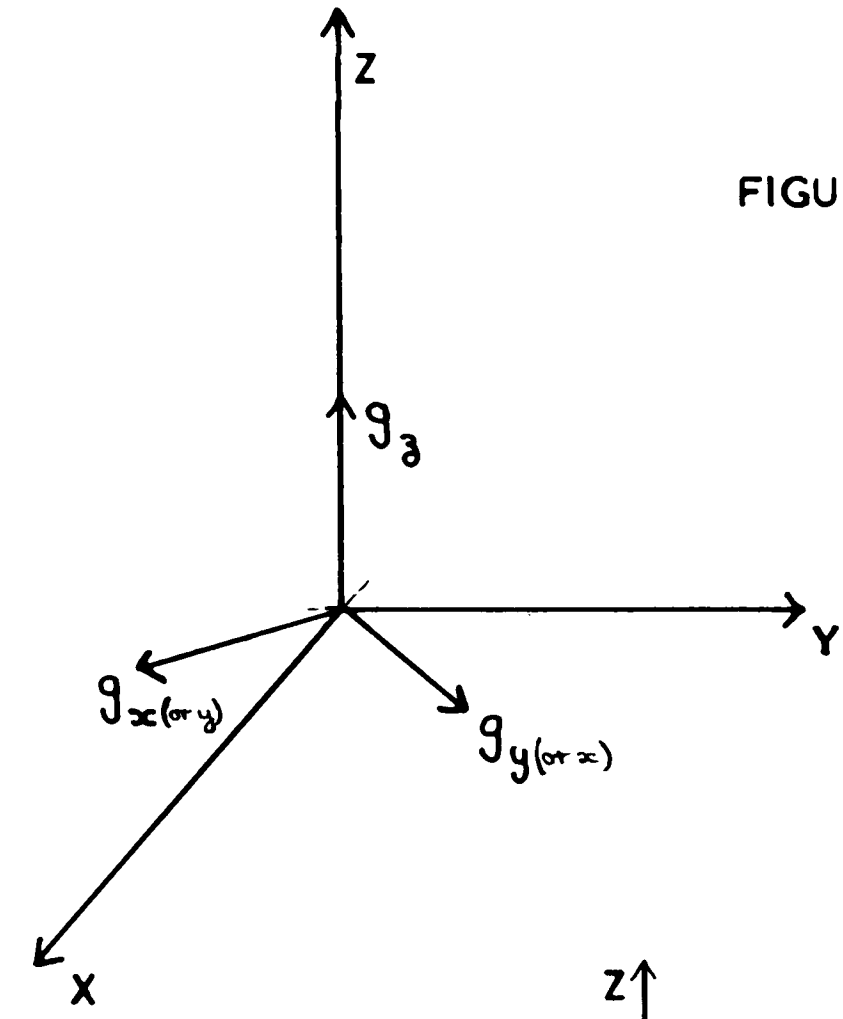


FIGURE 4·7a

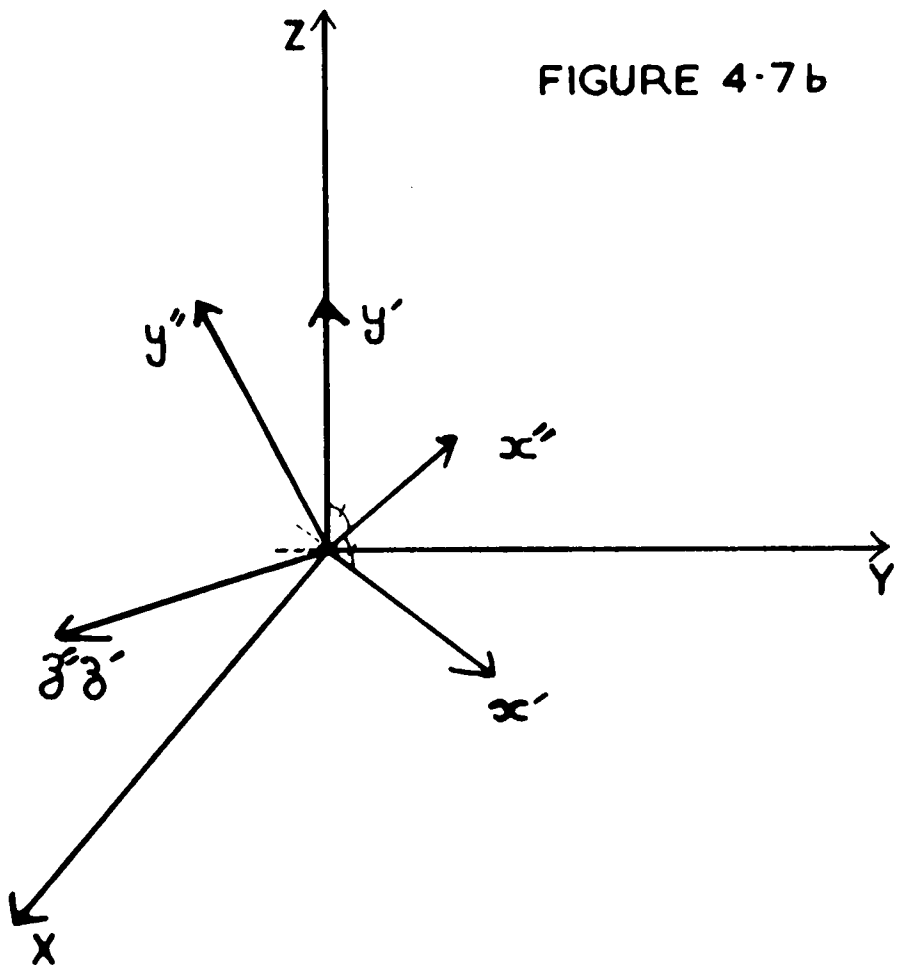


FIGURE 4·7b

$$|\alpha^+\rangle = a_1 |\tfrac{9}{2}\rangle + a_2 |\tfrac{1}{2}\rangle + a_3 |-\tfrac{7}{2}\rangle$$
$$|\alpha^-\rangle = -a_1 |-\tfrac{9}{2}\rangle - a_2 |-\tfrac{1}{2}\rangle - a_3 |\tfrac{7}{2}\rangle$$
$$|\beta^+\rangle = b_1 |\tfrac{5}{2}\rangle + b_2 |-\tfrac{3}{2}\rangle$$
$$|\beta^-\rangle = -b_1 |-\tfrac{5}{2}\rangle - b_2 |\tfrac{3}{2}\rangle \qquad (4.13)$$

Referred to axes (x',y',z'), they become (apart from a phase factor of modulus unity),

$$|\alpha^+\rangle = a_1 |\tfrac{9}{2}\rangle - a_2 |\tfrac{1}{2}\rangle + a_3 |-\tfrac{7}{2}\rangle$$
$$|\beta^+\rangle = b_1 |\tfrac{5}{2}\rangle - b_2 |-\tfrac{3}{2}\rangle \qquad (4.14)$$

Now the most general distortion of D_2 symmetry will split, and admix these two wavefunctions. If we ignore other admixtures from the $J = \frac{9}{2}$ manifold, and also from the $J = \frac{11}{2}$ manifold (whose Γ_8 state will be admixed even by a cubic field), we can write the ground doublet as

$$|+\rangle = c\,|\alpha^+\rangle + d\,|\beta^+\rangle$$
$$|-\rangle = \text{Kramer's conjugate.} \qquad \text{where } c^2 + d^2 = 1 \qquad (4.15)$$

From these we find,

$$g_z' = g_J\left[(5b_1^2 - 3b_2^2) + c^2\left\{(9a_1^2 + a_2^2 - 7a_3^2) - (5b_1^2 - 3b_2^2)\right\}\right]$$
$$g_x' = -g_J\left[cd(8b_1a_3 + 4\sqrt{6}\,a_2b_2) + c^2(6a_1a_3 + 5a_2^2) - (1-c^2)2\sqrt{21}\,b_1b_2\right]$$
$$g_y' = +g_J\left[cd(8b_1a_3 + 4\sqrt{6}\,a_2b_2) - c^2(6a_1a_3 + 5a_2^2) + (1-c^2)2\sqrt{21}\,b_1b_2\right]$$
$$\text{where } d = \pm\sqrt{1-c^2}, \quad g_J = 8/11 \qquad (4.16)$$

A short computer programme was written to calculate g_x', g_y' and g_z' from Equations (4.16), using as input data values

of a_1, a_2, a_3, b_1 and b_2, for each of x = 0, -0.20, -0.25, -0.3, ... -0.75, -0.80, -1.0 (Leask, private communication). For each value of x, the g values were calculated for c = 0 to c = 0.9 in steps of 0.1, and for c = 0.9 to c = 1.0 in steps of 0.01. The programme was checked by hand calculations for a few cases (See also Appendix IVB).

In comparing the calculated and experimental g values one is immediately faced with a number of ambiguities. In each case the moduli of the experimental and theoretical g values were compared to avoid ambiguities in sign (see Appendix I). There are two further ambiguities,

(a) between g_x, and g_y, because of the unknown sign of d

(b) taking g_x and g_y to be defined as in Table 3.1, either g_x or g_y can equal g_x, or g_z, as defined in Figure 4.7b. We can therefore only say that either g_x, or g_y, corresponds to g_z, and the other two theoretical values correspond to g_x or g_y. However this is sufficient to indicate that the parameters x and c lie within one of three specific zones. Curves were plotted to compare the experimental and calculated g values, and these indicated that there was approximate agreement in the three regions,

(i) when $x \approx -0.8$ to -1.0 (pure fourth order), $c \sim 0.2$ to 0.3.

(ii) when $x \approx -0.2$ to 0 (pure sixth order), $c \sim 0.3$

(iii) when $x \approx -0.65$ to -0.70, $c \sim 0.55$.

The most likely of these three values of x can be estimated on

the cubic model from an equation similar to (4.6), and taking $x_{Er} = -0.46$, we find $x_{Nd} = -0.53$, which is closest to (111). Working the other way if $x_{Nd} = -0.65$, $x_{Er} = -0.59$, which is slightly high but still in the region of the crossing; whereas if $x_{Nd} = -0.2$, or -0.4, x_{Er} becomes -0.18 or -0.75 respectively, values which are far from the expected crossing. Figure 4.8 shows the g values in region 3, and we must identify

$$g_x \text{ with } g_y$$
$$g_y \text{ with } g_z$$
$$g_z \text{ with } g_x \qquad (4.17)$$

We may therefore conclude that, in general, the principal g values of Nd^{3+} in garnet can be approximately accounted for by considering the splitting and admixture, by distortions of D_2 symmetry of the lowest Γ_8 quartet in a cubic field of $x \approx -0.65$ (that is $\frac{v_4^0}{v_6^0} \approx -10.2$). The admixture coefficient being $e \approx 0.55$, and the values of the wavefunction constants being given by,

$$a_1 = 0.3670 \qquad b_1 = 0.9953$$
$$a_2 = -0.5033 \qquad b_2 = -0.0968$$
$$a_3 = 0.7823$$

The agreement with experiment is reasonable within the severe approximations made, and a more detailed fit would require several more parameters to describe the admixture of other $J = \frac{9}{2}$ states, as well as the $J = \frac{11}{2}$ states which lie only about 1,800 cm^{-1} above (Elliott and Stevens, 1953a).

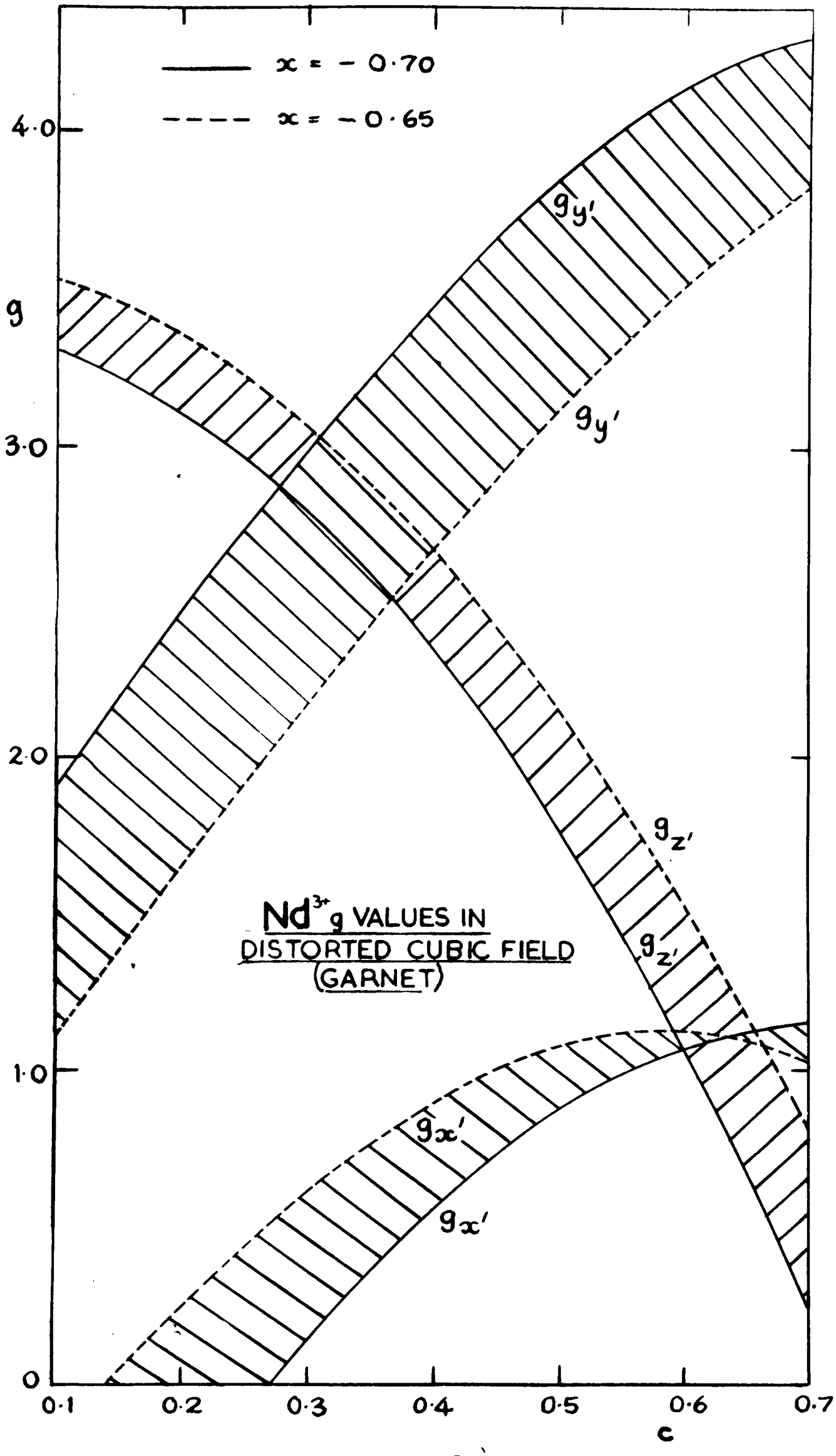

x = − 0·70
x = − 0·65
4·0
3·0
2·0
1·0
0
g
0·1
0·2
0·3
0·4
0·5
0·6
0·7
c
$g_{y'}$
$g_{y'}$
$g_{z'}$
$g_{z'}$
$g_{x'}$
$g_{x'}$
Nd^{3+} g VALUES IN
DISTORTED CUBIC FIELD
(GARNET)

FIGURE 4·8

4.7 Ytterbium in the cubic approximation

In contrast to the three cases just considered, the observed g values of Yb^{3+} can be accounted for quite accurately on the perturbed cubic model.

There are several simplifying features to a theoretical treatment of ytterbium which do not arise in most other rare earth ions. Within the lowest configuration of the free ion $(4f)^{13}$, which can be considered as a hole in an otherwise filled shell, there is only one term, ^2F, which gives rise to the two levels $^2F_{7/2}$ and $^2F_{5/2}$. For both of these L, S and J are rigorously good quantum numbers and there is no problem of intermediate coupling. The splitting between the two J states is large, about 10,000 cm^{-1}, & the upper ($J = \frac{5}{2}$) state can be neglected to a reasonable first approximation. For these reasons ytterbium has been one of the more extensively studied ions in the garnets.

A further simplifying feature arises from the fact that in the garnets the ground doublet of ytterbium appears to lie well below the next levels. This spacing is estimated as 570 cm^{-1} by Ball et al. (1960), from susceptibility measurements, and as 550 cm^{-1} by Pappalardo and Wood (1960) from optical work. More recently Wood (1962) (private communication) has found evidence of other levels lying lower than 550 cm^{-1}, but Tinkham et al. (1962) have attributed at least one of these to vibrational levels of the lattice. Dicke and Crosswhite (private communication) have repeated and extended, Pappalardo and Woods'

optical work, but no definite identification of the level at 550 cm^{-1} has been made, though it is probably from the split Γ_8.

The L.L.$^{\alpha}$. diagram for ytterbium in an 8-fold cubic field is shown in Figure 4.6, where it is seen that for $x > 0.2$ the lowest state is a Γ_7 doublet. Figure 4.9, after Pappalardo and Wood, shows the probable level structure in the garnets. The wavefunctions and energy levels of Yb^{3+} in a cubic field, as given by Pappalardo and Wood and checked by hand calculations, are given in Table 4.4. (As each representation occurs only once, the fourth and sixth order terms can be treated separately, and the cubic field matrix breaks up into simple 2 x 2 matrices). The two sets of signs given correspond to axes (x",y",z"), and (x',y',z') of Figure 4.7b. The energy levels are expressed in terms of Pappalardo and Woods' P, R, and P', where

$$P = 60\, A_4^0 \langle r^4 \rangle \beta_{J=7/2} = 60\, B_4^0 \ (J = 7/2)$$

$$R = 210\, A_6^0 \langle r^6 \rangle \gamma_{J=7/2} = 210\, B_6^0 \ (J = 7/2)$$

$$P' = 60\, A_4^0 \langle r^4 \rangle \beta_{J=5/2} = 60\, B_4^0 \ (J = 5/2) \qquad \ldots.(4.18)$$

The Γ_7 doublet has an isotropic g value of $g = 3g_J = 3.429$ Although the experimental g values are anisotropic (Table 3.1) the anisotropy is not great, and taking their R.M.S. average we find values for all lattices very close to 3.429 (Table 4.1). This strongly suggests that the Γ_7 state is appropriate to the garnets. With respect to the axes (x',y',z') (Figure 4.7), the most general distortion of D_2 symmetry will admix the four

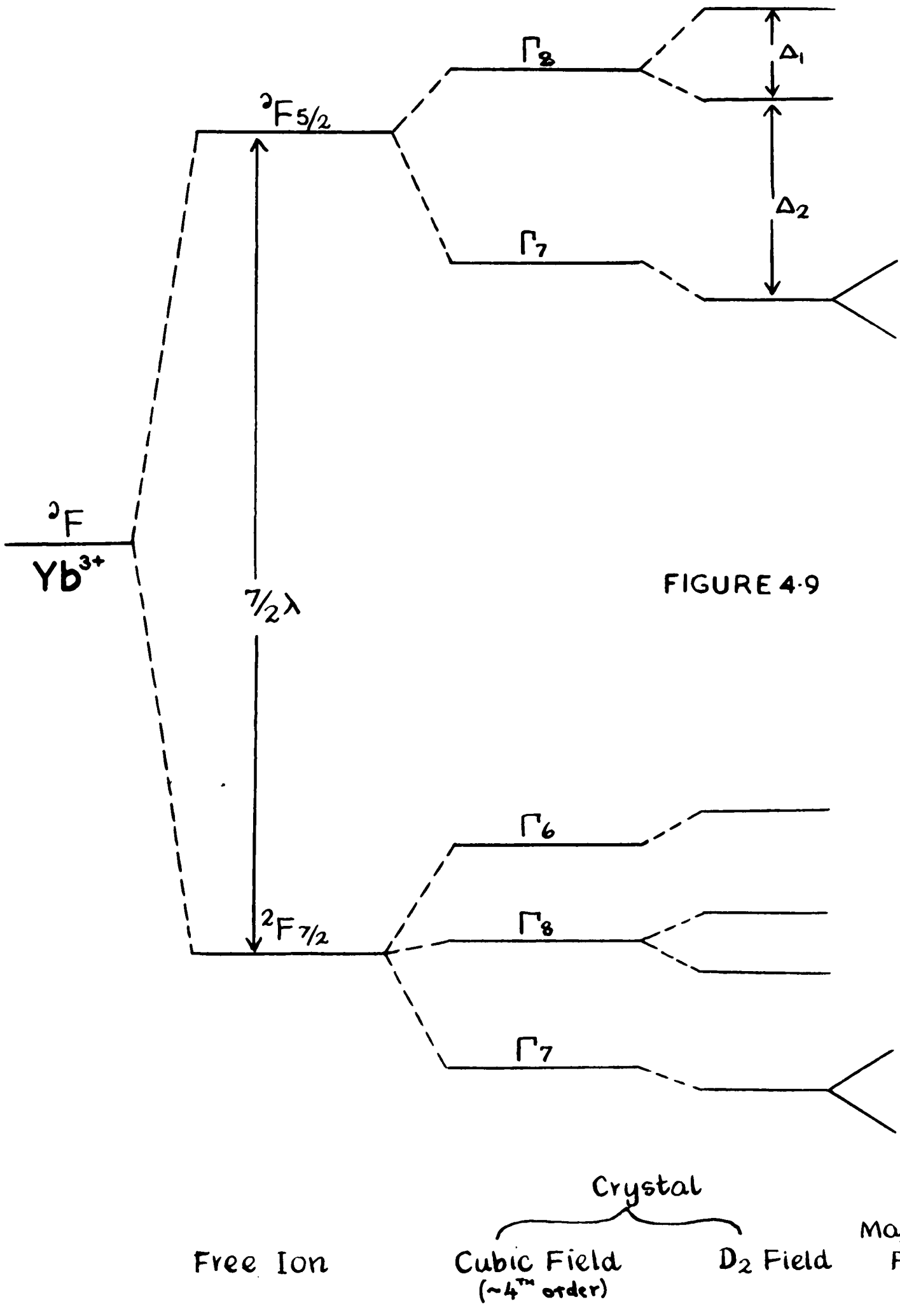

$^2F_{5/2}$
Γ_8
Γ_7
Δ_1
Δ_2
^2F
Yb^{3+}
$7/2\lambda$
$^2F_{7/2}$
Γ_6
Γ_8
Γ_7
Crystal
Free Ion
Cubic Field
(~4th order)
D_2 Field
Magnetic Field

FIGURE 4·9

Table 4.4

Energy levels, and wavefunctions of Yb^{3+} in an "eightfold" cubic field. The wavefunctions are expressed in terms of $|J, J_z\rangle$, and the upper signs correspond to all the axes taken parallel to the fourfold edges of the cube, (x",y",z") in Figure 4.7b, and the lower signs to the x and y axes being taken parallel to the twofold axes of the cube (x',y',z') in Figure 4.7b. The energy levels are expressed in terms of P, R, and P' defined in Equation (4.18).

J	Wave function	Description	Energy Level
$\frac{5}{2}$	$\|\varepsilon^+\rangle = \sqrt{\frac{5}{6}}\|\frac{5}{2}\rangle \pm \sqrt{\frac{1}{6}}\|-\frac{3}{2}\rangle$	Γ_8	2P'
	$\|\varepsilon^-\rangle = \sqrt{\frac{5}{6}}\|-\frac{5}{2}\rangle \pm \sqrt{\frac{1}{6}}\|\frac{3}{2}\rangle$		
	$\|\varepsilon^+\rangle = \|\frac{1}{2}\rangle$		
	$\|\varepsilon^-\rangle = \|-\frac{1}{2}\rangle$		
	$\|e^+\rangle = \frac{1}{\sqrt{6}}\|\frac{5}{2}\rangle \mp \sqrt{\frac{5}{6}}\|-\frac{3}{2}\rangle$	Γ_7	-4P'
	$\|e^-\rangle = \frac{1}{\sqrt{6}}\|-\frac{5}{2}\rangle \mp \sqrt{\frac{5}{6}}\|\frac{3}{2}\rangle$		
$\frac{7}{2}$	$\|a^+\rangle = \sqrt{\frac{5}{12}}\|\frac{7}{2}\rangle \pm \sqrt{\frac{7}{12}}\|-\frac{1}{2}\rangle$	Γ_6	14P - 140R
	$\|a^-\rangle = \sqrt{\frac{5}{12}}\|-\frac{7}{2}\rangle \pm \sqrt{\frac{7}{12}}\|\frac{1}{2}\rangle$		
	$\|c^+\rangle = \frac{1}{2}\|\frac{5}{2}\rangle \pm \frac{\sqrt{3}}{2}\|-\frac{3}{2}\rangle$	Γ_8	2P + 96R
	$\|c^-\rangle = \frac{1}{2}\|-\frac{5}{2}\rangle \pm \frac{\sqrt{3}}{2}\|\frac{3}{2}\rangle$		
	$\|b^+\rangle = \sqrt{\frac{7}{12}}\|\frac{7}{2}\rangle \mp \sqrt{\frac{5}{12}}\|-\frac{1}{2}\rangle$		
	$\|b^-\rangle = \sqrt{\frac{7}{12}}\|-\frac{7}{2}\rangle \mp \sqrt{\frac{5}{12}}\|\frac{1}{2}\rangle$		
	$\|a^+\rangle = \frac{\sqrt{3}}{2}\|\frac{5}{2}\rangle \mp \frac{1}{2}\|-\frac{3}{2}\rangle$	Γ_7	-18P - 72R
	$\|a^-\rangle = \frac{\sqrt{3}}{2}\|-\frac{5}{2}\rangle \mp \frac{1}{2}\|\frac{3}{2}\rangle$		

doublets, and neglecting the effect of the $J = \frac{5}{2}$ state, will give a ground doublet of

$$|\tfrac{1}{2}+\rangle = (1 + p^2 + q^2 + r^2)^{-\frac{1}{2}} \left[|a^+\rangle + p|b^-\rangle + q|c^+\rangle + r|d^-\rangle \right]$$
$$|\tfrac{1}{2}-\rangle = (1 + p^2 + q^2 + r^2)^{-\frac{1}{2}} \left[|a^-\rangle + p|b^+\rangle + q|c^-\rangle + r|d^+\rangle \right]$$
(4.19)

That is,

$$|\tfrac{1}{2}+\rangle = (1+p^2+q^2+r^2)^{-\frac{1}{2}} \left\{ \left[\sqrt{\tfrac{5}{6}} \,|\tfrac{5}{2}\rangle + |-\tfrac{3}{2}\rangle \right] + p\left[\sqrt{\tfrac{7}{12}} \,|-\tfrac{7}{2}\rangle + \sqrt{\tfrac{5}{12}} \,|\tfrac{1}{2}\rangle \right] + \right.$$
$$\left. + q\left[|\tfrac{1}{2}\rangle + \sqrt{\tfrac{5}{6}} \,|-\tfrac{3}{2}\rangle \right] + r\left[\sqrt{\tfrac{5}{12}} \,|-\tfrac{7}{2}\rangle - \sqrt{\tfrac{7}{12}} \,|\tfrac{1}{2}\rangle \right] \right\}$$
$|\tfrac{1}{2}-\rangle$ = Kramers conjugate ....(4.20)

The exact solution for p, q and r from the three experimental g values is feasible, but in practice it becomes very difficult on account of numerous ambiguities in signs. However, for small distortions p, q and r would be expected to be small, and we may neglect second order terms in these quantities. In this approximation we find, using equation (1.3)

$$g_{x'} = g_J \left[3 + P_0 - Q_0 \right]$$
$$g_{y'} = g_J \left[3 - P_0 - Q_0 \right]$$
$$g_{z'} = g_J \left[3 + 2Q_0 \right]$$

where $g_J = 6/7$

and $P_0 = 6p$

$$Q_0 = 2\sqrt{3}\, q \quad (4.21)$$

The mean, and R.M.S. of these values is $3g_J$ to within the approximation made. The modulus of the calculated g values has been taken as it is clear that they must all have the same sign as the cubic values when P_0 and Q_0 are zero. They must be compared with the moduli of the measured g values (cf. Appendix I).

We may note that there are no linear terms in r involved (as the magnetic field transforms like a vector and such a term has no matrix elements between the cubic Γ_7 and Γ_6 states), and so the complete wavefunction cannot be found in this manner.

Because of the experimental ambiguity between the directions of g_x and g_y (as defined in Table 3.1) we can derive two possible sets of P_o and κ_o. The theoretical values are defined in direction and we have the two cases:-

Case A		Case B	
$g_x = g_{x'}$		$g_x = g_{z'}$	
$g_y = g_{z'}$		$g_y = g_{x'}$	(4.21a)
$g_z = g_{y'}$		$g_z = g_{y'}$	

For each case P_o and κ_o were found in the three possible ways from pairs of g values and averaged. These "best fit" values are given in Table 4.5, and a comparison of the theoretical and experimental g values is given in Table 4.6 where it is seen that the discrepancy increases with distortion. In Figure 4.10, κ_o is plotted against P_o, and whilst this curve has no theoretical significance it does suggest that the distortions increase in a smooth manner as one goes from LGG→YAG. P_o and κ_o are also found to vary in a smooth manner if plotted against x~y. Again it is indicated that the principal g values in LGG may be expected to be closest to those in the larger YIG lattice if this trend continues.

As the values found for p and q are small (~0.05 and ~0.02 respectively) the neglect of second order terms appears

Table 4.5

Parameters P_o and Q_o found by fitting the Yb^{3+} experimental g values to formulae given in Equation (4.21). The two sets correspond to the ambiguity between experimental g_x and g_y values.

Lattice	Case A		Case B	
	$P_o = 6p$	$Q_o = 2\sqrt{3}\,q$	P_o	Q_o
LGG	0.288	0.069	0.247	0.110
YGG	0.365	0.090	0.328	0.148
LAG	0.546	0.151	0.500	0.198
YAG	0.613	0.177	0.572	0.218

Table 4.6

Best fit obtained for the g values using the results of Table 4.5 and Equation (4.21).

Lattice		g_x	g_y	g_z
LGG	Expmt.	3.65	3.56	2.99
	Theory	3.68	3.59	3.02
YGG	Expmt.	3.73	3.60	2.85
	Theory	3.77	3.63	2.88
LAG	Expmt.	3.84	3.74	2.59
	Theory	3.88	3.77	2.63
YAG	Expmt.	3.87	3.78	2.47
	Theory	3.93	3.83	2.53

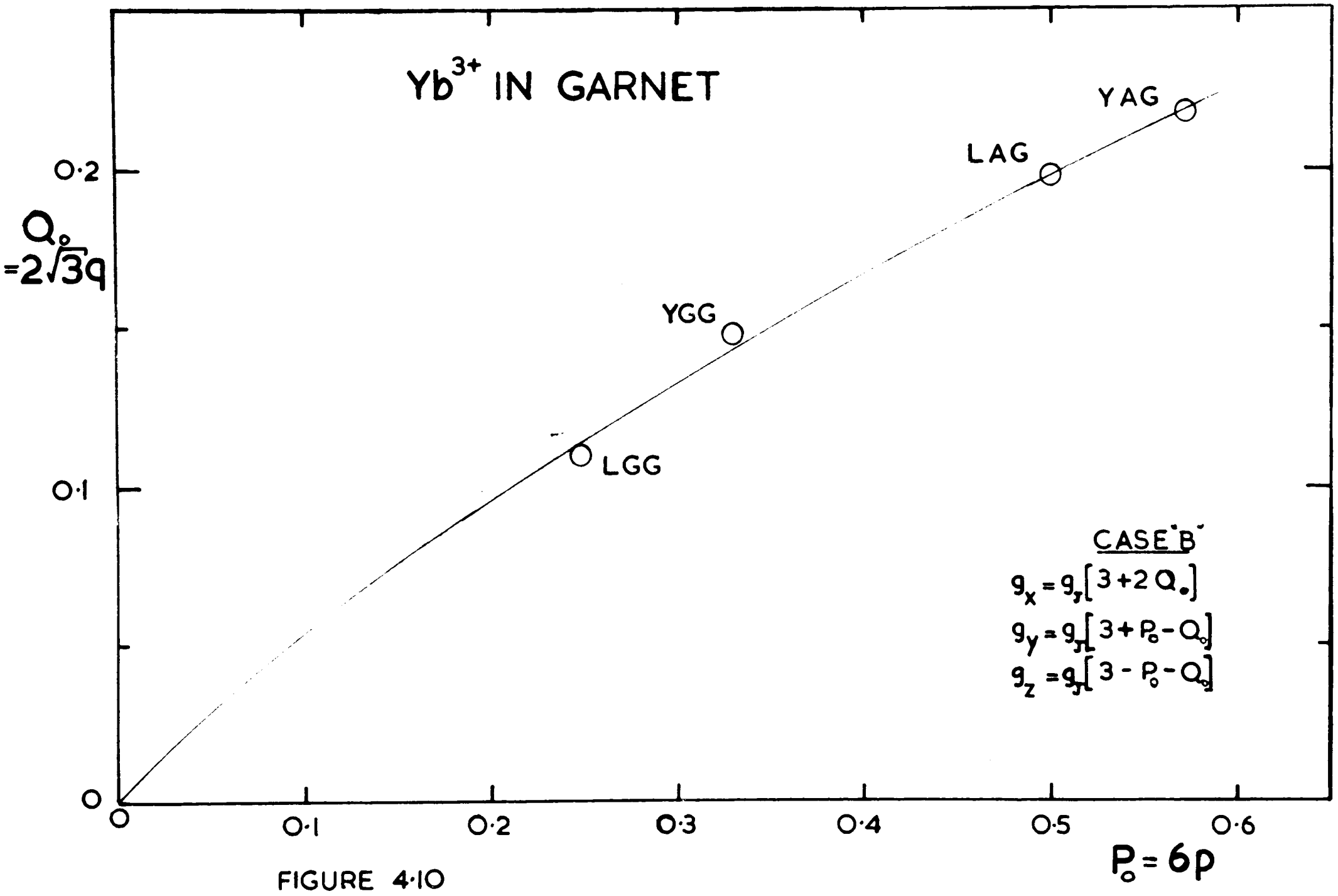

Yb3+ IN GARNET
YAG
LAG
YGG
LGG
0·2
0·1
0
Q₀ =2√3q
CASE 'B'
gx = gz[3+2Q₀]
gy = gz[3+P₀-Q₀]
gz = gz[3-P₀-Q₀]
0
0·1
0·2
0·3
0·4
0·5
0·6
P₀ = 6p

FIGURE 4·10

justified. However the remaining discrepancy between the theoretical and experimental values given in Table 4.6 must be attributed mainly to such terms, together with the effects of admixtures from the $J = \frac{5}{2}$ state. The latter effects will be discussed below, and it will be shown that they are of the order of 2% and will increase the theoretical g values, so that the parameter theory is not quite as good as it appears.

It might appropriately be mentioned here that Koster (1962) has given a wavefunction for the ground doublet of $|+\rangle = -0.6\,|-\frac{3}{2}\rangle + 0.80\,|\frac{5}{2}\rangle$ in terms of $|J_z\rangle$, where z is apparently taken along the crystallographic [001] direction. This has $g_x = g_y = 3.8$, and $g_z = 2.42$, which he claims fits the results for YAG, and is close to the cubic wavefunction

$$|+\rangle = +0.5\,|-\tfrac{3}{2}\rangle + 0.85\,|\tfrac{5}{2}\rangle$$

However, we cannot put much faith in this result, as

(a) there is a sign change in the coefficient of $|-\frac{3}{2}\rangle$ state between the two wave functions; and

(b) the cubic wavefunction is that of the Γ_7 doublet (Table 4.4) referred to a fourfold z axis, whereas the first wavefunction is expressed in terms of a co-ordinate system with z axis along the twofold "local" cube axis (cf. Figure 4.7 a,b) and in which the cubic Γ_7 would have states differing in J_z by two.

4.7.1 Admixture from $J = \frac{5}{2}\ \Gamma_7$ state

In order to estimate the order of magnitude of the effect of admixtures from the $J = \frac{5}{2}$ state we may consider the main cubic field alone, in which case only the Γ_7 will be admixed. The wave function of the pure $J = \frac{5}{2}\ \Gamma_7$, $|e^+\rangle$, is given in Table 4.4. Working in the (x",y",z") axes system, and a $|J, J_z\rangle$ representation, the lowest doublet becomes,

$$|+\rangle = \Gamma_7\left(\tfrac{7}{2}\right) + \varepsilon\,\Gamma_7\left(\tfrac{5}{2}\right)$$

$$= |a^+\rangle + \varepsilon\,|e^+\rangle \qquad (4.22)$$

So that $g = g_z = 2\,\langle + |\ L_z + 2S_z|\ + \rangle$

$$= 2g_J\,\langle a^+|\ J_z|\ a^+\rangle + 4\varepsilon\langle a^+|L_z + 2S_z|\ e^+\rangle$$

$$= 3.429 + 4\,\varepsilon\langle a^+|L_z + 2S_z|\ e^+\rangle \qquad (4.23)$$

(neglecting terms in ε^2)

The matrix element $\langle e^+|\ L_z + 2S_z|\ e^+\rangle$ can be found from the formula, given by Elliott and Stevens (1953a) and Van Vleck (1932),

$$\langle J+1,\ J_z|L_z + 2S_z|\ J,\ J_z\rangle = \langle J+1,\ J_z|\ S_z|\ J,\ J_z\rangle$$

$$= \langle J+1|\Lambda|\ J\rangle\left\{(J+1)^2 - J_z^2\right\}^{\frac{1}{2}} \qquad (4.24)$$

$\langle J+1|\Lambda|J\rangle = \langle\frac{7}{2}|\Lambda|\frac{5}{2}\rangle = \frac{1}{7}$ for Yb^{3+}, and we find $\langle a^+|\ L_z + 2S_z|\ e^+\rangle = \frac{\pm 4}{7\sqrt{3}}$. The sign depends on the phase relation between $|a^+\rangle$ and $|e^+\rangle$, and cannot be determined if the two manifolds have been treated separately in order to find the wave functions. We therefore have,

$$g = 3.429 + \Delta g, \text{ where } \Delta g = \pm\ \frac{16\varepsilon}{7\sqrt{3}} \qquad (4.25)$$

(In agreement with the formula found independently by Hayes and Twidell (1961)). The cubic crystal field has been diagonalised in an $|L, S, L_z, S_z\rangle$ representation spanning the whole ^2F manifold and it is found that $\Delta g > 0$, this will be described in Chapter 8.

In order to estimate ε, which is given by first order perturbation theory as

$$\varepsilon = \frac{\langle a^+ | \mathcal{H}_{CEF} | e^+ \rangle}{E_{7/2} - E_{5/2}} \qquad (4.26)$$

we rewrite $|a^+\rangle$ and $|e^+\rangle$ in an $|LSL_zS_z\rangle$ representation, using the Wigner coefficients $\langle L = 3, S = \frac{1}{2}, L_zS_z | L = 3, S = \frac{1}{2}, J\ J_z\rangle$ (a formula for which is given in Condon and Shortley (1935)).

If, operating within a manifold of states $|J = \frac{7}{2}, J_z\rangle$, we have the cubic crystal field Hamiltonian,

$$\mathcal{H}_{CEF}\ (J = \tfrac{7}{2}) = B_4^0\ (O_4^0 + 50O_4^4) + B_6^0\ (O_6^0 - 210O_6^4),$$

then the equivalent operator acting within a manifold of states $|L = 3, S = \frac{1}{2}, L_zS_z\rangle$ is

$$\mathcal{H}_{CEF}(L = 3, S = \tfrac{1}{2}) = \tfrac{7}{3} B_4^0(O_4^0 + 50O_4^4) + 7B_6^0(O_6^0 - 210O_6^4) \qquad (4.27)$$

since $B_n^m = A_n^m \langle r^m \rangle \Theta_n$ (Equation A2.20). The relevant Steven's multiplicative factors, Θ_n (see § A2.3.3) are listed in Table 4.7.

Using equation (4.27) we find

$$\langle a^+ | \mathcal{H}_{CEF} | e^+ \rangle = \pm \sqrt{3}\ \left[400\ B_4^0 + 30240 B_6^0\right] \qquad (4.28)$$

where again we have an ambiguity in sign because of the unknown

Table 4.7

Values of Stevens' multiplicative factors Θ_n for ytterbium, given for the two J manifolds, and for LS representation. Landé factors are also given.

	α_J	β_J	γ_J	s_J
$J = \frac{7}{2}$ *	$\frac{+2}{3^2 \times 7}$	$\frac{-2}{3 \times 5 \times 7 \times 11}$	$\frac{+2^2}{3^3 \times 7 \times 11 \times 13}$	$\frac{8}{7}$
$J = \frac{5}{2}$ †	$\frac{+2}{7 \times 5}$	$\frac{-2}{3^2 \times 5 \times 7}$	-	$\frac{6}{7}$
	α_L	β_L	γ_L	
$L = 3,\ S = 1$ ‡	$\frac{+2}{3^2 \times 5}$	$\frac{-2}{3^2 \times 5 \times 11}$	$\frac{+2^2}{3^3 \times 11 \times 13}$	

*From Elliott and Stevens (1953a)

†P. Levy (Private communication)

‡Calculated from row one, by equating matrix elements written in the two representations.

phase relationship. To obtain an order of magnitude estimate of ε we can use the data of Pappalardo and Wood (1960) to estimate B_4^0 and B_6^0. If we assume the 550 cm^{-1} splitting is that between Γ_7 and Γ_8. They also obtain Δ_1 = 160 cm^{-1} and Δ_2 = 290 cm^{-1} for the splittings of the $J = \frac{5}{2}$ state (Figure 4.9) so that the Γ_7 to Γ_8 cubic splitting would be ~370 cm^{-1}. From the energy levels given in Table 4.4 and Equation (4.18) we find

$$B_4^* \sim 0.28 \text{ cm}^{-1}, \text{ and } B_6^* \sim 0.006 \text{ cm}^{-1}$$

and taking $(E_{7/2} - E_{5/2}) = -10,300 \text{ cm}^{-1}$ we have from Equations (4.26) and (4.27), $\varepsilon \approx 0.0496$. This gives a change in g value of $\Delta g \sim +0.065$, i.e. about 2%. The values of $g_{RMS} = 3.43$ found experimentally therefore indicate that the distortions are not as small as first suggested by considering only the $J = \frac{7}{2}$ state.

4.7.2 Ratio of fourth to sixth order potential

As the cubic approximation appears to be quite successful for ytterbium, it is interesting to compare values of the L.L.W. parameter x for Yb^{3+} derived in several ways. The methods, some of which will concern later Chapters, will be discussed very briefly, and the comparison made in Table 4.8. Values of $\langle r^n \rangle$ from Table 4.3, in the appropriate units, were used when necessary. These methods are:-

(a) From $x_{Exp} = -0.46$, and using the appropriate form of Equation (4.6).

(b) Using the (non cubic) results of the fitting procedure

described in Chapter 8

(c) Using the optical measurements of Pappalardo and Wood. N.B. These can also be used to obtain a value of λ, from Equation (4.4) and (4.16) giving $\lambda \approx 24$ cm^{-1} for ytterbium.

(d) From a point charge calculation over the nearest eight oxygen ions considering them as at the corners of a perfect cube, as described in Appendix II and Chapter 7.

(e) From a point charge calculation over all ions in the lattice (non cubic potential) as described in Chapter 7.

We see, from Table 4.6 that the point charge calculations give far more emphasis to the fourth order terms than sixth, but this is not borne out by the two estimates based on experimental results. The values deduced from the erbium crossing for the ratios are about half the point charge values. This is in agreement with the findings of White (1962).

4.8 Consideration of the $J = \frac{5}{2}$ ytterbium state in the cubic approximation

In view of the success of the cubic approximation for the explanation of the measured g values of the lowest $J = \frac{7}{2}$ doublet, we shall now treat in a similar manner the lowest $J = \frac{5}{2}$ doublet. The principal g values of this state have been found from optical work by Wickersheim and White (1962). They are $g_x = 1.80$, $g_y = 1.98$ and $g_z = 0.35$, defined with respect to the axes shown in Figure 4.7a. Again there is an ambiguity between the directions of g_x and g_y.

Table 4.8

Various estimations of the value of x, defined by Equation (4.5), for ytterbium, assuming a cubic crystal field. Ratios of other parameters are also given.

Parameter \ Method	$x_{Er} \approx -0.46$	Best fit (Chapter 8)	Pappalardo & Wood (1960)	Point charge (Cube)	Point charge (Full Sum)
x_{Yb}	0.85	0.60	0.69	0.92	0.92
$\frac{F_4^0}{V_6^0}$	-10.0	-2.7	-4.0	-22	-21
$\frac{A_4^0}{A_6^0}(1-\rho^2)$	-9.0	-2.4	-3.6	-20	-19

If we neglect the $J = \frac{7}{2}$ state, we can rewrite the most general wavefunction in a D_2 symmetric crystal field, expressed with respect to axes (x',y',z') of Figure 4.7b in terms of the cubic wavefunctions given in Table 4.4. We have

$$|+\rangle = (1 + s^2 + t^2)^{-1/2} \left[|e^+\rangle + s|f^+\rangle + t\,|g^+\rangle \right]$$
$$|-\rangle = (1 + s^2 + t^2)^{-1/2} \left[|e^-\rangle + s\,|f^-\rangle + t\,|g^-\rangle \right]$$

(Taking the phase factor as + 1)

or,

$$|+\rangle = (1 + s^2 + t^2)^{-1/2} \left\{ \left[\frac{1}{\sqrt{6}} \left|\tfrac{5}{2}\right\rangle + \sqrt{\frac{5}{6}} \left|-\tfrac{3}{2}\right\rangle \right] + s\left|\tfrac{1}{2}\right\rangle + t\left[\sqrt{\frac{5}{6}} \left|\tfrac{5}{2}\right\rangle - \frac{1}{\sqrt{6}} \left|-\tfrac{3}{2}\right\rangle \right] \right\}$$

$|-\rangle$ = Kramers conjugate (4.29)

Again neglecting second order terms in s and t, we find (maintaining signs and identifying the $|+\rangle$ state with $\left|S' = \tfrac{1}{2}, S'_z = +\tfrac{1}{2}\right\rangle$, cf. Appendix I).

$$g_{x'} = g_J \left[\frac{5}{3} + S + T \right]$$
$$g_{y'} = g_J \left[\frac{5}{3} - S + T \right]$$
$$g_{z'} = -g_J \left[\frac{5}{3} - 2T \right]$$

where $S = 4\sqrt{\frac{5}{3}}\, s$

$T = \frac{4\sqrt{5}}{3}\, t$

$g_J = \frac{6}{7}$

(4.30)

We must consider the question of the signs of the g values a little more carefully here than in the $J = \frac{7}{2}$ case, as g_z is so small. It is assumed that the g_z has the same sign as the cubic value, that is, the distortion is not great enough to change its sign. The experimental g values are therefore given

the above theoretical signs for the comparison. The result of the calculations described in Chapter 8 suggest that this assumption is correct.

We again have two cases, as in Equation (4.21a), and averaging in the same manner as for the $J = \frac{7}{2}$ case, we find:-

Case A	Case B
S = 0.851	S = 0.950
T = -0.351	T = -0.247

Both giving $g_x = 1.86$, $g_y = 2.03$, and $g_z = 0.40$. Substituting the values for S and T into Equation (4.29) we find two possible wavefunctions:-

$$\text{Case A} \quad |+\rangle = 0.301\,|\tfrac{5}{2}\rangle + 0.165\,|\tfrac{1}{2}\rangle + 0.961\,|-\tfrac{3}{2}\rangle$$

$$\text{Case B} \quad |+\rangle = 0.333\,|\tfrac{5}{2}\rangle + 0.184\,|\tfrac{1}{2}\rangle + 0.947\,|-\tfrac{3}{2}\rangle \qquad (4.31)$$

(With respect to axes (x',y',z') of Figure 4.7b).

One could now treat these coefficients as a first approximation, which will help to remove the ambiguities, and deduce a wavefunction which gives the g values more exactly. However, this would not necessarily be consistent with the splittings, and a more rigorous treatment involving these as well will be given in Chapter 8. The wavefunctions given above form a useful check on those found in Chapter 8.

4.9 Conclusion

There is a very critical dependence of the principle g values of most rare earth ions investigated on their exact crystalline environment in the garnet lattice. Predictions of

their magnetic properties in the iron garnets cannot therefore be made directly from the resonance results, although for Yb^{3+} the trends in the g values suggest that the values in LGO may lie closest to those in YIG. As a first step in a more detailed analysis of the results a distorted cubic crystal field has been considered, and whilst this can account for some of the gross features of the observed g values, only in the case of Yb^{3+} does it allow a more detailed explanation. Any further discussion must be in terms of the actual crystal field parameters, and the most straightforward case of Yb^{3+} in YGG will be considered in Chapters 7 and 8.

CHAPTER 5

Direct application of the experimental g values to magnetically concentrated garnets

5.1 Introduction

In spite of the general conclusion of the previous chapter, the resonance g values may in two cases be applied directly to magnetically concentrated salts with some success. In this chapter the magnetic properties of DyAG, and YbIG, will be discussed to illustrate how useful the E.P.R. measurements can be in such cases. The discussion will be brief as it is mainly concerned with the work of other members of the group (who will be acknowledged where appropriate).

5.2 Antiferromagnetic ordering of dysprosium aluminium garnet

Dysprosium aluminium garnet (DyAG) orders antiferromagnetically at about $2.5^{\circ}K$. Below this temperature its susceptibility tends rapidly to zero (Ball et al 1962), in contrast to the behaviour of the usual cubic antiferromagnet whose susceptibility tends to a constant value. The susceptibility measurements of Leask and Wolf are shown in Figure 5.1.

This unusual behaviour can be explained very well in terms of the E.P.R. results for Dy^{3+} in the aluminium garnet lattices, which are given in Table 3.1 and illustrated in Figure 3.9. Although the oxygen structure parameters have not been determined for DyAG, the lattice constant (12.044 Å) lies close to that of YAG (12.000 Å) and it would therefore appear that the principal

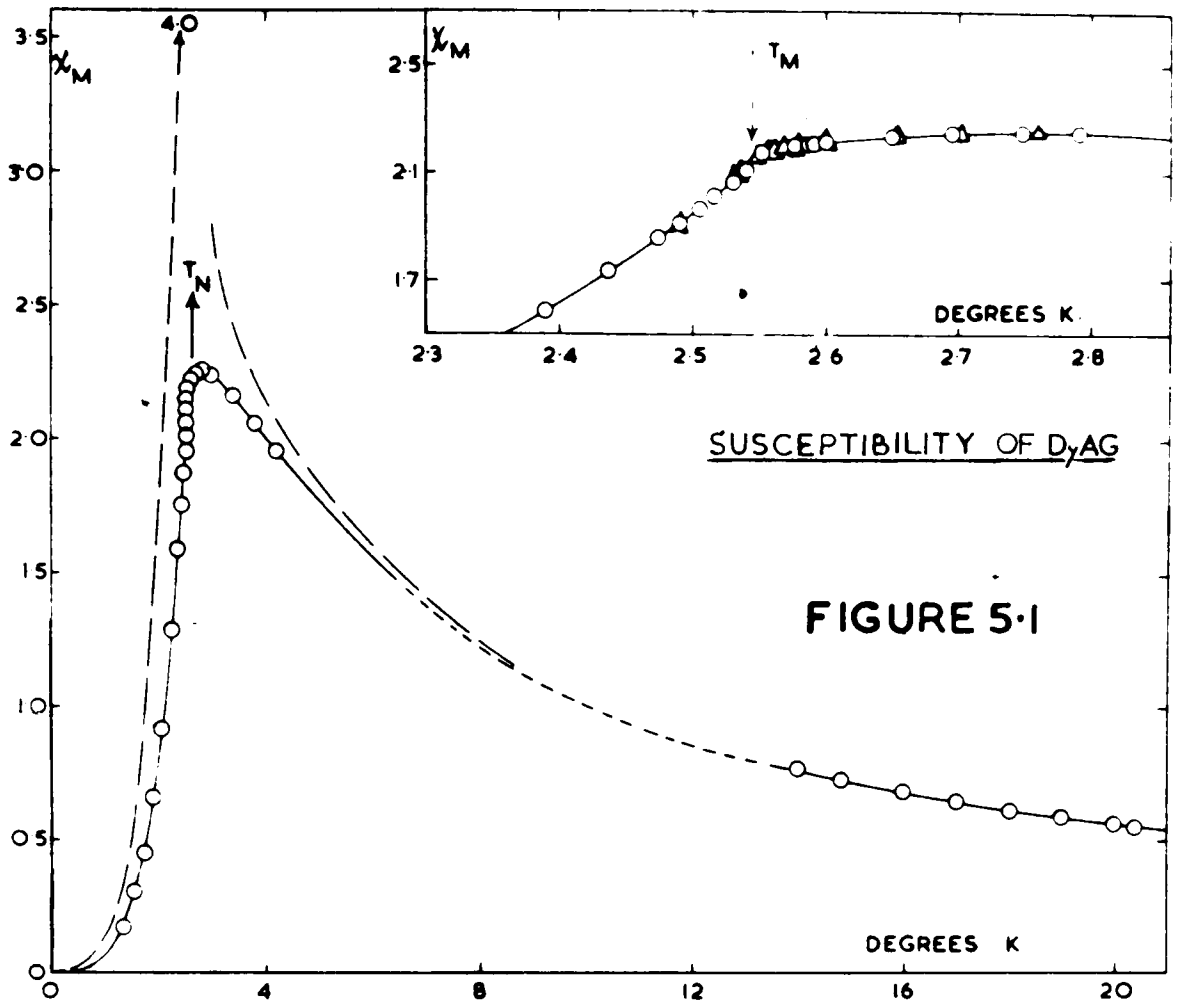


FIGURE 5·1

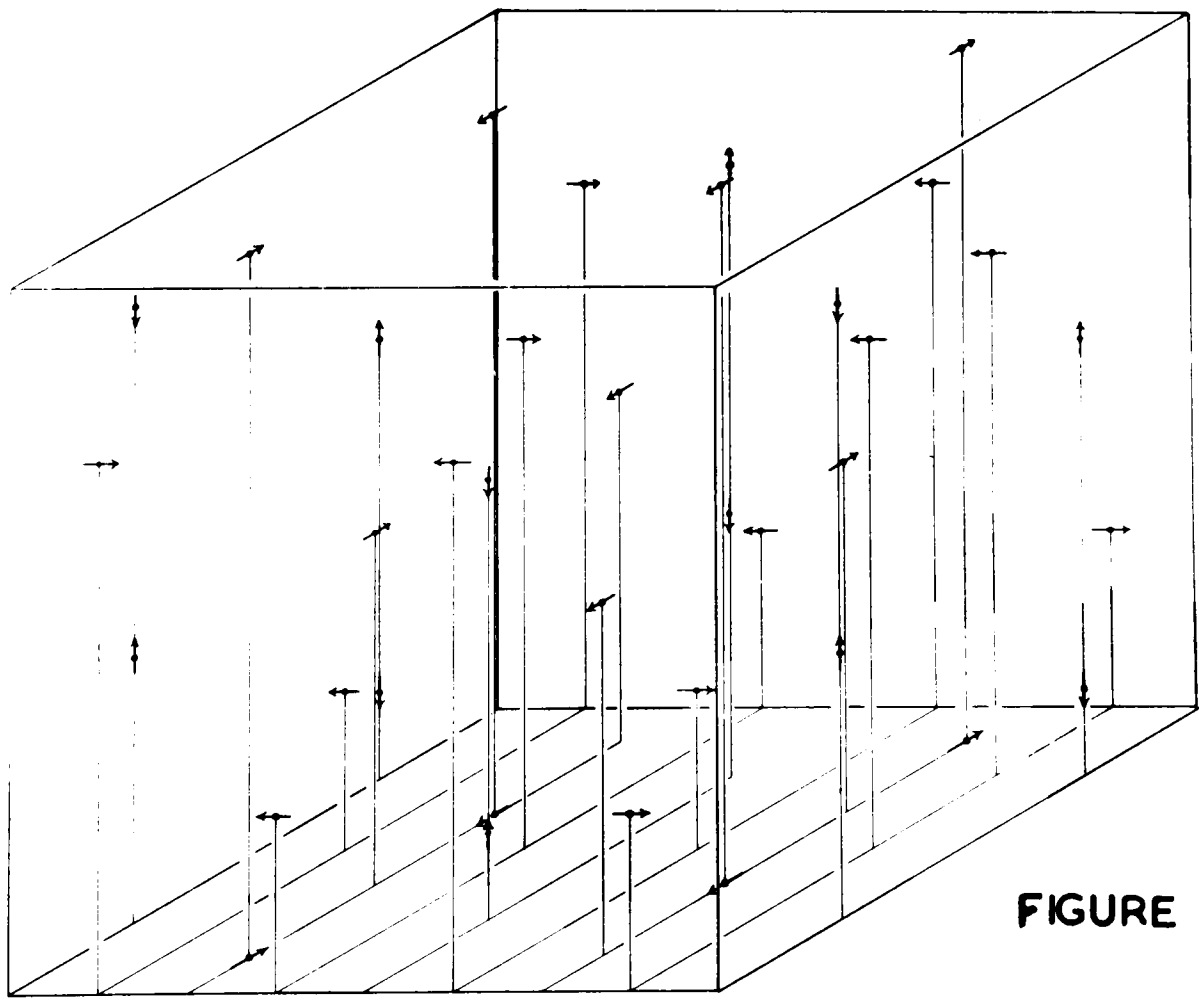


FIGURE 5·2

POSSIBLE SUB-LATTICE STRUCTURE FOR DYSPROSIUM ALUMINIUM GARNET.

g values of Dy^{3+} in YAG may be taken as a good estimate of those in DyAG, especially as the spectra in YAG and LAG show the same main features.

As a first approximation, the Dy^{3+} ion in DyAG may therefore be characterised at low temperatures by $S' = \frac{1}{2}$, $g_z = 18.0$, $g_x = g_y = 0$, and the compound should closely resemble a model of three orthogonal interpenetrating chains of Ising spins. A possible ordered state for such a model is shown in Figure 5.2, the moments on each ion are locked by the crystal field into one of two directions, which one being determined by the interaction with neighbouring ions. This arrangement was proposed on purely dipole-dipole interactions, and consists of antiferromagnetic chains parallel to each of the three cubic unit cell axes (X,Y,Z). It favours dipolar interactions between nearest and third nearest neighbours. Clearly for small external fields, $\chi \rightarrow \infty$ as $T \rightarrow 0$. Exchange interaction, generally expected to be small for rare earth ions, will here be even smaller than usual, since an isotropic exchange between real spins $\mathcal{H}_{ex} = J_{ex}\, \underline{S}^{(1)} . \underline{S}^{(2)}$ becomes of the form $\mathcal{H}_{int.} = \underline{S}^{(1)'} . \underline{\chi} . \underline{S}^{(2)'}$ in terms of the effective spins, and $\chi = 0$ if $g_x = g_y = 0$.

Leask and Wolf have considered possible alternative arrangements in some detail. They find that the {c} sites can be divided into two interpenetrating sublattices, where the sites on each sublattice include all the nearest neighbours of

each other. If dipolar interaction orders the ions on these two sublattices, the question remains as to how the sublattices align with respect to each other. They find that the arrangement described above has the lowest dipolar energy and that the alternative, consisting of ferromagnetic chains in the ± X, ± Y, ± Z directions, has an energy 30% higher.

Assuming dipolar interactions only, and the simple Ising model, Leask and Wolf have calculated the susceptibility above T_N using a standard series expansion method. From the arrangement of Figure 5.2 they also calculated the small field susceptibility below T_N, and estimated the Néel temperature. Their results, represented by the dashed curves of Figure 5.1, show reasonable agreement with experiment in view of the fact that they used no adjustable constants. The estimated value of T_N of 2.68°K is remarkably close to the most recent experimental value of 2.49°K (Wyatt 1963).

Specific heat measurements (Wyatt 1963) have enabled an estimation of the interaction energy to be made, which shows that the interactions are in fact not entirely dipolar, there being a contribution of at least 30% due to exchange. Measurements on the magnetic moment of $DyAlO_3$ in high fields (Wyatt 1963) confirm the Ising model of the lattice and lead to an estimated value of $g_z = 18 \pm 1$. They show a very interesting spin flipping phenomenon when the ion, still contrained by the crystal field, flips over against the ordering field if an external field is applied.

In conclusion we may say that the results of the E.P.R. experiments on Dy^{3+} in YAG enable an explanation of the main antiferromagnetic ordering process in DyAG to be made. The bulk magnetic properties can be interpreted quite well in terms of a model of Ising spins with dipolar interactions only.

5.3 Canting effects in the rare earth iron garnets

In the ferrimagnetic iron garnets the rare earth ions are subject to exchange forces from two Fe^{3+} sublattices consisting of irons on the [a] and (d) sites which, below the ordering temperature (~ 550°K) are strongly aligned antiparallel to each other. As there are more (d) sites than [a] sites in the ratio 3:2 there is a net spontaneous magnetic moment due to the Fe^{3+} of $(3-2) \times \frac{5}{2} \times 2\mu_B = 5\mu_B$, per formula unit $R_3Fe_5O_{12}$, along the [111] direction. At relatively high temperatures the rare earth moment will be aligned antiparallel to the resultant iron moment (considering rare earth ions in the second half of the series, ions in the first half will align parallel (Wolf 1961[b])). However at lower temperatures, when only a few of the rare earth levels are populated, the situation will become more complicated since the large anisotropic crystal field effects indicated by the E.P.R. results will now act on the ion. The relative sizes of the interactions inthe iron garnets being :-

R.E. - C.E.F. > R.E. - Fe > R.E. - R.E.

Wolf (1962[c]) has considered the case of a Kramers ion, and

shown that at low temperatures canting of the rare earth moments will occur. That is the rare earth ions will in general form six sublattices, each lattice consisting of ions whose moments make a fixed angle with the direction of the net iron moment. An outline of this theory will now be given, and the case of YbIG considered quantitatively.

Neglecting the small rare earth-rare earth interactions, we consider the low temperature case of an odd electron rare earth ion when only the lowest Kramers doublet is populated. This doublet will be split by the interaction with the iron spins and to first order this can be considered in terms of an isotropic exchange field - $\underline{H}_e$, in the direction of the iron sublattice magnetisation, acting on the fictitious spins through an anisotropic exchange tensor $\underline{Q}$. By symmetry $\underline{Q}$ has the same principal axes as the magnetic $\underline{g}$ tensor. The interaction is therefore represented by $\mathcal{H}_1 = \underline{H}_e \cdot \underline{Q} \cdot \underline{s}'$. In order to calculate the magnetic moment $\underline{M}$ of a particular rare earth sublattice, we derive an expression for the total free energy F of the individual ions subject to the exchange effects of the iron sublattices, together with a small arbitrarily oriented magnetic field $\underline{H}_o$. The component of $\underline{M}$ along one of the principal directions (α) of the $\underline{g}$ tensor is then given by $M_\alpha = - \frac{\partial F}{\partial H_{o\alpha}}$. The calculation of $\underline{M}$ at $T = 0^\circ K$ is particularly simple as the free energy is then identical with the spectroscopically measured internal energy, and to first

order F (per ion) becomes equal to the lowest eigen value of the Hamiltonian

$$\mathcal{H} = H_0 \cdot \underline{G} \cdot \hat{S}' + \mu_B H_0 \cdot \underline{g} \cdot \hat{S}' \qquad (5.1)$$

which is $E_- = -\frac{1}{2}\left[\sum_{\alpha=x,y,z} (H_{e\alpha} G_\alpha + \mu_B H_{e\alpha} g_\alpha)^2\right]^{\frac{1}{2}}$ (5.2)

So that at T = 0, provided that the exchange energy is independent of H_0,

$$M_\alpha = \frac{N \mu_B g_\alpha}{2} \cdot \frac{(H_{e\alpha} G_\alpha + \mu_B H_{e\alpha} g_\alpha)}{\left[\sum_\alpha (H_{e\alpha} G_\alpha + \mu_B H_{e\alpha} g_\alpha)^2\right]^{\frac{1}{2}}} \qquad (5.3)$$

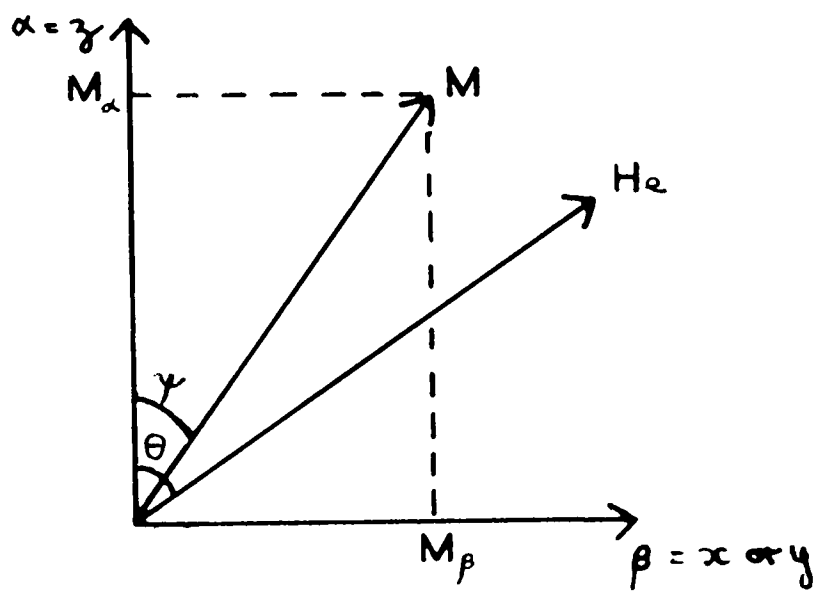
where N is the number of ions.

The spontaneous moment produced by the exchange field alone can be found by putting $H_0 = 0$. If, as shown in Figure 5.3, H_e lies in one of the principal planes of the $\underline{g}$ tensor, the induced magnetisation will also lie in that plane, and its components will be related by

$$\tan\gamma = \frac{M_\beta}{M_\alpha} = \frac{g_\beta G_\beta H_{e\beta}}{g_\alpha G_\alpha H_{e\alpha}} = \frac{g_\beta G_\beta}{g_\alpha G_\alpha} \tan\theta \qquad (5.4)$$

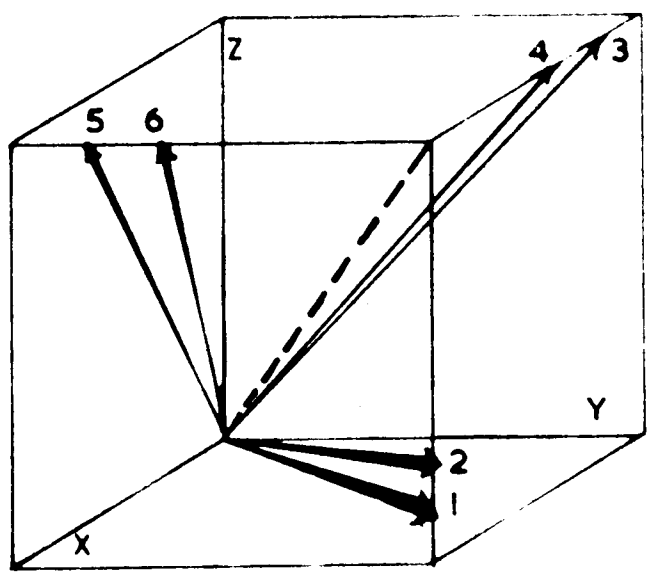
where θ is the angle between H_e, and the principal axis α, and γ is the angle between M and α.

Now if H_0 is small, the iron sublattice, and therefore H_e, will be parallel to one of the <111> axes, so that $\tan\theta = \sqrt{2}$, and we may identify $g_\alpha G_\alpha$ with $g_x G_x$ for every ion, and $g_\beta G_\beta$ with either $g_x G_x$ or $g_y G_y$. The six inequivalent rare earth ions now fall into one of these two types (cf. the E.P.R. spectra



θ = 54° 44′

FIGURE 5·3



$[Yb^{3+}]$ $g_x > g_y > g_z$.

FIGURE 5·4

along the [111] direction in Figure 3.5).

The interaction tensor $\underline{Q}$ has only been determined for the one case of YbIG (Wickersheim 1961, Wickersheim and White 1962), using optical techniques. The most recent values of the exchange splittings of the ground doublet, ΔE_α, which are proportional to Q_α, are listed in Table 5.1. The principal g

Table 5.1

Principal Value	YbIG (g)	LGG (g)	YbIG(Δ... cm^{-1})
x	3.7 ± 0.15	3.65	30.6 ± 0.2
y [illegible]	3.6 ± 0.15	3.56	2[illegible].1 ± 0.1
z	2.6 ± 0.1	2.99	11.8 ± 0.2

values given for Yb in YbIG were determined by Wickersheim by noting the increase in splitting of the doublet in an applied magnetic field, but the inaccuracies are so large it is probably better to use the values found in LGG.

Using these values we can predict that the two groups of ions will have canting angles of $22^{\circ}40'$ and $20^{\circ}15'$. Figure 5.4 shows such a canting system. Wolf (1962) has given tentative canting arrangements for other rare earth ions.

Canting in the garnets has been observed experimentally, but only for the case of HoIG for which no E.P.R. data is available (Herpin et al. 1960).

5.3.1 Spontaneous moment at 0°K of YbIG

At low temperatures the spontaneous moment of YbIG differs very much from the value of $(\frac{8}{7}\cdot\frac{7}{2}\cdot 3 - 5)\mu_B = 7\mu_B$, per formula unit, expected if the R.E.-Fe exchange was very much greater than the crystalline electric field effects on the rare earth ion. The measured value of $0.25\mu_B$ (Pauthenet 1958), indicates large crystal field effects and indeed compares well with the value calculated using the R.M.S. E.P.R. results given in Table 4.2, assuming no canting, i.e. $(3.42 \times \frac{1}{2} \times 3 - 5)\mu_B = 0.13\mu_B$ However, using Equation (5.3) and Table 5.1 we find moments of $1.80\mu_B$, and $1.75\mu_B$ at angles of 22°40' and 20°15' respectively to the [111], and averaging these we find a net moment at 0°K per formula unit of $\sim 0 \pm 0.02\mu_B$. That is, the rare earth moment almost cancels the net iron moment. It is therefore left for second order effects to account for the observed value of $0.25\mu_B$, and an order of magnitude estimate of these, from the temperature independent susceptibility measurements (Ball et al. 1960), shows them to be about $0.15\mu_B$.

Thus the E.P.R. results for Yb^{3+} in the diamagnetic garnets enable the ferrimagnetic ordering of YbIG at 0°K to be discussed quantitatively, particularly with respect to the canting angles and spontaneous moment.

CHAPTER 6

The calculation of the crystal field [illegible] from a point charge model of the crystal lattice and a discussion of the validity of the model

6.1 Introduction

The basic principles, and methods, of calculating the eigenvalues and eigen-functions of rare earth ions in crystal fields, as used in Chapter 4, are very well established. However the various notations used, and the actual calculations of the parameters A_n^m occurring in the perturbing Hamiltonian from a definite crystallographic model, have been the cause of considerable confusion. A general account of such calculations has therefore been written, and is given in Appendix II, to which the reader who is unfamiliar with the problem is referred. It is the aim of Appendix II to correlate the different notations in a straightforward manner, with particular reference to cubic crystal fields, and to illustrate how the Hamiltonian may be determined on a simple point-charge model of static ions. Some relevant basic principles, and general rules, are also mentioned in Appendix II. A brief discussion of the validity of the point charge model is given in the next section. This model is used in Chapter 7 to calculate the crystal field at the rare earth {c} site in the garnets, and the results are used in Chapter 8 to help to reduce the number of parameters V_n^m ($= A_n^m \langle r^n \rangle$) to be fitted to the available experimental

data for Yb^{3+} in YGG.

The basic expression used in Chapter 7, Equation (A2.10) is repeated here for convenience. It gives the electrostatic potential at a point (r,Θ,ϕ) near the origin, due to k charges q_j at (R_j,Θ_j,ϕ_j), as,

$$V(r,\Theta,\phi) = \sum_{n=0}^{\infty} \sum_{\alpha} r^n \; \gamma_{n\alpha} \; Z_{n\alpha}(\Theta,\phi)$$

$$\text{where } \gamma_{n\alpha} = \sum_{j=1}^{k} \frac{4\pi}{(2n+1)} \; q_j \; \frac{Z_{n\alpha}(\Theta_j,\phi_j)}{R_j^{(n+1)}} \qquad \text{(A2.10)}$$

The $Z_{n\alpha}$ are defined by Equation (A2.8).

6.2 Discussion of the validity of an ionic model of the crystal lattice

Before using the point charge model to calculate the ratios of crystal field parameters and thereby reduce the number to be fitted to experimental data, a brief discussion of the validity of such calculated ratios, and of the model in general, will be given.

Although the model is frequently used (for example Dillon and Walker 1961, Thomas 1962) there has previously been little evidence to suggest the extent of its validity for rare earth ions, and at first sight it appears to be very crude. However, Hutchison and Wong (1958), including induced electric dipoles as well as point charges, have calculated the ratio A_6^6/A_6^0 for a $LaCl_3$ lattice, and by fitting the remaining three parameters

have explained their E.P.R. results with considerable success. A rigorous determination of the "external" crystalline potential near a rare earth ion, assuming that covalency effects are small so that the electron charge clouds are localised about the ions, should include a self consistent calculation of the potential near that site due to all the point charges and induced electric moments on other sites. Provided that there is no overlap of charge clouds, this potential should then be well determined, as it is only necessary to expand to terms of sixth order. However, to determine how much of this external potential the 4f electrons "see", one must investigate the screening effect due to the distortion of the outer rare earth shells, and this in itself is a complex many-bodied problem. A complete calculation of A_n^m is therefore very lengthy, and to find V_n^m one requires an accurate value of $\langle r^n \rangle$, for which Freeman and Watson's (1962) Hartree-Fock values are probably the best available at the present time.

In order to provide a direct test of the validity of a simple ionic model, a comparison was made between the experimentally well-determined crystalline electric field (C.E.F.) parameters, V_2^0, V_4^0, V_6^0 and V_6^6, for Pr^{3+} in $PrCl_3$ and $PrBr_3$ (Margolis 1961), and those calculated on the ionic model. Full details of this comparison are given in Hutchings and Ray (1963). The contributions to A_n^m from point charges at the position of all ions in the lattice were found on the Oxford

University Mercury computer, using two programmes similar to those used for the garnets described in Chapter 7 and Appendix IV. The contributions to A_n^m from electric dipoles and quadrupoles, induced at the halide sites by the point charge electric field at these sites, were also calculated. For this a general expression, derived by D. K. Ray, for the contribution of induced moments of any order to the C.F. parameters was used. The calculated parameters A_n^m were then multiplied by $\langle r^n \rangle$ values from hydrogenic, Hartree, or Hartree-Fock wavefunctions and compared with the experimental values of V_n^m.

The results of these calculations showed that although the contributions from the induced moments were of comparable magnitude to those from the point charges, especially for second order terms, the dipolar contribution and quadrupolar contribution were of opposite sign. Their net contribution, however, was significant, and larger than the error in the point charge values due to structure parameter uncertainties, though it decreased as n increased. Large but systematic differences were found between the calculated and experimental A_n^m's. The calculated value of A_2^o was 20 to 30 times the experimental value, that of A_4^o showed quite reasonable agreement, and both A_6^o and A_6^6 were about 4 to 10 times smaller. However, the ratio A_6^6/A_6^o was in good agreement with the experimental ratio, especially if only the point charge values were used.

The large discrepancies between calculated and experimental values of A_n^m could arise from covalency effects (changing the value of $\langle r^n \rangle$), higher order induced moments on neighbouring ions, or screening effects of the other rare earth electrons. Ray (1963) has estimated the screening effect of the rare earth orbitals, due to their distortion in the "external" crystal field, and finds that the major contribution comes from the 5s and 5p electrons. He calculates that the value of A_2^0 seen by the 4f electrons is about half that of the external field, thus bringing the calculated value nearer the experimental value, and that the screening is the same for all parameters of the same value of n. It appears that screening effects are largest for the second order terms.

It might be mentioned that in spite of the large discrepancies likely in the calculated values, the point charge model may in certain circumstances be used directly. For example, it may be used to distinguish between the 4, 6, and 8-fold cubic fields, discussed in Appendix II, which each lead to very different magnetic properties of the ion, (Lea, Leask and Wolf 1962).

6.2.1 Conclusion

One may therefore conclude that, from the case considered, it seems that it would be a reasonable approximation to reduce the number of parameters to be fitted to experimental data by calculations of their ratios on a simple point charge model.

This method will be used in Chapter 8 for the case of Yb^{3+} in YAG.

CHAPTER 7

Point charge calculations of the garnet crystal field

7.1 Introduction

In Chapter 4 the need for a more detailed analysis of the crystal field at the rare earth {c} site was indicated, and in this chapter the methods of Chapter 6 and Appendix II will be used to calculate the nine parameters A_n^m describing the crystal field in five garnet lattices. The calculations are based on a simple ionic point-charge model of the lattice. The results will be used in Chapter 8 to reduce the number of C.F. parameters, $V_n^m = A_n^m \langle r^n \rangle$, to be fitted to experimental data in the case of Yb^{3+} in YGG. The calculations were also carried out to provide an indication of how the C.F. parameters might vary with the structure parameters, and so help to understand the garnet crystal field in general, and possibly indicate how the properties of a rare earth ion in several lattices might be predicted once its properties in one lattice had been established.

The nine values of A_n^m for each lattice were determined, firstly summing over the nearest O^{2-} ions only, and secondly including a summation over all ions (~ 5,000 in number) with-in a radius of $8a_0$ from the site in question. The results are given in Tables 7.5 and 7.6 and are discussed in § 7.4. The calculations are described in the next two sections.

7.2 Crystallography and co-ordinate systems used

The structure of the garnets has been discussed briefly in §3.2, and a model of the unit cell shown in Figure 3.1. The positions of the ions with respect to axes (X,Y,Z), parallel to the cubic unit cell axes, are given in the "International Tables of X-ray crystallography". The positions of the {c}, [a] and (d) sites depend only on a_o, the lattice constant, whereas those of the oxygen "h" sites depend also on the structure parameters x, y and z. The values of these structure constants used in the calculations are given in Table 4.1.

For the purpose of the calculations the particular rare earth site at $(\frac{1}{8},\frac{1}{4},\frac{1}{8})$ was singled out for consideration. The nearest four [a] sites, six (d) sites and eight "h" sites to this rare earth ion are given in Table 7.1. A photograph of these eight oxygen ions is shown in Figure 3.2 and their positions are plotted for the case of YGG in Figures 7.1a and b, where the distortions from a cubic arrangement can be seen. The dotted lines are the three axes of twofold rotation symmetry and are parallel to the principal axes of the g tensor. The distance of the oxygens from the {c} site is either r_1 or r_2, given by the expressions in Table 7.1. These distances are given for the relevant lattices in Table 7.2.

As the calculations were being carried out it became evident that different axes from those originally chosen would be more convenient. The several local axes used, with origin at the $(\frac{1}{8},\frac{1}{4},\frac{1}{8})$ rare earth ion, are shown in Figures 7.2a and b. We

Table 7.1

Positions of the neighbouring sites to the {c} site at $(\frac{1}{8},\frac{1}{4},\frac{3}{8})$; with respect to axes (X,Y,Z) parallel to the unit cell axes. r_1 and r_2 are the two nearest neighbour h site distances.

"h" sites

$\frac{1}{8}+y,\ z,\ \frac{1}{8}-x$	$\frac{1}{4}+z,\ \frac{1}{4}+y,\ \frac{1}{4}+x$	At distance r_1
$\frac{3}{4}-z,\ \frac{1}{4}-y,\ \frac{1}{4}+x$	$\frac{1}{8}-y,\ \frac{1}{8}-z,\ \frac{1}{8}-x$	
$\frac{1}{8}+x,\ y,\ \frac{1}{8}-z$	$\frac{1}{4}+y,\ \frac{1}{4}+x,\ \frac{1}{4}+z$	At distance r_2
$\frac{3}{4}-y,\ \frac{1}{4}-x,\ \frac{1}{4}+z$	$\frac{1}{8}-x,\ \frac{1}{8}-y,\ \frac{1}{8}-z$	

$$r_1 = \left[y^2 + (\tfrac{1}{4} - z)^2 + (\tfrac{1}{8} - x)^2\right]^{\frac{1}{2}}$$

$$r_2 = \left[x^2 + (\tfrac{1}{4} - y)^2 + (z - \tfrac{1}{8})^2\right]^{\frac{1}{2}}$$

(d) sites	$\frac{1}{8},\frac{1}{4},\frac{5}{8}$	$\frac{1}{8},\frac{1}{4},\frac{1}{8}$	$\frac{3}{8},0,\frac{1}{4}$	
	$\frac{1}{4},\frac{1}{8},\frac{3}{8}$	$\frac{3}{4},\frac{3}{8},\frac{1}{8}$	$\frac{5}{8},\frac{1}{4},\frac{1}{4}$	
[a] sites	$\frac{1}{8},0,\frac{1}{8}$	$\frac{1}{2},\frac{1}{2},\frac{1}{2}$	$\frac{1}{4},\frac{1}{4},\frac{1}{4}$	$\frac{3}{4},\frac{1}{4},\frac{1}{4}$

Table 7.2

Distances r_1 and r_2, calculated using the parameters given in Table 4.1.

Lattice	a_o (Å)	r_1 (Å)	r_2 (Å)
LAG	11.906	2.28	2.39
YAG	12.000	2.30	2.43
LGG	12.188	2.30	2.40
YGG	12.280	2.34	2.42
YIG	12.376	2.36	2.43

POSITIONS OF 8 NEAREST O^{2-} NEIGHBOURS

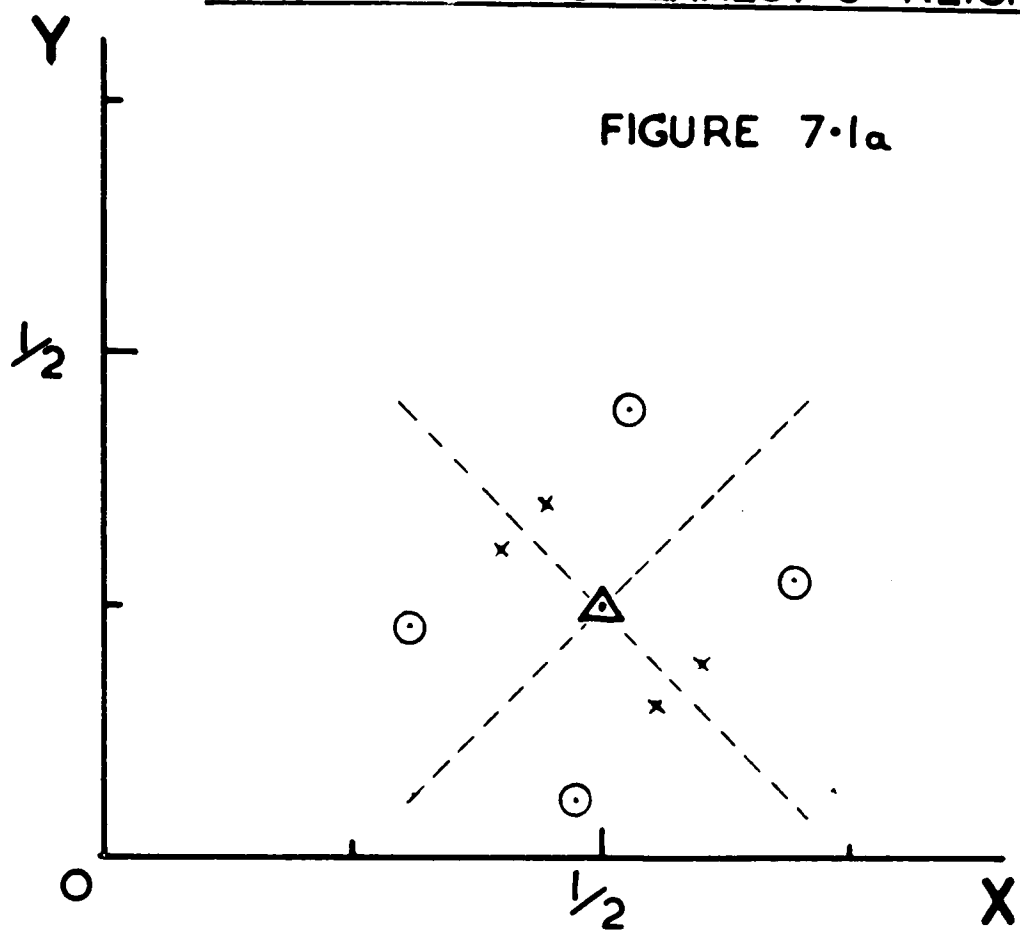


FIGURE 7·1a

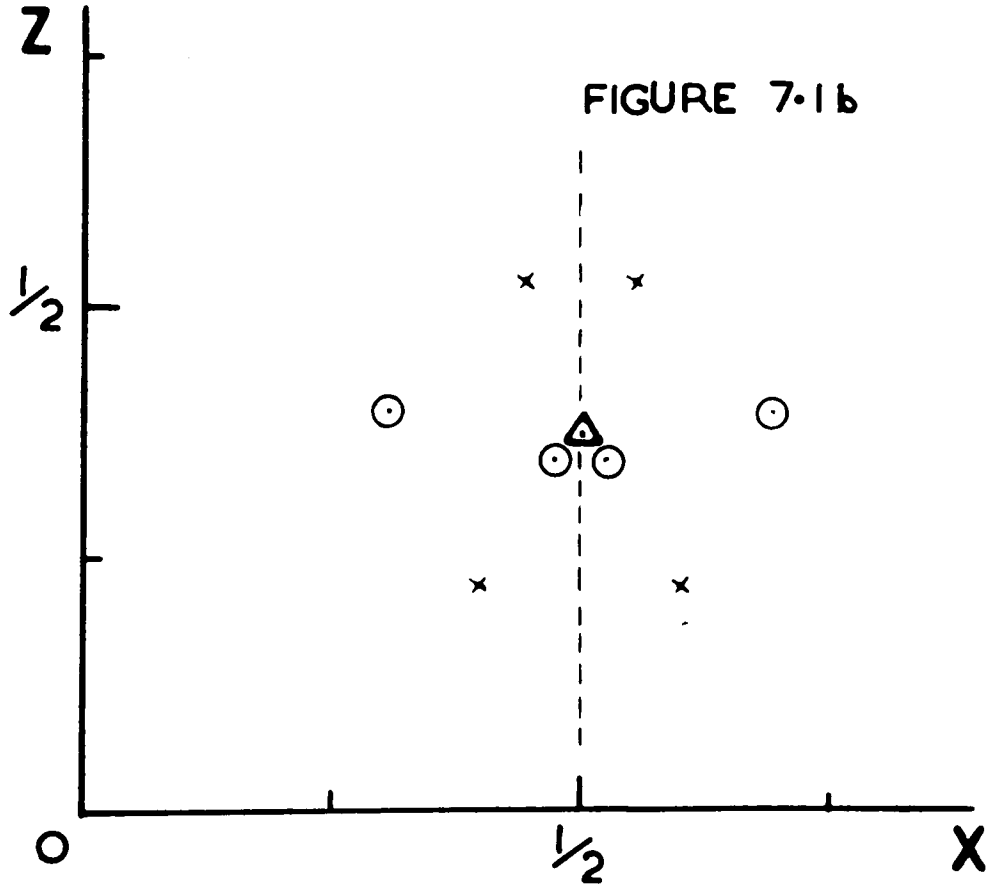


FIGURE 7·1b

△ {C} SITE $(\frac{1}{2}, \frac{1}{4}, \frac{3}{8})$

× DISTANCE r_1 FROM {C} SITE

⊙ DISTANCE r_2 FROM {C} SITE

} FOR YGG IN UNITS OF a_o

LOCAL AXES CHOSEN FOR SITE AT $(\frac{1}{2}, \frac{1}{4}, \frac{3}{8})$

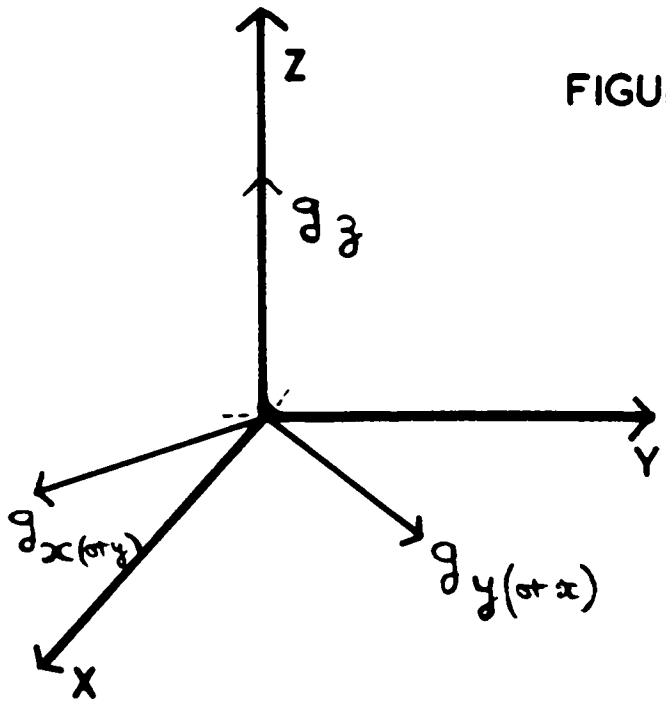


FIGURE 7·2a

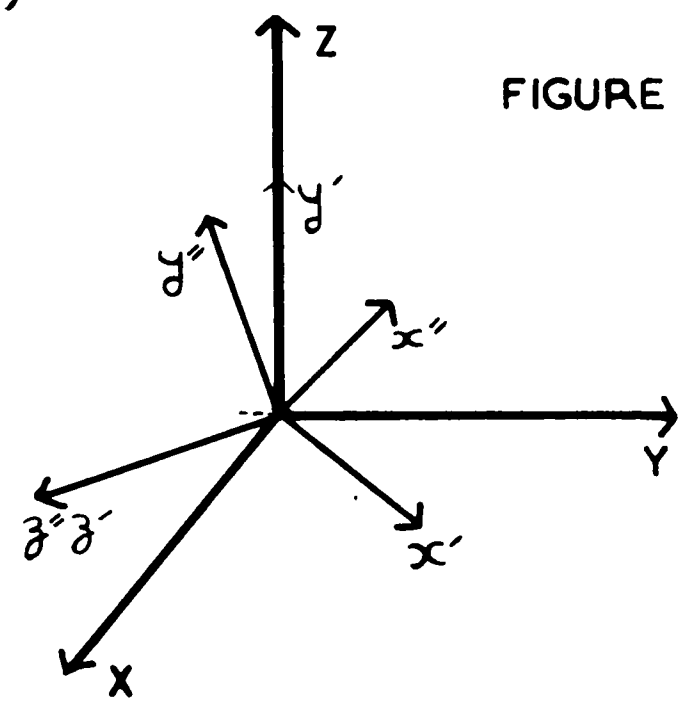


FIGURE 7·2b

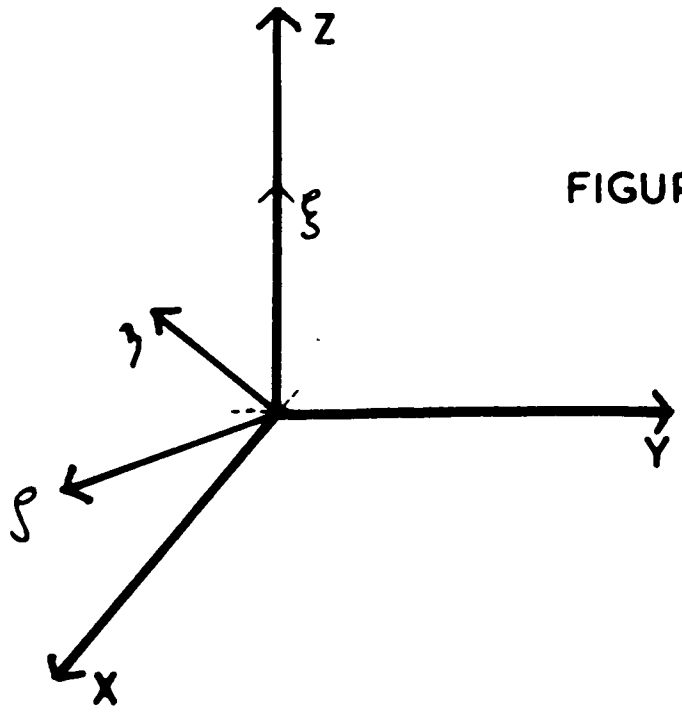


FIGURE 7·2c

define the g tensor axes as in Figure 7.2a; axes (x",y",z") parallel to what would be fourfold axes of the cube of oxygens were it undistorted, as in Figure 7.2b; and a set of symmetry axes (x',y',z') also as shown in Figure 7.2b. (These are the same as those shown in Figures 4.7a and b, and are repeated here for convenience). A further set of axes (ξ, η, ζ) are used for the fitting procedure of Chapter 8, these are shown in Figure 7.2c, they are the axes (x',y',z') rotated through 90° about z'.

With respect to axes (x",y",z") there are even order terms γ_{20}, γ^{s}_{22}, γ_{40}, γ^{s}_{42}, γ^{c}_{44}, γ_{60}, γ^{s}_{62}, γ^{c}_{64} and γ^{s}_{66}, occurring in the expansion of the potential (Equation (A2.10)) near the {e} site. If the D_2 symmetry axes (x',y',z') are chosen, these become γ_{20}, γ^{c}_{22}, γ_{40}, γ^{c}_{42}, γ^{c}_{44}, γ_{60}, γ^{c}_{62}, γ^{c}_{64} and γ^{c}_{66}. There are also some odd n terms (γ^{s}_{32}, γ^{s}_{52}, γ^{s}_{54} with respect to axes (x',y',z)) but these were not considered as they have zero matrix elements within a given configuration (§ A2.3.2).

7.3 The calculations

Two computer programmes were written in order to calculate quantities proportional to the parameters A^{m}_{n}. These programmes will be described here briefly, further details are given in Appendix IVC and D.

7.3.1 The calculation of the crystalline potential due to nearest neighbours only

We may express the electrostatic potential at a point (r,θ,ϕ) near the rare earth site as origin in the form,

$$V(r,\theta,\phi) = |e| \Big\{ r^2 \alpha_{20} Y_2^0 + r^2 \alpha_{22}^s i(Y_2^{-2} - Y_2^2) + r^2 \alpha_{22}^c (Y_2^{-2} + Y_2^2) +$$

$$+ r^4 \alpha_{40} Y_4^0 + r^4 \alpha_{42}^s i(Y_4^{-2} - Y_4^2) + r^4 \alpha_{42}^c (Y_4^{-2} + Y_4^2) + \ldots.$$

$$\ldots + r^6 \alpha_{66}^c (Y_6^{-6} + Y_6^6) \Big\} \qquad (7.1)$$

where we have expanded up to terms of 6^{th} order. The $\alpha_{n\alpha}$ are then related to the $\gamma_{n\alpha}$, defined by Equation (A2.10) with the charge q_j written in units of $|e|$, by

$$\alpha_{n0} = \gamma_{n0}$$

$$\alpha_{n\alpha} = \frac{\gamma_{n\alpha}}{\sqrt{2}} \quad (\alpha \neq 0)$$

And the γ_{nm}^c are related to A_n^m by Equation (A2.18).

A computer programme, C.F.P.II described in Appendix IVC, was written to calculate the coefficients $\alpha_{n\alpha}$, with even n and m, using Equation (A2.10). The position and magnitude in units of $|e|$, of each contributing charge was required as data, together with the lattice constant. The co-ordinate system used could be varied, and for the case of the garnets was chosen to be (x",y",z") of Figure 7.2b. The programme was checked by the following tests:-

(1) The potential due to eight charges at the corners of a cube was found to correspond to the values listed in Table A2.2,

the remaining coefficients vanishing.

(ii) The potentials determined in the case of the garnets were found to correspond to D_2 symmetry to within the error expected from the structure parameters.

(iii) The potential due to the four nearest [a] sites, as given in Table 7.2, agreed with that calculated by hand.

(iv) The coefficients due to the eight nearest neighbours in YIG were compared with corresponding values calculated by Dillon and Walker (1961) and were found to agree to within ½% of their corrected values. (Their original sixth order terms were in error). The slight discrepancies could easily arise from slightly different structure parameters being used or from rounding errors. The ratios of the terms of the same n also agreed with those of Obata (private communication). N.B. These comparisons were made on calculations based on a different set of structure parameters than those given in Table 4.1 and used for the final calculations described in this Chapter.

This programme was used to determine some of the results given in Table 7.5 and also for some of the calculations described in §6.2. The errors in the coefficients given in Table 7.5 arising from uncertainties in the structure parameters, were estimated by taking the extreme values of the parameters for YIG and calculating the potential due to the nearest oxygens. It was found that errors of ~10% occurred in the "non cubic" coefficients, compared with ~3% in the "cubic" coefficients. The small $d^6_{\bar{6}}$ coefficient was not well determined as it is

extremely sensitive to the parameters chosen, and the values of β_6^6 (proportional to α_{66}^*) given in Table 7.5 can only be considered to be of the correct order of magnitude.

7.3.2 The calculation of the contribution of all ions in the lattice to the crystal field parameters

Using the programme described in §7.3.1 it was found that other ions besides the nearest eight oxygens contributed significantly to the crystalline potential. One can see from Table 7.1 that there are triply ionised (d) site ions only $a\sqrt{4}$ Å above and below the {c} site in question. A full summation, including the contribution of all ions within a distance $2a_o$ of the {c} site, was therefore carried out, using the programme "C.F.F. Full Sum" described in Appendix IVD. This programme calculated directly the coefficients in the crystal field Hamiltonian, β_n^m (in $(\text{Å})^{-(n+1)}$), which are related to the A_n^m of Equations (A2.18) and (A2.19) by $\beta_n^m = \frac{A_n^m}{-|e|}$. If the mean radial wavefunctions $\langle r^n \rangle$ are also expressed in Å units, then the crystal field parameters V_n^m are given in cm^{-1} by

$$V_n^m = A_n^m \langle r^n \rangle = -1.1614 \times 10^5 \ \beta_n^m \ \langle r^n \rangle \qquad (7.2)$$

The axes chosen for these calculations were the symmetry axes (x',y',z') shown in Figure 7.2b. The co-ordinates and charges of the c, a and d sites were fed in as data, and the total contribution of each type of site found separately and added by hand. This was only necessary for one lattice, but

was actually done for two to check. The contributions of these ions (whose positions depend only on a_o) in other lattices being found by multiplying by the appropriate scaling factor. The contribution of the h sites, which were split into three groups, had to be found separately for each lattice; the structure parameters (x;y;z) were fed in as data for each case, and the positions of the 96 ions in the unit cell were calculated from expressions for their co-ordinates, in terms of x, y, and z, written into the programme. Finally the total contributions from c, a, d, and h sites were added by hand. (The calculation was not carried out completely on the computer in order to avoid using the storage drum).

Besides giving the total contribution from ions within a distance $2a_o$ from the {c} site origin, the programme also printed the contributions from ions lying within shells differing in radius by $a_o/4$, thus showing the convergence of the summation. A typical output, for the [a] sites in YAG, is shown in Table 7.3. The lowest two numbers in each column are dummies, the others represent the contributions from [a] site ions lying within shells the inner radii of which increase by $\frac{1}{4}a_o$ as one moves up the column.

The programme was checked in several ways:-

(i) In the case of the h sites the first shell contained only the eight nearest neighbours. The results for this shell agreed exactly with those calculated using "C. [illegible]. II" when they

Table 7.3

YAG [a] Sites

```
01   389
02   359
03   280
04   431
04   382
05   401
05   352
06   420
00   643 a0=12.000
****************
```

β_2^0	β_2^2	$\propto Y_{22}^s$
5.30426, -6	1.59128, -5	-5.99698,-12
2.40922, -4	7.22767, -4	-7.16227,-12
-1.39919, -4	-4.19757, -4	2.50111,-12
-6.57343, -4	-1.97203, -3	3.20597,-11
1.39672, -3	4.19015, -3	-4.54747,-12
3.79555, -3	1.13866, -2	-5.91172,-11
5.68948, -3	1.70685, -2	3.85626,-10
4.31808,-78	4.31808,-78	0.00000,-128
4.31808,-78	4.31808,-78	0.00000,-128
4.31808,-78	4.31808,-78	0.00000,-128
1.03307, -2	3.09921, -2	****************

β_4^0	β_4^2	β_4^4
-4.88221, -7	7.25071, -7	-1.71604, -6
1.54027, -7	-7.66298, -7	3.83731, -9
2.08926, -6	-2.31801, -6	8.12829, -6
-4.63329, -6	1.56601, -5	-7.50632, -6
-6.33345, -6	3.08447, -5	-8.22584, -7
4.25955, -5	-6.85649, -5	1.44413, -4
-1.53364, -3	3.14662, -3	-4.52160, -3
4.31808,-78	4.31808,-78	4.31808,-78
4.31808,-78	4.31808,-78	4.31808,-78
4.31808,-78	4.31808,-78	4.31808,-78
-1.50026, -3	3.12220, -3	-4.37910, -3

β_6^0	β_6^2	β_6^4	β_6^6
-1.54380,-10	-1.14493, -9	-4.21791,-10	-2.51885, -9
3.48821,-10	2.81991, -9	1.69848, -9	6.20381, -9
5.86960,-10	1.24102, -8	2.73865, -8	2.73024, -8
-3.56442, -9	3.87035, -9	8.72379, -8	8.51478, -9
2.30513, -9	6.38356, -8	1.55866, -7	1.40438, -7
-5.60516,-10	-1.81578, -7	-5.69277, -7	-3.99472, -7
1.51567, -5	-8.51418, -5	-5.90743, -4	-1.87312, -4
4.31808,-78	4.31808,-78	4.31808,-78	4.31808,-78
4.31808,-78	4.31808,-78	4.31808,-78	4.31808,-78
4.31808,-78	4.31808,-78	4.31808,-78	4.31808,-78
1.51556, -5	-8.52425, -5	-5.91041, -4	-1.87533, -4

had been multiplied by the correct factors, and the change of axes had been taken into account. For this change of axes:-

$$\begin{aligned}
&\alpha_{no} \text{ w.r.t. } (x'',y'',z'') = + \alpha_{no} \text{ w.r.t. } (x',y',z') \\
&\alpha^{s}_{n2} \quad " \quad = - \alpha^{c}_{n2} \quad " \\
&\alpha^{c}_{n4} \quad " \quad = - \alpha^{c}_{n4} \quad " \\
&\alpha^{s}_{n6} \quad " \quad = + \alpha^{c}_{n6} \quad "
\end{aligned} \tag{7.3}$$

(11) The co-ordinates of the ions fed into the programme were checked carefully by eye. As an additional check a summation was made for $\sum_j \frac{x_j y_j}{r_j^5}$ (proportional to γ^{s}_{22}) which should vanish by symmetry. Any error in an ion's position would give a non zero value for this term. Being of "second order" it is slowly converging and provides a critical test, and in all cases it was found to be zero.

(111) The c, a, and d site contributions were found for both YGG and YAG, and when scaled appropriately they agreed within the convergence error.

The additions by hand were also carefully checked.

Within the (large) approximation of the point charge model there are three sources of error in these results.

(1) Convergence error

As can be seen from Table 7.3, this is only appreciable for the second order coefficients. As a test a summation was made for these terms over all [a] sites within $4a_o$ of the rare earth site in YAG. The results are compared in Table 7.4.

Table 7.4

	β_2^0	β_2^2
Summation up to r = $2a_0$	1.0331×10^{-2}	3.0992×10^{-2}
Summation up to r = $4a_0$	1.0471×10^{-2}	3.1413×10^{-2}

It is seen that the convergence error is ~ 3% in these terms. As the second order parameters calculated on a point charge model are the least reliable, for the reasons given in §6.2, summations over further shells to improve this accuracy were not carried out.

(ii) Uncertainties in the structure parameters

A test to determine the errors in the coefficients arising from uncertainties in the structure parameters, in the case of the LGG h sites, was described in § 7.3.1. The errors in the "full sum" non-cubic coefficients will not be so large as for the nearest oxygens only, as the c, a and d sites contribute considerably to these coefficients, and their positions are known to 1 part in 12,000. In the case of β_6^6 they make a larger contribution than the h sites by an order of magnitude. Thus the full sum errors due to this cause are ~ 2% in β_4^0, β_4^4, β_6^0 and β_6^4, and ~ 5% in other coefficients.

(iii) Systematic Error due to contraction

The structure parameters given in Table 4.1 were determined at 290°K, and since a_0 has a thermal expansion coefficient of

$\sim 10^{-5}$ deg^{-1} (Geller et al. 1957), the coefficients will be subject to a systematic increase at low temperatures. This may amount to ~ 5 - 7% for the sixth order terms.

The results of the calculations are given in Tables 7.5 and 7.6. Most of the values given in Table 7.5 were taken from the contribution of the first shell of h sites. It must be emphasized that the errors given above are those inherent in the numerical calculation, and for practical purposes these values of β_n^m will be subject to far greater uncertainties due to the point charge approximation discussed in §6.2.

7.4 Discussion of the results

It is seen from Tables 7.5 and 7.6 that there is an appreciable contribution from ions more distant than the eight nearest oxygen neighbours. This immediately casts doubts on calculations based solely on the contributions from the nearest neighbours such as those of Dillon and Walker (1961) and Thomas (1962). These additional contributions are mainly to the "non-cubic" terms, although the β_6^2 coefficient due to the nearest neighbours only is of very appreciable size. In all cases the β_2^2 coefficients is of different sign for the full sum from that due to the nearest neighbours only.

In general the "distortions" from a cubic potential are large, indicating the severity of the cubic model approximation used in Chapter 4. The coefficients are of similar order of magnitude for each lattice, and apart from the second order

Table 7.5

Values of β_n^m, defined as in Equation (7.2) calculated on the basis of a point-charge ionic model of the garnet lattice, and including only the eight nearest neighbour oxygen ions of the rare earth site. The axes chosen are (x',y',z') as shown in Figure 7.2b. The errors in these values are discussed in §7.3.1 (and §7.3.2. (iii)).

Coeff. \ Lattice	LGG	YGG	LAG	YAG	YIG
β_2^0	-1.98×10^{-2}	-1.21×10^{-2}	$+2.35 \times 10^{-3}$	$+7.61 \times 10^{-3}$	-8.64×10^{-3}
β_2^2	$+3.56 \times 10^{-2}$	$+2.50 \times 10^{-2}$	$+4.46 \times 10^{-2}$	$+4.84 \times 10^{-2}$	$+2.41 \times 10^{-2}$
β_4^0	$+1.14 \times 10^{-2}$	$+1.04 \times 10^{-2}$	$+1.13 \times 10^{-2}$	$+1.03 \times 10^{-2}$	$+1.00 \times 10^{-2}$
β_4^2	$+3.01 \times 10^{-3}$	$+1.76 \times 10^{-3}$	$+2.78 \times 10^{-3}$	$+2.50 \times 10^{-3}$	$+1.71 \times 10^{-3}$
β_4^4	-3.79×10^{-2}	-3.63×10^{-2}	-4.21×10^{-2}	-3.89×10^{-2}	-3.61×10^{-2}
β_6^0	-4.72×10^{-4}	-4.38×10^{-4}	-6.18×10^{-4}	-5.84×10^{-4}	-4.53×10^{-4}
β_6^2	-1.22×10^{-3}	-8.79×10^{-4}	-1.55×10^{-3}	-1.63×10^{-3}	-7.47×10^{-4}
β_6^4	-9.00×10^{-3}	-8.12×10^{-3}	-9.23×10^{-3}	-8.07×10^{-3}	-7.86×10^{-3}
β_6^6	-8.64×10^{-5}	-2.48×10^{-4}	-5.41×10^{-5}	-2.69×10^{-4}	-2.73×10^{-6}

Table 7.6

Values of β_n^m, defined as in Equation (7.2) calculated on the basis of a point charge ionic model of the garnet lattice, and including all ions within a distance $2a_o$ of the rare earth site. The axes chosen are (x',y',z') as shown in Figure 7.2b. The errors in these values are discussed in § 7.3.2.

Coeff. \ Lattice	LGG	YGG	LAG	YAG	YIG
β_2^0	-4.08×10^{-2}	-5.07×10^{-2}	-1.47×10^{-2}	-0.73×10^{-2}	-2.65×10^{-2}
β_2^2	-1.45×10^{-2}	-2.36×10^{-2}	-0.85×10^{-2}	-0.36×10^{-2}	-2.35×10^{-2}
β_4^0	$+10.74 \times 10^{-3}$	$+9.84 \times 10^{-3}$	$+10.60 \times 10^{-3}$	$+9.69 \times 10^{-3}$	$+9.47 \times 10^{-3}$
β_4^2	$+9.67 \times 10^{-3}$	$+8.13 \times 10^{-3}$	$+10.30 \times 10^{-3}$	$+9.77 \times 10^{-3}$	$+7.84 \times 10^{-3}$
β_4^4	-2.86×10^{-2}	-2.73×10^{-2}	-3.16×10^{-2}	-2.87×10^{-2}	-2.75×10^{-2}
β_6^0	-5.24×10^{-4}	-5.08×10^{-4}	-6.78×10^{-4}	-6.39×10^{-4}	-5.00×10^{-4}
β_6^2	-1.99×10^{-3}	-1.61×10^{-3}	-2.45×10^{-3}	-2.49×10^{-3}	-1.44×10^{-3}
β_6^4	-10.21×10^{-3}	-9.27×10^{-3}	-10.67×10^{-3}	-9.44×10^{-3}	-8.96×10^{-3}
β_6^6	-1.56×10^{-3}	-1.64×10^{-3}	-1.77×10^{-3}	-1.87×10^{-3}	-1.33×10^{-3}

terms, do not show gross differences between the aluminium and gallium garnets, thus the explanation of the Dy^{3+} and Er^{3+} g values given in §4.4 and §4.5 seems justified. The coefficients might be expected to show similar trends to those observed in the g values of Nd^{3+} and Yb^{3+} (Table 3.1), but in general this is not so. However, for four ratios of parameters, given in Table 7.7, it is seen that a similar variation does occur. The

Table 7.7

Values of A_4^4/A_4^0, A_6^4/A_6^0, A_4^0/A_6^0, and A_2^0/A_4^0, calculated from the coefficients given in Table 7.6, compared with the ratios for a purely cubic field.

Ratio	Cube	LGG	YGG	LAG	YAG	YIG
A_4^4/A_4^0	-5	-2.67	-2.77	-2.97	-2.96	-2.90
A_6^4/A_6^0	+21	19.5	18.3	15.7	14.8	17.9
A_4^0/A_6^0	-	-20.5	-19.4	-15.6	-15.2	-18.9
A_2^0/A_4^0	0	-3.80	-3.12	-1.39	-0.75	-2.80

ratio A_6^4/A_6^0 is nearest the cubic value for LGG whereas the reverse is true for A_4^4/A_4^0. These trends are also observed in the ratios A_4^0/A_6^0 and A_2^0/A_4^0 where one might have expected the variation with a_0 to predominate.

In contrast to the conclusions reached in §4.2 and §4.7 the coefficients for YIG lie closest to those of YGG, suggestin

the magnetic properties in the iron garnet should lie closest to those in YGG, rather than LGG.

When experimentally determined parameters become available for one ion in each lattice, it will be extremely interesting to compare the ratio of calculated and experimental values for each parameter in each lattice, as this should be constant if screening effects are the same. This should be particularly true for the variation between yttrium and lutetium lattices, as any covalency effects should then be also constant. In general these results will provide a far more crucial test of the simple point charge model than that carried out on $PrCl_3$ and described in §6.2.

7.5 Summary

The general results of the calculations are summarised below.

(a) There are significant contributions to the C.E.F. parameters from ions more distant than the eight nearest neighbours, especially in "non cubic" terms.

(b) The distortions from a cubic field are quite large.

(c) There are no striking differences between Al and Ga lattices.

(d) The trend observed in the Nd^{3+} and Yb^{3+} g values is only followed by a few ratios of the parameters.

(e) The parameters of YIG are closest to those of YGG.

The results of this chapter will be used in Chapter 8, taking note of the conclusions of §6.2 regarding the validity of the point charge model.

CHAPTER 8

The determination of a possible set of crystal field parameters for Yb^{3+} in YGG

8.1 Introduction

The advantages of a theoretical treatment of Yb^{3+}, rather than any other rare earth ion, have been discussed in §4.7. Consequently this ion has been the object of extensive study in the garnets, and will now be considered in detail with a view to obtaining a set of crystal field parameters. Unfortunately there are as yet insufficient experimental data to enable the parameters to be determined from experiment alone. The results of the point charge calculations described in the previous chapter were therefore used to estimate the ratios of fourth, and sixth, order parameters of different m, and thereby reduce the number of parameters to be fitted to the available data. As the garnets form good regular crystals with most of the "ideal" properties outlined in Chapter 1, these ratios should only be subject to the limitations of this simple model discussed in §6.2.

Ayant and Thomas (1962) (see also Thomas 1962) have previously considered the case of Yb^{3+} in YGG and before describing the present calculations their treatment will be briefly discussed. With respect to the D_2 symmetry axes the crystal field Hamiltonian at the {c} site is given by ,

$$\mathcal{H} = B_2^0 O_2^0 + B_2^2 O_2^2 + B_4^0 O_4^0 + B_4^2 O_4^2 + B_4^4 O_4^4 + B_6^0 O_6^0 + B_6^2 O_6^2 + B_6^4 O_6^4 + B_6^6 O_6^6 \qquad (8.1)$$

where $B_n^m = A_n^m \langle r^n \rangle \theta_n = V_n^m \theta_n^m$, as given in Equations (A2.19) and (A2.20). Ayant and Thomas estimated the values of A_n^m from a point charge calculation over the nearest eight oxygen ions only and they neglected A_4^2 and sixth order terms on the strength of these calculations. Taking a value of $A_4^0 \langle r^4 \rangle$ estimated from susceptibility measurements and the calculated ratio of A_4^4/A_4^0 they fitted $A_2^0 \langle r^2 \rangle$ and A_2^2/A_2^0 to the experimental g values using perturbation theory. However, as the mean g value for small distortions from a cubic field is constant they actually fitted two parameters to two unknowns and their results can therefore have little definite physical significance. Apart from their approximation in considering nearest neighbours only, there is evidence both from the discussion of §6.2 and from the estimations made in §4.7 from Pappalardo and Woods' optical work that the sixth order terms are more important than indicated by point charge calculations.

For the determination of the parameters described here, a new set of local axes, (ξ, η, ζ) of Figure 7.2a were chosen. The values of β_n^m with respect to these axes are easily found from those listed in Table 7.6, as

$$\begin{aligned}
\beta_n^0 \text{ w.r.t. axes } (\xi,\eta,\zeta) &= \beta_n^0 \text{ w.r.t. axes } (x',y',z') \\
\beta_n^2 \quad " \quad " \quad " &= -\beta_n^2 \quad " \quad " \quad " \\
\beta_n^4 \quad " \quad " \quad " &= \beta_n^4 \quad " \quad " \quad " \\
\beta_n^6 \quad " \quad " \quad " &= -\beta_n^6 \quad " \quad " \quad "
\end{aligned} \tag{8.2}$$

As the C.E.F. parameters of n = 6 do not affect the J = 5/2 state to first order, V_2^0 V_2^2 & V_4^0 were first found approximately by considering only this state, using the calculated values of V_4^4/V_4^0 and V_4^2/V_4^0, and fitting to the available experimental data. The whole ^2F term was then considered and all four parameters V_2^0, V_2^2, V_4^0 and V_6^0 fitted, using calculated ratios for the other sixth order terms. The results will be discussed in § 8.4.

8.2 Experimental data for Yb^{3+} in XOO

The splitting of the ^2F term in cubic and D_2 symmetry crystal fields is shown in Figure 4.9. (N.B. This diagram assumes the field is predominantly 4th order, cf. Figure 4.6; the experimental results, however, are quite general but do approximate to Γ_7 states lowest). There has, up to now, been published only sufficient experimental data to provide seven independent, definite, pieces of information, and these are given in Table 8.1. They are the two splittings of the J = 5/2 multiplet, and the three g values of the lowest J = 5/2 and J = 7/2 doublets. The g values of the J = 5/2 doublet provide only two independent pieces of information, as within the J = 5/2 manifold they can be expressed in terms of two parameters (cf. § 4.6). As mentioned in § 4.7, there is a level at 550 cm^{-1} above the lowest J = 7/2 state, but its identification is not at all certain. The g values given in Table 8.1 are subject to ambiguity between the direction of g_x and g_y, but

Table 8.1

Experimental optical and E.P.R. data on YbY^{3+} in YOC. The results of several authors is given to indicate reliability. The axes chosen are shown in Figure 7.2a.

	J = 5/2		J = 5/2 lowest doublet			J = 7/2 lowest doublet		
Author	Δ_1 cm^{-1}	Δ_2 cm^{-1}	g_x	g_y	g_z	g_x	g_y	g_z
Boakes et al. (1959)						3.73 (±0.01)	3.60 (±0.01)	2.850 (±0.015)
Pappalardo & Wood (1960)	160	290						
Wickersheim & White (1962)			1.80	1.98	0.35	3.73	3.60	2.85
Crosswhite (Priv. Comm. 1961)	153	282	1.80	1.98	0.41	3.73	3.60	2.85
Crosswhite (Priv. Comm. 1962)	153	274	1.80	1.98	0.35	3.73	3.60	2.85

the correlation between the numbers is definite, that is 1.80 is measured in the same direction as 3.73 etc. Values for Δ_2 of both 262 cm^{-1} and 274 cm^{-1} were used in the fitting, but the latter is probably more correct (Crosswhite, private communication).

8.3 The fitting procedure

The results of the point charge calculations given in Table 7.6 indicate that none of the nine parameters is likely to be small enough to neglect. The fact that terms of n = 2 and 6 may well be important is indicated firstly by the crystal lattice, where the two nearest (d) sites mentioned in §7.3.2. have axial symmetry about the Z axis of the unit cell and therefore give rise to n = 2, 4, and 6 terms for the axes (ξ, η, ζ) chosen; and secondly by the axial symmetry of the Yb^{3+} g values, again about the Z axis. All nine parameters have, therefore, to be treated on an equal basis.

Assuming that the ratios of the parameters can be taken from the point charge values, there are three unknowns:- $A_2^0\langle r^2\rangle$, $A_4^0\langle r^4\rangle$, and $A_6^0\langle r^6\rangle$. However since the second order (n = 2) terms are not well determined on the point charge model (see §6.2 and §7.3.1) these were both fitted independantly, and $A_2^0\langle r^2\rangle$, $A_2^2\langle r^2\rangle$, ($\frac{\quad}{\quad}$), $A_4^0\langle r^4\rangle$ and $A_6^0\langle r^6\rangle$ were taken as adjustable parameters. The other parameters, expressed as ratios with respect to $A_4^0\langle r^4\rangle$ and $A_6^0\langle r^6\rangle$ were given the values estimated from the full point charge

summations (Table 7.6). These ratios are given in Table 8.2, and are denoted by $\xi_0, \eta_0, \zeta_0, \Omega$, and (H), (ξ_0 η_0 and ζ_0 must not be confused with the axes (ξ, η, ζ)).

Table 8.2

Values of ratios of A_n^m/A_n^0 for XOO (From Table 7.6) expressed w.r.t. axes (ξ, η, ζ)

$$\xi_0 = \frac{A_4^2}{A_4^0} = -0.8262 \qquad \zeta_0 = \frac{A_6^2}{A_6^0} = -3.176$$

$$\eta_0 = \frac{A_4^4}{A_4^0} = -2.769 \qquad \Omega = \frac{A_6^4}{A_6^0} = +16.27$$

$$(H) = \frac{A_6^6}{A_6^0} = -3.240$$

Pappalardo and Wood (1960) find the splitting between the $J = 7/2$ and $J = 5/2$ states to be 10,300 cm^{-1}, which gives spin-orbit coupling constant λ of -2943 cm^{-1}. As discussed in §4.7, because of this large splitting the pure J state g values are only affected by the presence of the other state by ~ 2%. However one might expect the energy level positions to be affected by $\sim \frac{(G_x E_x)^2}{10,300}$ i.e. by ~5 - 10%, and although splittings would be affected to a smaller extent; the presence of the other state is clearly important. In spite of this fact, the fitting was carried out in two stages as described below. Subsequent tests showed that, for the order of magnitude of the C.E.F. parameters found, Δ_1 was hardly affected by the presence of

the $J = 7/2$ state whereas Δ_2 was changed by about 20%.

For each of the two stages of fitting, the adjustable C.E.F. parameters in the appropriate Hamiltonian were varied to give a minimum value of a function F, defined in a general manner below as equal to the sum of the squares of the differences between experimental and theoretical splittings and g values, with appropriate weighting factors (ω).

$$F = \omega_1(\Delta_1^e - \Delta_1^t)^2 + \omega_2(\Delta_2^e - \Delta_2^t)^2 + \sum_{\substack{i = 5,7,9 \\ J = 5/2}} \omega_i(g_i^e - g_i^t)^2 + \sum_{\substack{j = 5,7,9 \\ J = 7/2}} \omega_j(g_j^e - g_j^t)^2$$

where $\omega_j = 0$ for the first stage ($J = 5/2$) of fitting. ...(6.3)

So that in effect $F = f(V_2^0, V_2^2, V_4^0)$

or $F = f(V_2^0, V_2^2, V_4^0, V_6^0)$, in the two cases.

The minimisation of F with respect to these variables was carried out using a computer routine written by M. J. D. Powell. A separate programme was used for each stage, "Yb 5/2 Fit", and "$Yb^{2}F$ Full Fit", and these are described in Appendix IV F and G. The iterative method (Powell 1962) used in the minimisation is similar to the method of steepest descents but has second order convergence. It allows a minimum of F to be found from poor starting values of the parameters, which is not possible with methods such as that of least squares.

As F is such a complex function of the parameters V_n^m there are a large number of minima in the three, or four, dimensional surface which they form. The programmes were therefore run

many times with starting parameters of different signs and magnitudes to ensure that the lowest minimum was found. The "fitted" crystal field parameters being taken as those giving this lowest minimum, provided the results were physically consistent.

In fitting to the experimental data one is immediately faced with several ambiguities which add to the difficulty of finding the correct minimum. Firstly there is the experimental ambiguity that while $g_z = g_J$, g_x or g_y can equal either g_γ or g_J ; and secondly there is the problem of the signs of the g values as discussed in Appendix I.

As only three separate pieces of experimental information are required to fit the three parameters in the J = 5/2 fit, for example, the first ambiguity was overcome by fitting in the first place to only Δ_1 Δ_2 and g_z. It was then possible to compare the calculated values of g_γ and g_J with the experimental values, and correlate them according to their magnitude.

The second ambiguity was overcome by giving the experimental values the theoretical signs. Although possible, fitting to the moduli of the g values was avoided as it was liable to be misleading. Again it was possible to fit at first to only one g value, g_z, with only two alternatives of sign, and to give g_x and g_y the theoretical signs of this best fit when fitting to the full data.

Before giving the results, the crystal field matrices and

formulae used will be discussed. A brief account of the tests made on the programmes will also be given.

8.3.1 Fitting to the J = 5/2 state data alone

Within a manifold of states of $J = 5/2$ the D_2 symmetry crystal field Hamiltonian may be written, with respect to axes (ξ, η, ζ) of Figure 7.2c, as

$$\mathcal{H} = V_2^0 \alpha_J O_2^0 + V_2^2 \alpha_J O_2^2 + V_4^0 \beta_J (O_4^0 + \xi_0 O_4^2 + \eta_0 O_4^4) \quad (8.4)$$

where $V_n^m = A_n^m \langle r^n \rangle$. ξ_0 and η_0 are given in Table 8.2 from the point charge model. $\alpha_J = \frac{2}{35}$, and $\beta_J = \frac{-2}{9 \times 33}$ for Yb^{3+}, from Table 4.7. The matrix of this Hamiltonian, referred to a basis of states within a manifold of $J = 5/2$, splits into two identical 3 x 3 matrices (Kramer's theorem), one of which is given in Table 8.3. Numerical values of α_J, β_J, ξ_0 and η_0

Table 8.3

Matrix of the crystal field Hamiltonian for Yb^{3+} in YGO (Equation (8.4)), referred to a basis of states $|J, J_\zeta\rangle$ within a manifold of $J = 5/2$

	$\left\|\frac{5}{2}, \frac{5}{2}\right\rangle$	$\left\|\frac{5}{2}, \frac{1}{2}\right\rangle$	$\left\|\frac{5}{2}, -\frac{3}{2}\right\rangle$
$\left\langle\frac{5}{2}, \frac{5}{2}\right\|$	$+0.57143\ V_2^0$ $-0.38095\ V_4^0$	$+0.18070\ V_2^2$ $+0.14930\ V_4^0$	$+0.47167\ V_4^0$
$\left\langle\frac{5}{2}, \frac{1}{2}\right\|$	$+0.18070\ V_2^2$ $+0.14930\ V_4^0$	$-0.45714\ V_2^0$ $-0.76190\ V_4^0$	$+0.24244\ V_2^2$ $-0.11128\ V_4^0$
$\left\langle\frac{5}{2}, -\frac{3}{2}\right\|$	$+0.47167\ V_4^0$	$+0.24244\ V_2^2$ $-0.11128\ V_4^0$	$-0.11429\ V_2^0$ $+1.1429\ V_4^0$

have been substituted. The other matrix has identical matrix elements if the basis states are written $|-\frac{5}{2}\rangle$, $|-\frac{3}{2}\rangle$, $|\frac{1}{2}\rangle$ instead of $|\frac{5}{2}\rangle$, $|\frac{3}{2}\rangle$, and $|-\frac{1}{2}\rangle$.

The lowest eigenstate of this matrix may be written in terms of states $|J_z\rangle$ as

$$|+\rangle = a\,|\tfrac{5}{2}\rangle + b\,|\tfrac{1}{2}\rangle + c\,|-\tfrac{3}{2}\rangle$$

with Kramers conjugate (8.5)

$$|-\rangle = -a\,|-\tfrac{5}{2}\rangle - b\,|-\tfrac{1}{2}\rangle - c\,|\tfrac{3}{2}\rangle$$

Then from Equations (1.3),

$$g_z = -g_J\left[2\sqrt{5}\,ac + 3b^2 + 4\sqrt{2}\,bc\right]$$
$$g_z = -g_J\left[2\sqrt{5}\,ac + 3b^2 - 4\sqrt{2}\,bc\right]$$
$$g_y = g_J\left[5a^2 + b^2 - 3c^2\right] \qquad (8.6)$$

The fitting was carried out with the programme "Yb $\frac{5}{2}$ Fit" (see Appendix IV F) which used the matrix of Table 8.3, and Equations (8.6), to calculate F from Equation (8.3).

The programme was tested in several ways.

(i) The matrix was carefully checked by eye, and also by checking its eigenvalues and eigenvectors with those obtained by feeding the matrix elements individually into Programm CL171a (Appendix IV E).

(ii) The programme was checked against "Yb^{2}F Full Fit" as described in test (IV) on that programme.

(iii) Trial fits were made where the "experimental data" was calculated from given crystal field parameters using Programme CL171b (Appendix IV E). Starting from parameters

about 10% different from these, the programme found the correct values, and reduced F to 10^{-5} if either the correct sign, or the moduli, of the g values were taken. A trial starting with the three parameters of opposite sign, however, did not find the true minimum, but one for which F = 6,500, although two of the "fitted" parameters had the correct sign. This latter check emphasised the need to start near the "true" parameters if the "correct" minimum was to be found.

8.3.2 Fitting to the data for the full ^2F term

In order to fit the data for both the $J = 5/2$ and $J = 7/2$ states, the matrix of the crystal field Hamiltonian, given by Equation (8.7) below, was written referred to a basis of states $|L = 3, S = \frac{1}{2}, L_J, S_J\rangle$. The D_2 symmetry crystal field Hamiltonian may be written, with respect to axes (ξ, η, ζ) as

$$\mathcal{H} = V_2^0 \alpha_L O_2^0 + V_2^2 \alpha_L O_2^2 + V_4^0 \beta_L (O_4^0 + \xi_0 O_4^2 + \eta_0 O_4^4) +$$

$$+ V_6^0 \gamma_L (O_6^0 + \zeta_0 O_6^2 + \Omega O_6^4 + \textcircled{H}\, O_6^6) + \lambda L.S. \qquad (8.7)$$

where the ratios ξ_0, η_0, ζ_0, Ω, and $\textcircled{H}$, are defined in Table 8.2. For Yb^{3+}, $\alpha_L = \frac{2}{45}$, $\beta_L = \frac{-2}{45.11}$ and $\gamma_L = \frac{4}{27.11.13}$, as given in Table 4.7; and $\lambda = -2943$ (Pappalardo and Wood 1960).

The matrix again splits into two identical matrices, one half being given in Table 8.4, where $\lambda' = \lambda/2$. A typical eigenstate of this matrix may be written, in terms of states $|L_J, \text{Sign of } 2S_J\rangle$, as

$$|+\rangle = a|3, +\rangle + b|1, +\rangle + c|-1, +\rangle + d|-3, +\rangle + e|2, -\rangle + f|0, -\rangle + g|-2, -\rangle$$

	$\lvert 3,+\rangle$	$\lvert 1,+\rangle$	$\lvert -1,+\rangle$	$\lvert -3,+\rangle$	$\lvert 2,-\rangle$	$\lvert 0,-\rangle$	$\lvert -2,-\rangle$
$\langle 3,+\rvert$	$3\lambda'$ $15\alpha V_2^0$ $180\beta V_4^0$ $180\gamma V_6^0$	$\sqrt{15}\alpha V_2^2$ $18\sqrt{15}\beta\xi_0 V_4^0$ $24\sqrt{15}\gamma\Sigma_0 V_6^0$	$12\sqrt{15}\beta\gamma_0 V_4^0$ $60\sqrt{15}\gamma\Omega V_6^0$	360γ ⑪ V_6^0	0	0	0
$\langle 1,+\rvert$	$\sqrt{15}\alpha V_2^2$ $18\sqrt{15}\beta\xi_0 V_4^0$ $24\sqrt{15}\gamma\Sigma_0 V_6^0$	λ' $-9\alpha V_2^0$ $60\beta V_4^0$ $2700\gamma V_6^0$	$6\alpha V_2^2$ $-60\beta\xi_0 V_4^0$ $360\gamma\Sigma_0 V_6^0$	$12\sqrt{15}\beta\gamma_0 V_4^0$ $60\sqrt{15}\gamma\Omega V_6^0$	$\lambda'\sqrt{10}$	0	0
$\langle -1,+\rvert$	$12\sqrt{15}\beta\gamma_0 V_4^0$ $60\sqrt{15}\gamma\Omega V_6^0$	$6\alpha V_2^2$ $-60\beta\xi_0 V_4^0$ $360\gamma\Sigma_0 V_6^0$	$-\lambda'$ $-9\alpha V_2^0$ $60\beta V_4^0$ $2700\gamma V_6^0$	$\sqrt{15}\alpha V_2^2$ $18\sqrt{15}\beta\xi_0 V_4^0$ $24\sqrt{15}\gamma\Sigma_0 V_6^0$	0	$\lambda'\sqrt{12}$	0
$\langle -3,+\rvert$	360γ ⑭ V_6^0	$12\sqrt{15}\beta\gamma_0 V_4^0$ $60\sqrt{15}\gamma\Omega V_6^0$	$\sqrt{15}\alpha V_2^2$ $18\sqrt{15}\beta\xi_0 V_4^0$ $24\sqrt{15}\gamma\Sigma_0 V_6^0$	$-3\lambda'$ $15\alpha V_2^0$ $180\beta V_4^0$ $180\gamma V_6^0$	0	0	$\lambda'\sqrt{6}$
$\langle 2,-\rvert$	0	$\lambda'\sqrt{10}$	0	0	$-2\lambda'$ $0.V_2^0$ $-420\beta V_4^0$ $-1080\gamma V_6^0$	$\sqrt{30}\alpha V_2^2$ $-3\sqrt{30}\beta\xi_0 V_4^0$ $-48\sqrt{30}\gamma\Sigma_0 V_6^0$	$60\beta\gamma_0 V_4^0$ $-360\gamma\Omega V_6^0$
$\langle 0,-\rvert$	0	0	$\lambda'\sqrt{12}$	0	$\sqrt{30}\alpha V_2^2$ $-3\sqrt{30}\beta\xi_0 V_4^0$ $-48\sqrt{30}\gamma\Sigma_0 V_6^0$	$-12\alpha V_2^0$ $360\beta V_4^0$ $-3600\gamma V_6^0$	$\sqrt{30}\alpha V_2^2$ $-3\sqrt{30}\beta\xi_0 V_4^0$ $-48\sqrt{30}\gamma\Sigma_0 V_6^0$
$\langle -2,-\rvert$	0	0	0	$\lambda'\sqrt{6}$	$60\beta\gamma_0 V_4^0$ $-360\gamma\Omega V_6^0$	$\sqrt{30}\alpha V_2^2$ $-3\sqrt{30}\beta\xi_0 V_4^0$ $-48\sqrt{30}\gamma\Sigma_0 V_6^0$	$2\lambda'$ $0.V_2^0$ $-420\beta V_4^0$ $-1080\gamma V_6^0$

Table 8.4

Matrix of the crystal field Hamiltonian for Yb^{3+} in YGG, (Equation 8.7), referred to a basis of states $\lvert L_z S_z\rangle$ within the ^2F term.

with Kramer's Conjugate,

$$|\bar{+}\rangle = -a|-3,-\rangle - b|-1,-\rangle - c|1,-\rangle - d|3,-\rangle - e|-2,+\rangle$$
$$- f|0,+\rangle - g|2,+\rangle \quad \ldots(8.8)$$

Using these in Equation (2.3) we have

$$g_\zeta = -\left[(2ag\sqrt{6} + 2de\sqrt{6} + 2bg\sqrt{10} + 2ce\sqrt{10} + 2cf\sqrt{12} + 2bf\sqrt{12}) + (4ad + 4bc + 4eg + 2f^2)\right]$$

$$g_\gamma = -\left[(2ag\sqrt{6} - 2de\sqrt{6} - 2bg\sqrt{10} + 2ce\sqrt{10} - 2cf\sqrt{12} + 2bf\sqrt{12}) + (4ad + 4bc - 4eg - 2f^2)\right]$$

$$g_J = \left[8a^2 + 4b^2 - 4d^2 + 2e^2 - 2f^2 - 6g^2\right] \quad \ldots(8.9)$$

The general matrix of Table 8.4 was written into the programme "Yb^2F Full Fit" used for the second stage of fitting, and described in Appendix IV C. In most cases the point charge ratios given in Table 8.2 were fed in as data. The g values were calculated from the above formulae (Equation (8.9)).

The programme was tested in the following manner

(1) Using it to diagonalise the matrix (see Appendix IV C) with a cubic crystal field of:-

(a) point charge values for V_4^0 and V_6^0 (Table 9.7)

(b) $\zeta_0 = \zeta_0 = (H) = 0$, $\gamma_0 = -5$ and $\Omega = +21$ (corresponding to a perfect cube of oxygens).

(c) $\lambda = -10^5$ cm^{-1} (so that the spin-orbit coupling $\gg$ C.F., giving pure "J" states)

the programme gave the correct "pure J state" g values of 10/7 and 24/7. This result is shown in the lower portion of Table 8.6 (no. D1) where the results of other diagonalisation tests are also given.

(ii) With the same data as for test (1) but with $\lambda = -2943\ cm^{-1}$, the matrix was diagonalised to determine the effect on the g values of the nearby J state. It is seen from run No. D2, Table 8.6, that the g value of each Γ_7 is raised by the same amount, ~1%. This has been discussed in §4.7 (where an estimation of the effect was made for a larger value of V_6^0).

(iii) The programme gave the correct parameters for a trial fit similar to that carried out in test (iii) on "Yb 5/2 Fit".

(iv) Taking the three parameters given by a fit using "Yb 5/2 Fit" (those of run no. 7 given in Table 8.5) and diagonalising the matrix with a value of $\lambda = -5 \times 10^6\ cm^{-1}$, the programme gave the same splittings and J = 5/2 g values, as "Yb 5/2 Fit" (run no. D3 of Table 8.6). As the two matrixes were written in different representations this formed a rigorous cross check.

(v) To establish the effect of the J = 7/2 state on the J = 5/2 splittings, diagonalisations were made for some values of V_2^0, V_2^2 and V_4^0 fitted by the "Yb 5/2 Fit" programme, and a value of V_6^0 of ~ 75 cm^{-1}. These showed that only Δ_2 was appreciably affected, by about 20%.

8.3.3 Sequence of fitting

Fitting was mainly carried out with the "Yb 5/2 Fit" programme, as this was faster and could be used to decide between the various ambiguities. Some principal results, from

both stages, are given in Table 8.5 (5/2 Fit) and Table 8.6 (^{2}F Fit). The upper numbers in each row represent starting parameters and experimental data, and the lower numbers the fitted parameters and calculated splittings and g values. n is the number of pieces of information fitted to, and F_n the final value of F calculated from the n splittings and g values. The figure in brackets in the last column is the weighting factor given to the square of the difference in g values.

The initial starting values taken were the point charge values:-

$$V_2^0 = +\ 613\ cm^{-1},\ V_2^2 = -\ 474\ cm^{-1};\ V_4^0 = -66\ cm^{-1},\ V_6^0 = +\ 4cm^{-1} \qquad (8.10)$$

(Calculated from the coefficients in Table 7.6, and values of $\langle r^n \rangle$ (in Å) from Table 4.3), but with V_2^0 and V_2^2 reduced to 100 cm^{-1} and - 100 cm^{-1} respectively in view of the results of the investigation on $PrCl_3$ discussed in §6.2. It was found that V_2^2 changed sign in the fit and the result was close to that of run no. 1 in Table 8.5. As V_2^0 and V_2^2 were the least well determined parameters their starting values were allowed to take all possible signs, each combination being fitted to Δ_1, Δ_2, + g_z, and - g_z, whilst V_4^0 was assumed to have the point charge sign. Most of these fits tended to require a positive V_2^2, and although F_3 was usually reduced to zero, the other two g values seldom resembled the experimental values. In cases where V_4^0 was initially given a positive value the

Table 6.5

Results of runs of the "Yb 5/2 Fit" programme

No.	n	$V_2^0 cm^{-1}$	$V_2^2 cm^{-1}$	$V_4^0 cm^{-1}$	Δ_1	Δ_2	g_5	g_3	g_J	$\frac{(\omega_1)}{F_n}$
1	3	220	-180	-160	153	262	-0.35	(-1.80)	(-1.98)	(10,000)
		208	187	-151	153	262	0.35	-1.95	-2.15	10^{-4}
2*	5	220	180	-150	153	262	0.35	-1.80	-1.98	(100,000)
		206	175	-152	153	262	0.30	-1.88	-2.17	4578
3	5	206	176	-152	153	262	0.35	-1.80	-1.98	g_3, g_5 ($\times 10^9$)
		-0.76	12.05	-12.0	5	22	-0.30	-1.80	-1.98	84,070
4	5	-0.76	12.05	-12	153	262	-0.35	-1.98	-1.80	g_3, g_5 ($\times 10^9$)
		-2.4	6.4	-5.3	4	9	-0.41	-1.98	-1.80	90,000
5	3	-75	200	-200	153	262	-0.35	(-1.80)	(-1.98)	(10,000)
		-97	258	-167	153	262	-0.35	-2.19	-1.68	10^{-5}
6	5	-97	258	-167	153	262	-0.30	-1.98	-1.80	(10,000)
		-95	216	-171	146	265	-0.44	-2.04	-1.74	192
7†	5	-30	100	-50	153	274	-0.35	-1.98	-1.80	(10,000)
		-94	222	-176	149	276	-0.43	-2.03	-1.75	135

Table 8.6

Results of runs of the "Yb ^2F Full Fit" programme

No.	Mod. or Sign	V_2^0 cm^{-1}	V_2^2 cm^{-1}	V_4^0 cm^{-1}	V_6^0 cm^{-1}	Δ_1 cm^{-1}	Δ_2 cm^{-1}	J = 5/2			J = 7/2			$\|(\omega_i, j_\xi)\|$
								g_ξ	g_η	g_ζ	g_ξ	g_η	g_ζ	F_n
1	M4	208	187	-151	4	153	274	|-0.35|	(-1.80)	(1.98)	|-2.85|	(3.73)	(-3.60)	(10,000)
		210	209	-165	46	153	274	-0.35	-1.96	2.21	-2.85	4.19	-3.33	10^{-5}
2*	38	210	209	-165	46	153	274	-0.35	-1.80	1.98	-2.85	3.73	-3.60	(10,000)
		203	200	-176	74	146	277	-0.28	-1.79	2.28	-2.99	3.94	-3.39	2,053
3†	38	-97	258	-167	74	153	274	0.35	-1.98	1.80	-2.85	3.60	-3.73	(10,000)
		-86	297	-193	72	152	276	0.27	-2.14	1.92	-2.94	3.42	-3.65	1,031
(4)	S8	-86	297	-193	72	153	274	0.35	-1.98	1.80	-2.85	3.60	-3.73	(10,000)
		-77	370	-253	196	153	274	0.44	-2.07	1.91	-3.00	3.72	-3.73	644

DIAGONALISATION ONLY

No.	V_2^0 cm^{-1}	V_2^2 cm^{-1}	V_4^0 cm^{-1}	V_6^0 cm^{-1}	Δ_1 cm^{-1}	Δ_2 cm^{-1}	J=5/2 ε_ζ	J=5/2 ε_η	J=5/2 ε_ζ	J=7/2 ε_ζ	J=7/2 ε_η	J=7/2 ε_ζ	Comment
D1	0	0	-89	4	0	203	1.429	-1.429	1.429	-3.429	3.429	-3.429	Cube $\lambda = -10^5$ cm^{-1}
D2	0	0	-89	4	0	201	1.445	-1.445	1.445	-3.445	3.445	-3.445	Cube $\lambda = -2943$ cm^{-1}
D3	-34	222	-176	74	149	276	0.44	-2.03	1.75	-3.00	3.62	-3.80	$\lambda = -5 \times 10^6$ cm^{-1}

fit was very poor.

The best fit found by the "Yb 5/2 Fit" programme was that of run no.7 of Table 8.5. There are two reasons why this is better than that of run no. 2. Firstly, as the wavefunctions and g values of a J = 5/2 doublet depend on only two parameters, a strong fit to two of them, by very heavy weighting, should give the third with the correct sign according to the formulae for the g values chosen. Two strong fits to g_3 and g_5 were made in runs no. 3 and 4, both giving g_5 as negative, the same sign as in fit no. 7. Secondly, we can correlate the signs of the calculated g values in the two programmes by comparing runs 7 of Table 8.5, and D3 of Table 8.6 where it is seen that g_5 has the same sign as for the cubic case, as do the other two g values. It is probably unlikely that distortions would be so great as to change the sign of g_5 from its cubic value.

The values of parameters given by the first stage of fitting were then used as starting values in the "Yb ^2F Full Fit" programme, together with the point charge value of V_6^0. Typical results are given in Table 8.6, where run no. 3 represents the best overall fit having g values of the correct sign. Two further points may be noted:-

(1) Run no. 4 of Table 8.6 was carried out using values of the ratios $f_0 = -0.169$, $f_3 = -3.48$, $f_5 = -1.92$, $\Omega = 17.7$, and $\langle H \rangle = -0.54$ calculated on a point charge model of nearest neighbours only, Table 7.5. It is seen that although F is smaller,

the fit has been partly brought about by a very large value of the "free" V_2^2, and has almost axial symmetry about g_z . The full summation values of ratios must be given more weight than those used here.

(11) By slightly changing each of the values of the ratios in turn from the values in Table 8.4 and diagonalising the matrix with values of the parameters as given by run no. 3 in Table 8.6, it was found that F decreased when ζ_o and (H) decreased, and when ζ_o , ζ_o , and Ω increased.

Finally we may note that, as seen from Table 8.6, the fits give the correct correlation between the values of g_x and g_y for the two states (cf. Table 8.1).

8.4 Discussion of results and conclusions

The best fit results of run no. 7 of Table 8.5, and run no. 3 of Table 8.6, are compared in Table 8.7 with the values calculated solely from the point charge models. It must be

Table 8.7

Various estimations of the C.F. Parameters for Yb^{3+} in YGG

Comment	$V_2^o cm^{-1}$	$V_2^2 cm^{-1}$	$V_4^o cm^{-1}$	$V_6^o cm^{-1}$
Point charge values (n.n. only)	+242	+498	-91	+3.6
Point charge n.n. values, if cubic	0	0	-89	+4
Point charge values (Full Sum)	+613	-474	-86	+4
Best Fit (Yb 5/2 Fit)	-94	+222	-176	-
Best Fit (Yb ^2F Full Fit)	-86	+297	-193	+72

emphasized that the sole criterion for these fits has been a physically consistent minimum value of F when values for the ratios of Table 8.2 are fixed by the point charge model. These ratios may be a severe approximation to the true values, and the main discrepancies in the fit found, which should be good as the whole $(4f)^{13}$ configuration is considered, must be attributed to the values taken for these ratios. There is the danger that the four "free" parameters may have been varied excessively to force the fit as appears to have been the case of run no. 4 of Table 8.6, where ratios were taken from the nearest neighbours only. A further danger is that the sixth order terms will be determined mainly by the three ground state g values alone, and these are also strongly dependent on the lower order terms which affect all the splittings and g values to the same extent. A similar fitting procedure has been carried out by Leask et al. (1963) on cerium magnesium nitrate, where a crystal field of C_{3v} symmetry was fitted to purely experimental data, and it was found that some parameters had to be given excessively large values in order to fit all the data within experimental accuracy. Their results illustrate the danger of purely computational fitting, and also cast some doubts on the validity of the conventional crystal field approach when applied to the magnetic properties of several J states.§ However this approach has been used successfully in many other cases (e.g. for europium ethyl sulphate (Judd 1959)).

The best fit values of the C.F. parameters given in Table 8.7 show that V_2^0 and V_2^2 have opposite signs to their point charge values. However it is these parameters which are poorly determined on the point charge model, and to which induced moments on neighbouring ions make the largest contribution. In the garnets these contributions may well be large, as the oxygen sites are of very low symmetry, and could reverse the overall sign of the second order terms. In magnitude, the fitted parameters are smaller than the point charge values calculated for V_2^0 and V_2^2, twice as big as those calculated for V_4^0 and about 20 times that calculated for V_6^0. They thus show a similar relation to the calculated values as that found for $PrCl_3$ (§ 6.2).

In Table 8.8 the wavefunctions found for the lowest $J = 5/2$

Table 8.8

Coefficients of the states $|J = 5/2, J_z\rangle$ in the lowest doublet of the $J = 5/2$ state of Yb^{3+} in cubic and D_2 (YGG) crystal fields. The wavefunction is given by equation (8.5).

Comment	a	b	c
Pure Cube	-0.408	0	-0.913
Force fit to g_z , g_z (No. 4 of Table 8.6)	-0.312	+0.174	-0.934
Best Fit of Yb 5/2 Fit. Run No. 7 of Table 8.5.	-0.323	+0.177	-0.930
Case B of §4.6, Ptb. theory	-0.333	+0.184	-0.947

doublet are given, and a comparison is made between the various fits. The corresponding wavefunction found from perturbation theory in §4.8, that is with $g_x = g_y = g_z$, is also given. (The sign of b has been changed from that in Equation (4.31) in order to refer the wavefunction to axes (ξ , η , ζ)). The properties of the state are probably best described by the wavefunction from the J = 5/2 fit no. 7, as it is seen from Table 8.5 that both splittings and g values are close to the experimental values. The fact that this fit is so good, in spite of the neglect of the J = 7/2 state, could be explained by considering the Hamiltonian of Equation (8.4) as an "effective crystal field Hamiltonian" operating within a J = 5/2 manifold but including effects of the 7/2 state. This effective Hamiltonian must have the same form as Equation (8.4) because of the D_2 symmetry, and it is conceivable that the fourth order terms would have the same ratio. The V_n^m's fitted would then not be the true V_n^m's, as given by the full ^2F fit, but effective parameters.

From the results of the best ^2F full fit, Table 8.7, we have a possible set of crystal field parameters for Yb^{3+} in YCO:-

$A_2^0 \langle r^2 \rangle = -86 \text{ cm}^{-1}$ $A_4^0 \langle r^4 \rangle = -193 \text{ cm}^{-1}$ $A_6^0 \langle r^6 \rangle = +72 \text{ cm}^{-1}$

$A_2^2 \langle r^2 \rangle = +297 \text{ cm}^{-1}$ $A_4^2 \langle r^4 \rangle = +159 \text{ cm}^{-1}$ $A_6^2 \langle r^6 \rangle = -229 \text{ cm}^{-1}$

$A_4^4 \langle r^4 \rangle = +535 \text{ cm}^{-1}$ $A_6^4 \langle r^6 \rangle = +1315 \text{ cm}^{-1}$

$A_6^6 \langle r^6 \rangle = -233 \text{ cm}^{-1}$

where the axes chosen are (ξ , η , ζ) of Figure 7.2c. (8.11)

The errors in these parameters are mainly determined by the validity of the approximations made, and may therefore amount to up to-50% of the values given in some cases. They represent estimations made using a conventional approach, and a point charge model of the lattice. It will be extremely interesting and a rigorous test of the methods used, to compare the results with parameters obtained completely from experimental work, if and when sufficient data become available.

These parameters give wavefunctions for the lowest doublets in each J state of the form of Equation (8.8) where the coefficients are listed in Table 8.9. Cubic wavefunctions (for a large λ) are given for comparison. The energy levels of the

Table 8.9

Coefficients, in Equation (8.8) for the wavefunction of the lowest doublet in the two J states of Yb^{3+} in YGG. Cubic wavefunctions are given for comparison (in the case of $\lambda \rightarrow -\infty$)

State	a	b	c	d	e	f	g
Γ_7 $J = \frac{5}{2}$ (Cubic)	0	0.468	0	0.378	-0.771	0	-0.154
Lowest doublet "J = 5/2"	-0.007	0.529	-0.168	0.285	-0.768	0.132	-0.059
Γ_7 $J = \frac{7}{2}$ (Cubic)	0	0.422	0	0.327	0.268	0	0.802
Lowest doublet "J = 7/2"	0.097	0.322	-0.128	0.307	0.272	-0.162	0.822

"J = 7/2" state are at :-

$$0\ cm^{-1},\ 517\ cm^{-1},\ 697\ cm^{-1},\ \text{and}\ 796\ cm^{-1} \qquad (8.12)$$

The value of 517 cm^{-1} for the first excited state is close to the 550 cm^{-1} fitting found by Pappalardo and Wood (1960).

Finally it may be noted that if the parameters of Equation (6.11) can be taken with confidence, in particular the value of V_2^0, the ambiguity between the experimental values of g_x and g_y for Yb^{3+} is removed. In fact g_x, the larger of the two values as listed in Table 3.1, will lie along fourfold axis of the nearest neighbour oxygen "cube."

CHAPTER 9

Interaction shifts observed in the weakly paramagnetic garnet lattices

9.1 Introduction

In this chapter, the results, given in Table 3.2, of the measurements on Yb^{3+} in weakly paramagnetic garnet lattices will be discussed. Under normal circumstances, if the concentration of rare earth ions in a crystal lattice is increased the additional magnetic and exchange interactions between the ions generally broaden the absorption and so preclude the study of individual ions by paramagnetic resonance. However, sharp resonances should be observed in cases where a Kramers ion is incorporated in a paramagnetic lattice in which the magnetic moments of the host ions do not contain time dependent components. That is when the host ions are in a singlet ground state at the temperature of the experiment and their moment arises only from the second order Zeeman effect. In these cases the line should not be broadened, but only shifted by the interactions, as will be shown in § 9.2. The case of Yb^{3+} in a paramagnetic garnet exhibiting only a temperature independent susceptibility appeared to be a suitable system in which to observe such an effect, and sharp resonances were observed in TmAG, TmGG, and EuGG. The results for Yb^{3+} in TmAG are believed to show an unambiguous interaction shift.

Resonance has previously been observed from individual ions in paramagnetic lattices in two other cases. (1) when

the probe ion has a much longer relaxation time than the host ions, in which case there will be neither a shift nor a broadening due to the fast relaxing host ions (Scovil 1951).

(ii) In some concentrated paramagnetic salts of Kramers ions, where the general interactions are weak and predominantly due to nearest neighbours only, it is possible to resolve the broad line observed at low temperatures into a main line, and satellite lines due to the nearest neighbour interactions. This will occur in crystals where the magnetic ions are separated by many intervening diamagnetic ions, as for example in neodymium ethyl sulphate (Scovil 1951).

A third possibility is the case where a probe ion is incorporated in a salt of different Kramers host ions which are strongly polarised by a high magnetic field at low temperatures. In this case the host ions will be mainly in a singlet state which has a finite magnetic moment, and their interaction with the probe ion will shift its resonance line position. Such a case is Er^{3+} in dysprosium ethyl sulphate and experiments on this will be mentioned in Chapter 13.

9.2 Theory of the g tensor shift produced by singlet state neighbours

Consider the interaction of a pair of ions, ion 1 the probe Kramers ion whose paramagnetic resonance we wish to observe, and ion 2 a neighbour with a low lying singlet state. Let us specifically consider ion 1 to have a lowest Kramers doublet

derived from a total angular momentum $J^{(1)}$, and represented by an effective spin $S' = \frac{1}{2}$. Its interaction with a magnetic field in the absence of other interactions is given by $\mathcal{H}_m^{(1)} = \mu_B \underline{H} \cdot \underline{g} \cdot \underline{S}'$. For ion 2 let us specifically consider a rare earth type ion characterised by a total angular momentum $J^{(2)}$, with Lande factor $g_J^{(2)}$, which is split by the crystalline electric field into states $|0\rangle$, $|1\rangle$, ... $|n\rangle$; of which $|0\rangle$, the lowest in energy, is a singlet. Let the relative energy of $|1\rangle$ be $\Delta_1 \gg kT$. For this ion the interaction with a magnetic field is represented by $\mathcal{H}_m^{(2)} = \mu_B g_J^{(2)} \underline{H} \cdot \underline{J}^{(2)}$. This has no first order effect on the ground state, since a singlet has no magnetic moment in the absence of an applied field, and we must therefore consider the effect of this term simultaneously with the interaction between the ions.

We may consider a general interaction between these ions of the form

$$\mathcal{H}_1(1,2) = \sum_{\alpha\beta} \mathcal{J}_{\alpha\beta} U_\alpha(J^{(1)}) V_\beta(J^{(2)}) \qquad \alpha, \beta = x, y, z \qquad (9.1)$$

where U_α and V_β are dimensionless functions of $J^{(1)}$ and $J^{(2)}$. For example, for isotropic exchange coupling between the real spins of the ions

$$\mathcal{H}_1(1,2) = \mathcal{J}\, \underline{S}^{(1)} \cdot \underline{S}^{(2)} = \mathcal{J}(g_J^{(1)} - 1)(g_J^{(2)} - 1)\, \underline{J}^{(1)} \cdot \underline{J}^{(2)}$$
$$= \sum_\alpha \mathcal{J}(g_J^{(1)} - 1)(g_J^{(2)} - 1)\, J_\alpha^{(1)} J_\alpha^{(2)}$$

The interaction must be time invariant, and in general this is brought about by both U_α and V_β changing sign with time

reversal. This will be the case if U_α and V_β are linear functions of angular momentum - as they are for isotropic exchange, magnetic dipole coupling, and the usual form of anisotropic exchange. We shall use this symmetry to reduce the number of matrix elements, and we exclude here interactions such as $(\underline{S}^{(1)}.\underline{S}^{(2)})^2$.

The simplest way of calculating the second order effect of the simultaneous action of $\mathcal{H}_m^{(1)}$, $\mathcal{H}_m^{(2)}$, and $\mathcal{H}_1(1,2)$ in the total Hamiltonian

$$\mathcal{H} = \mathcal{H}_m^{(1)} + \mathcal{H}_m^{(2)} + \mathcal{H}_1(1,2), \qquad (9.2)$$

is to use the "spin Hamiltonian" approach of Pryce (1950) (see also Bleaney and Stevens (1953)). This consists of calculating the perturbations produced by one of the dynamic variables (usually $\underline{L}$, the orbital angular momentum) while keeping the others (usually $\underline{S}$, the spin) in the form of an operator. Here we shall consider explicitly the terms involving ion 2, while keeping the terms involving ion 1 in the form of operators written in terms of the components of the fictitious spin $S' = \frac{1}{2}$. This approach leads naturally to a spin Hamiltonian of the usual form for the Kramer's ion 1 subject to the influence of its "singlet state" neighbours.

Following the procedure and a notation similar to that of Bleaney and Stevens (1953) we write,

$$\mathcal{H}' = \mu_B \underline{H}.\underline{g}.\underline{S}' + \mu_B \alpha_J \underline{H}.\underline{\Lambda}^{(2)} + \sum_{\alpha\beta} \lambda_{\alpha\beta} U_\alpha^{(1)} V_\beta^{(2)} \qquad (9.3)$$

and corresponding to their equation (7.9) we find the first

order spin Hamiltonian $\mathcal{H} = \mu_B \underline{H} \cdot \underline{g} \cdot \underline{S}'$, with no effect from ion 2 since $\langle 0 | J^{(2)} | 0 \rangle = \langle 0 | V_\beta^{(2)} | 0 \rangle = 0$ for a singlet state resulting from an electrostatic field. (By postulate $V_\beta^{(2)}$ changes sign with time reversal like the components of $\underline{J}^{(2)}$).

To second order these terms will become

$$-\mu_B^2 \Lambda_{\alpha\beta} \times H_\alpha H_\beta - \mu_B \cdot f''_{\alpha\beta} \times H_\alpha U_\beta^{(1)} - d_{\alpha\beta} U_\alpha^{(1)} U_\beta^{(1)} \qquad (9.4)$$

corresponding to Bleaney and Stevens' equation (7.10). In general U_α is a function of the total angular momentum of ion 1, but if we consider only effects within a ground state doublet spanned by the fictitious spin $S' = \frac{1}{2}$, we know that a Hermitian operator can always be represented by a suitable combination of Pauli spin matrices and the unit matrix, and we may therefore write quite generally

$$U_\alpha = u_{\alpha x} S'_x + u_{\alpha y} S'_y + u_{\alpha z} S'_z + u_\alpha 1$$
$$= \underline{u}_\alpha \underline{S}' + u_\alpha 1 \qquad (9.5)$$

where $\underline{u}$ and u_α are suitable constants. If, as we suppose U_α changes sign with time reversal, $u_\alpha = 0$. The effective part of the second order terms may therefore be written in the form of a spin Hamiltonian

$$\mu_B \underline{H} \cdot \underline{f}' \cdot \underline{S}' + \underline{S}' \cdot \underline{d}' \cdot \underline{S}' \qquad (9.6)$$

where $\underline{f}'$ and $\underline{d}'$ are second rank tensors. Of these the terms in d' will again not be detectable by paramagnetic resonance between the levels of the ground state doublet, as may be seen by transferring $\underline{g}'$ to its principal axes, and using the fact

that for a spin of $S' = \frac{1}{2}$, $S_x^2 = S_y^2 = S_z^2 = \frac{1}{4}1$. (For ions with more than two energy levels a term of this kind will produce additional splittings, and for such ions it may also be necessary to include additional terms from the operator equivalents for U_α (Equation 9.5)).

We therefore have that for a Kramers doublet, $S' = \frac{1}{2}$, the most general spin Hamiltonian representing a type 2 neighbour's interaction is of the form $\mu_B \underline{H} \cdot \underline{f}' \cdot \underline{S}'$ where f' is a dimensionless second rank tensor. If we now sum the interactions of all ions of type 2 in a sphere containing many ions, the net interaction with ion 1 will be represented by $\mathcal{H}_1(1,2) = \mu_B \underline{H} \cdot \underline{f} \cdot \underline{S}'$, where $f = \Sigma f'$. On the basis of symmetry we know that the principal axes of f will generally coincide with those of the magnetic g tensor, and only if the point symmetry has no n fold axis of symmetry will the orientation of the g and f' tensors be completely arbitrary. So that the complete Hamiltonian for ion 1 in the garnets will be,

$$\mathcal{H} = \mu_B \underline{H} \cdot \underline{g} \cdot \underline{S}' + \mu_B \underline{H} \cdot \underline{f} \cdot \underline{S}' = \mu_B \underline{H} \cdot (\underline{g} + \underline{f}) \underline{S}' \qquad (9.7)$$

and the spectrum should still obey a g tensor variation. The magnitude of $f \approx \mathcal{J}/E$, will generally be quite small, but may easily amount to several per cent of the usual crystal field g tensor.

9.3 Discussion of the measured g tensors in weakly paramagnetic lattices

In order to determine if there is an observable interaction

shift in the case of Yb^{3+} resonances investigated we must first estimate the g values expected from crystal field interactions alone. We have seen in §4.2 that the g values of Yb^{3+} vary smoothly in the four diamagnetic lattices, and it is possible to interpolate the g values for other lattices if the oxygen structure parameters x, y and z are known, using Figures 4.1 and 4.2. Unfortunately no measurements have been made of these structure parameters for TmGG, TmAG, and LuGG. However, by plotting x and y against a_o for lattices where they are known, it is possible to interpolate the values below for TmGG and TmAG.

Table 9.1

	TmGG	TmAG
x	-0.0263	-0.0301
y	0.0564	0.0524

Using these values and Figures 4.1 and 4.2 we can make two independent interpolations of the g values expected in TmGG and TmAG if the only difference from YAG was a small change in the crystal field. These are given in Table 9.2 and it is seen that there is general agreement between the two sets of estimates.

From Figures 3.13 - 3.16 we see that in general the observed H_4 spectrum of Yb^{3+} (and Er^{3+}) in the paramagnetic lattices can be fitted quite well to a g tensor . The experimental results for Yb^{3+} in the Tm garnets are given in Table 9.2, and it is seen

Table 9.2

Lattice		g_x	g_y	g_z
TmHG	Estimated from x	3.70	3.58	2.91
	Estimated from y	3.69	3.58	2.88
	Average	3.70	3.58	2.89
	cf. Experimental value	3.72	3.56	2.94
TmAG	Estimated from x	3.85	3.76	2.54
	Estimated from y	3.86	3.76	2.53
	Average	3.86	3.76	2.54
	cf. Experimental value	4.02	3.76	2.55

from this table that in at least one case, that of g_x in TmAG, there is a significant shift from the value expected from crystal field effects alone. If this shift is interpreted in terms of the theory given in §9.2, it leads to a value of f_x = 0.16, which is well outside the combined interpolation ($\pm$0.03) and experimental ($\pm$0.01) errors.

We may note that one might also expect a small shift from shape dependent demagnetisation effects. The effective local field at the Kramers ion may be written as

$H_{loc.} = H_{ext} + H_{dep} + H_1 + H_2$, where in the usual manner H_{ext} = applied field outside specimen, H_{dep} = surface depolarisation field, H_1 = polarisation (Lorentz) field due to a fictitious ellipsoidal surface taken in the sample around the

ion, and H_2 is due to those ions inside this surface. For a spherical surface H_2 is taken into account in the theory of §9.2, and the demagnetisation shift will be $H_{dem} + H_1$ $(= -N_1 M + \frac{4\pi}{3} M)$. The samples were roughly in the form of spheres, but even for extreme shapes the shifts expected from such effects were estimated from susceptibility measurements to be $\lesssim 1\%$.

Susceptibility measurements (Wolf et al. 1962) have shown that TmAG and TmGG have non magnetic ground states with splittings $\sim 100^{\circ}K$ to the next excited state. TmAG has twice the temperature independent susceptibility of TmGG, indicating appreciably smaller splittings, or larger magnetic field matrix elements, to the excited state, in this garnet. For this reason, and also from the fact that the ions are closer, one would expect a larger shift in TmAG. It is significant that the only unambiguous shift is found for this case. If the rare earth-rare earth interactions are $\sim 1^{\circ}K$, as found in other garnets, one would expect shifts of $\approx g/\Delta_1 \sim 0.01$ in g, which is roughly of the order of that observed.

In the case of Yb^{3+} in YbGG the experimental g values fall near the curves of Figure 4.1 and 4.2 for diamagnetic lattices; this is to be expected since the next excited state lies $400^{\circ}K$ above the lowest J = 0 singlet.

9.4 Conclusion

The resonance of Yb^{3+} in TmAG is believed to show a field induced interaction shift due to the singlet state Tm^{3+} ions. Unfortunately the shift is too small, with subsequent large errors, to be quantitatively useful, but it does indicate a new method of investigating the interaction of ions in these special cases. There are clearly other cases where more significant shifts may be observed, in particular the use of S state ions as probes would have the advantages of larger interactions and less dependence on the lattice than other Kramers ions. For example Gd^{3+} in thulium ethyl sulphate should show such an effect. S state ions could also be used to explore the relative sizes of the interactions at two sites in a crystal, for example at the [a] and (d) sites in the garnets using Fe^{3+} in TmAG. However they have the disadvantage, mentioned in §9.2, that the interaction effects will be more complicated than for an $S' = \frac{1}{2}$ ion, and will necessitate the separation of the g tensor from other terms in the interaction Hamiltonian.

CHAPTER 10

Paramagnetic resonance from pairs of Gd^{3+} ions in lanthanum trichloride: Experimental Results

10.1 Introduction

Anhydrous gadolinium trichloride, $GdCl_3$, is one of the few known ionic ferromagnets, ordering at 2.2°K (Wolf et al, 1962[b]). The fact that it is possible to obtain large single crystals, its simple hexagonal crystal structure, and the relative ease with which the ordering can be investigated in the helium range, make it in many ways the ideal ionic ferromagnet. The susceptibility and specific heat of $GdCl_3$ have been investigated in detail (Wolf et al 1962[b], Garton et al 1962). The results show that the ordering can be explained in terms of dipolar and isotropic exchange interactions between the ions, the isotropic exchange constant for nearest neighbouring ions has been found to be of the order of 0.1 cm^{-1}.

It is therefore of considerable interest to investigate the interactions between a pair of Gd^{3+} ions from their resonance in the isostructural diamagnetic compound $LaCl_3$. Unfortunately the lattice constants of $LaCl_3$ are slighily larger than those of $GdCl_3$ so that it may not be valid to use any resonance results directly for the interpretation of the properties of $GdCl_3$, the converse is also true. Since the exchange interactions found from the bulk measurements are of the same order as the

estimated dipolar interaction, it should be possible to obtain measurements of the exchange constants directly from the pair resonance line positions.

An extensive spectrum, attributed to pair transitions, has been observed in samples of 1% Gd in $LaCl_3$, and measurements of the spectrum will be described in this Chapter. Its theoretical interpretation will be discussed in Chapter 11. It has not yet been possible to obtain an exact fit for all the resonance lines observed, mainly because the crystal field effects are not known with certainty (thereby increasing the number of unknown parameters). However, providing certain assumptions regarding the crystal field can be made with validity, it is possible to estimate J_{ex} for nearest neighbour ions.

In order to investigate the crystal field variations with lattice, measurements have been made on the single ion resonance of Gd^{3+} in $LaCl_3$ and $LaBr_3$, and these will be described in §10.3. The pair spectrum will be described in § 10.4.

10.2 Crystallography, and orientation of samples

$LaCl_3$ has the hexagonal crystal structure of $Y(OH)_3$, (Zachariasen 1948), with space group C $6_{3/m}$. There are two molecules per unit cell, the ionic positions of which are given together with relevant lattice constants in Table 10.1. The point symmetry at the rare earth site is C_{3h}. All the rare earth trichlorides of elements in the first half of the series

Table 10.1

Position of ions in the hexagonal $LaCl_3$ structure, space group $C_{63/m}$

La^{3+} at $(\frac{2}{3},\frac{1}{3},\frac{1}{4})$ $(\frac{1}{3},\frac{2}{3},\frac{3}{4})$

Cl^- at $(x,y,\frac{1}{4})$ $(\bar{y},x-y,\frac{1}{4})$ $(y-x,\bar{x},\frac{1}{4})$

$(\bar{x},\bar{y},\frac{3}{4})$ $(y,y-x,\frac{3}{4})$ $(x-y,x,\frac{3}{4})$

where $x = 0.29$, $y = 0.38$

Lattice constants[+]:-

	a_o	c_o
$LaCl_3$	7.483 Å	4.375 Å
$GdCl_3$	7.363 Å	4.105 Å
$LaBr_3$	7.967 Å	4.510 Å

[+]Wyckoff, Vol. II (1960)

(Ce to Gd) crystallise with this structure, which is illustrated in Figure 10.1. From Figure 10.1 it is seen that for a typical La^{3+} site X, there are two nearest neighbour (n.n.) sites lying at a distance of $\pm$ 4.375 Å along the $\underline{c}$ axis. There are six next nearest neighbours (n.n.n.) at 4.84 Å (e.g. ions Y, Z in Figure 10.1), and six next-next nearest neighbours (n.n.n.n.) at the corners of a hexagon centred at X. These are at distances of 7.483 Å.

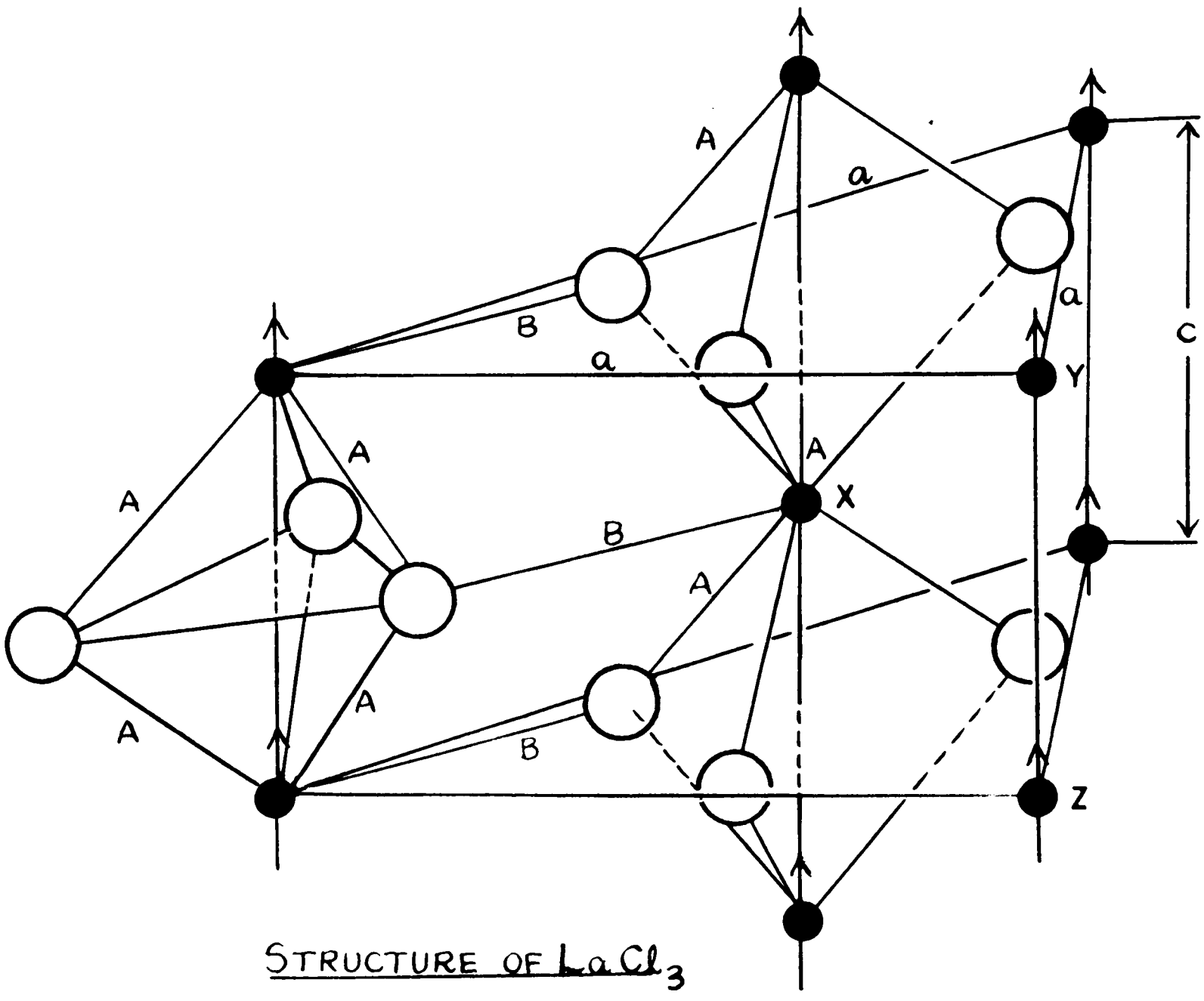
The crystals were grown by Dr. G. Garton and Mr. S. Itzcovitz using the Bridgman-Stockbarger method. Their quality

● = La^{3+}

○ = Cl^-

a = 7·483 Å

c = 4·375 Å



STRUCTURE OF $LaCl_3$

FIGURE 10·1

was found to be extremely dependent on the conditions of growth, and many samples which appeared macroscopically good were found to be multicrystalline in their microscopic properties. The single ion Gd^{3+} lines often split when the field was at an angle to the c axis, indicating angles between the axes of different sections of the multicrystals of up to 10^{o} in some cases. Consequently a large number of samples were investigated and only the very best used for quantitative measurement. Most of the samples contained 1% Ce^{3+} ions to relax the Gd^{3+} ions at $20^{o}K$, and a good test of their quality was to ensure that the very anisotropic Ce^{3+} resonance line observed at $4.2^{o}K$ did not split off axis.

The crystals are very hygroscopic and were handled either in a dry box, or under dried paraffin. The c axis could be found roughly from the intersection of two cleavage planes, or from striations in the crystal. In difficult cases the extinction of plane polarised light parallel and perpendicular to the c axis was used. The crystals were then attached to a goniometer head with Durofix and accurately oriented, usually with the c axis horizontal, by Laue back reflection of X-rays. A typical photograph is shown in Figure 10.2 where the sixfold symmetry is clearly seen. During the X-ray orientation the crystals were protected either by use of a small perspex box containing P_2O_5, with a window of "Siranwrap" (shown in Figure 10.3), or by covering them with a mixture of vaseline and

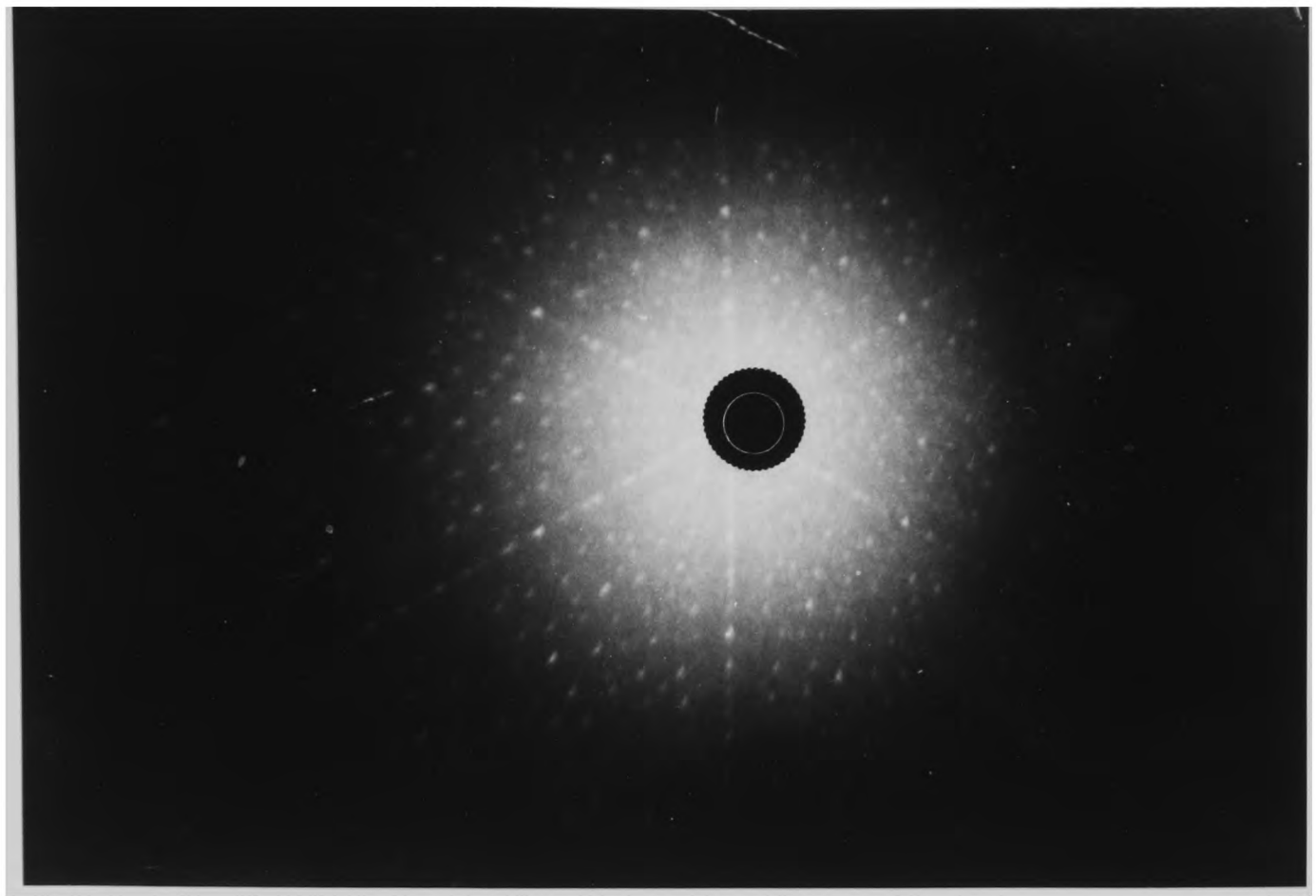


FIGURE 10·2

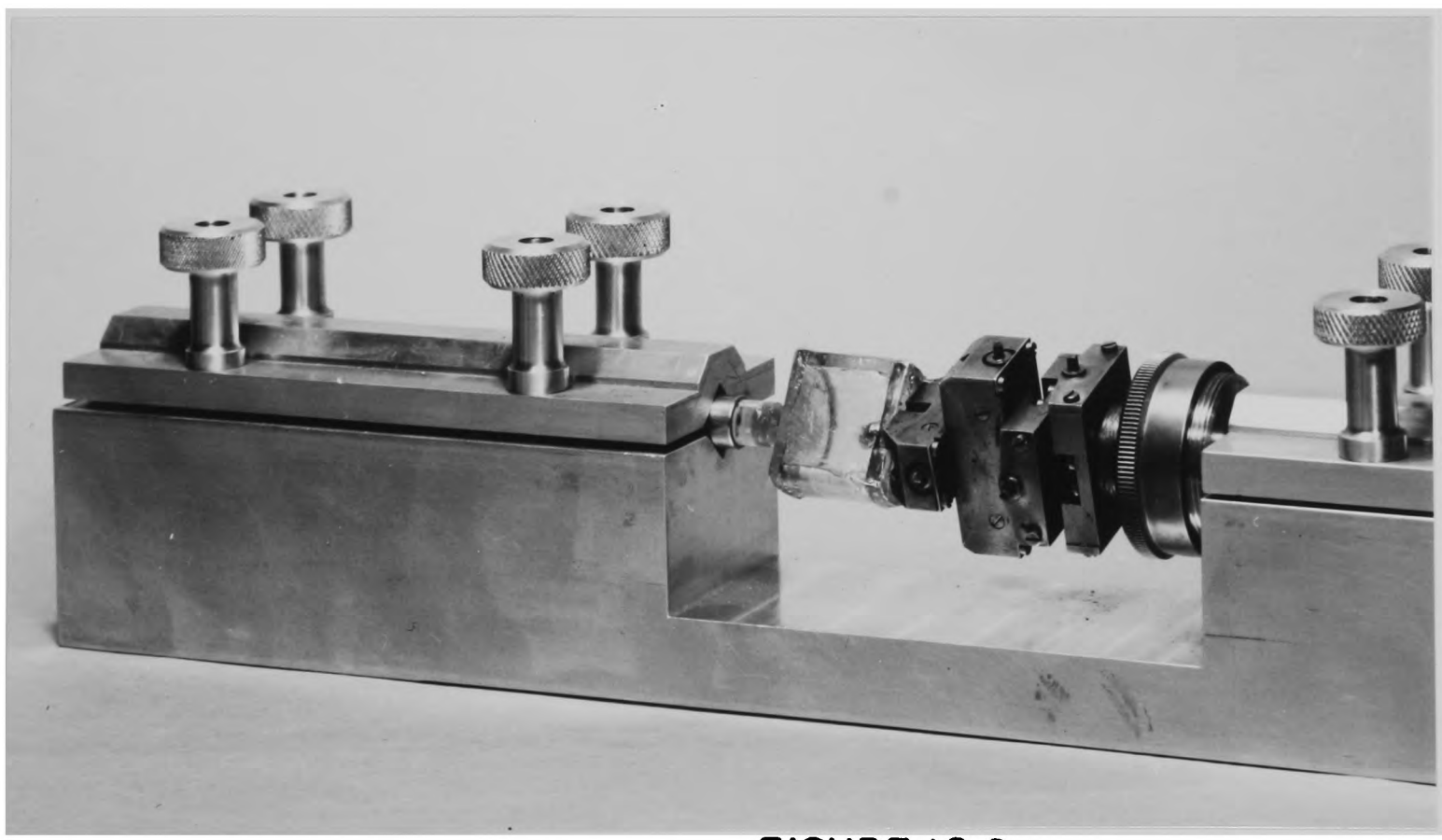


FIGURE 10·3

paraffin. They were then embedded in Araldite in the specimen holder using the mounting block shown in Figure 10.3. This was placed in a dry box. Finally the Durofix was dissolved away with dry ethyl acetate. (N.B. Some of the crystal orientation was carried out by Mr. S. Itzcovitz).

10.3 The single ion resonance of Gd^{3+} in $LaCl_3$ and $LaBr_3$

$Gd^{3+}, (4f)^7$, has a ground state $^8S_{7/2}$, and in a crystal field of C_{3h} symmetry can be represented by a spin Hamiltonian of the form,

$$\mathcal{H} = \mu_B g \underline{H}.\underline{S} + B_2^0 O_2^0 + B_4^0 O_4^0 + B_6^0 O_6^0 + B_6^6 O_6^6 \qquad (10.1)$$

acting within a manifold of $S = 7/2$. (Elliott and Stevens 1953b). The notation is of Equation (A2.20), where the B_n^m are experimental parameters, and are only related to the crystal environment through a high order perturbation. The axis of quantisation is along the g direction.

10.3.1 Gd^{3+} in $LaCl_3$

The parameters for Gd^{3+} in $LaCl_3$ at 290°K and 90°K have been determined by Hutchison et al (1957) and are given in Table 10.2. (The coefficients b_n^m are related to B_n^m at the end of § A2.3.3). They show a remarkable temperature dependence, i.e. dependence on the lattice spacing. However Hutchison et al. do not give parameters for 20°K, and although they state that there was little change in their values between 90°K and

$20^{\circ}K$, the measurements they give at $20^{\circ}K$ do not agree at all well.

The spectrum from Gd^{3+} impurity ions in an X-ray oriented sample of 1% Ce in $LaCl_3$ was therefore measured at $20^{\circ}K$ and at X Band frequencies. 115 Kc/s phase sensitive video detection was used, and the magnetic field measured by simultaneous display of N.M.R. The microwave frequency was read from the calibrated dial of the L.F.E. source used, and corrections made from the resonance of a d.p.p.h. sample as described in § 3.4. The angular variation of the spectrum is shown in Figure 10.4 and the results are given in Table 10.2. No hyperfine lines were observed, the half intensity line width was ~ 3g.

The spectrum was analysed in a similar manner to that described by Hutchison et al (1957) and Bleaney et al (1954) and involved only the diagonal terms in the Hamiltonians for the parallel (Equation (10.1)), and perpendicular field directions. The z axis of quantisation being taken along the direction of $\underline{H}$ in each case. Values of b_2^0 and b_4^0 found from the two directions agreed well. The sample was oriented with the crystallographic axes $\underline{a}$ and $\underline{b}$ at 30° to the horizontal, so that $\cos 6\phi$ (Bleaney et al 1954) was an extremum, enabling $|b_6^6|$ to be found from the perpendicular direction. (It was assumed that the $\phi = 0$ direction lies along a hexagonal axis of the unit cell). The positive sign of b_2^0 was confirmed from K Band measurements with $\underline{H}$ along the $\underline{c}$ axis, when the highest field

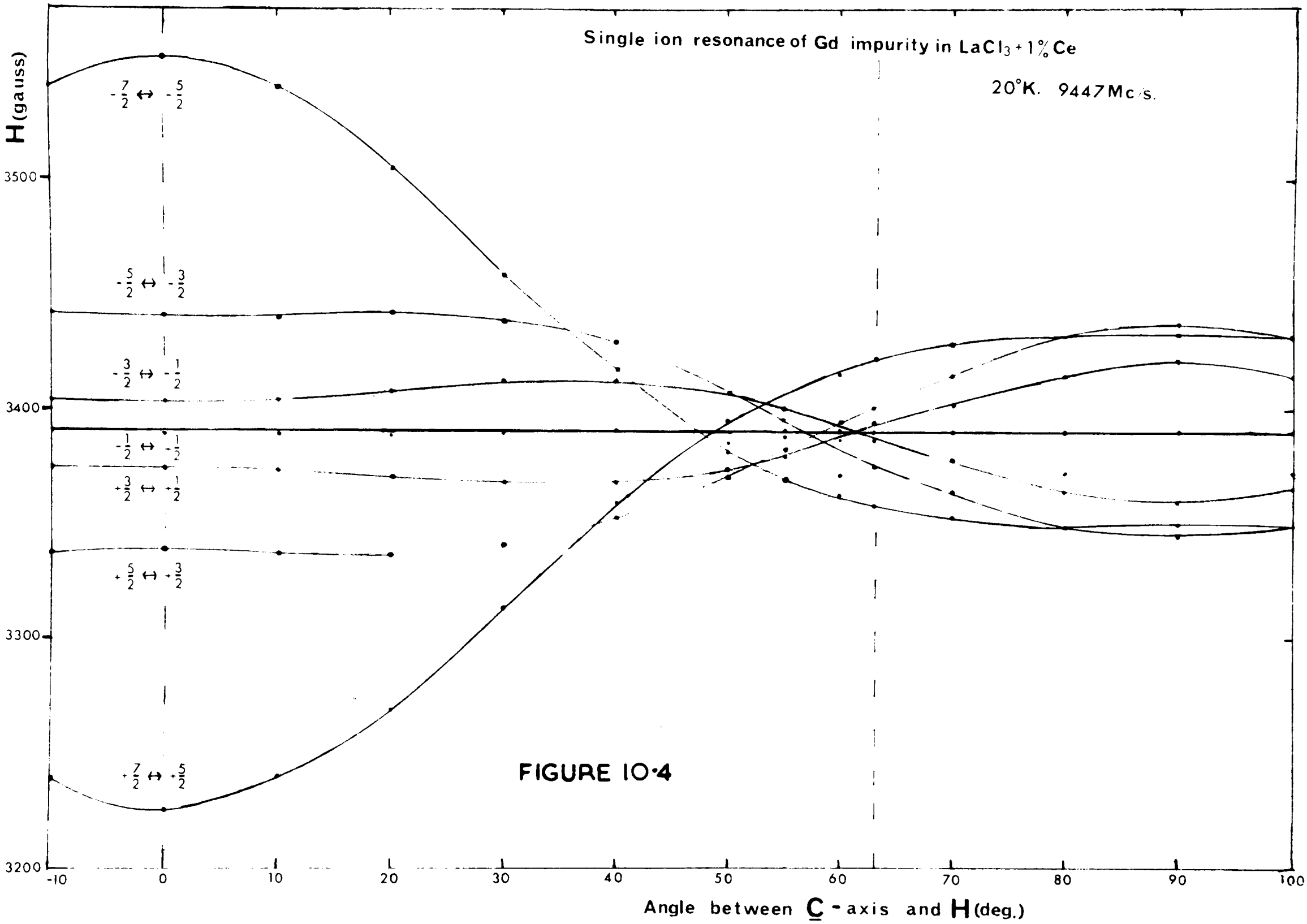

Single ion resonance of Gd impurity in $LaCl_3$ + 1% Ce
20°K. 9447 Mc/s.
H (gauss)
3500
3400
3300
3200
$-\frac{7}{2} \leftrightarrow -\frac{5}{2}$
$-\frac{5}{2} \leftrightarrow -\frac{3}{2}$
$-\frac{3}{2} \leftrightarrow -\frac{1}{2}$
$-\frac{1}{2} \leftrightarrow -\frac{1}{2}$
$+\frac{3}{2} \leftrightarrow +\frac{1}{2}$
$+\frac{5}{2} \leftrightarrow +\frac{3}{2}$
$+\frac{7}{2} \leftrightarrow +\frac{5}{2}$
-10
0
10
20
30
40
50
60
70
80
90
100
Angle between C - axis and H (deg.)

FIGURE 10·4

Table 10.2

Lattice	g	$b_2^0 \times 10^4$ cm^{-1}	$b_4^0 \times 10^4$ cm^{-1}	$b_6^0 \times 10^4$ cm^{-1}	$\lvert b_6^6 \rvert \times 10^4$ cm^{-1}
$LaCl_3$ 290°K*	1.991 (± 0.001)	8.36 (± 0.10)	1.68 (± 0.04)	0.64 (± 0.15)	-
$LaCl_3$ 90°K*	1.991 (± 0.001)	16.0 (± 0.02)	2.13 (± 0.05)	0.25 (± 0.05)	1.40 (± 0.3)
$LaCl_3$ 20°K	1.992 (± 0.001)	18.0 (± 0.2)	2.14 (± 0.05)	0.23 (± 0.05)	0.13 (± 0.07)
$LaBr_3$ 20°K	1.991 (± 0.001)	67.6 (± 0.3)	11.11 (± 0.06)	3.46 (± 0.06)	-

*From Hutchison et al (1957)

Parameters occurring in Equation (10.1) for Gd^{3+} ions in two hexagonal lattices.

line was seen to be more intense than the lowest field line. The results differ significantly from those of Hutchison et al at 90°K only in the values of b_2^0 and $|b_6^6|$.

10.3.2 Gd^{3+} in $LaBr_3$

In order to investigate further the variation of the parameters b_n^m with lattice dimensions, measurements at X Band were made on samples of 1% Gd in $LaBr_3$, prepared and X-ray oriented by Mr. R. Shore. $LaBr_3$ has the same structure as $LaCl_3$, but larger lattice constants (Table 10.1). Unfortunately these samples showed evidence of multicrystalline growth, but gave a good spectrum along the $\underline{c}$ axis with half intensity line width ~25g. Straightforward 50c/s field modulation and video detection were used, the field and frequency being measured as described in §10.3.1. The spectrum with $\underline{H}$ along the $\underline{c}$ axis was symmetric about the central line to within ± 1g, the lines were identified from their relative intensities and the values of b_n^0 found as for $LaCl_3$. It was not possible to determine the sign of b_2^0 at X Band and it has been assumed to be positive in Table 10.2, as for $LaCl_3$. A specimen with the $\underline{c}$ axis vertical, so that $\underline{H}$ could be swept in the perpendicular plane, showed a 60° symmetry in line positions, but the spectrum could not be fitted using second order perturbation theory. As the b_6^6 parameter is not immediately necessary in connection with the pair problem the spectrum was not analysed further, an estimation of its value showed it may be as large as 15 cm^{-1}. Apart from higher

order terms, the discrepancy could be due to apparent line shifts arising from the multicrystalline growth. A weaker spectrum at lower fields due to forbidden transitions, and not observed in $LaCl_3$, was evident in $LaBr_3$ when $\underline{H}$ was not along the $\underline{c}$ axis.

10.4 The spectrum from pairs of Gd^{3+} ions in $LaCl_3$

In this section the measurements made on samples of Gd^{3+} in $LaCl_3$ will be described together with a brief account of the evidence leading to the conclusion that most of the lines observed are due to pair transitions. The measurements were made at both X and K Band frequencies. Unless stated otherwise the magnetic fields quoted were measured from calibrated potentiometer readings of the magnet exciting current (see §2.5). 115 Kc/s phase sensitive detection (P.S.D.) was mainly used, with both chart and oscilloscope display. The X Band microwave frequency was read off the calibrated dial of the L.F.E. stabilised source, and the K Band frequency found from a calibrated cavity wavemeter. Unless stated the measurements were made at 20°K on X-ray oriented samples. The sample used for the K Band measurements was oriented with reference to a cleavage plane in which the direction of the $\underline{c}$ axis was identified using polarised light.

10.4.1 The general nature of the pair spectrum

A small crystal of 100% $GdCl_3$ was first investigated at

X Band frequencies, and at 20°K and 4.2°K. It gave a broad resonance centred about $g_{eff} = 2$, of half intensity full width ~ 2-3000 g, thus suggesting a possible extent in field of the pair spectrum of this order.

A sample of 1% Gd (1% Ce) $LaCl_3$ was then examined and at 20°K showed a complex spectrum of lines ~ 1/1000th the intensity of the single ion resonances. These extended over ~ ± 2,500 gauss from the central $|+\tfrac{1}{2}\rangle \rightarrow |-\tfrac{1}{2}\rangle$ single ion line. Their intensity is in rough agreement with that expected for pair transitions from calculations similar to those of Griffiths et al (1959). All subsequent quantitative measurements were made on samples of this concentration.

Because of the possibility of multicrystalline growth increasing the number of lines observed, several samples, which fulfilled the criterion described in § 10.2, were investigated. The results of measurements on some of these samples with H along the g axis are given in Table 10.3, where the X Band results are also given. In general it is seen that the same lines occurred in most of the samples. Samples B10 and B17 were from the same crystal batch, but B49 was from a different preparation.

From Table 10.3 and Figure 10.5 (where the angular variation of the spectrum at X Band is shown) it is seen that the main feature of the spectrum along the g axis, attributed to n.n. pair transitions, is a grouping of the lines. The

Table 10.3

Survey of the relative positions, w.r.t. the central main Gd^{3+} line, of the largest n.n. pair lines measured in several oriented samples of 1% Gd (1% Ce) $LaCl_3$ when H//c (n.n.) axis. (Errors of up to (± 12g) are likely for columns A–C, and (± 20g) for columns D–F).

	20°K					290°K
	X BAND			K BAND		K BAND
GROUP OR LINE	A B10 (9551 mc/s)	B B17 (9551 mc/s)	C† B49 (9373 mc/s)	D B49 (25.91 Kmc/s)	E B49 (25.91 Kmc/s)	F B49 (25.83 Kmc/s)
1	+2574	–	+2590	+2572	+2587	+2554
	–	+2566	+2564	+2546	+2561	+2530
	–	+2512	+2523	+2504	+2520	+2476
	–	+2470	+2484	+2465	+2478	+2426
	–	+2447	+2447	+2432	+2449	+2384
2	+2224	+2212	+2217	+2209	+2225	+2206
	+2186	+2183	+2186	+2175	+2186	+2162
	+2147	+2147	+2145	+2137	+2151	+2114
	+2105	+2103	+2108	+2105	+2114	+2069
	–	–	+2096	+2091	–	+2045
3	–	–	–	+1988s	+1972s	–
	–	–	–	+1922s	+1926s	–
	+1861	+1857	+1860	+1851	+1866	+1845
	+1783	+1781	+1779	+1776	+1788	+1765
	–	–	–	+1752	+1761s	+1707
	+1733	+1730	+1732	+1729 } +1719 }	+1737	+1682
	–	–	–		–	–
4	+1465	+1478	+1480	+1475	+1487	+1473
	+1373	–	+1388	+1382	+1382	–
	–	+1369	+1374	+1366	–	+1354
	+1333	+1336	+1329	+1330	+1343	+1303
5	+1093	+1091	+1087	+1082	+1094	+1080
6	+ 958	+ 960	+ 949	+ 950	+ 957	+ 936
7	+ 681	+ 685	+ 678	+ 679	+ 692	+ 677
	+ 510	+ 430	+ 515	+ 520	≀	≀
	≀	≀	≀	≀	≀	≀
CENTRAL MAIN LINE	0(3427g)	0(3425g)	0(3360g)	0(9305g)	0(9306g)	0(9260g)
	≀	≀	≀	≀	≀	≀
		– 477	– 515	– 521	≀	≀

Table 10.3 Contd.

	20°K					290°K
	X BAND			K BAND		K BAND
GROUP & LINE	A B10 (9551mc/s)	B B17 (9551mc/s)	+C B49 (9373mc/s)	D B49 (25.91Kmc/s)	E B49 (25.91Kmc/s)	F B49 (25.83Kmc/s)
8	- 681	- 677	- 678	- 679	- 674	- 677
9	- 950	- 949	- 948	- 948	- 940	- 930
10	-1092	-1084	-1085	-1089	-1077	-1084
11	-	-1252s	-1244s	-	-	-
	-1344	-1344	-1332	-1331	-1318	-1306
	-	-	-1365	-1369	-1366	-1354
	-1385	-1386	-	-1383	-	-
	-	-	-	-1435s	-	-
	-1490	-1478	-1479	-1480 / -1489	-1475	-1478
12	-	-	-1685*	-	-	-
	-	-1720	-	-1724	-1721	-1692
	-1744	-1746	-1733	-1738	-1743	-1715
	-	-	-	-1753	-	-
	-1786	-1789	-1781	-1786	-1775	-1771
	-1866	-1864	-1858	-1862	-1854	-1859
13	-	-	-2093	-2095	-2086s	-2058
	-2108	-2113	-2104	-2110	-2102s	-2084
	-2152	-2152	-2146	-2147	-2142	-2126
	-2191	-2189	-2188	-2186	-2181	-2176
	-2226	-2222	-2223	-2225	-2217	-2226
14	-2452	-2450	-2454	-2443	-2440	-2401
	-2493	-2485	-2479	-2479	-2472	-2444
	-2533	-2525	-2527	-2520	-2514	-2496
	-2571	-2558	-2560	-2559	-2557	-2555
	-2598	-2594	-2591	-2589	-2582	-2580

* "Half field" line

s = very small

† Some fields measured with N.M.R. (±5γ error)

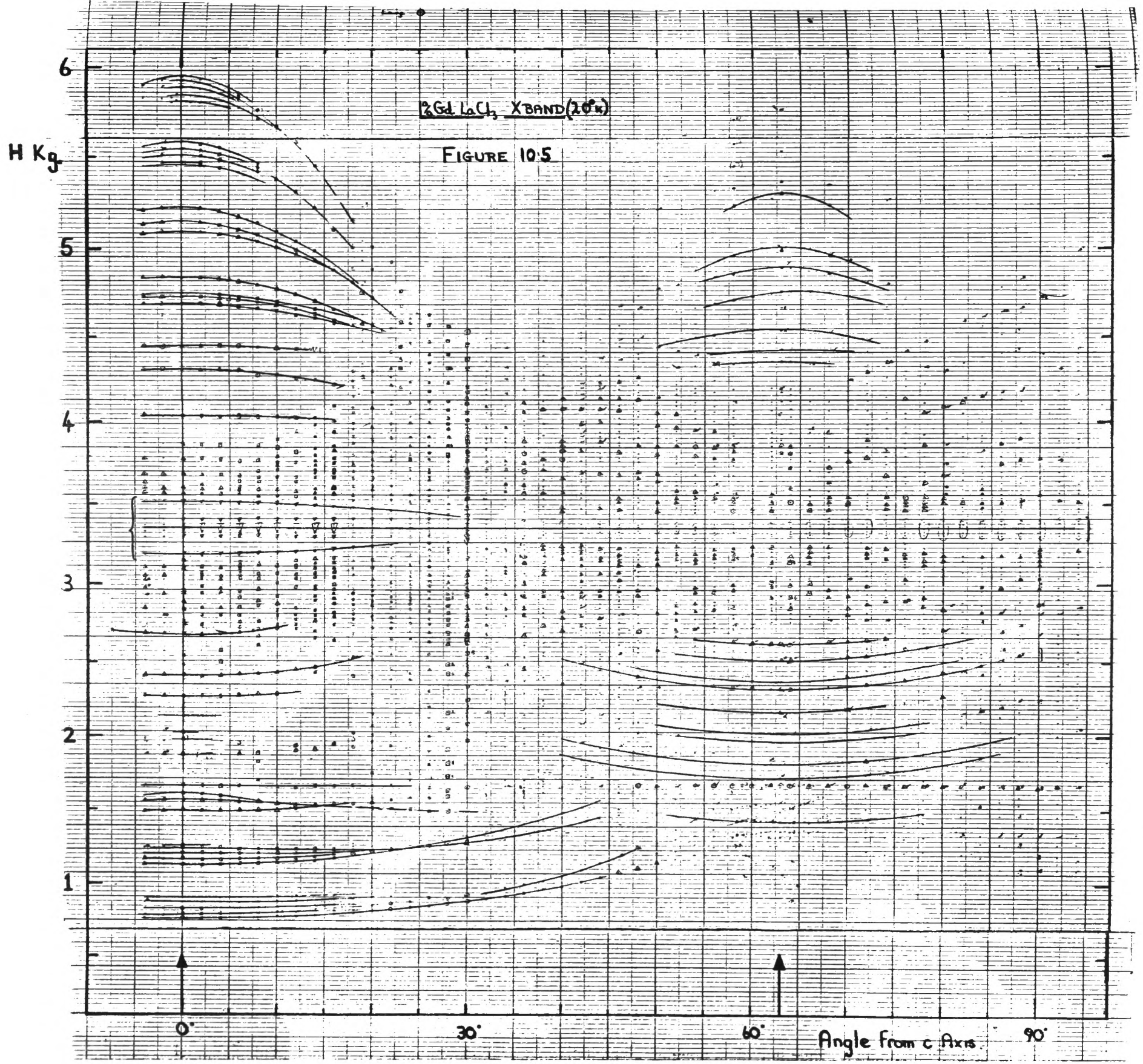


FIGURE 10.5

outermost lines form four distinct groups in which four or more lines are resolved, and there are three inner apparently well resolved lines. These groups and lines have been numbered 1 to 14 in Table 10.3, they will be described further in §10.4.2. It is also seen from Figure 10.5 that there are several lines turning at 63° from the g axis, and these, attributed to n.n.n. pair transitions, will be discussed in §10.4.3.

10.4.2 <u>The nearest neighbour pair spectrum</u>

The lines turning along the g axis are attributed to n.n. pair transitions since they have the correct symmetry and their relative position from the central line is of the correct order of magnitude (see §11.4). Lines from further neighbours along the g axis e.g. two ions separated by 2c, would have the same symmetry but would be closer in by a factor of about ½. Lines from n.n.n. pairs would be expected to cross along the g axis, but none were positively identified in this direction. They would be expected to lie close in on account of their small diagonal dipolar interaction when H is in this direction. Very many lines due to the more distant neighbours were observed with ΔH <~600g and these have not been fully analysed. The isolated Gd^{3+} main line positions (bracketed in Figure 10.5) were found to agree well with the measurements described in §10.3.1.

The most accurate values found for the relative line positions of the n.n. pairs are listed in Table 10.4. These were measured at X Band by simultaneous video display of N.M.R. unless stated. However it must be pointed out that few of the lines were completely resolved, and the "centre" of each line was taken as the mid-point between maximum and minimum values of the derivative of the absorption. The true line positions may be shifted from these values and there may be weaker lines hidden by the stronger ones. The half intensity full widths of the lines were ~ 10-20 gauss. From Table 10.4 it is seen that for most of the lines observed above the central line there is a corresponding one at the same relative position below, to within the accuracy of the measurements. The measurements made at K Band agree within the error with those made at X Band, two sets of readings are given in Table 10.3 (D and E) to illustrate the likely error.

The angular variation of the lines at X and K Band frequencies can be seen from Figures 10.5 and 10.6. At X Band the lines at low magnetic field have a less pronounced variation than the corresponding high field ones, and some show subsidiary maxima. At K Band, however, all the lines above, and below, the central line show the same general angular variation.

A typical chart recording of the spectrum along the g axis at X Band is reproduced in Figure 10.7 (line 8 is not

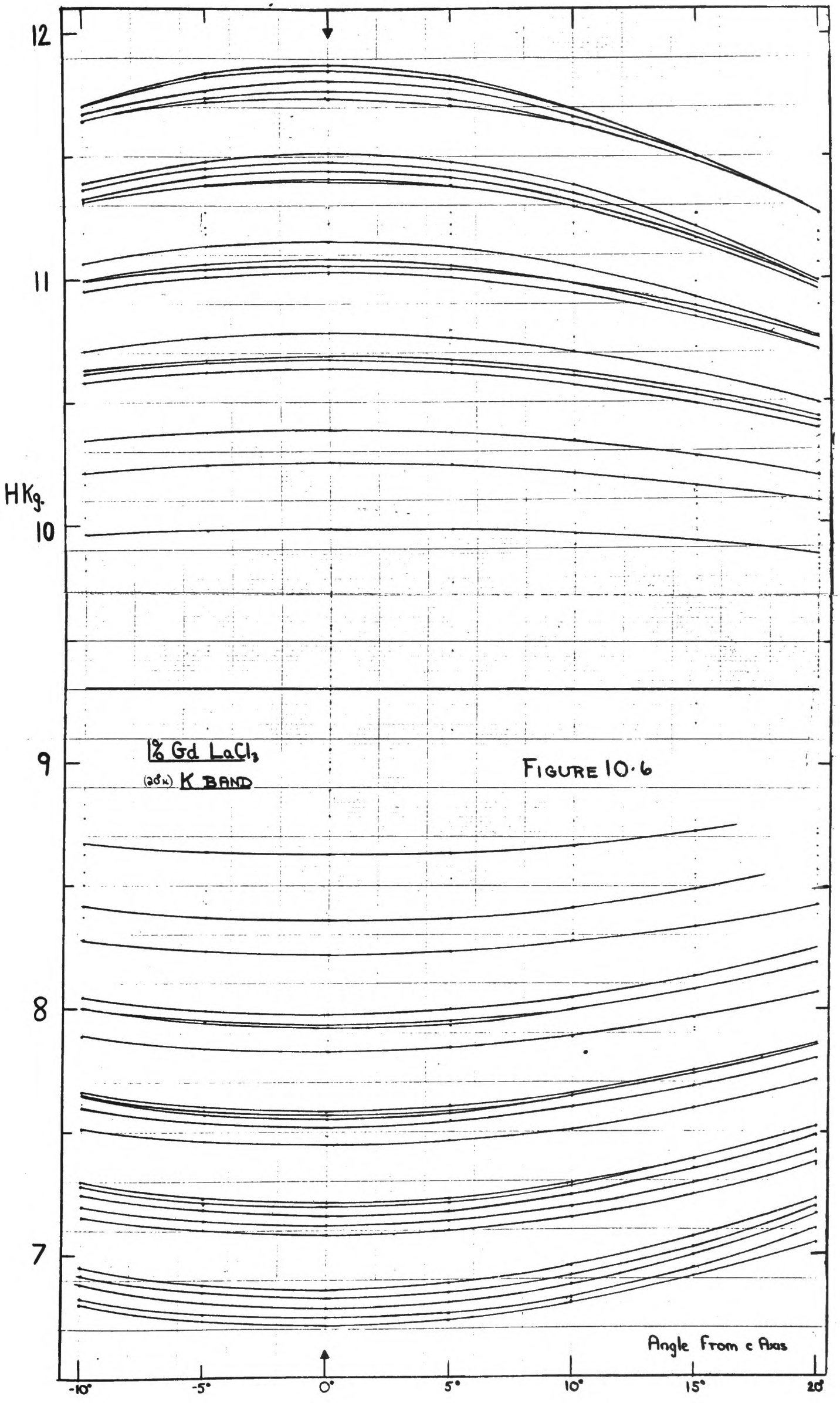
Table 10.4

Summary of the most accurate values found for the relative positions of the largest n.n. Gd^{3+} pair lines in 1% Gd (1% Ce) $LaCl_3$ (B49). H//g axis, 20°K. Measurements were made at X Band, with errors of (± 5g) unless stated.

Group or Line	ΔH gauss	Group or Line	ΔH gauss
1*	+2590 +2564 +2523 +2484 +2447	14*	-2591 -2560 -2527 -2479 -2454
2	+2217 +2188 +2145 +2108 +2096*	13	-2223 -2188 -2146 -2104 -2093*
3	+1660 +1779 +1752† +1732 +1719†	12	-1658 -1781 -1753† -1733 -1724†
4	+1480 +1388* +1374 +1329	11	-1479 -1382 -1365 -1332
5	+1087	10	-1085
6	+ 949	9	- 948
7	+ 678	8	- 678

*Error (± 10g). Measured at X Band using calibrated magnet current.

†Error (± 15g). Measured at K Band using calibrated magnet current.


12
11
HKg.
10
9
8
7
1% Gd LaCl3
(20K) K BAND
FIGURE 10·6
Angle From c Axis
-10°
-5°
0°
5°
10°
15°
20°

shown), the single ion Gd^{3+} lines, attenuated by a factor of 100 are given for comparison. It is seen that the intensity of the lines generally decreases as their distance from the centre increases. The highest field groups 1 and 2, at K Band, are shown in Figure 10.8.

A careful search was made at X Band for lines higher in field than those of group 1, using both 115 Kc/s and 50 c/s P.S.D. with chart display. No lines larger in intensity than $1/35^{th}$ of the lines of group 1 were observed up to 10.6 Kg.

Additional transitions

The X Band measurements showed an isotropic line at half the field of the central main line. This has been observed in other systems, and may possibly be due to a pair of ions separated by a large enough distance so that their interactions do not affect the single ion levels significantly but admix the states sufficiently to give a finite transition probability for a "$\Delta S_z = 2$" transition (A. Harris, private communication). The angular variation of the lines of group 11 in Figure 10.5 is not well determined, and it is possible that some "forbidden" single ion transitions occur at this field since at K Band these lines are well resolved (see Figure 10.6). However no forbidden transitions of the intensity of those observed in 1% $Gd LaBr_3$ (§10.3.2.) were observed and it is unlikely that many of the low field lines are due to such transitions. In this connection it is

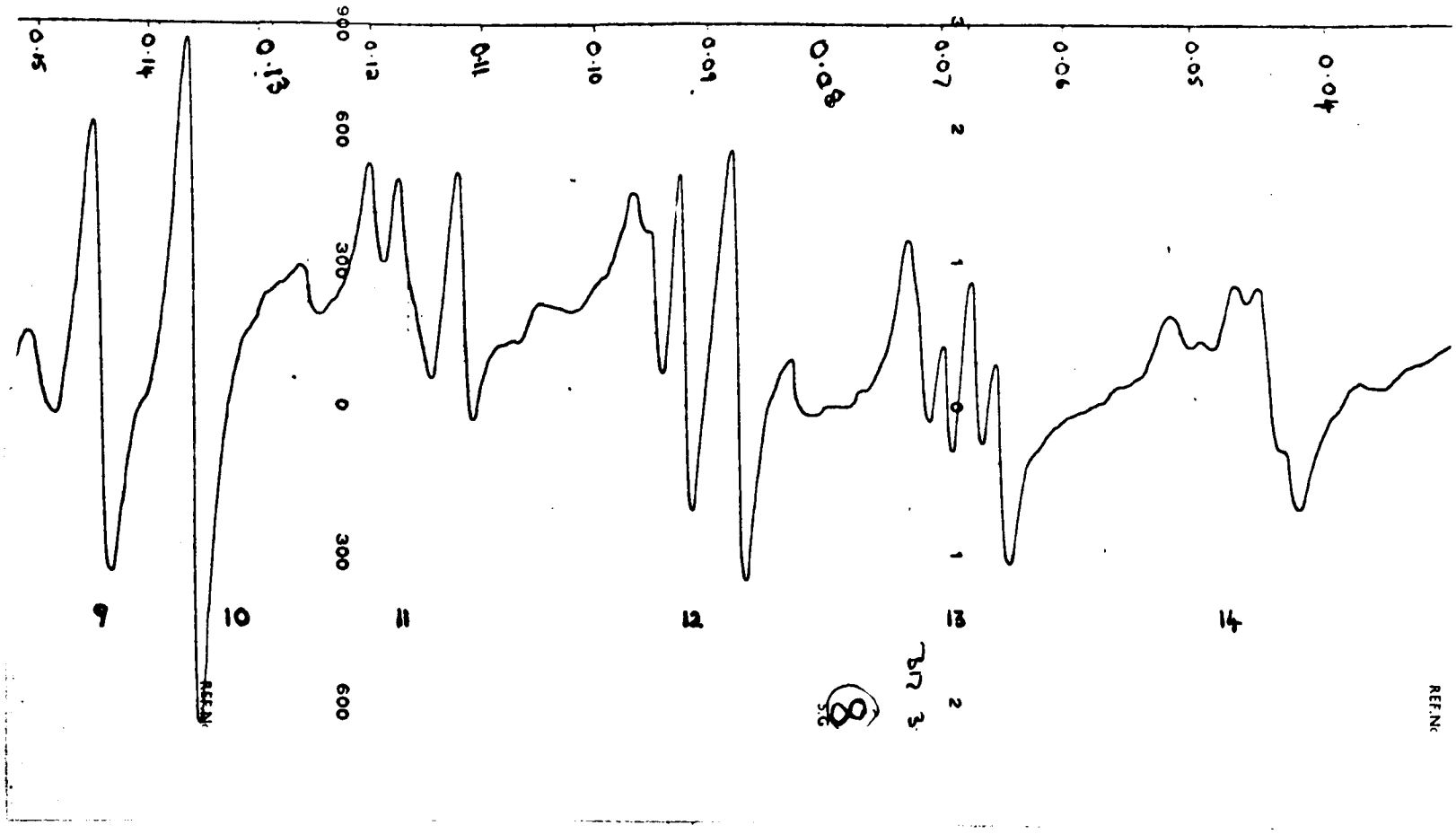
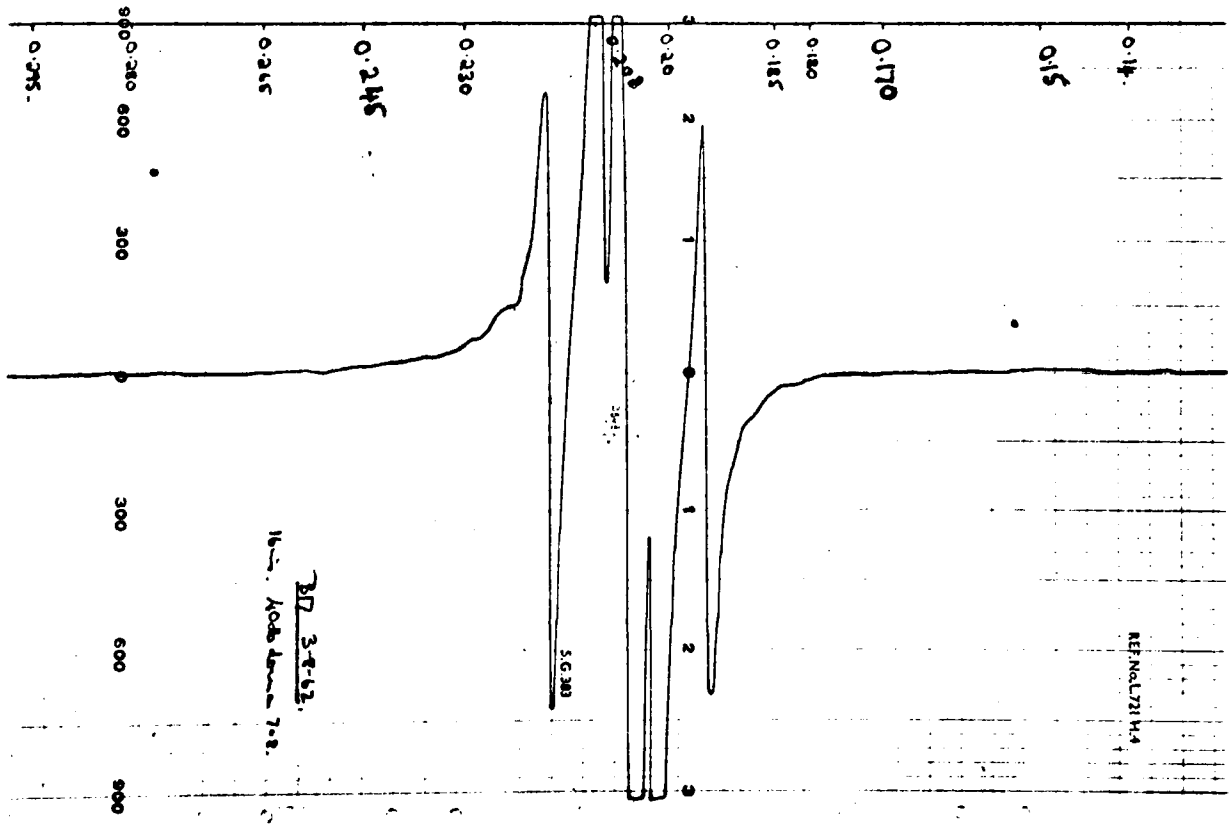


FIGURE 10.7 Gd^{3+} in $LaCl_3$, 20° K

Above: X Band pair spectrum. H// c axis

Below: Single ion lines attenuated by 1/100



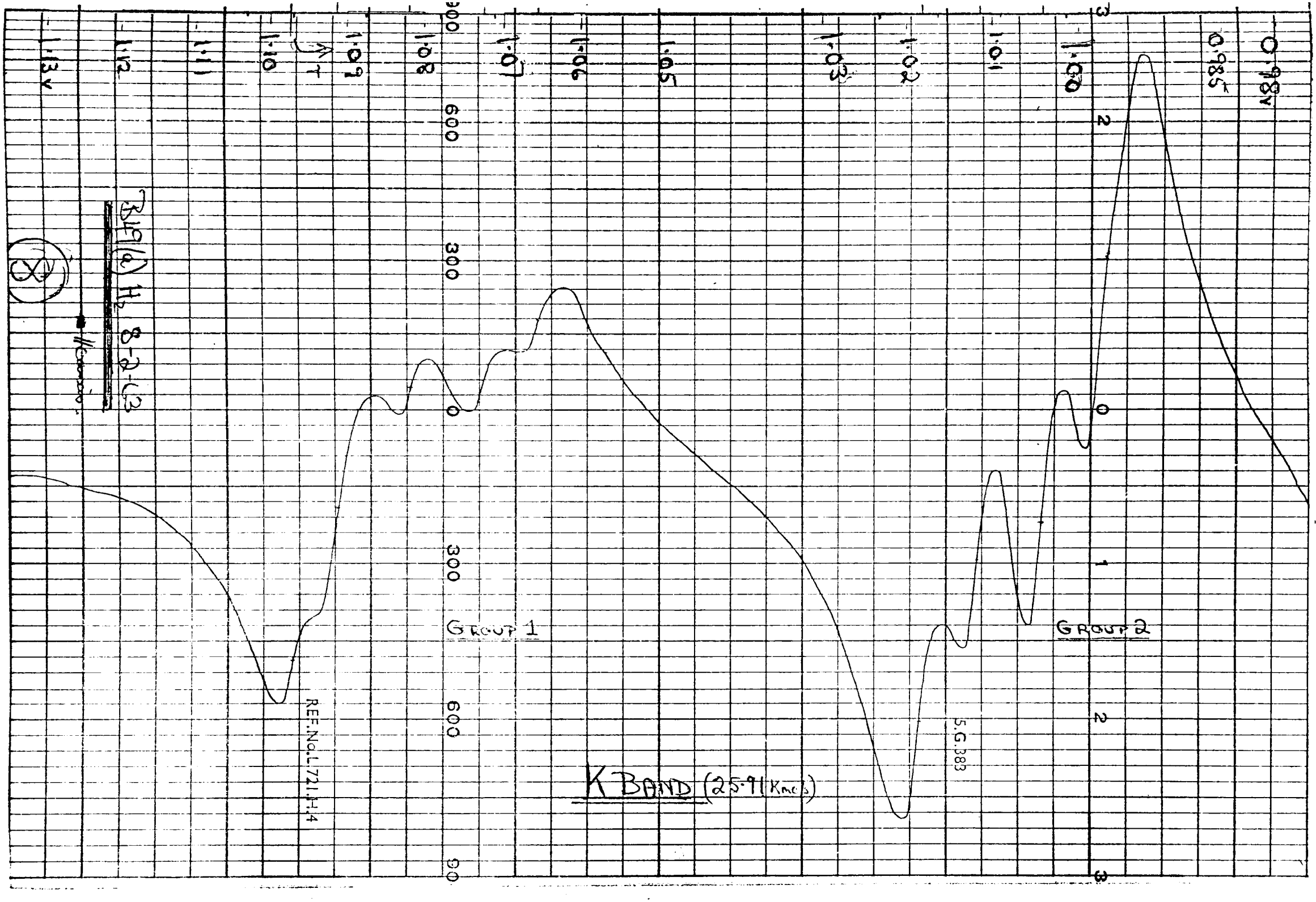

0·98V
0·985
1·00
1·01
1·02
1·03
1·05
1·06
1·07
1·09
1·10
1·11
1·12
1·13V
3
2
1
0
300
600
300
0
300
600
900
GROUP 1
GROUP 2
K BAND (25·91 KMc/s)
REF. No. L721.H.4
S.G.383
RH7(a) H2 8-2-63

FIGURE 10·8

interesting to note that in one sample three isotropic lines at 554g, 485g, and 408g were observed at a frequency of 9550 mc/s. The centre one of these occurs close to 1/7 of the field of the central line (489g) and such a "$\Delta S_z = \pm 7$" transition could arise between the $|S_z = +7/2\rangle$ and $|S_z = -7/2\rangle$ single ion states through admixtures by the small b_6^6 term of the $|S_z = -5/2\rangle$ and $|S_z = +5/2\rangle$ states respectively.

Temperature Variation

A sample was investigated at helium temperatures down to 2.0°K at X Band, and to 1.4°K at K Band. No definite conclusions could be drawn from these experiments except that the lines tended to become saturated and not resolved. At K Band the highest groups were very much reduced in intensity, thus indicating that the high field lines arise from transitions between positive T_z states (see §11.2).

Measurements were possible at 290°K at K Band frequencies because of the higher sensitivity of this spectrometer, and the results are given in Table 10.3. Unfortunately the large error on the values prohibits a detailed comparison with the 20°K results, but the grouping remains and the shifts in line position appears to be relatively small. There is evidence of a possible assymmetry about the central line. (The values given are the average of oscilloscope and chart readings).

10.4.3 The next nearest neighbour pair spectrum

The sample used for the determination of the angular variation shown in Figure 10.5 was oriented so that the magnetic field could be swept from along, to perpendicular to, the g axis through the n.n.n. direction. That is the plane XYZ of Figure 10.1 was horizontal. This was accomplished by ensuring that one of the three intense lines of spots on the Laue photograph, which lie at 30° to the hexagonal axes a and b (G. Garton, private communication) was horizontal. The lines turning at 63° are attributed to n.n.n. pairs, as the symmetry angle is close to that calculated for $LaCl_3$, 63.15°. The spectrum was not so well defined in this direction as along the c axis, possibly due to crystal imperfections. The line positions are summarized in Table 10.5, they are not exactly symmetrical about the central line although in some cases they are nearly so. In general their intensity decreases as their position relative to the main line increases.

The observation of these lines at the expected angle helps considerably to justify the assumption that most of the weak lines observed in the samples investigated are due to pair transitions.

Table 10.5

Resonance field and relative positions of lines turning at 63° from the g axis, attributed to n.n.n. pair transitions in 1% Gd (1% Ce) $LaCl_3$, 20°K. Errors (± 15g)

(ν = 9373 mc/s)

H gauss	ΔH gauss	Comment	H gauss	ΔH gauss	Comment
5553	+2176	Max.	2930	-427	
5356	+2001	Max.	2650	-499	
5302	+1945	Max.	2623	-734	Min.
4990	+1633	Max.	2521	-836	Min.
4895	+1538	Max.	2373	-984	Min.
4759	+1402	Max.	2326	-1031	Min.
4669	+1312	?	2171	-1186	Min.
4542	+1185	Max.	2020	-1337	Min.
4427	+1070	Max.	1967	-1390	Min.
4359	+1002	Max.	1821	-1536	Min.
4194	+ 837	Max.	1727	-1630	Min.
4129	+ 772	Max.	1677	-1680	½ Field Line
4062	+ 705		1431	-1926	Min.
3933	+ 576		1325	-2032	?
3893	+ 536				
3860	+ 503				
3817	+ 460				
↓	↓				
3357	0	Central Line			
↓	↓				

10.4.4 Further relevant experiments

In this sub-section, a brief mention will be made of additional experiments made at X Band frequencies which help to verify that the lines observed are due to pair transitions.

1% Gd $LaCl_3$ In order to rule out the possibility that the observed lines were due to non magnetic $Gd^{3+} - Ce^{3+}$ pairs, i.e. due to distortions of the crystal field by the Ce^{3+} ions, a sample containing no Ce^{3+} ions was investigated at 20°K. This showed the same spectrum along the $\underline{c}$ axis as observed in samples containing cerium.

Irradiated 1% Gd 1% Co $LaCl_3$ In case any of the lines observed were caused by radiation damage during orientation, a sample was subjected to an intense X-ray beam for 9 hours. This showed no additional lines.

0.1% Gd (1% Ce) $LaCl_3$, and 5% Gd (1% Ce) $LaCl_3$ In these samples the intensities of the spectrum observed were roughly in accordance with that expected from pair transitions. In the 0.1% sample the pair lines were barely visible, whilst in the 5% sample they were between ~ 1/75th and ~ 1/200th of the single ion lines and slightly broader than in the 1% samples.

1% Gd $LaBr_3$ An extensive spectrum of small lines probably due to pair transitions was observed in this sample. The spectrum with $\underline{H}$ along the $\underline{c}$ axis extended to ~ 2,200g above the central line, but bore no resemblance to that observed in $LaCl_3$.

10.5 Conclusion

The microwave spectrum of a nearest neighbour pair of Gd^{3+} ions in $LaCl_3$ has been thoroughly investigated and the positions of the observable lines established. The spectrum is symmetric about the central main line. It consists of four outer groups of lines, and three inner lines which appear to be well resolved. The groups are separated by ~ 370g and the spacing between the outer lines of each group is ~ 130g. The intensity of the transitions generally decreases as their position relative to the central line increases.

The spectrum due to the next nearest neighbour pair transitions has also been measured. In contrast to the n.n. spectrum it does not show any outstanding features.

Measurements of the single ion crystal field parameters for Gd^{3+} in $LaBr_3$ emphasize their large dependence on the exact dimensions of lattices with this structure. This confirms the conclusions of Hutchison et al. (1957) from their experiments on Gd^{3+} in $LaCl_3$.

CHAPTER 11

Paramagnetic resonance from pairs of Gd^{3+} ions in lanthanum trichloride: Theoretical discussion

11.1 Introduction

In this chapter the measurements made on the pair spectrum of Gd^{3+} in $LaCl_3$ will be discussed in terms of a suitable Hamiltonian for the pair. As mentioned in §1.4 and §10.1, in such a case of a weak exchange interaction it should be possible to determine all the interaction constants directly from the resonance line position. The Hamiltonian is described in §11.2 where the difficulties arising from the number of unknown parameters are pointed out. The problem has been treated from the start on the Oxford University Mercury computer, and the methods of calculation will be described in §11.3. The results of the calculations are discussed in §11.4.

11.2 The pair Hamiltonian

The general spin Hamiltonian for a pair of interacting ions has been given in Equation (1.5). For S state ions anisotropic exchange is expected to be small, and it has been assumed for the case of two neighbouring Gd^{3+} ions that the only interaction is due to a dipolar contribution and isotropic exchange of the Heisenberg form $\mathcal{H}_{ex} = J_{ex}\, \underline{S}^{(1)}.\underline{S}^{(2)}$. The Hamiltonian for the nearest neighbour pair, written in

terms of individual spin operators, will therefore be,

$$\mathcal{H}_p = g\mu_B \underline{H}(\underline{S}^{(1)}+\underline{S}^{(2)}) + \mathcal{H}_c^{(1)} + \mathcal{H}_c^{(2)} + J_{ex}\,\underline{S}^{(1)}.\underline{S}^{(2)} + \frac{g^2\mu_B^2}{r^3}(\underline{S}^{(1)}.\underline{S}^{(2)} - 3S_z^{(1)}S_z^{(2)}) \qquad (11.1)$$

where $\mathcal{H}_c^{(1)} = B_2^0 O_2^{0(i)} + B_4^0 O_4^{0(1)} + B_6^0 O_6^{0(1)}$ (neglecting the small B_6^6 term). The z axis of quantisation is taken along $\underline{c}$ axis joining the two ions, which are a distance r apart. (The weak hyperfine interaction of the minority isotopes with a nuclear spin has been neglected).

11.2.1 Approximate values of the parameters in the Hamiltonian

It was originally hoped that the interpretation of the observed spectrum in terms of the above Hamiltonian would be straightforward, as J_{ex} was known roughly from the bulk measurements, α could be estimated from the known crystal structure, and the crystal field interaction had been determined and found to be small by Hutchison et al (1957). However this has not proved to be the case, and the difficulty of estimating the parameters will now be outlined.

(a) The exchange constant. As the lattice parameters for $LaCl_3$ are somewhat larger than for $GdCl_3$ (cf. Table 10.1), the exchange constants may be expected to be somewhat different in the two cases. Apart from this uncertainty, however, the analysis of the susceptibility results has proved ambiguous. The original analysis, by C. D. Marquard and A. F. G. Wyatt

(private communication) of the results of Wolf et al (1962) assumed $J_{ex}(n.n.) \gg J_{ex}(n.n.n.)$. It was based on a Bethe-Peierls-Weiss model, and gave

$$J_{ex}(n.n.) = -0.1038 \text{ cm}^{-1}$$

$$J_{ex}(n.n.n.) = +0.0032 \text{ cm}^{-1}$$

Attempts were therefore made to interpret the n.n. pair spectrum along the g axis in terms of a ferromagnetic exchange. As will be discussed in §11.4 no fit can be found for an exchange constant of this sign, and only for a weak antiferromagnetic exchange is there any agreement with the observed spectrum. However more recent analysis of further susceptibility measurements, using a high temperature series expansion method, have indicated two alternative possibilities (Wyatt and Marquard, private communication). These are

$$\text{(i)} \begin{cases} J_{ex}(n.n.) = +0.112 \text{ cm}^{-1} \\ J_{ex}(n.n.n.) = -0.086 \text{ cm}^{-1} \end{cases}, \text{or (ii)} \begin{cases} J_{ex}(n.n.) = -0.153 \text{cm}^{-1} \\ J_{ex}(n.n.n.) = +0.0018 \text{cm}^{-1} \end{cases}$$

The first set, with an antiferromagnetic n.n. exchange constant appears to fit the susceptibility results better. (The error in these values is at least ± 25%).

It might appropriately be mentioned here that the n.n. ions have three possible super-exchange paths, each via one intervening chlorine ion, whereas the n.n.n. ions have only two such paths (Figure 10.1). The relevant distances are listed in Table 11.1 below, (A and B are the rare earth $-Cl^-$ distances labelled in Figure 10.1). However as the

Table 11.1

	r(n.n.) (Å)	r(n.n.n.) (Å)	A(Å)	B(Å)
$LaCl_3$	4.375	4.843	2.99*	2.97†
$GdCl_3$	4.105	4.721	2.86†	3.05†

*Hutchison et al. (1958). †Wolf et al. (1961b)

mechanism of the interaction in $GdCl_3$ is not yet fully understood, no conclusions can be drawn from the crystallography alone.

(b) <u>The dipolar interaction.</u> It should be possible to estimate the dipolar constant $\alpha = \frac{g^2\mu_B^2}{r^3}$, quite accurately from the known lattice dimensions. However the separation of two Gd^{3+} ions in $LaCl_3$ probably lies somewhere between the rare earth site separation in $LaCl_3$ and $GdCl_3$.

$\alpha = 0.02049$ cm^{-1} for $LaCl_3$ spacing.

$\alpha = 0.02461$ cm^{-1} for $GdCl_3$ spacing.

(c) <u>The crystal field</u> The crystal field seen by a member of the pair may well be different from that seen by the isolated Gd^{3+} ions since the neighbouring site is occupied by a Gd^{3+} ion instead of a La^{3+} ion. Measurements on other systems have shown this effect to be ~3% for Cr^{3+} pairs in ruby (Statz et al. 1961) and ~30% for M_n^{2+} pairs in ZnF_2 (Brown et al 1961). But because of the very great dependence of the parameters b_n^m on the structure constants found for the single ions (§10.5)

the difference may be much greater for Gd^{3+} pairs in this structure. In fact there is a possibility of additional terms occurring, due to a lowering of the symmetry through distortions caused by the adjacent Gd^{3+} ion. The neglect of the b_6^6 term may therefore not be justified, though the symmetry of the spectrum about the central line suggests such off diagonal terms are small (see § 11.4.1). The similarity of the pair spectrum at 20°K and 290°K suggests that the variation with lattice size of the crystal field seen by a member of the pair may not be as great as that found for the isolated ion, or alternatively, the pair line position may not be so dependent on the crystal field.

Of the five parameters to be fitted to the observed spectrum only the dipolar constant, $\propto$, may therefore be estimated with some confidence. J_{ex} may be expected to lie between + 0.2 and - 0.2 cm^{-1}, and the parameters b_n^m must be considered as unknown. As all of these quantities affect the pair line position to a considerable extent (see § 11.4), their exact determination presents a formidable problem until transitions may be identified with certainty. The experimentally observed grouping, and the overall spread, of the n.n. lines must be regarded as a major clue to the interpretation of the spectrum.

11.3 The calculation of the resonance line positions

The calculation of the resonance line positions is simplest when the magnetic field lies along the g axis, and only this case has been considered in detail. The Hamiltonian may then be rewritten as

$$\mathcal{H}_p = G(S_z^{(1)} + S_z^{(2)}) + J(S_+^{(1)}S_-^{(2)} + S_-^{(1)}S_+^{(2)}) + DS_z^{(1)}S_z^{(2)} + \mathcal{H}_c^{(1)} + \mathcal{H}_c^{(2)} \qquad (11.2)$$

where $G = g\mu_B H_z = 9.2956 \times 10^{-5} H_z \text{ cm}^{-1}$ (H_z in gauss)

$J = \frac{1}{2}(J_{ex} + \alpha)$, $D = J_{ex} - 2\alpha$, and $\alpha = \frac{g^2\mu_B^2}{r^3}$

For a large J_{ex} (as in most of the previous systems investigated) the problem can be treated by perturbation theory in a representation of states $|S^{(1)}S^{(2)}\ T\ T_z\rangle$, where $\underline{T} = \underline{S}^{(1)} + \underline{S}^{(2)}$ (Owen 1961). However for the present example of a weak exchange there is no such advantage in working in this representation. For example if $J_{ex} \sim -\alpha$, the matrix of $\mathcal{H}_p$ will be almost diagonal in a representation of states $|S^{(1)}S^{(2)}S_z^{(1)}S_z^{(2)}\rangle$. Between these two cases perturbation theory cannot be used, and the problem was therefore treated from the start on a computer.

The 64 x 64 matrix of $\mathcal{H}_p$, written with respect to a basis of states $|S^{(1)}S^{(2)}S_z^{(1)}S_z^{(2)}\rangle$ breaks up into fifteen matrices the basis states of which are each characterised by a constant value of $S_z^{(1)} + S_z^{(2)} = T_z$. This can be seen from the fact that the only off-diagonal elements are due to the

coefficient of J, and this operator will only connect states of the same $S^{(1)}_z + S^{(2)}_z$. Considering these matrices individually the magnetic field term will be simply $G\ T_z\ 1_{op}$ and may be considered separately. The only difference between the matrices with basis states of positive and negative T_z is due to this term. The eight matrices with basis states of positive and zero T_z are given in Appendix VA, they are listed in increasing order p (where $T_z = 8 - p$). In Appendix VB the corresponding matrices written with respect to a basis of states $|S^{(1)}S^{(2)}T\ T_z\rangle$ are given. These were found using the computer programme described below and are written in terms of J_{ex} and α, rather than J and D. It is seen that only states of the same symmetry (i.e. T odd or even) are coupled since $S^{(1)}_z S^{(2)}_z$, O^0_2, O^0_4 and O^0_6 all couple states of ΔT = even no.

11.3.1 The computer programme

The matrices of Appendix VA, with respect to a basis $|S^{(1)}_z S^{(2)}_z\rangle$, were written into the programme. For given values of J_{ex}, α, b^0_2, b^0_4, b^0_6 and H (though as H is always diagonal it was only used to test the programme) the programme could:-

(a) Calculate the matrix elements of the matrices (denoted by Δ) with respect to a basis $|S^{(1)}_z S^{(2)}_z\rangle$.

(b) Diagonalise these matrices and print the eigenvalues and eigenfunctions in terms of states $|S^{(1)}_z S^{(2)}_z\rangle$.

(c) Transform the matrices so that they were referred to a basis of states $|T\ T_z\rangle$. For this the necessary Clebsch-

Gordon coefficients were first calculated from a Library programme, and arranged into matrices $\underline{U}$. The transformed matrices (denoted by $\underline{A}'$) were then found from the relation $\underline{A}' = \underline{U}\underline{A}\tilde{\underline{U}} = \underline{U}\underline{A}\underline{U}^{-1}$ (cf. Mandl 1957, p.95).

(d) Diagonalise the matrices $\underline{A}'$, and print the eigenvalues, and eigenfunctions in terms of states $|TT_z\rangle$.

(e) Calculate and print the field for resonance, and relative intensities, of all the possible microwave transitions between the energy levels of the pair. For this $\tilde{\nu}$ (the wave number of the microwaves) had to be fed in as data and H put = 0. The matrices were transformed and diagonalised with respect to a $|T\ T_z\rangle$ representation. The resonance fields for transitions $\Delta T = 0, \Delta T_z = \pm 1$, were then calculated in a straightforward manner from the equation

$$g \mu_B H = |\tilde{\nu}| \mp (E_{pn} - E_{p+1,n'}) \qquad (11.3)$$

E_{pn} is the energy of the n^{th} level of the p x p matrix (where n = 1 for the highest level). If both the - and + signs are taken, this equation gives the fields for all possible transitions between both positive and negative T_z states. Any negative fields found must be taken as positive. A typical output of the programme is given in Table 11.2, where the integers on the left are the values of p and n for the levels concerned. The relative intensities, assumed to be given solely by the transition probabilities, were found from the relation,

D= -3.34499996, -2; J= 1.67249998, -2; G= 4.31808422, -78
J_{ex}= 1.11 50000, -2; H= 0.0000000, -128; α= 2.2300000, -2
CEF= 0.00000, -128, 0.00000, -128 0.00000, -128

$\check{\nu}$ = 3.1855300, -1

	h	m	h+1	m'	H_1	H_2	I
**	1	1	2	1	5945.87	907.99	14.0000
**	2	1	3	1	5586.02	1267.84	25.8462
*	2	1	3	3	907.99	5945.87	0.1538
*	2	2	3	2	5945.87	907.99	12.000
**	3	1	4	1	5226.17	1627.69	35.4545
*	3	1	4	3	1267.84	5586.02	0.3916
*	3	2	4	2	5586.02	1267.84	21.5385
*	3	2	4	4	907.99	5945.87	0.4615
*	3	3	4	1	9904.20	-3050.34	0.0000
*	3	3	4	3	5945.87	907.99	10.1538
**	4	1	5	1	4866.32	1987.54	42.6667
*	4	1	5	3	1627.69	5226.17	0.7879
*	4	1	5	5	-3050.34	9904.20	0.0000
*	4	2	5	2	5226.17	1627.69	28.3636
*	4	2	5	4	1267.84	5586.02	1.1748
*	4	3	5	1	8824.66	-1970.80	0.0000
*	4	3	5	3	5586.02	1267.84	17.6224
*	4	3	5	5	907.99	5945.87	0.9231
*	4	4	5	2	9904.20	-3050.34	0.0000
*	4	4	5	4	5945.87	907.99	8.4615
**	5	1	6	1	4506.47	2347.38	47.1429
*	5	1	6	3	1987.54	4866.32	1.5238
*	5	1	6	5	-1970.80	8824.66	0.0000
*	5	2	6	2	4866.32	1987.54	32.0000
*	5	2	6	4	1627.69	5226.17	2.3636
*	5	2	6	6	-3050.34	9904.20	0.0000
*	5	3	6	1	7745.11	-891.25	0.0000
*	5	3	6	3	5226.17	1627.69	22.0606
*	5	3	6	5	1267.84	5586.02	2.3497
*	5	4	6	2	8824.66	-1970.80	0.0000
*	5	4	6	4	5586.02	1267.84	14.0979
*	5	4	6	6	907.99	5945.87	1.5385
*	5	5	6	1	12423.14	-5569.28	0.0000
*	5	5	6	3	9904.20	-3050.34	0.0000
*	5	5	6	5	5945.87	907.99	6.9231

	h	n	h+1	n'	H_1	H_2	I
**	6	1	7	1	4146.63	2707.23	48.0000
*	6	1	7	3	2347.38	4506.47	3.1429
*	6	1	7	5	-891.25	7745.11	0.0000
*	6	1	7	7	-5569.28	12423.14	0.0000
*	6	2	7	2	4506.47	2347.38	31.4286
*	6	2	7	4	1987.54	4866.32	4.5714
*	6	2	7	6	-1970.80	8824.66	0.0000
*	6	3	7	1	6665.57	188.29	0.0000
*	6	3	7	3	4866.32	1987.54	22.8571
*	6	3	7	5	1627.69	5226.17	4.7273
*	6	3	7	7	-3050.34	9904.20	0.0000
*	6	4	7	2	7745.11	-891.25	0.0000
*	6	4	7	4	5226.17	1627.69	16.5455
*	6	4	7	6	1267.84	5586.02	3.9161
*	6	5	7	1	10623.90	-3770.04	0.0000
*	6	5	7	3	8824.66	-1970.80	0.0000
*	6	5	7	5	5586.02	1267.84	10.9650
*	6	5	7	7	907.99	5945.87	2.3077
*	6	6	7	2	12423.14	-5569.28	0.0000
*	6	6	7	4	9904.20	-3050.34	0.0000
*	6	6	7	6	5945.87	907.99	5.5385
**	7	1	8	1	3786.78	3067.08	42.0000
*	7	1	8	3	2707.23	4146.63	7.9999
*	7	1	8	5	188.29	6665.57	0.0000
*	7	1	8	7	-3770.04	10623.90	0.0000
*	7	2	8	2	4146.63	2707.23	24.0000
*	7	2	8	4	2347.38	4506.47	9.4286
*	7	2	8	6	-891.25	7745.11	0.0000
*	7	2	8	8	-5569.28	12423.14	0.0000
*	7	3	8	1	5586.02	1267.84	0.0000
*	7	3	8	3	4506.47	2347.38	18.8571
*	7	3	8	5	1987.54	4866.32	9.1429
*	7	3	8	7	-1970.80	8824.66	0.0000
*	7	4	8	2	6665.57	188.29	0.0000
*	7	4	8	4	4866.32	1987.54	15.2381
*	7	4	8	6	1627.69	5226.17	7.8788
*	7	4	8	8	-3050.34	9904.20	0.0000
*	7	5	8	1	8824.66	-1970.80	0.0000
*	7	5	8	3	7745.11	-891.25	0.0000
*	7	5	8	5	5226.17	1627.69	11.8182
*	7	5	8	7	1267.84	5586.02	5.8741
*	7	6	8	2	10623.90	-3770.04	0.0000
*	7	6	8	4	8824.66	-1970.80	0.0000
*	7	6	8	6	5586.02	1267.84	8.2238
*	7	6	8	8	907.99	5945.87	3.2308
*	7	7	8	1	13502.68	-6648.83	0.0000
*	7	7	8	3	12423.14	-5569.28	0.0000
*	7	7	8	5	9904.20	-3050.34	0.0000
*	7	7	8	7	5945.87	907.99	4.3077

$$I \propto |\langle \psi_{p,n} | T_x | \psi_{p+1,n'} \rangle|^2 \qquad (11.4)$$

where ψ_{pn} and $\psi_{p+1,n'}$ are the wavefunctions of the two eigenstates expressed in terms of states $|\Gamma\, T_g\rangle$. Further details of the programme are given in Appendix IVH.

The programme was tested in several ways:-

(i) With $J_{ex} = 1$, and all other parameters zero, the correct eigenvalues and eigenfunctions for the diagonalised $\underline{\Delta}$ matrices were found; the coefficients of the basis states $|S_g^{(1)} S_g^{(2)}\rangle$ in the eigenfunctions being equal to the Clebsch-Gordon coefficients. The correct transformed $\underline{A}'$ matrices was also found.

(ii) With G = 1, and all other parameters zero, the correct transformed $\underline{\Delta}'$ matrices were given. This essentially checked the normalisation and orthogonality of the Clebsch-Gordon coefficients.

(iii) With D = 1, and all other parameters zero, the correct eigenvalues were found for the transformed $\underline{\Delta}'$ matrices.

(iv) With only the crystal field parameters non zero, the energy level differences gave the same resonance fields as for the single ion transitions.

(v) The diagonal elements of O_2^0 referred to a basis of states $|\Gamma\, T_g\rangle$ (Appendix VB) agreed with those calculated from the formula given by Owen (1961) in all cases tested.

(vi) The transition probabilities, and resonance fields, given by the programme agreed with those calculated by hand

from the energy levels and eigenfunctions in several cases tested.

11.4 The results of the calculations

Only the principal results of the calculations will be given in full. Most of the work has been devoted to the nearest neighbour pair spectrum, and although no detailed interpretation has been found, for certain values of the parameters J_{ex} and α, a grouping of the theoretical lines occurs. If, as seems likely, this represents the experimental situation a value for the exchange constant can be estimated.

11.4.1 The nearest neighbour pair spectrum

The symmetry of the observed line positions above and below the central main line, especially at X Band where there is a large factor between the resonance fields of the outer lines (~ 840g and ~ 6Kg), justifies the use of a Hamiltonian of the form of Equation (11.2) containing no terms which couple states of different T_z. The overall spread of the spectrum is of the order of that expected (see below) but in general the number of lines observed is somewhat less than that found theoretically, possibly due to the fact that several are unresolved. For a large J_{ex} one would expect 26 main transitions $\Delta T = 0, \Delta T_z = \pm 1$ above, and below, the central line, if all levels were populated; but this number increases for small J_{ex} when the states of different T become admixed.

Since the resonance line position varies considerably with the values of all five parameters it is very difficult to establish the identity of any one line with certainty. The temperature variation of the spectrum in the helium range does not help in this respect unless very high fields are used, since all levels are almost equally populated for values of $|J_{ex}| \approx 0.1\ cm^{-1}$.

Only the high field lines need be considered on account of the symmetry of the spectrum. The spectrum expected at X Band from a ferromagnetic exchange of $J_{ex} = -0.1056\ cm^{-1}$ was first calculated. As a starting point the value of α for $LaCl_3$ spacing was assumed ($0.020495\ cm^{-1}$) and the line positions determined for various values, including negative signs, of the crystal field parameters b_n^o. However no agreement with the observed spectrum was found, and for most values of the parameters b_n^o lines at fields greater than 6Kg are predicted, whereas none were observed.

The variation of line position with J_{ex} was therefore determined, and is shown in Figure 11.1. For this the 90^oK values of the crystal field parameters b_n^o for the isolated ions (Table 10.2) were used, and as pointed out in §11.2.1 these may be different from those of the pair. The central region for $|J_{ex}| < 0.04\ cm^{-1}$ was investigated more carefully using a value of $\alpha = 0.023\ cm^{-1}$, that is for a spacing of ions between that in $LaCl_3$ and $GdCl_3$, and is shown in Figure 11.2.

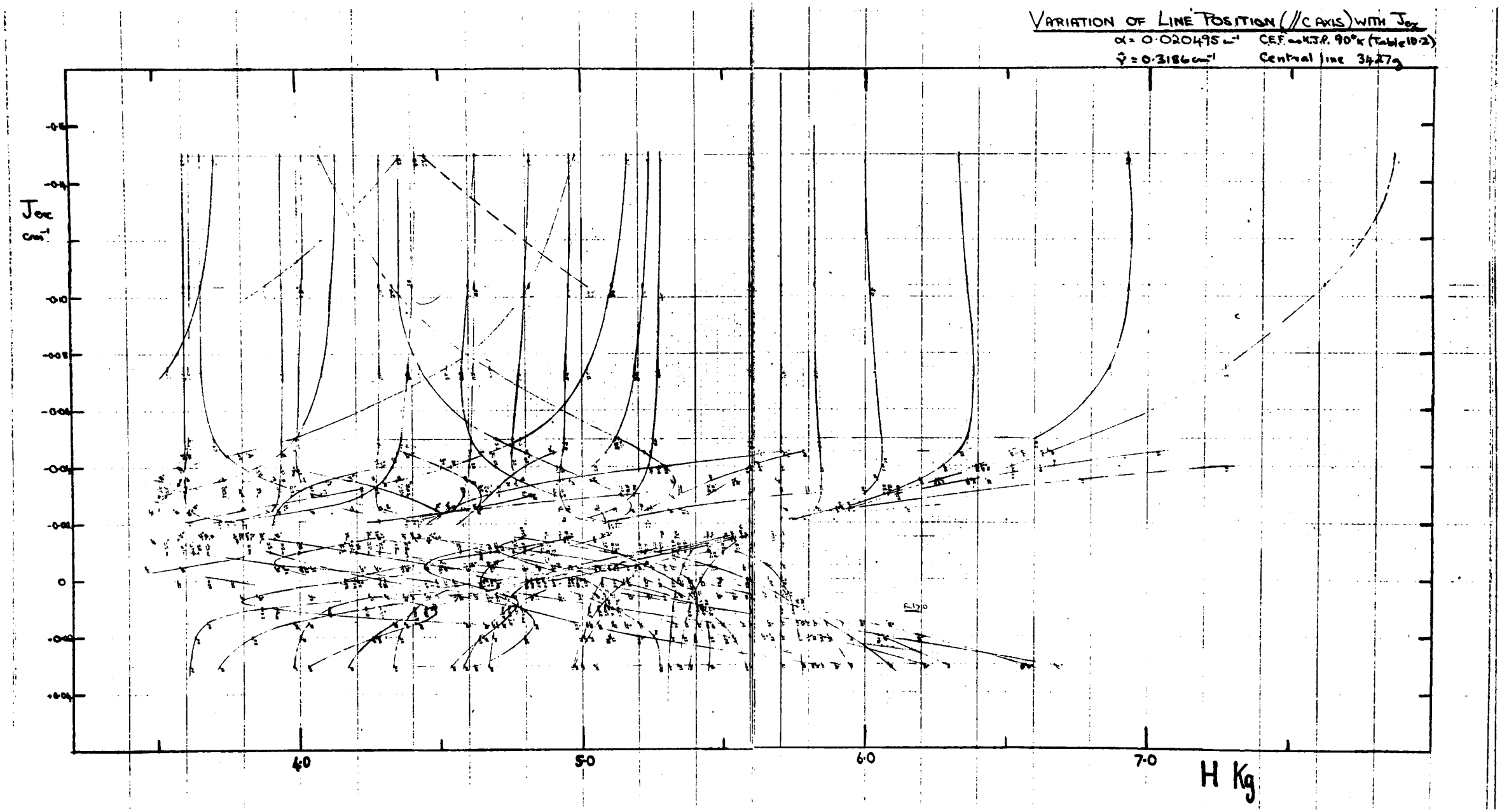

VARIATION OF LINE POSITION (// C AXIS) WITH J_{ex}
α = 0·020495 cm^{-1} C.E.F. — H.J.P. 90°K (Table 10·2)
$\bar{\nu}$ = 0·3186 cm^{-1} Central line 34·17
J_{exc} cm^{-1}
-0·15
-0·1
-0·05
0
+0·05
4·0
5·0
6·0
7·0
H Kg

FIGURE 11·1

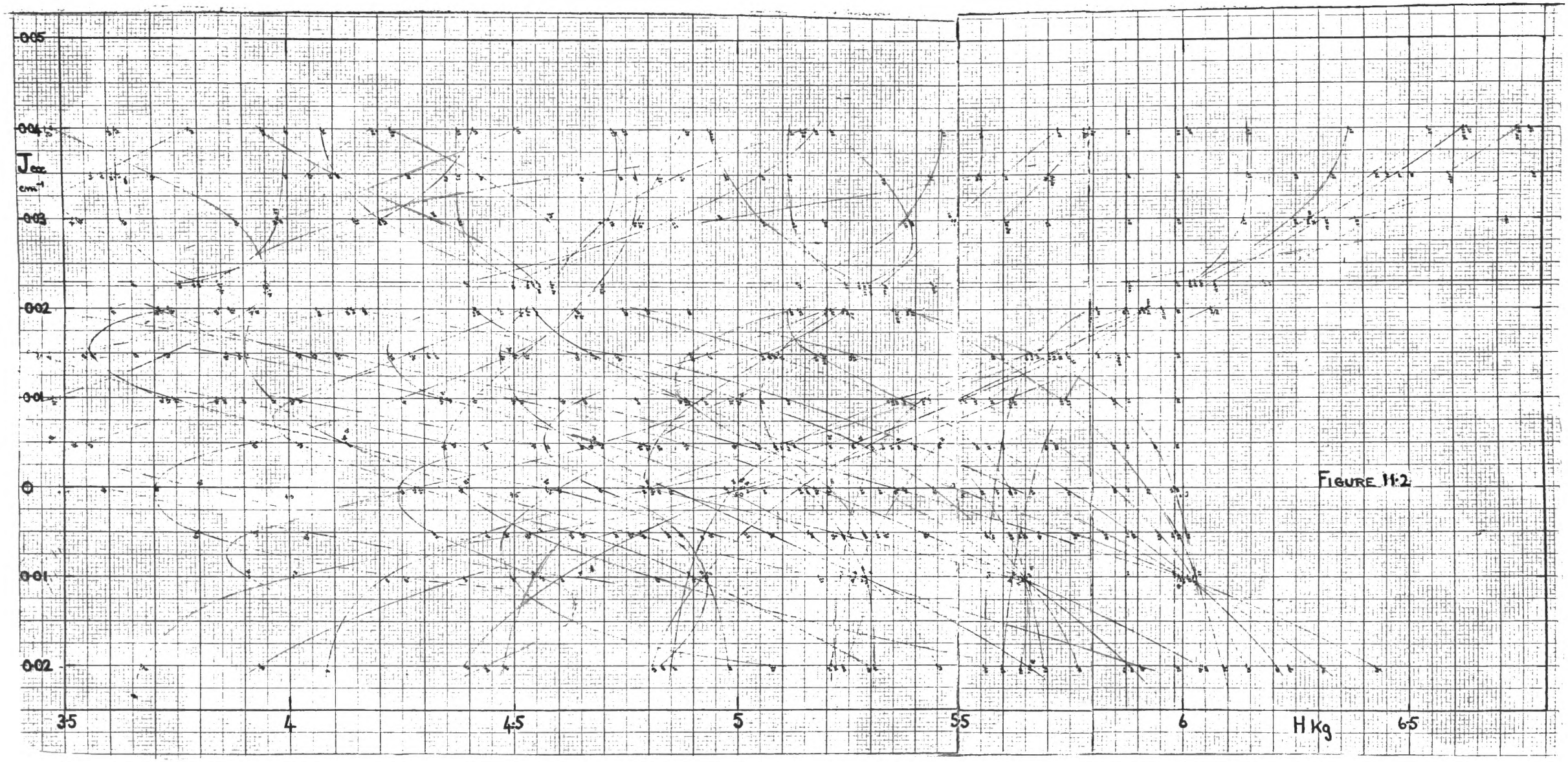


FIGURE 11·2

VARIATION OF N.N. LINE POSITION (H // c AXIS) WITH J_{ex}

$\alpha = 0.023 cm^{-1}$ C.E.F. as H.J.P. 90°K (Table 10.2)

$\tilde{\nu} = 0.3186 cm^{-1}$ Central line :- 3427g.

FIGURE 11·2

The main features of these results are,

(i) Only two lines are independent of J_{ex}. These are the $|T = 7, T_z = 7\rangle \rightarrow |T = 7, T_z = 6\rangle$ and $|6,6\rangle \rightarrow |6,5\rangle$, transitions. Their separation is due to the crystal field interaction, and their relative position from the central main line is $\frac{21\alpha}{2}$. It thus appears that these will occur in the outer groups 1 or 2.

(ii) For values of $|J_{ex}| > 0.03$ cm^{-1} lines occur at fields greater than 6Kg.

(iii) The overall spread of the spectrum increases with α.

(iv) The transitions plotted are those with a transition probability greater than $\sim \frac{1}{20}^{th}$ of that of the largest line expected. It is seen that their number decreases as $|J_{ex}|$ increases. For large $|J_{ex}|$ the line positions become independent of J_{ex}.

(v) When $J_{ex} = -\alpha$, i.e. $J = 0$ in Equation (11.2) the spectrum simplifies into four similar, equally spaced, groups of lines which are split by the crystal field by the same amount as for the isolated ion main lines.

(vi) For most values of J_{ex} there is little agreement with the observed spectrum. But when $J_{ex} \sim +0.01$ cm^{-1} a grouping of the outer lines does occur, and especially if $\alpha = 0.023$ cm^{-1} these closely resemble the experimentally observed grouping.

This latter region of grouping was investigated further, and it was found that when $J_{ex} = \alpha/2$, and $H = b_n^m = 0$, an unexpected degeneracy in the eigenvalues of $\mathcal{H}_p$ occurs, and the 36 zero field energy levels coalesce into 8. These levels are shown in Figure 11.3, where they are labelled according to their value of p and n (defined in §11.3.1). The symmetry (T odd or even) and values of T_z of the eigenstates are also given. The resonance fields for the seven distinct transitions between the levels are given in Table 11.2 and are plotted in Figure 11.4(A). They were calculated for $J_{ex} = 0.01115\ cm^{-1}$ and $\alpha = 0.0223\ cm^{-1}$, values chosen to give the closest agreement with experiment. The experimental line positions, with approximate relative intensities, are shown in Figure 11.4(c) and it is seen that the observed grouping may well arise from a situation where $J_{ex} \approx \alpha/2$. Indeed, unless the crystal field is very much different from that of the isolated ions, causing a similar grouping for different values of J_{ex} and α, it does appear that this is the correct region of J_{ex}.

The coincident lines of Figure 11.4(A) may be split by a different value of either α, or J_{ex}, as well as by the crystal field. An example of the crystal field effect is shown in Figure 11.4(B). It is seen from Figure 11.4 that although the general trends of the intensities found theoretically agree with those observed there are differences,

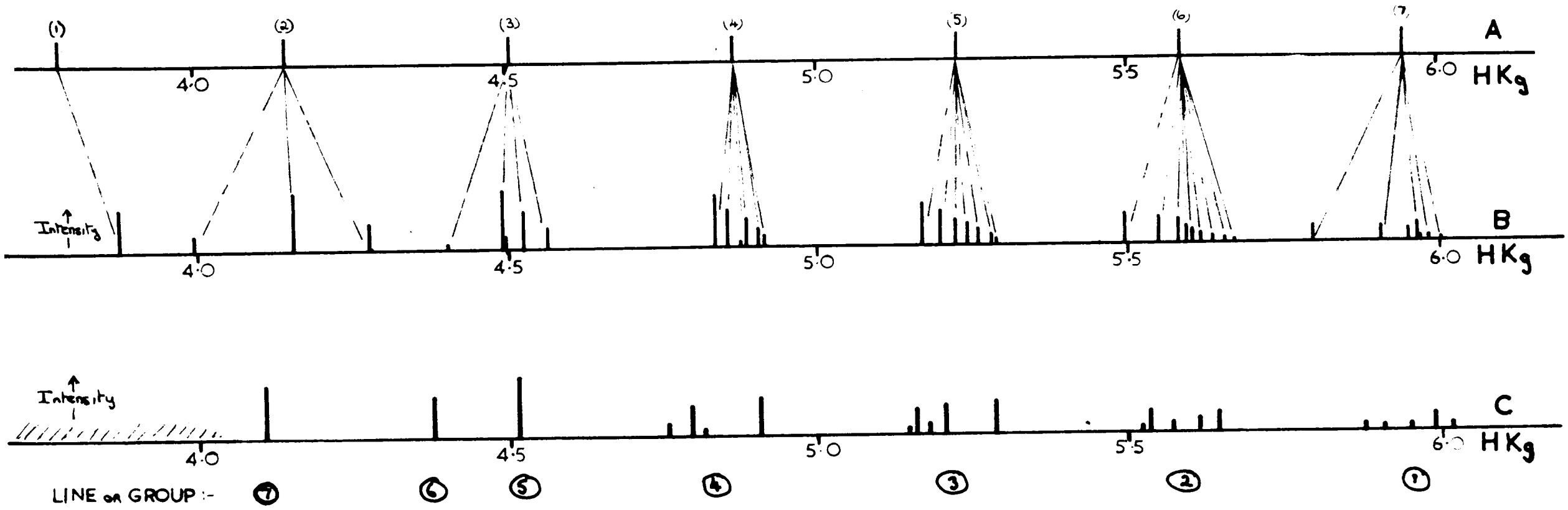
ZERO FIELD ENERGY LEVELS OF $\mathcal{H}_p$ WHEN $J_{ex} = \frac{\alpha}{2}$, CEF=0

DEGENERACY	ENERGY	EIGENFUNCTION Listed: E_{hn} T_z Symmetry (T odd or even)
1	$84 J_{ex}$	81 0 σ
3	$81 J_{ex}$	82, 71 0, ±1 e, σ
5	$75 J_{ex}$	83, 72, 61 0, ±1, ±2 σ, e, σ
7	$66 J_{ex}$	84, 73, 62, 51 0, ±1, ±2, ±3 e, σ, e, σ
9	$54 J_{ex}$	85, 74, 63, 52, 41 0, ±1, ±2, ±3, ±4 σ, e, σ, e, σ
11	$39 J_{ex}$	86, 75, 64, 53, 42, 31 0, ±1, ±2, ±3, ±4, ±5 e, σ, e, σ, e, σ
13	$21 J_{ex}$	87, 76, 65, 54, 43, 32, 21 0, ±1, ±2, ±3, ±4, ±5, ±6 σ, e, σ, e, σ, e, σ
15	0	88, 77, 66, 55, 44, 33, 22, 11 0, ±1, ±2, ±3, ±4, ±5, ±6, ±7 e, σ, e, σ, e, σ, e, σ

FIGURE II-3

NEAREST NEIGHBOUR PAIRS OF Gd^{3+} IN LaCl

Comparison of experimental line positions with those calculated from the Hamiltonian, Equation (11·2), using values of J_{exc} and a which give approximate agreement with the form of spectrum observed.



A: Theoretical line positions for $J_{exc} = a/2 = 0.01115 cm^{-1}$., No C.E.F., $\bar{\nu} = 0.3186 cm^{-1}$. (no. in brackets = no. of coincident "main" pair lines).

B: Theoretical splitting of coincident lines by C.E.F. of Hutchison et al. (Table 10·2, 90°K).

C: Experimental positions of largest pair lines, $\bar{\nu} = 0.3186 cm^{-1}$, with (very) approx. relative intensities.

FIGURE 11·4

and the number of theoretical lines is also greater. This is particularly true for the inner groups where apparently resolved single lines are observed experimentally. However Figure 11.4(B) is for a special case, and it is found that for slightly different values of α, J_{ex}, or b_n^m, it is quite possible for some of the lines to coincide, and for their relative positions within the groups to change. This can also be seen from Figure 11.2.

The experimentally observed grouping of the lines thus appears to be somewhat fortuitous, but it may be noted that no such grouping is found for Gd^{3+} pairs in $LaBr_3$, nor for the n.n.n. pairs in $LaCl_3$ (§10.4).

The angular variation of the spectrum has not yet been considered theoretically. The variation in high fields at K Band should be the easier case to treat by perturbation theory, once the identification of states has been fully established.

11.4.2 The next nearest neighbour pair spectrum

Only a relatively brief theoretical analysis of the n.n.n. pair problem has been made. Experimentally (Table 10.5) the lines are not exactly symmetric about the central main line, as expected since there will be crystal field terms b_n^m with $m \neq 0$ when $\underline{H}$ and z are in this direction. If the z axis of quantisation is taken along $\underline{r}$, the line joining the ions, the Hamiltonian of Equation (11.2) may be taken to represent the

situation to first order in the crystal field. The value of α, appropriate to a spacing of ions between that in $LaCl_3$ and $GdCl_3$, is 0.0157 cm^{-1}. An estimate of the effective crystal field parameters to first order may be obtained from solving the equations for $\underline{H}$ along the $\underline{g}$ axis given by Bleaney et al. (1954) using the averaged relative line positions at 63° to the $\underline{g}$ axis (Figure 10.4). (That is, quantising along the n.n.n. axis the crystal field will contain terms b_n^m for most even n and m, but to first order only those of m = 0 are considered). These effective parameters are found to be

$$b_2^0 \text{ (eff)} = -3.4 \times 10^{-4} cm^{-1}$$

$$b_4^0 \text{ (eff)} = -0.45 \times 10^{-4} cm^{-1}$$

$$b_6^0 \text{ (eff)} = +9.0 \times 10^{-6} cm^{-1}$$

so that crystal field effects are expected to be small.

Two regions of values of J_{ex} have been considered, and whilst no definite account of the observed spectrum has been possible, the number and spread of lines shows greater agreement for a value of $J_{ex}(n.n.n.) \sim -0.086\ cm^{-1}$ (i.e. ferromagnetic) than with $J_{ex}(n.n.n.) \sim 0$.

11.5 Conclusion

Although it has not yet been possible to make a detailed interpretation of the n.n. pair spectrum of Gd^{3+} ions in $LaCl_3$, it does appear that the grouping of the observed lines may well correspond to a situation where $J_{ex} \sim \alpha/2$. Since,

for a relation $J_{ex} = \alpha/2$ and no crystal field interaction, it has been found that an unexpected degeneracy of the levels occurs, and the theoretical pair spectrum coalesces into seven lines equally spaced on either side of the central main line. Although unlikely, it is conceivable that the experimentally observed grouping could arise from a very different value of J_{ex}, and to a lesser extent of α, if the crystal field interaction for each member of the pair differs greatly from that for the isolated ions. With this reservation in mind, it may be concluded that the isotropic exchange constant for n.n. ions is $J_{ex} = +0.011\ (\pm 0.005)\ cm^{-1}$, antiferromagnetic in sign, and that the dipolar interaction constant, $\alpha = \frac{g^2\beta^2}{r^3} = 0.022\ (\pm 0.002)\ cm^{-1}$.

Positive confirmation of the above values can only come from an exact fit of all the lines. In this connection it may help to identify transitions if very high fields for resonance and low temperatures could be used, providing saturation could be avoided. (Using 4 or 8 mm. wavelengths at $0.1^{\circ}K$ for example). In this way only the states of large negative T_g would be populated, and the transitions between them could be identified. A further theoretical analysis of the spectrum would best be undertaken using perturbation theory, in the region of $J_{ex} = \alpha/2$. Using the matrices of Appendix VB, the matrix of $\mathcal{H}_p$ could be rewritten with respect to a basis of the states which diagonalise $\mathcal{H}_p$ when

$J_{ex} = \alpha/2$ and $b_n^m = 0$.

No thorough analysis of the next nearest neighbour spectrum has been made, but it does appear unlikely that $J_{ex} \sim 0$. Thus, providing the change in lattice spacing from $LaCl_3$ to $GdCl_3$, does not alter the sign of the exchange interaction, both the n.n. and n.n.n. pair spectra indicate that the first of the two alternative results of the susceptibility analysis given in § II.2.1 is more likely to be correct.

CHAPTER 12

Electron paramagnetic resonance of rare earth ions in the monoclinic yttrium trichloride structure

12.1 Introduction

Although the anhydrous trichlorides of ions in the second half of the rare earth series, from dysprosium to lutetium, have a monoclinic crystal structure, and are not simple in this respect, the magnetic ions in these compounds do lie close together ($\sim 4\mathring{A}$) and the concentrated salts show some interesting ordering properties. Preliminary susceptibility measurements on the monoclinic trichlorides of Kramers ions (A. P. D. Hyatt, private communication) show that $DyCl_3$ becomes antiferromagnetic at about 2.45°K, and $ErCl_3$ remains paramagnetic down to 1.3°K. The behaviour of $YbCl_3$ in the helium range is not yet fully understood.

In order to help to understand these susceptibility measurements, and to provide information on the general properties of rare earth ions in this structure, measurements have been made of the principal g values of Dy^{3+}, Er^{3+}, and Yb^{3+} in the isostructural monoclinic $LaCl_3$ and YCl_3 lattices. Of more academic interest only, the principal g values of Ce^{3+} and Nd^{3+} in YCl_3 have been measured. These measurements are complementary to those of Hutchison and Wong (1958) on the resonance of rare earth ions in $LaCl_3$, which has the hexagonal structure of the concentrated anhydrous chlorides of ions in the first half of the rare earth series, cerium to gadolinium,

(the structure of $TbCl_3$ is uncertain).

The results will be discussed in §12.5. At the present time they can only be compared directly with the susceptibility measurements. As a source of information on the crystal field at the rare earth site, the principal g values will require supplementary data from optical and other work, more data being required than in the case of the garnets as the point symmetry at this site is very low (C_2). However to a first approximation the six nearest chlorine ions may be considered to form a distorted octahedron about the rare earth site, and as a preliminary theoretical discussion the results will be considered briefly in terms of such an approximation.

12.2 Crystal structure of YCl_3 and the directions of the principal axes of the g tensors

The anhydrous trichlorides of ions from the second half of the rare earth series $DyCl_3$ to $LuCl_3$, and also YCl_3, have been found by Templeton and Carter (1954) to have the true monoclinic structure of $AlCl_3$. The space group of this structure is $C_{2/m}$, and Figure 12.1 shows a photograph of a model of one unit cell, (constructed by Mr. R. Shore). Considering the case of YCl_3, there are four Y^{3+} (g) sites (the black balls in Figure 12.1) per unit cell, and twelve Cl^- sites (white balls). The Y^{3+} ions lie in layers, parallel to the (001) planes, which are separated by about 6Å. The point symmetry at the Y^{3+} site is C_2, there being a twofold rotation axis parallel to the b

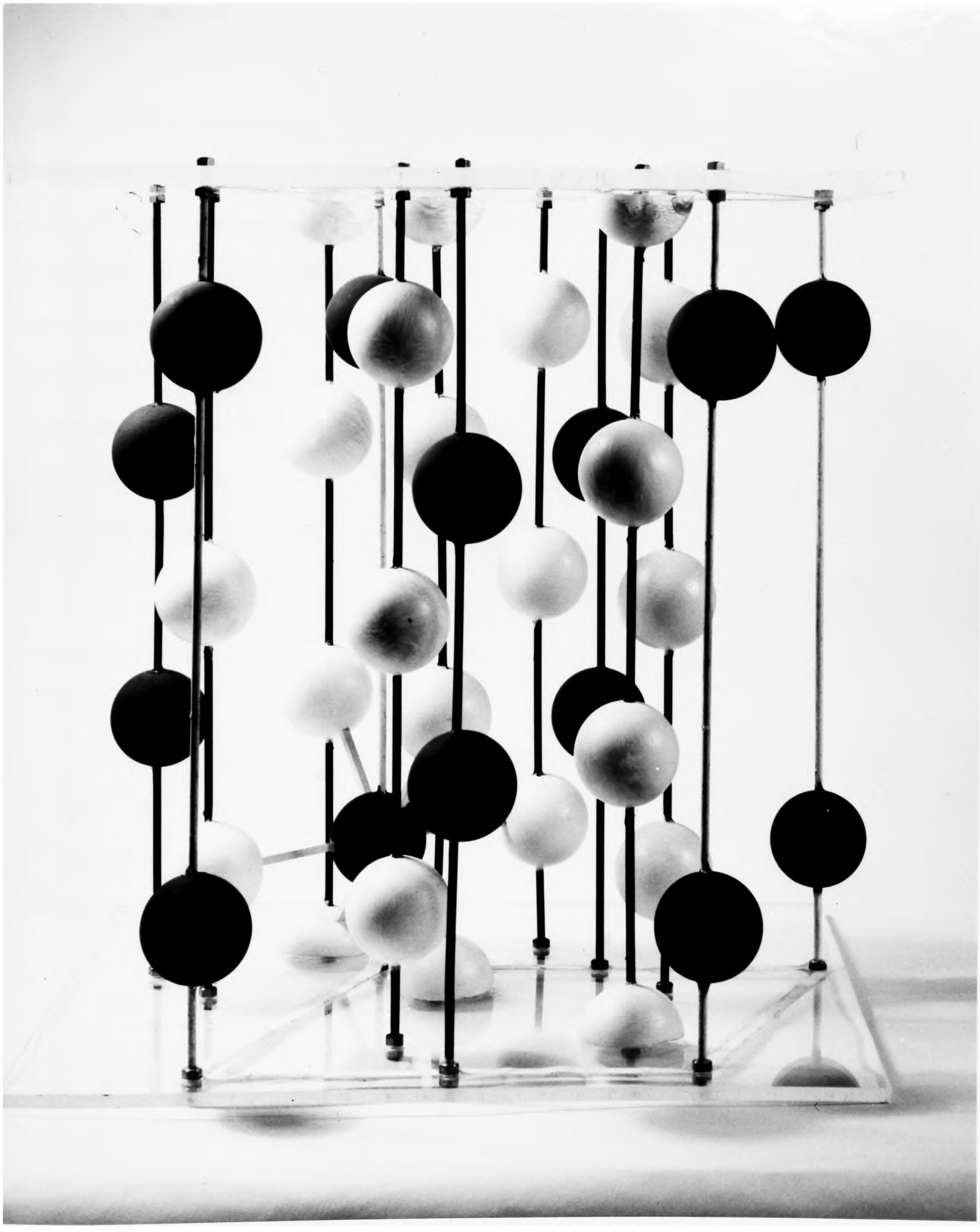


FIGURE 12·1

axis of the crystal. The six nearest neighbour Cl^- ions form a distorted octahedron about the Y^{3+} site, with three pairs of Cl^- ions at distances of 2.58Å, 2.63Å, and 2.69Å, from the site. However, the axes of the octahedron bear no simple relation to the crystallographic axes, nor, as will be seen, to the principal axes of the g tensor. The positions of the ions are given in Table 12.1 together with values of the lattice parameters for YCl_3 and $LuCl_3$. Figure 12.2 shows a [010] projection of the unit cell.

Table 12.1

Positions of ions in the monoclinic YCl_3 structure, space group $C_{2/m}$.

Equivalent positions:- (0,0,0) & $(\frac{1}{2},\frac{1}{2},0)$

Y^{3+} in 4(g) positions $\pm$ (0,y,0) where y = 0.166

Cl^- in 4(i) positions $\pm$ (x,0,z) where x = 0.211, y = 0.247

Cl^- in 8(j) positions $\pm$ (x,y,z) where x = 0.229, y = 0.179

$\pm$ (x,$\bar{y}$,z) z = 0.760

	a(Å)	b(Å)	c(Å)	β
YCl_3	6.92	11.94	6.44	111.0°
$LuCl_3$	6.71	11.60	6.39	110.4°

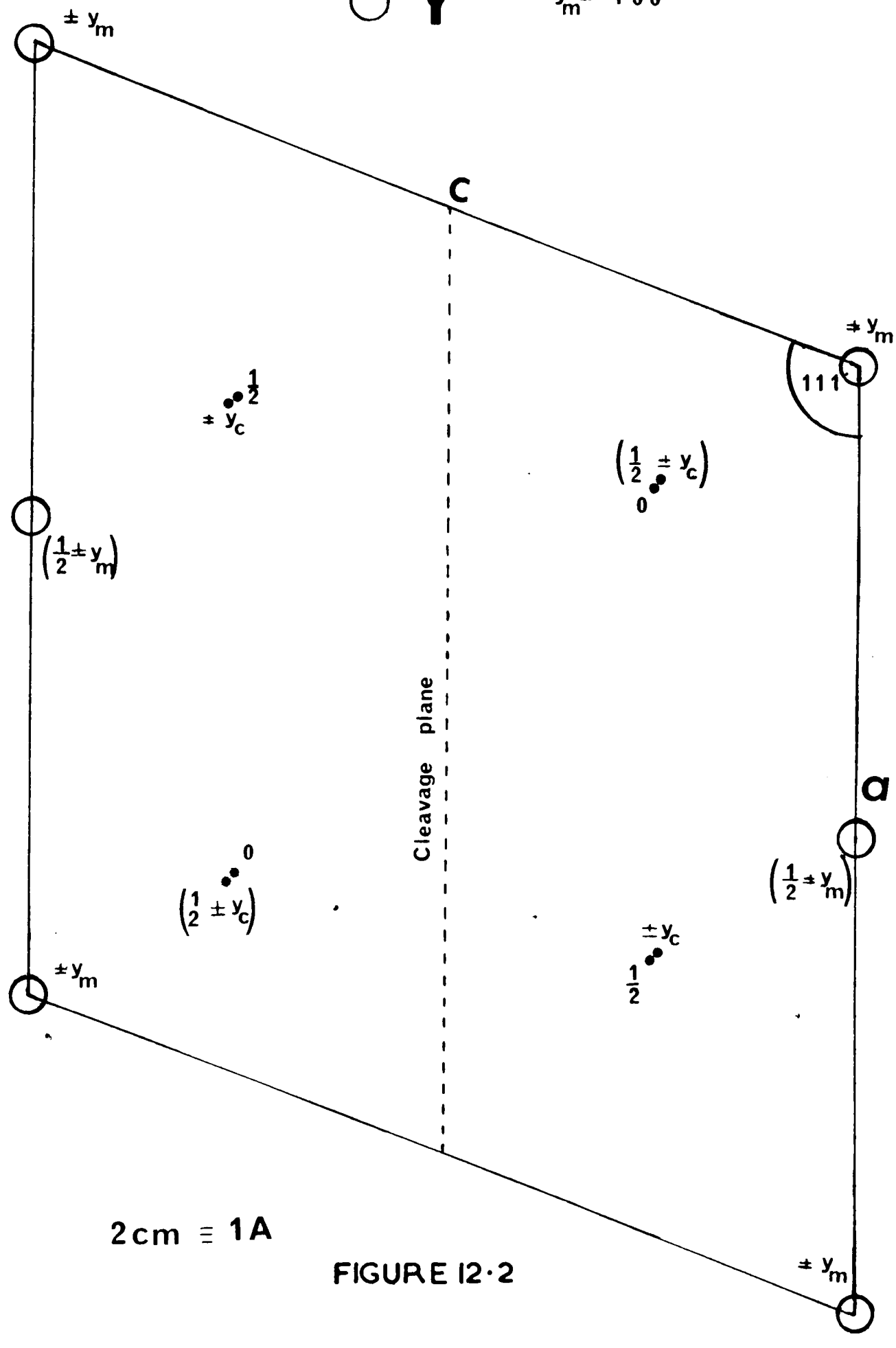
By a simple argument we can now show that the four rare earth sites are magnetically equivalent. From the point symmetry at the Y^{3+} sites, one principal g value (g_b) lies along the b axis. The other two principal g values must

YCl_3 Structure

[010] Projection

• **Cl** $y_c = \cdot 179$

○ **Y** $y_m = \cdot 166$



2cm ≡ 1A

FIGURE 12·2

therefore lie in a plane perpendicular to this axis, that is in a plane parallel to the (010) mirror plane which bisects the unit cell. Since the Y^{3+} site at (0,y,0) is crystallographically equivalent to that at ($\frac{1}{2}$,$\frac{1}{2}$ + y,0), these sites must also be magnetically equivalent. Furthermore, the sites at ($\frac{1}{2}$,$\frac{1}{2}$ + y,0) and ($\frac{1}{2}$,$\frac{1}{2}$ - y,0) are mirror images in the (010) plane through ($\frac{1}{2}$,$\frac{1}{2}$,0), as one axis of the g tensor lies perpendicular to this reflection plane, the g tensor at one site can only be reflected into itself again at the other. These sites must therefore also be magnetically equivalent, and by similar arguments so must (0,y,0) and (1,1 - y, 0). This conclusion is verified by the observation of only one resonance line.

Figure 12.3 shows the directions of the principal g values, which are denoted by g_1, g_2 and g_3, relative to the axes of the crystal a, b, and c. g_a is the effective g value in the direction of the a axis, and α the angle between g_1 and the a axis; g_1, g_a and g_2 all lying in the (010) mirror plane.

The crystals have a layer like appearance and cleave very easily parallel to the (001) plane. They are very hygroscopic and are rapidly hydrolised by the atmosphere, and were therefore handled either in a dry box or under dry paraffin.

12.3 Crystal orientation and experimental procedure

The crystals were grown by Dr. G. Garton and Mr. R. Shore using the Bridgman-Stockbarger method. Most of the crystals prepared were of sufficiently good quality to enable measurements

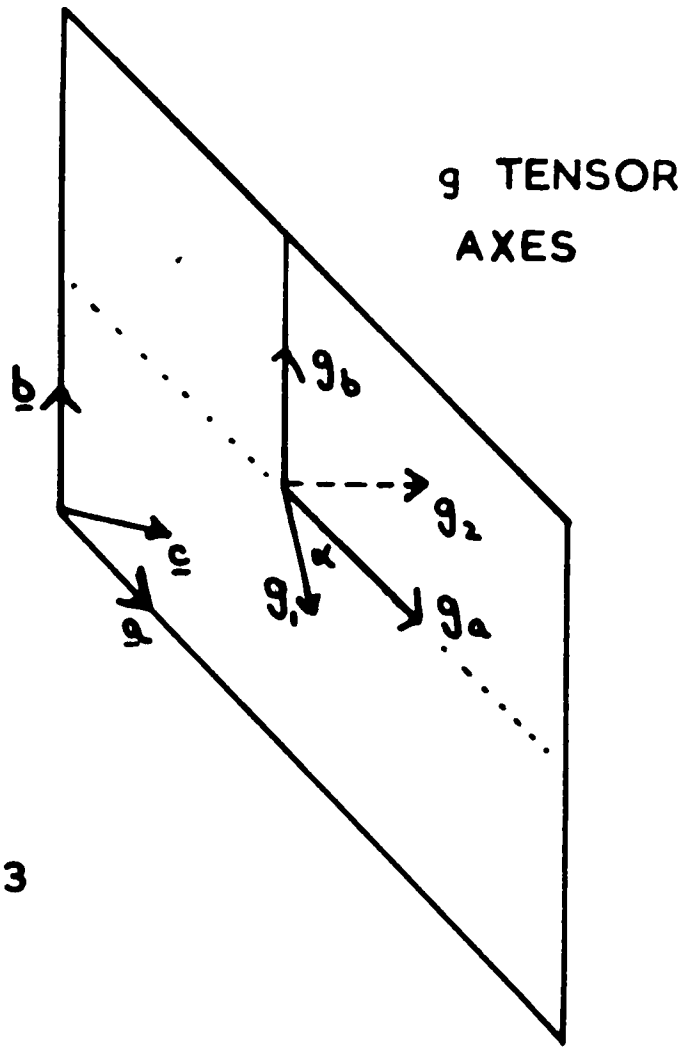


FIGURE 12·3

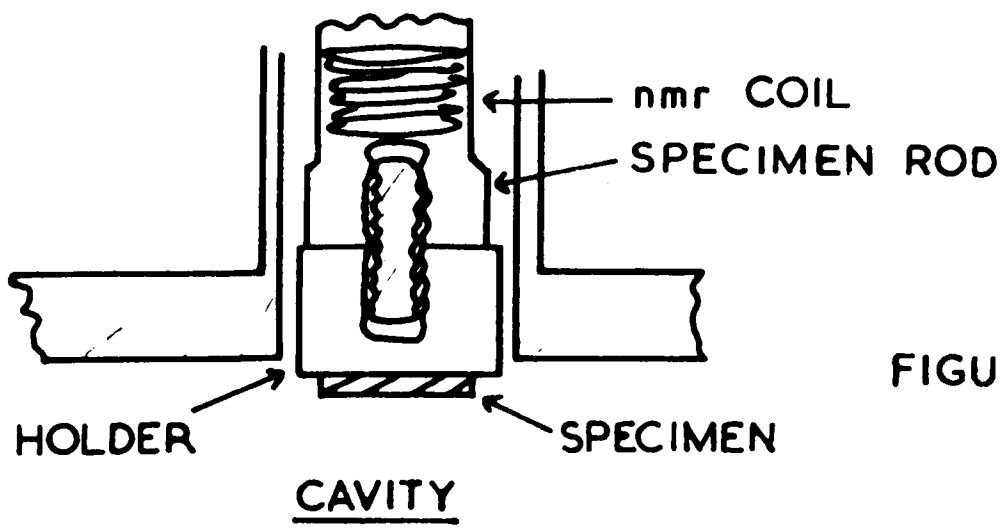


FIGURE 12·4

to be made on them, although a few showed evidence of multi-crystalline growth. In this respect their conditions of growth appear to be far less critical than those of crystals with the $LaCl_3$ structure.

The resonance was investigated at X Band frequencies. Two experiments were performed on each crystal. In the first the magnetic field was swept in the (001) cleavage plane to determine g_a and g_b, and in the second the magnetic field was swept in the (010) mirror plane to determine g_1 and g_2. The angle α was then calculated from the formula

$$g_a^2 = g_1^2 \cos^2\alpha + g_2^2 \sin^2\alpha \qquad (12.1)$$

The orientation of the crystal for the first experiment was achieved by cleaving the crystal into a thin rectangular block with faces parallel to the (001) plane. This was then attached with Apiezon grease to the plane face of perspex specimen holder, as shown in Figure 12.4.

For the second experiment it was essential that the crystal was oriented with the mirror plane accurately horizontal. This orientation was carried out by Mr. R. Shore and the procedure used will be briefly outlined. As the crystals were optically clear, they could be roughly oriented by the use of highly convergent polarised light, viewing normal to the cleavage plane. The Bertrand lens interference images showed two "eyes" where the optic axes cut the crystal surface. The line joining these "eyes" was found to lie parallel to the b axis for both

YCl_3 and $LuCl_3$ by measuring the lattice constant in this direction from a rotation-transmission X-ray photograph. Thus the mirror plane, lying perpendicular to both the b axis and cleavage plane, could be found approximately. The crystal was finally aligned using Laue back-reflection of white X-rays. The X-ray beam was passed normal to the (001) cleavage plane when the photograph showed a line of mirror symmetry containing the (010) plane. The techniques used for the X-ray orientation, and the transfer of the crystal to the specimen holder were similar to those described in §10.2. The accuracy of the alignment of the crystal in the cavity was estimated to be $\sim 2^{\circ}$. The mounted crystals were found to suffer no ill effects on cooling to helium temperatures.

All measurements were made at helium temperatures, although resonance from Yb^{3+} ions was also observed at $20^{\circ}K$. Straightforward video detection was found to be sufficient in all cases, the magnetic field being modulated at 50 c/s. The magnetic field was measured by simultaneous observation of N.M.R., corrections being made using a sample of d.p.p.h. attached to the crystal as described in § 3.4. The apparatus and magnet were carefully levelled to minimise misorientation error. The N.M.R. frequency was measured with a Hewlett-Packard frequency counter, and the microwave frequency from the calibrated dial of the L.F.E. stabilised source used. Random and systematic errors were estimated as for the garnets (§ 3.4). misorientation errors were estimated from the accuracy of orientation of the

samples and reproducibility of results.

12.4 Experimental Results

The principal g values of the ions investigated are given in Table 12.2. The experiments were made on samples containing 1% rare earth ions, and in some cases the accuracy of the measurements was limited by the broadening and slight splitting of the E.P.R. line due to crystal distortions. That distortions were the main cause of the broadening was shown by the fact that a sample of 0.1% Dy in YCl_3 gave no reduction in line width. Half intensity full widths were of the order of 30-100 gauss. In most cases the resonance was visible over the whole of the spectrum and was measured every 10°, the g values being determined from a straight line graph in the usual manner. A typical spectrum is shown in Figure 12.5, where the measurements in both planes are given. In the cases where the lines split at angles between the two turning values, greater weight was given to the measurements at the turning values.

The intensity of the resonance from Ce^{3+} and Nd^{3+} was much lower than that from the other three ions, probably due to the fact that these ions did not fit the lattice so well and entered in a smaller concentration. The Ce^{3+} resonance was only observable at the turning points when the field was swept in the (010) mirror plane. In the case of Nd^{3+} the width of the line varied from 12 gauss at g_2, to 100 gauss at g_1, when the field was swept in this plane, thus indicating that some

Table 12.2

Results for the principal g values (g_1, g_2, g_b) of rare earth ions in YCl_3 and $LuCl_3$. The axes chosen are shown in Figure 12.3

Ion	Lattice	g_a	g_1	g_2	g_b	α
Dy^{3+}	YCl_3	6.78 ± 0.03	6.86 ± 0.03	3.02 ± 0.06	9.34 ± 0.03	± 9° (± 5°)
	$LuCl_3$	7.16 ± 0.03	7.21 ± 0.02	3.16 ± 0.05	8.84 ± 0.02	± 7° (−7°) (+4°)
Er^{3+}	YCl_3	8.29 ± 0.03	8.27 ± 0.05	3.78 ± 0.05	7.70 ± 0.03	0 (± 8°)
	$LuCl_3$	8.35 ± 0.02	8.34 ± 0.02	3.51 ± 0.03	7.92 ± 0.02	0 (± 5°)
Yb^{3+}	YCl_3	2.985 ± 0.004	2.99 ± 0.02	1.53 ± 0.02	2.957 ± 0.006	0 (± 9°)
	$LuCl_3$	2.96 ± 0.01	2.95 ± 0.01	1.58 ± 0.01	2.96 ± 0.01	0 (± 5°)
Ce^{3+}	YCl_3	1.595 ± 0.005	1.60 ± 0.01	0.66 ± 0.02	1.708 ± 0.003	0 (± 10°)
Nd^{3+}	YCl_3	1.170 ± 0.008	1.16 ± 0.03	2.63 ± 0.02	1.653 ± 0.005	0 (± 8°)

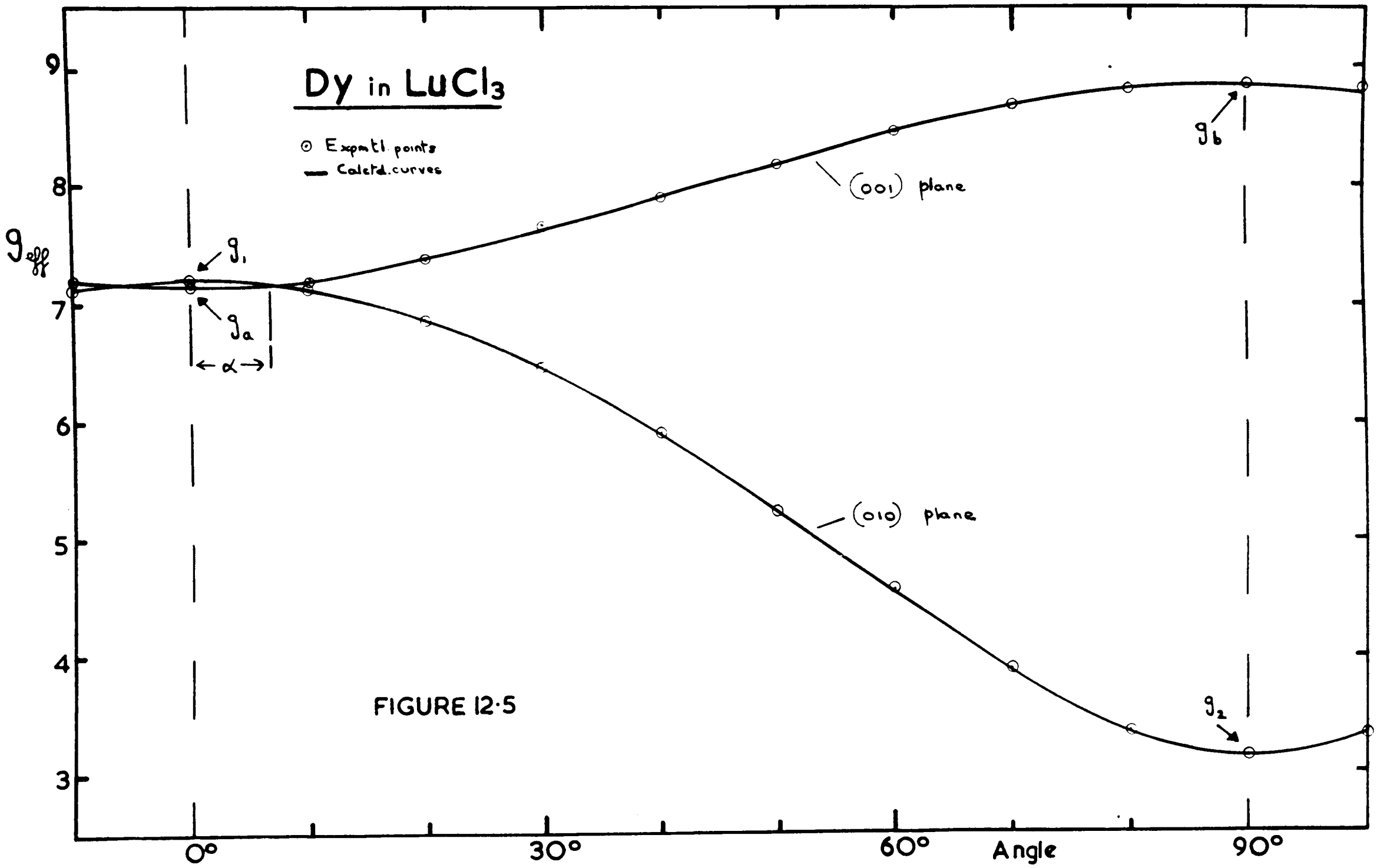

Dy in LuCl3
⊙ Expmtl. points
— Calcfd. curves
(001) plane
(010) plane
g1
ga
gb
g2
α
geff
9
8
7
6
5
4
3
0°
30°
60°
90°
Angle

FIGURE 12·5

distortions may be due to the (001) planes of the crystal rotating relative to each other.

Using polarised light to determine the direction of the b axis, a distinction was made between the two turning values observed in the (001) cleavage plane for Nd^{3+}, and Yb^{3+} in YCl_3. Impurities of Dy^{3+} and Er^{3+} in both the 1% Nd^{3+} and 1% Ce^{3+} samples enabled g_b to be correlated for all cases. The principal g values of these impurities agreed well with those measured in the corresponding 1% samples.

In order to check the orientation of crystals with the (010) mirror plane horizontal, measurements were repeated on different samples of Dy^{3+} in $LuCl_3$ and YCl_3, and of Ce^{3+} and Nd^{3+} in YCl_3. In all cases agreement with the first measurements was within experimental error. Measurements made in this plane on impurities of Er^{3+} in the 1% Yb^{3+} in $LuCl_3$ and 1% Ce^{3+} in YCl_3 samples also agreed with those in the 1% Er^{3+} samples.

The angles α given in Table 12.2, determined from Equation (12.1), were found in most cases to be almost zero. The large errors are due to the fact that the g value changes very slowly with angle near the turning points. In the case of Dy^{3+} however the angle was finite, and a direct measurement in YCl_3 gave it to be $\pm 7^{\circ}$ ($\pm 4^{\circ}$) in good agreement with that obtained from Equation (12.1). The sign of the angle, as it is defined in Figure 12.3, has not yet been determined. It requires a

determination of the direction of the c axis from X-ray work in the actual sample used.

Although resonance from 1% Gd^{3+} in YCl_3 was observed at 20°K it was not measured because of the complex analysis involved in terms of a crystal field of such low symmetry as C_2. Resonance from 1% Sm^{3+} in YCl_3 was also observed but occurred at or beyond the limit of the available magnetic field. A sample of 1% Pr^{3+} in YCl_3 gave no resonance.

The hyperfine structure of Dy^{3+}, Er^{3+}, and Yb^{3+} was measured when possible, but has not been fully analysed as it is irrelevant to the immediate aim of the investigation. A sample of 5% Dy^{3+} in YCl_3 showed satellite lines which, from their angular variation, were possibly due to pairs of Dy^{3+} ions.

12.5 Discussion

In Table 12.3 the R.M.S. of the observed principal g values are given, together with the Curie constants calculated from $C = 0.09383\ \overline{g_i^2}$. It is seen from both Tables 12.2 and 12.3 that the principal g values of the ions measured are not very dependent on their host trichloride lattice, in contrast to the large variations found in the garnet lattices. Reliable predictions of their values in the concentrated trichlorides may therefore be made. However the agreement between the calculated and experimental Curie constant in the case of $ErCl_3$ is poor, and a further investigation of the latter is required.

Table 12.5

Values of the r.m.s. of the principal g values given in Table 12.4, and calculated Curie constants. Experimental values for the Curie constant are given for comparison (Hyatt 1968).

Ion	Host	$g_{r.m.s.}$	$C_{calc.}$	$C_{exp.}$
Y^{3+}	YCl_3	6.91 (± 0.03)	4.48 (± 0.04)	-
	$LuCl_3$	6.83 (± 0.03)	4.38 (± 0.05)	
Er^{3+}	YCl_3	6.88 (± 0.03)	4.44 (± 0.04)	7.5
	$LuCl_3$	6.94 (± 0.03)	4.52 (± 0.04)	
Yb^{3+}	YCl_3	2.58 (± 0.02)	0.626 (± 0.04)	-
	$LuCl_3$	2.58 (± 0.01)	0.624 (± 0.02)	
Ce^{3+}	YCl_3	1.404 (± 0.015)	-	-
Nd^{3+}	YCl_3	1.91 (± 0.04)	-	

The antiferromagnetic ordering of $DyCl_3$ cannot be explained in any simple manner in terms of the E.P.R. measurements, (cf. DyAG, discussed in § 5.2), but it is not surprising in view of the layer like structure of the crystal, with ions lying as close as ~4Å within each layer, whilst the layers are separated by ~6Å.

An interpretation of the principal g values in terms of the exact crystal field is completely out of the question until a large number of further experimental data become available. For a crystal field of C_2 point symmetry there are 14 parameters in the crystal field Hamiltonian if one considers only one configuration, and 23 if one includes odd order terms. Prather (1961) lists the coefficients occurring in the expansion of the potential, Equation (A2.10). The even order terms are,

$$\gamma_{20}\ \gamma^c_{22} \qquad \gamma_{40}\gamma^c_{42}\ \gamma^s_{42}\ \gamma^c_{44}\gamma^s_{44} \qquad \gamma_{60}\ \gamma^c_{62}\ \gamma^s_{62}\ \gamma^c_{64}\ \gamma^s_{64}\ \gamma^c_{66}\ \gamma^s_{66}$$

(the term γ^s_{22} vanishing if suitable axes are chosen).

However the nearest six chlorine ions may to a first approximation be considered to form a distorted octahedron about the rare earth site, and if we neglect further neighbours we may consider the rare earth ion as situated in a six-fold co-ordinated cubic field. The axes of the octahedron do not bear any simple relation to the g tensor principal axes, but by comparing the values of $g_{R.M.S.}$ with the expected g values from

a cubic field, it is possible to determine the nature of the ground state in this cubic approximation.

Each ion will be considered briefly, with reference to the tables and diagrams of Lea, Leask and Wolf (1962), (L.L.W.). In the diagrams referred to in the following paragraphs, the appropriate sign of W (Equation (4.4)) has been taken into account, so that the energies of the levels are given by multiplying E by $|W|$.

An estimate of the relative importance of fourth to sixth order terms based on a point charge model is given from Table A2.3, by $V_4^0/V_6^0 = \frac{26R^2}{3} \cdot \frac{\langle r^4 \rangle}{\langle r^6 \rangle}$. Taking $\langle r^6 \rangle / \langle r^4 \rangle \sim 4(\text{a.u.})^2$ (Table 4.3) and R = 2.6Å, this gives $V_4^0/V_6^0 \approx 56$. However, as has been seen in the case of the garnets, the sixth order terms are likely to be more important than indicated by such a simple model by a factor ~ 10.

(a) Cerium (J = 5/2)

The lowest J state of cerium, J = 5/2, is unaffected by sixth order crystal field terms. In a six-fold co-ordinated cubic field the ground state is a Γ_7 doublet with an isotropic g = 1.43. The value of $g_{R.M.S.} = 1.40$, given in Table 12.5, lies quite close to this, and suggests that an octahedral field may be a good first approximation.

(b) Praseodymium (J = 4)

In an octahedral field Pr^{3+} has a Γ_1 singlet state lowest (L.L.W.) and the fact that no resonance was observed from 1½

Pr^{3+} in YCl_3 is consistent with this approximation.

(c) Neodymium (J = 9/2)

The L.L.S. diagram for Nd^{3+} in an octahedral field is reproduced in Figure 12.6, where it is seen that there can be either a Γ_6 doublet or Γ_8 quartet state lowest. As the Γ_6 doublet has an isotropic g value of 2.66, which does not correspond to the value of $g_{R.M.S.} = 1.91$, it is probable that in this approximation the $\Gamma_8^{(2)}$ state lies lowest. That is $x < 0.82$, or $V_4/V_6 < 25$.

(d) Dysprosium (J = 15/2)

The L.L.S. diagram for Dy^{3+} in an octahedral field is the same as that for Er^{3+} in an eightfold cubic field given in Figure 4.5. The value found for $g_{R.M.S.} = 6.91$ lies between the isotropic g values expected from the two possible lowest doublets; $g = 6.67$ (Γ_6) and $g = 7.56$ (Γ_7), although it suggests that the Γ_6 is more likely to be lowest in this approximation. The g values of Dy^{3+} do not show such a large dependence on the host trichloride lattice as found in the garnets, and this suggests that the appropriate L.L.S. parameter x lies away from the crossing in Figure 4.5.

(e) Erbium (J = 15/2)

Figure 4.4, that for Dy^{3+} in an eight-fold cubic field, is the appropriate L.L.S. diagram for Er^{3+} in an octahedral field. Of the two possible ground states in this approximation, the Γ_7 doublet is more probable as the value found for $g_{R.M.S.} = 6.9$ is

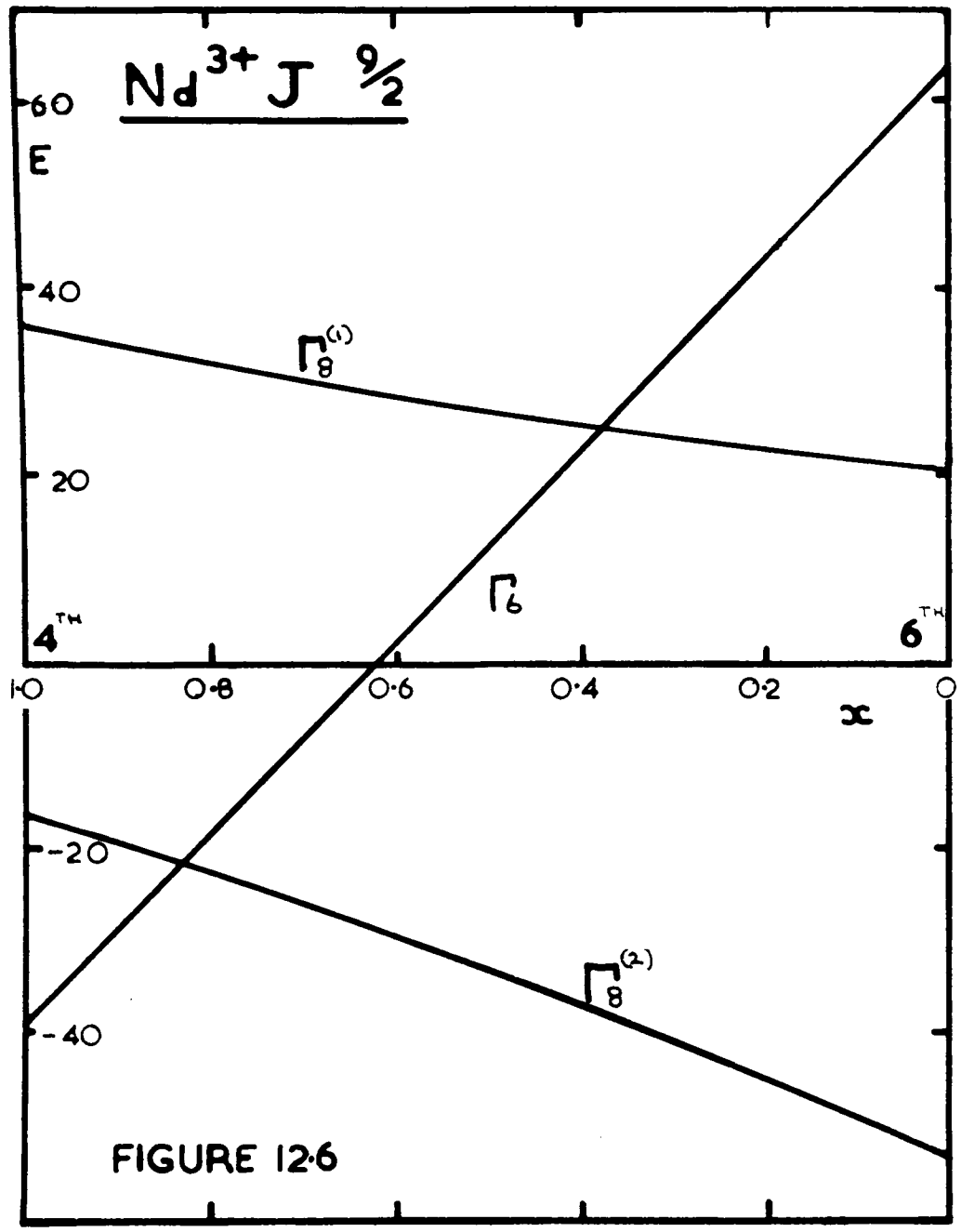


FIGURE 12·6

ENERGY LEVELS IN A SIXFOLD CUBIC CRYSTAL FIELD

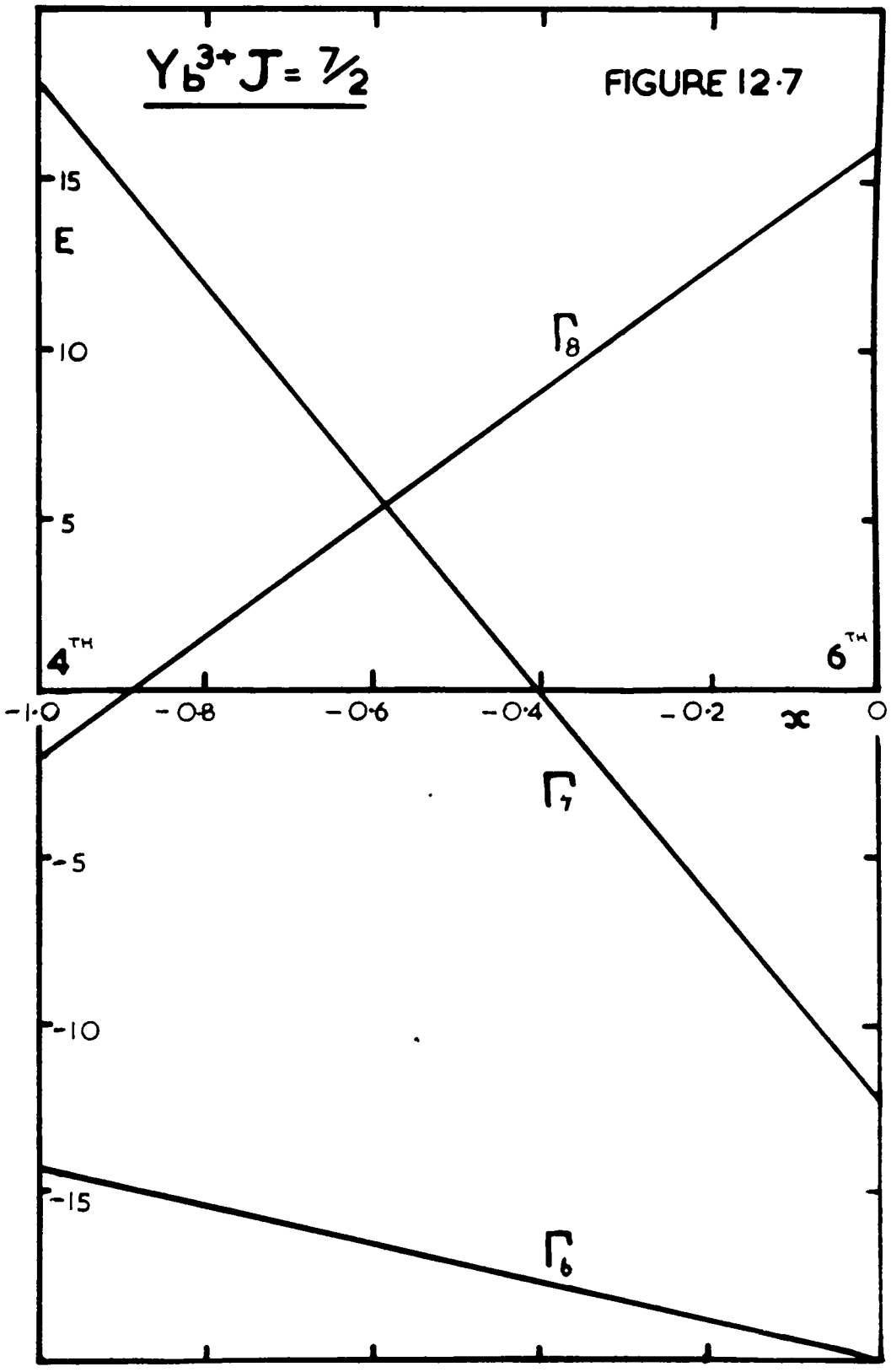


FIGURE 12·7

close to the isotropic g = 6.80 of this state. This suggests that x < 0.57, or V_4/V_6 < 14.3, in this case. Again there is far less dependence of the principal g values on the host lattice than in the case of the garnets.

(f) Ytterbium (J = 7/2)

The appropriate L.L.S. diagram for Yb^{3+} in an octahedral field is given in Figure 12.7, and it is seen that there is only one possibility, that of the Γ_6 doublet with g = 2.67 as ground state. The experimental value of $g_{R.M.S.}$ = 2.56 corresponds quite closely to this, the small difference, and quite large anisotropy in the g values, suggesting that the admixture of other states by the crystal field is larger than in the garnets.

12.6 Conclusion

From the preliminary discussion above, we may conclude that a sixfold co-ordinated cubic field may be taken as a fair first approximation to the crystal field at the rare earth site in the monoclinic trichlorides. In this approximation the results for Er^{3+} and Nd^{3+} indicate that sixth order terms may well be important. Further experimental data is required before a more detailed analysis of the crystal field is attempted.

As the measured g values show only a small variation with lattice it will be possible to use them directly for the quantitative explanation of bulk magnetic measurements. However only preliminary susceptibility results are at present available,

and the agreement between the calculated and experimental Curie constant of $ErCl_3$ suggests that further investigation of the latter is necessary.

Finally it might be noted that because of the small distances between neighbouring rare earth sites, these structures may form good host lattices in which to study the interactions of magnetic ions from their pair spectra.

CHAPTER 13

Miscellaneous E.P.R. experiments on systems of possible interest

13.1 Introduction

In all scientific research there is a certain amount of work undertaken which gives negative or inconclusive results. Nevertheless it is important that such work does not go completely unrecorded, and in this chapter the results of experiments which fall into this category will be briefly discussed.

13.2 Resonance from pairs of Ce^{3+} ions in $LaCl_3$

Lanthanum trichloride forms a good lattice in which to investigate the interaction between rare earth ions as the nearest neighbour lattice sites are separated by only 4.375 Å along the hexagonal c axis (cf. §10.2). Hutchison et al. (1958) have found that Ce^{3+} in $LaCl_3$ has principal g values $g_{\parallel} = 4.037\ (\pm 0.002)$ and $g_{\perp} = 0.17\ (\pm 0.08)$, and from these values one might expect $CeCl_3$ to show interesting dipolar ordering properties below $1^{\circ}K$, in a similar manner to dysprosium ethyl sulphate (Cooke et al 1959[b]). It is therefore of special interest to investigate the interaction between cerium ions in this lattice. As cerium has no nuclear spin the pair spectrum should simply consist of two lines for each pair.

13.2.1 Nearest neighbour pairs-theory

The most general interaction between two ions of effective spin $S' = \frac{1}{2}$ may be represented by

$$\mathcal{H}_1 (1,2) = \underline{S}^{(1)} . \underline{\underline{K}} . \underline{S}^{(2)} \qquad (13.1)$$

The spin Hamiltonian of the pair will therefore be (cf. Equation (1.5))

$$\mathcal{H}_p = \mu_B \underline{H} . \underline{\underline{g}}^{(1)} . \underline{S}^{(1)} + \mu_B \underline{H} . \underline{\underline{g}}^{(2)} . \underline{S}^{(2)} + \underline{S}^{(1)} . \underline{\underline{K}} . \underline{S}^{(2)} \qquad (13.2)$$

If the only interactions are isotropic exchange anisotropic exchange and dipolar, by symmetry $\underline{\underline{K}}$ would be expected to have only two non zero terms: $K_{xx} = K_{yy} = K_\perp$, and $K_{zz} = K_{//}$. The z axis is taken along the $\underline{r}$ direction joining the two ions, a distance r apart. If it is assumed, as a first approximation, that for the two identical ions $g^{(1)}_{//} = g_{//}$ and $g^{(1)}_{\perp} = 0$, then the Hamiltonian may be rewritten as

$$\mathcal{H}_p = G(S^{(1)}_z + S^{(2)}_z) + D\, S^{(1)}_z S^{(2)}_z + J(S^{(1)}_+ S^{(2)}_- + S^{(1)}_- S^{(2)}_+) \qquad (13.3)$$

where $G = g_{//} \mu_B H \cos\theta$, ($\theta$ being the angle between $\underline{H}$ and the $\underline{r}$ axis).

$$D = K_{//} \quad , \text{ and } J = \tfrac{1}{2} K_\perp$$

$\mathcal{H}_p$ may easily be diagonalised exactly, and when $\theta = 0$ the resonance fields of the allowed transitions are given by

$$H_0 = \frac{h\nu}{g_{//}\mu_B} \qquad \text{(Single ion)}$$

$$\left.\begin{aligned} H_1 &= H_0 + x \\ H_2 &= H_0 - x \end{aligned}\right\} \text{(Pair transitions); where } x = \frac{K_\perp - K_{//}}{2g_{//}\mu_B} \qquad (13.4)$$

For the above approximation regarding $g_\perp$, $K_{//} = (J_{ex} - 2\alpha + P_{//})$ and $K_\perp = (J_{ex} + P_\perp)$; where J_{ex} is the isotropic exchange constant, $\underline{P}$ the anisotropic exchange tensor, and $\alpha = \frac{g_{//}^2 \mu_B^2}{r^3}$. If α can be estimated, it should therefore be possible to determine $(P_\perp - P_{//})$ from the observed spectrum. J_{ex} however cannot be found from the line position, as mentioned in §1.4. (This may be seen from symmetry arguments alone, and is true for $\mathcal{H}_p$ (equation 13.3) with no approximations made). For r = 4.375 Å, as in $LaCl_3$, the value of $\alpha/g_{//}\mu_B$ = 430 gauss.

If, as discussed in §11.2.1, the crystal field seen by a member of the pair is different from that seen by an isolated ion, $g_{//}$ will be altered for the pair and the resonant lines will appear asymmetric about the central single ion line.

When the magnetic field makes a small angle with the $\underline{g}$ axis, the pair lines will be separated from the central line by $\pm \frac{\lambda}{\cos \theta}$ gauss.

13.2.2 Nearest neighbour pairs - experiments

The crystals were grown and oriented by Mr. S. Itzcovitz in a similar manner to that described in §10.2. Several samples showed evidence of multicrystalline growth and measurements were made only on the very best.

Samples of 1% and 5% Ce^{3+} concentration were investigated

at X Band frequencies, and at 4.5°K. 115 Kc/s phase sensitive detection and chart display were used; the magnetic field being measured from the calibrated magnet exciting current, and the microwave frequency from the calibrated dial of the L.F.D. source. The positions of the more definite lines observed in both samples are given in Table 13.1. The g value

Table 13.1

Resonance fields of lines observed at 4.2°K in samples of 1% and 5% Ce^{3+} in $LaCl_3$ when H is along the g axis, some of which are possibly due to pair transitions. (Errors in H ~ ± 6g, in ΔH ~ ± 12g). Intensities relative to the main Ce^{3+} line in the 1% sample are given.

		X-ray oriented 1% Ce. 9419 mc/s		Eye oriented 5% Ce. 9454 mc/s	
Comment	Rel. Int.	H gauss	ΔH gauss	H gauss	ΔH gauss
Definite	~0.05%	2290	+636	2289	+633
?	<0.05%	2224	+570	2215	+559
?	<0.05%	2056	+402	2063	+407
Definite	~ 8%	1698	+ 44		
MAIN	100%	1654	0	1656	0
Definite	~10%	1621	- 33		
Definite	~0.2%	769	-885	763	-893

found for the main Ce^{3+} line was $g_{//} = 4.07$ (± 0.03) which is slightly larger than that found by Hutchison et al. (1958).

All the lines listed appeared to have a minimum along the g axis, and most were smaller than expected for pair transitions (i.e.~1% of the main line intensity).

As none of the lines observed are symmetric about the main line it is difficult to identify which may arise from pairs of ions. The effective g values of these lines do not agree with those of any possible rare earth impurities. The larger inner lines, resolved only in the 1% sample, are probably due to more distant neighbours. The low field line at ~765 g was more definite than any of the others observed, and it is possible that the weaker line at ~2290g is the corresponding high field transition for the n.n. pair. In which case from Equation (13.4) $g_{//}$ (pair ion) = 4.4, α = 0.10 cm^{-1}, and $(P_{\perp} - P_{//})$ = 0.11 cm^{-1}. However more experimental data is required before these values can be taken with any confidence.

The most puzzling feature about the spectrum is the small size of the "pair" lines, this may arise from the concentration being less than the nominal 1%; the lowest field line was relatively larger in the 5% sample. It might be mentioned that in cerium ethyl sulphate the presence of a low lying excited doublet gives rise to an appreciable quadrupole-quadrupole interaction between the ions (Bleaney 1961). This has been neglected here as the splitting to the next excited state is larger in $CeCl_3$ (Hutchison et al. 1958), but it may

still affect the line position considerably.

13.3 E.P.R. of magnetic ions in ThO_2

ThO_2 has the cubic crystal structure of CaF_2, the thorium ions form a face-centred lattice each ion being surrounded by eight oxygen ions at the corners of a cube. It is therefore an ideal lattice for the investigation of the properties of tetravalent ions in a cubic crystal field. The resonance of three such ions was investigated in small but perfect crystals of ThO_2 grown by Dr. J. Chadwick.

13.3.1 Tb^{4+} in ThO_2

Tb^{4+}, with electronic configuration $(4f)^7$ has an $^8S_{7/2}$ ground state, and a nuclear spin of $I = 3/2$. A crystal of ThO_2 containing nominally 1% Tb was investigated at helium temperatures and resonance attributed to Tb^{4+} ions observed. The spectrum consisted of anisotropic groups of four lines each with an overall spread of ~ 90g, the groups being separated by ~ 2-300 g. Line widths were ~ 5g. This sample has since been thoroughly investigated by J. Murrell (private communication) and it has been found that Tb^{4+} has a very large zero field splitting for an S state ion in a cubic field (cf. Gd^{3+} below).

13.3.2 U^{4+} in ThO_2, Gd^{3+} in ThO_2

U^{4+} with an electronic configuration of $(5f)^2$ has the same lowest state, $^3H_4$, as Pr^{3+} $(4f)^2$. In an eightfold cubic field there is the possibility of either a Γ_5 triplet (large 4^{th} order terms) or a Γ_1 singlet (large 6^{th} order terms) lowest, (Lea et al. 1962). Llewellyn (1956) has observed a resonance in powders of solid solutions of U^{4+} in ThO_2, with $g \sim 2.7$, even at room temperature, and also in ThO_2 powder containing U^{5+} ions, with $g \sim 1.25$. U^{5+}, with a configuration $(5f)^2$ has a Γ_8 state lowest in an eightfold cubic field (cf. Ce^{3+} $(4f)^1$).

Several samples in the form of small perfect crystals containing 1% and 5% uranium were investigated at X Band frequencies and at temperatures between 290°K and 4°K, but no resonance which could unambiguously be attributed to U^{4+} or U^{3+} was observed. 50 c/s video, and 115 Kc/s P.S.D. were used, and the regions of field for $g \sim 2.7$ and $g \sim 1.25$ were carefully investigated.

One sample containing nominally 5% U^{4+} gave a very weak spectrum centred at $g \sim 2$. This sample was oriented (by Dr. Chadwick) with the (110) plane horizontal, and the spectrum at 4.2°K plotted out using 115 Kc/s phase sensitive video detection. The spectrum, shown in Figure 13.1, was found to be due to impurity ions of Gd^{3+}. Values of the parameters c and d (defined at the end of § A2.3.3) were

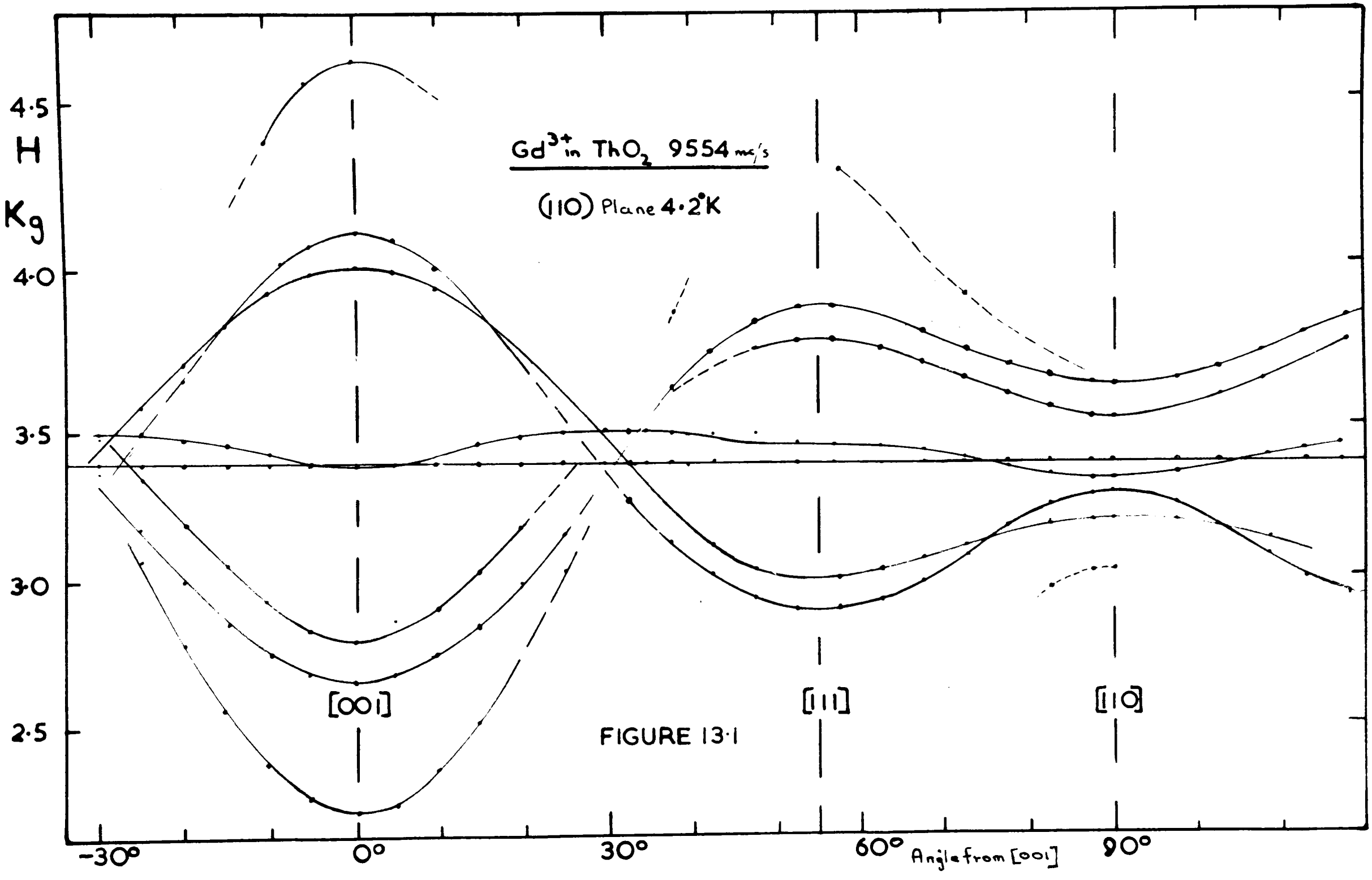

Gd^{3+} in ThO_2 9554 mc/s
(110) Plane 4·2°K
H
Kg
4·5
4·0
3·5
3·0
2·5
[001]
[111]
[110]
−30°
0°
30°
60°
90°
Angle from [001]

FIGURE 13·1

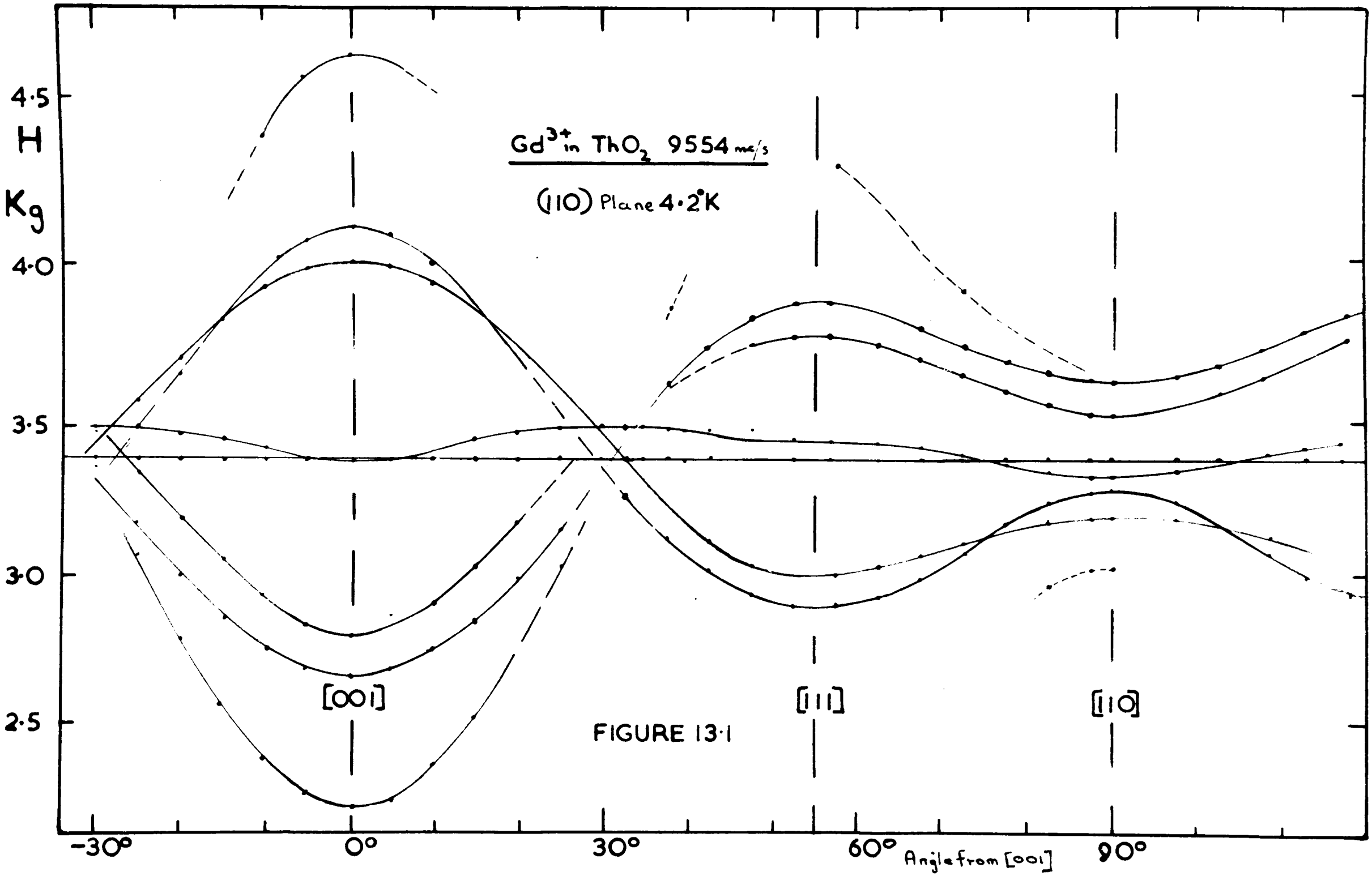

Gd^{3+} in ThO_2 9554 mc/s
(110) Plane 4·2°K
H
Kg
4·5
4·0
3·5
3·0
2·5
[001]
[111]
[110]
-30°
0°
30°
60°
90°
Angle from [001]

FIGURE 13·1

determined from the spectrum in the [001] direction, and agree within the experimental error with those of Low and Shaltiel (1958). They are compared below.

Table 13.2

	e(gauss)	d(gauss)	g
Present measurement (4.2°K)	241 (±4)	1.0(± 5)	2.00 (±0.01)
Low and Shaltiel (90°K)	242.0 (± 0.8)	1.8(±0.8)	1.991 (±0.001)

The large errors being due to the method of field measurement, using calibrated ammeter readings of the magnet exciting current.

Besides the Gd^{3+} spectrum two other isotropic lines were observed. A line with g = 4.33 ± 0.04 was observed at 4.2°K, and does not correspond with any known g value in a cubic field. At both 20°K and 4.2°K an isotropic line, 15 gauss wide, with g = 2.003 (± 0.001) was observed. If there are no Jahn-Teller distortions (see § A2.3.2) the Γ_5 triplet would give a resonance at g = 2, as can easily be seen from the wavefunctions of Lea et al (1962). (Terms of the form S_1^2 allowed in the spin Hamiltonian for S' = 1 would take the form $h(S_x^2+S_y^2+S_z^2)$ in a cubic field, and appear as an additive constant). It is possible that this second isotropic line was from the Γ_5 triplet of U^{4+}, but if so a much stronger resonance would have

been expected.

A crystal from the same batch as that giving the resonance described above was analysed for uranium (by a Harwell group) and found to contain about 1%. Its colour, a light green, also suggested the presence of U^{4+}. In one batch of crystals the colour was blood red, suggesting the presence of U^{5+} but these only gave one broad weak resonance at $g \sim 2$. Subsequent reduction of these crystals in a hydrogen furnace caused their colour to change to light green, again indicating U^{4+}.

No definite conclusion can therefore be made. There appear to be three possible explanations of the observations:

(a) Uranium did not enter the lattice as U^{4+}, in spite of the colour.

(b) A Γ_1 level is lowest in the cubic field of ThO_2, giving no resonance.

(c) The line at $g = 2$ was from the Γ_5 level, in spite of its low intensity.

It will require large crystals of completely unambiguous composition to enable the correct answer to be found. It is also puzzling that the results of Llewellyn on powders were not verified.

13.3.3 Pr^{4+} in ThO_2

No resonance was observed at X Band frequencies and

helium temperatures from a sample of 5% Pr in ThO_2. Pr^{4+}, with a configuration $(5f)^1$, has the same lowest multiplet, $^2F_{5/2}$, as Ce^{3+}, $(4f)^1$. In an eightfold cubic field this has a ground Γ_8 quartet, and if Pr^{4+} ions had been present in the sample resonance should have been observed from this state, Bleaney (1959).

13.4 Measurements on Er^{3+} in dysprosium ethyl sulphate

In §9.1 it was mentioned that a possible method of investigating the interaction between paramagnetic ions was to place a probe ion in a paramagnetic lattice in which the ions are "forced" into a singlet state by the application of a large magnetic field at low temperatures. Er^{3+} in dysprosium ethyl sulphate ($DyES$) forms a possible system in which to observe such an effect as the ground doublet of Dy^{3+} in this lattice has a large $g_{\parallel}$ (~ 10.8) and small $g_{\perp}$ (~ 0) (Cooke et al. 1959), giving no resonance yet capable of being split by a large amount by a magnetic field. Er^{3+} has a fairly small $g_{\parallel}$ of 1.47 and its resonance therefore occurs at a reasonably high field at X Band frequencies. At helium temperatures the relaxation time of the Dy^{3+} ions should be sufficiently long to give rise to a triplet structure of the Er^{3+} resonance line, similar to that observed in concentrated $NdES$ (Bleaney et al. 1951). For predominantly dipolar interactions, the satellites should be separated by the classical

value of $\Delta H = 2g_{\parallel(Dy)}\mu_B/r^3$ from the central line, and have half its intensity if both Dy^{3+} states are equally populated. At 2^0K and 5 Kg, $\frac{1}{2}g_{\parallel(Dy)}\mu_B H \approx kT$, and as the temperature is lowered the lower field satellite line should increase in intensity relative to the other two lines, leading ultimately to a single line in the position of the lowest satellite.

This effect was observed at X Band frequencies and helium temperatures in a sample of 1% Er in Dy_2S_3. The broad Er^{3+} resonance showed a structure similar to that described above although not well resolved. A rough measurement gave the spacing of the lines as ~ 600 g, compared with the calculated (classical) dipolar separation of 590g, and as the temperature was lowered the lower field line increased in intensity.

Clearly the experiment would be best performed at K Band frequencies (which were not available at the time of the experiment) in a field ~ 15 Kg, a carefully shaped specimen being necessary for accurate measurements.

13.5 The investigation by E.P.R. of rare earth ions in yttrium nitride

Yttrium nitride has a simple sodium chloride cubic lattice structure and would therefore appear ideal as a host for the study of rare earth ions in a sixfold cubic field. However both powdered and sintered samples containing a small amount of rare earth ions gave no definite resonance

whatsoever at X Band when investigated at 90°K, 20°K, or at 4°K, with high sensitivity. It appears that these compounds are semiconductors, and their conductivity is still high at helium temperatures precluding investigation by usual paramagnetic techniques. Samples investigated included 1% Gd, 1% Er, 1% Ce, and 1% Yb in YN , the last two ions have isotropic g values, g = 1.43 (Ce^{3+}) and g = 2.67 (Yb^{3+}), in a sixfold cubic field, and should give a sharp resonance even when in powder form. Some strange field dependent detuning effects were observed at helium temperatures with these samples, but were not explained.

APPENDIX I

The theoretical determination of the principal g values, and a discussion of their sign

If we consider a magnetic field acting on a Kramers rare earth ion in a crystalline electric field, we may normally treat the magnetic field as a perturbation on the wavefunctions of the ion in the crystal. For doubly degenerate crystal field levels (Kramers doublets) these wavefunctions may be written as,

$$|+\rangle = a\,|J,J_z\rangle + b\,|J',J'_z\rangle + c\,|J'',J''_z\rangle + \ldots.$$

$$|-\rangle = (-1)^{J+J_z} a^*\,|J,-J_z\rangle + (-1)^{J'+J'_z} b^*\,|J',-J'_z\rangle + (-1)^{J''+J''_z} c^*\,|J'',-J''_z\rangle + \ldots \quad (A1.1)$$

or

$$|+\rangle = a\,|L_z,S_z\rangle + b\,|L'_z\,S'_z\rangle + c\,|L''_z,\,S''_z\rangle + \ldots$$

$$|-\rangle = (-1)^{L_z+S_z} a^*\,|-L_z,-S_z\rangle + (-1)^{L'_z+S'_z} b^*\,|-L'_z,-S'_z\rangle + (-1)^{L''_z+S''_z} c^*\,|-L''_z,-S''_z\rangle + \ldots \quad (A1.2)$$

in the two representations usually used. The overall phase relation between $|+\rangle$ and $|-\rangle$ is arbitrary.

On a perturbation approach we consider the magnetic field interaction operator $\mathcal{H}_M$ acting within a particular manifold of two such Kramers states. This operator is (Equation 1.1)

$\mathcal{H}_M = \mu_B \mathbf{H}\cdot(\mathbf{L} + 2\mathbf{S})$, $(= \mu_B g_J \mathbf{H}\cdot\mathbf{J}$ if only one J state is involved, where g_J = Landé factor).

We may also represent the interaction by considering the doublet as arising from a fictitious spin $S' = \frac{1}{2}$ (Pryce 1950) the two states $|S'_z = \frac{1}{2}\rangle$ and $|S'_z = -\frac{1}{2}\rangle$ being split by an effective spin Hamiltonian,

$$\mathcal{H}' = \mu_B \underline{H} \cdot \underline{g} \cdot \underline{S}' \qquad \text{(Al.3)}$$

This equation may be regarded as defining the effective g tensor, a purely theoretical concept. If we choose a co-ordinate system in which $\underline{g}$ is diagonal, and consider an applied field $\underline{H} = \underline{i}\, H_x + \underline{j}\, H_y + \underline{k}\, H_z$, then by definition, the operator

$$\mu_B \left[H_x g_x S'_x + H_y g_y S'_y + H_z g_z S'_z \right] \quad \left(\begin{array}{l} \text{Acting within a manifold} \\ \text{of two effective spin} \\ \text{states } |S'=\frac{1}{2},\ S_z = \pm\frac{1}{2}\rangle \end{array} \right)$$

$$\equiv \mu_B \left[H_x(L_x + 2S_x) + H_y(L_y + 2S_y) + H_z(L_z + 2S_z) \right]$$

$$\left(\begin{array}{l} \text{Acting within a manifold of true angular momentum} \\ \text{states } |+\rangle \text{ , and } |-\rangle \end{array} \right). \qquad \text{(Al.4)}$$

So that with the normal definitions of the Pauli spin matrices,

	$\lvert\frac{1}{2}\rangle$	$\lvert-\frac{1}{2}\rangle$
$\langle\frac{1}{2}\rvert$	$\frac{H_z g_z}{2}$	$\frac{H_x g_x}{2} - \frac{iH_y g_y}{2}$
$\langle-\frac{1}{2}\rvert$	$\frac{H_x g_x}{2} + \frac{iH_y g_y}{2}$	$-\frac{H_z g_z}{2}$

$\equiv$

	$\lvert+\rangle$	$\lvert-\rangle$
$\langle+\rvert$	$H_z A$	$H_x B - iH_y C$
$\langle-\rvert$	$H_x B + iH_y C$	$-H_z A$

(Al.5)

where $A = \langle + | L_z + 2S_z | + \rangle = -\langle - | L_z + 2S_z | - \rangle$

$B = \langle + | L_x + 2S_x | - \rangle$

$-iC = \langle + | L_y + 2S_y | - \rangle$ (AI.6)

We may now equate the individual matrix elements, in particular the coefficients of H_x, H_y and H_z, to find the g values. However there are two causes for ambiguity. Firstly we do not know whether to identify $|+\rangle$ with $|+\frac{1}{2}\rangle$ (as above) or $|-\frac{1}{2}\rangle$, this will affect the sign of g_y and g_z. Secondly we do not know the phase of $|+\rangle$ relative to $|-\rangle$, this will affect the sign of g_x and g_y. In spite of these ambiguities, however, we can show that the product $g_x g_y g_z$ will always have a definite sign:-

If we take the above definitions of A, B and C to hold when $|+\frac{1}{2}\rangle$ is identified with $|+\rangle$, and when $|+\rangle$ and $|-\rangle$ have a definite phase relation, then we have:-

$$g_x = 2B,\ g_y = 2C,\ g_z = 2A;\ g_x g_y = 4BC;\ g_x g_y g_z = 8ABC \quad \text{(AI.7a)}$$

If we keep the identity, but reverse the phase, we have:-

$$g_x = -2B,\ g_y = -2C,\ g_z = 2A;\ g_x g_y = 4BC;\ g_x g_y g_z = 8ABC \quad \text{(AI.7b}$$

If we identify $|+\rangle$ with $|-\frac{1}{2}\rangle$, but have phases as in (AI.7a) we have:-

$$g_x = 2B,\ g_y = -2C,\ g_z = -2A;\ g_x g_y = -4BC;\ g_x g_y g_z = 8ABC \quad \text{(AI.7c)}$$

If we identify $|+\rangle$ with $|-\frac{1}{2}\rangle$, but have phases as in (AI.7b) we have

$$g_x = -2B,\ g_y = 2C,\ g_z = -2A;\ g_xg_y = -4BC;\ g_xg_yg_z = 8ABC \qquad (A1.7d)$$

Thus $g_xg_yg_z$ is independent of both choices. Pryce (1959) has pointed out that the only physical observables are $|g_x|$, $|g_y|$, $|g_z|$, and $g_xg_yg_z$. The sign of $g_xg_yg_z$ can be found from the relative intensities of transitions induced by circularly polarised light, and

$g_xg_yg_z > 0$ for "electron like" g values.

$g_xg_yg_z < 0$ for "non-electron like" g values.

(Dr. M. O'Brien, private communication). The sign will depend on the interaction of the ion with the crystal field.

When comparing theory with experiment the question of the signs of the g values must be borne in mind, and the experimental values given signs consistent with the theory. Some examples will be considered.

(1) When the Kramers states are explicitly stated, that is a, b, c ... etc. are known, and we wish to calculate the g values, we must first make a choice of identity and phase. The calculated sign of the product should then be consistent with the experimental sign (if known).

(2) If we wish to determine the state from the experimental g values by varying the values of a, b, c, etc. until the calculated and experimental values agree; then, having made a choice of identity and phase, there will only be one ambiguity - that in the sign of the product. That is, varying

each parameter in turn will create a surface in a 3 dimensional space formed by the g values, and this space will divide into two sets of four quadrants, the four quadrants in each set being equivalent. If the sign of the product is known from experiment, then the ambiguity is removed.

(3) If we wish to determine the state from the experimental g values by solving algebraic equations for a, b and c, such equations must be based on a particular choice of identity and phase and there will be no a priori indication of the appropriate signs to be given to the experimental g values. All four (or eight if the sign of the product is unknown) signs must therefore be tried. However, if it is known that the state represents a perturbation on a known wavefunction, then the g values can be given the signs appropriate to this unperturbed known state.

The discussion of Pryce (1959) implies that in cases of axial, and cubic, symmetry the phase or/and identity must be chosen so that the g values have signs consistent with the symmetry. For example in cubic symmetry a choice must be made for both so that $g_x = g_y = g_z$. This could be used to remove some of the ambiguities in the above discussion. However, there seems to be no a priori reason why such a choice should be made in every symmetric case, though it may be convenient. This point does not appear to be fully understood.

APPENDIX II

The calculation of the perturbing crystal field Hamiltonian from a point charge ionic model of the crystal lattice, and the determination of its matrix elements

A2.1 Introduction

An introduction to this appendix is given in §6.1

A2.2 Determination of the perturbing Hamiltonian

On the basis of a simple point charge ionic model the determination of the perturbing Hamiltonian is primarily the evaluation of the electrostatic potential $V(r,\theta,\phi)$ due to the surrounding point charges, at a point (r,θ,ϕ) near the origin at the magnetic ion in question.

$$V(r,\theta,\phi) = \sum_j \frac{q_j}{|(\underline{R}_j - \underline{r})|} \qquad (A2.1)$$

where q_j is the charge at the j^{th} neighbouring ion, distance R_j from the origin.

If the magnetic ion has charge q_i at (r_i,θ_i,ϕ_i) then the perturbing crystalline potential energy will be

$$H_c = \sum_i q_i V_i = \sum_i \sum_j \frac{q_i q_j}{|(\underline{R}_j - \underline{r}_i)|} \qquad (A2.2)$$

We are normally only concerned with $\sum_i$ over electrons in unfilled shells, as the crystal field affects closed shells only in a much higher order perturbation.

The crystalline potential, Equation (A2.1) may be

calculated in Cartesian co-ordinates, or directly in terms of spherical harmonics. [7] These two methods and their connection will be considered below for crystal fields of cubic symmetry.

A2.2.1 Evaluation of the crystalline electric potential near a magnetic ion in terms of Cartesian co-ordinates

As an illustration we shall give, in a frequently quoted form, an expression for the potential energy of a charge at a point (x,y,z), near the magnetic ion as origin, for three arrangements of charges giving a cubic crystalline electric field. That is, near an origin of cubic point symmetry. The simplest three such arrangements are:

1) When the charges are placed at the corners of an octahedron. (6-fold co-ordination)

2) When the charges are placed at the corners of a cube. (8-fold co-ordination)

3) When the charges are placed at the corners of a tetrahedron. (4-fold co-ordination)

The results given here have been derived in full detail in Hutchings (1963) §2 using an elementary, but tedious, Cartesian expansion of Equation (A2.2). We shall see in §A2.3.2 that it is only necessary to expand the potential up to sixth order terms.

The axes chosen are shown in Figure A2.1 and A2.2 for the six and eightfold cases respectively. For the tetrahedral (fourfold) case the even order terms in the potential follow

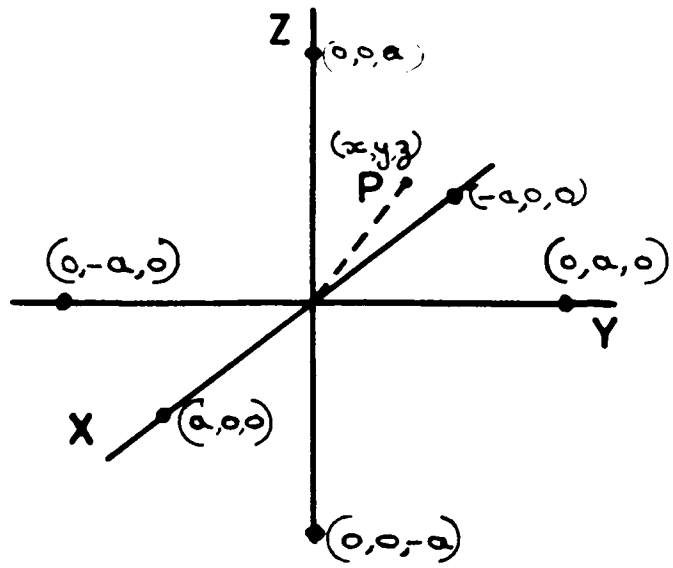


FIGURE A2·1

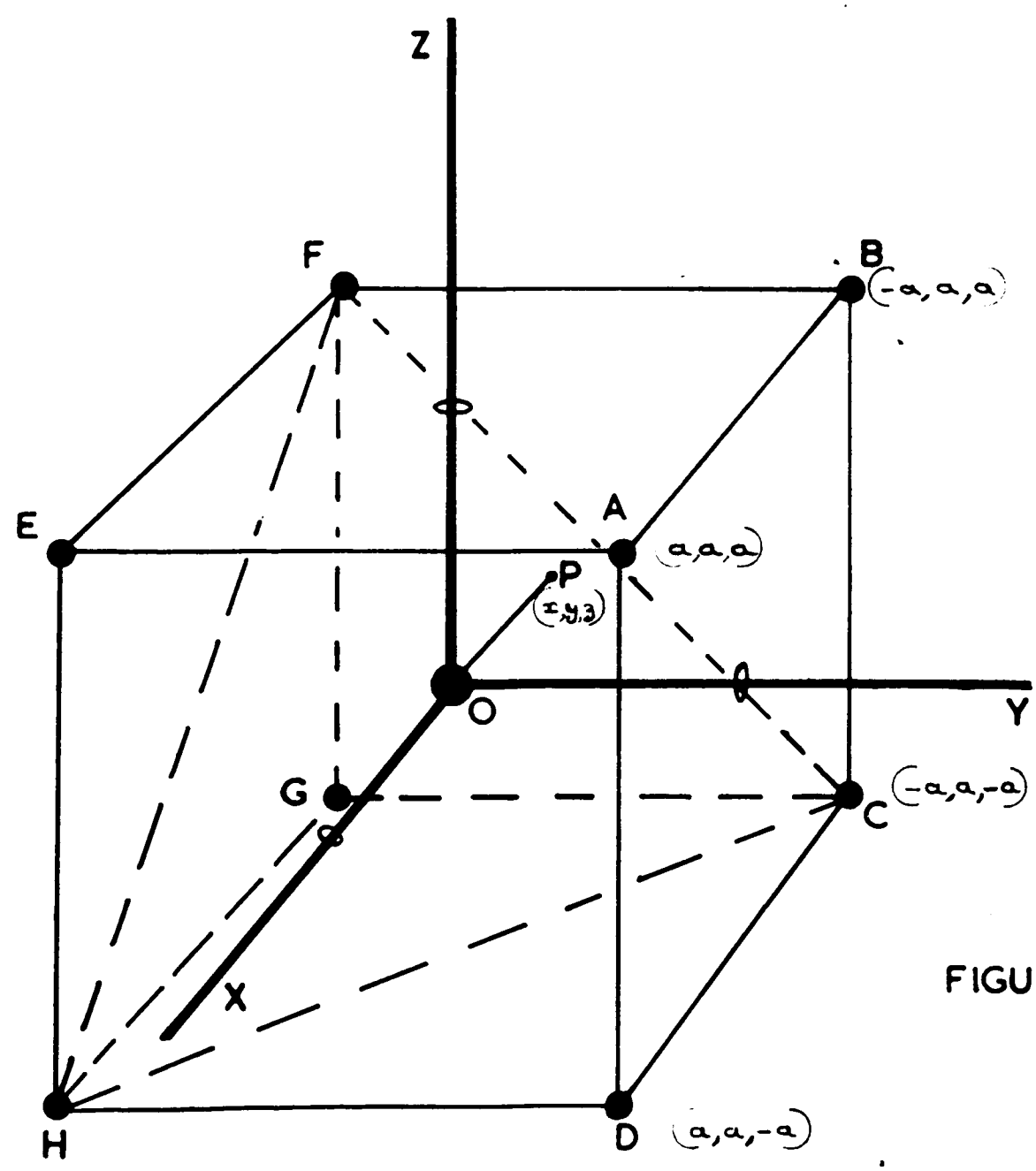


FIGURE A2·2

immediately from the eightfold case if one considers the four charges at AFBC, or EHGD, in Figure A2.2. The even order terms in the potential are then just half the values for the eightfold case, as described in Hutchings (1963). There will however be additional odd order terms in this case as there is no centre of symmetry, but these will not affect the energy levels of the ion if only one configuration is considered (see §A2.3.2).

For axes chosen as described above, the potential energy W_c of a charge q' at (x,y,z) in the potentials due to these three arrangements of charges is given by

$$W_c = C_4\left[(x^4+y^4+z^4) - \tfrac{3}{5}r^4\right] + D_6\left[(x^6+y^6+z^6) + \tfrac{15}{4}(x^2y^4+x^2z^4+y^2x^4+y^2z^4+z^2x^4+z^2y^4) - \tfrac{15}{14}r^6\right] \qquad (A2.3)$$

where the coefficients are given in Table A2.1; d is the distance of the point charges q from the origin in each case.

	C_4	D_6
8-fold co-ordination	$-\frac{70qq'}{9d^5}$	$-\frac{224qq'}{9d^7}$
6-fold co-ordination	$\frac{35qq'}{4d^5}$	$-\frac{21qq'}{2d^7}$
4-fold co-ordination	$-\frac{35qq'}{9d^5}$	$-\frac{112qq'}{9d^7}$

Table A2.1

The form of the expression for W_e given in Equation (A2.3) is frequently quoted, but there is often confusion over the magnitude and sign of the coefficients, (see for example Low (1960) p.15, N.B. There is an error in sign of D_6 in his eq. 5.5). Before its matrix elements can be conveniently found from tables, it must be rearranged as in §A2.4.1.

An alternative to the direct expansion method of calculating the results described in Hutchings (1963) is to make use of Taylor's series, expanding up to n = 6

$$V(x,y,z) = \sum_{n=0}^{n=6} \frac{1}{n!} \left(x \frac{\partial}{\partial x} + y \frac{\partial}{\partial y} + z \frac{\partial}{\partial z}\right)^n V(0,0,0).$$

A2.5 Evaluation of the crystalline electric potential near a magnetic ion in terms of spherical harmonics

It is far more convenient to express the crystalline electric potential due to surrounding point charges in spherical harmonics, or tesseral harmonics, for two reasons. Firstly a general formula for its evaluation can easily be derived, and secondly it is far easier to calculate the matrix elements of the potential energy in this form.

The method of calculation is discussed in Griffith (1961) p.197 and Prather (1961) p.6. It is based on the spherical harmonic addition theorem. This expresses the angle ω between two vectors $\underline{r}$ and $\underline{R}$ in terms of their polar angles (θ_1, ϕ_1) and (θ_j, ϕ_j).

$$P_n^0(\cos\omega) = \frac{4\pi}{(2n+1)} \sum_{m=-n}^{n} (-1)^m Y_n^{-m}(\theta_j,\phi_j)\, Y_n^m(\theta_1,\phi_1) \quad (A2.4)$$

(see Griffith , p.75, for example). Where the Legendre functions P_n^m (where we use the term Legendre functions to cover both the Legendre polynomials P_n^0, and the associated Legendre polynomials P_n^m ($m \neq 0$)), and spherical harmonics, Y_n^m, are defined as:-

$$\left.\begin{aligned} P_n^0(\mu) &= \frac{1}{2^n n!}\frac{d^n}{d\mu^n}(\mu^2-1)^n \\ P_n^{|m|}(\mu) &= (1-\mu^2)^{\frac{|m|}{2}}\frac{d^{|m|}}{d\mu^{|m|}}P_n^0(\mu) \end{aligned}\right\} \quad \mu = \cos\theta$$

$$Y_n^m(\theta,\phi) = (-1)^{\frac{m+|m|}{2}}\sqrt{\frac{(2n+1)(n-|m|)!}{2(n+|m|)!}}\frac{1}{\sqrt{2\pi}}P_n^{|m|}(\cos\theta)e^{im\phi} \quad (A2.5)$$

Some of the more relevant Legendre functions, and spherical harmonics are listed in Appendix III, Tables A3.1 and A3.2. More complete lists are given by Prather (1961, p.4 (with different normalisation of the Legendre functions from those defined in Equation (A2.5)), and also by Jahnke and Emde (1945) p.107 and 110.

Now the potential $V(r,\theta,\phi)$, at a point (r,θ,ϕ), due to a number of charges q_j at $\underline{R}_j$ is given by Equation (A2.1),

$$V(r,\theta,\phi) = \sum_j \frac{q_j}{|(\underline{R}_j - \underline{r})|}$$

If ω is the angle between $\underline{r}$ and $\underline{R}$ then

$$\frac{1}{|(\underline{R}-\underline{r})|} = \sum_{n=0}^{\infty}\frac{r^n}{R^{(n+1)}}P_n^0(\cos\omega), \quad R>r \quad (A2.6)$$

(See for example, Margenau & Murphy (1956) p.100).

In order to avoid the use of imaginary quantities, we define tesseral harmonics, as:-

$$Z_{no} = Y_n^o$$

$$\left.\begin{aligned} Z_{nm}^c &= \frac{1}{\sqrt{2}}\left[Y_n^{-m} + (-1)^m Y_n^m\right] \\ Z_{nm}^s &= \frac{i}{\sqrt{2}}\left[Y_n^{-m} - (-1)^m Y_n^m\right] \end{aligned}\right\} \quad m > 0 \qquad (A2.7)$$

that is,

$$Z_{no} = Y_n^o$$

$$Z_{nm}^c = \sqrt{\frac{(2n+1)}{2}\frac{(n-m)!}{(n+m)!}}\, P_n^m(\cos\theta)\frac{\cos m\phi}{\sqrt{\pi}}$$

$$Z_{nm}^s = \sqrt{\frac{(2n+1)}{2}\frac{(n-m)!}{(n+m)!}}\, P_n^m(\cos\theta)\frac{\sin m\phi}{\sqrt{\pi}} \qquad (A2.8)$$

Then from the spherical harmonic addition theorem, Equation (A2.4)

$$P_n^o(\cos\omega) = \frac{4\pi}{(2n+1)} \sum_\alpha Z_{n\alpha}(\underline{r})\, Z_{n\alpha}(\underline{R}) \qquad (A2.9)$$

where the Z's are evaluated for the points $\underline{r}$ and $\underline{R}$, and the summation is over α, that is for each n, there are terms Z_{no} Z_{nm}^c and Z_{nm}^s for all m. Hence if $V(r,\theta,\phi)$ is due to a charge q_j at $\underline{R}_j$, using Equations (A2.6) and (A2.9), in (A2.1)

$$V(r,\theta,\phi) = q_j \sum_{n=0}^{\infty} \frac{r^n}{R_j^{(n+1)}} \left\{ \sum_\alpha \frac{4\pi}{(2n+1)} Z_{n\alpha}(\theta_j,\phi_j) Z_{n\alpha}(\theta,\phi) \right\},$$

and for k charges

$$V(r,\theta,\phi) = \sum_{n=0}^{\infty} \sum_\alpha r^n \gamma_{n\alpha} Z_{n\alpha}(\theta,\phi),$$

$$\text{where } \gamma_{n\alpha} = \sum_{j=1}^{k} \frac{4\pi}{(2n+1)} q_j \frac{Z_{n\alpha}(\theta_j,\phi_j)}{R_j^{(n+1)}} \quad . \qquad (A2.10)$$

This is a very convenient form in which to write the potential. If the $Z_{n\alpha}$ are expressed in Cartesian co-ordinates, there is an immediate correspondence between them and Stevens' "operator equivalents", which can be used for the evaluation of the matrix elements. These will be discussed in §A2.3.3. The tesseral harmonics used here are identical with those of Griffith (1961) p.200, and Prather (1961) p. 4, although Prather uses the notation $C_n^m = Z_{nm}^c$; $S_n^m = Z_{nm}^s$. Prather, 1961, p.4 & 5, gives expressions for the C_n^m and S_n^m's up to order n = 6, m = 6, in terms of Cartesian co-ordinates (x,y,z). A few of the more commonly occurring Z_{nm}^e are listed in Appendix III, Table A3.3.

An alternative way of expressing V is to write it directly in spherical harmonics, using the form of the spherical harmonic addition theorem in Equation (A2.4). Dropping the i's,

$$V(r,\theta,\phi) = \sum_j \frac{q_j}{|R_j - r|} = \sum_j q_j \sum_n \frac{r^n}{R_j^{(n+1)}} \cdot \frac{4\pi}{(2n+1)} \cdot \sum_{m=-n}^{n} \Big((-1)^m Y_n^{-m}(\theta_j,\phi_j) Y_n^m(\theta,\phi) \Big).$$

$$\therefore V(r,\theta,\phi) = \sum_n \sum_{m=-n}^{n} r^n \gamma'_{nm} Y_n^m(\theta,\phi),$$

$$\text{where } \gamma'_{nm} = \sum_j \frac{4\pi}{(2n+1)} \frac{q_j}{R_j^{(n+1)}} (-1)^m Y_n^{-m}(\theta_j,\phi_j) \qquad (A2.11)$$

Using Equation (A2.10) we can easily calculate the potential in polar co-ordinates, due to the three forms of cubic

crystalline environment. Full details of the derivation are given in Hutchings (1963), §3, where it is seen that most of the $\gamma_{n\alpha}$ are zero, and the only relevant $Z_{n\alpha}$ are:-

$$Z_{00} = \frac{1}{2\sqrt{\pi}} \; ; \; Z_{40} = \frac{1}{16\sqrt{\pi}} \left(35\cos^4\theta - 30\cos^2\theta + 3\right)$$

$$Z_{60} = \frac{1}{32}\sqrt{\frac{13}{\pi}} \left(231\cos^6\theta - 315\cos^4\theta + 105\cos^2\theta - 5\right)$$

$$Z^c_{44} = \frac{3}{16}\sqrt{\frac{35}{\pi}} \sin^4\theta \cos 4\phi$$

$$Z^s_{64} = \frac{3}{32}\sqrt{\frac{91}{\pi}} \left(11\cos^2\theta - 1\right)\sin^4\theta \cos 4\phi \qquad \text{(A2.12)}$$

Substituting for these in Equation (A2.10) we find that, for axes chosen as in §A2.2.1, (and again considering only the even order terms in the tetrahedral case), the potential energy W_c of a charge q' at (r,θ,ϕ) in the three cases is given by

$$W_c = D'_4\left[Y^0_4(\theta,\phi) + \sqrt{\frac{5}{14}}\left(Y^4_4(\theta,\phi) + Y^{-4}_4(\theta,\phi)\right)\right] +$$

$$+ D'_6\left[Y^0_6(\theta,\phi) - \sqrt{\frac{7}{2}}\left(Y^4_6(\theta,\phi) + Y^{-4}_6(\theta,\phi)\right)\right] \qquad \text{(A2.13)}$$

If the potential is due to charges q, at a distance d from the origin, the coefficients are given in Table A2.2.

Table A2.2

	D_4'	D_6'
8-fold co-ordination	$-\frac{56}{27}\sqrt{\pi}\,\frac{qq'r^4}{d^5}$	$\frac{32}{9\sqrt{13}}\sqrt{\pi}\,\frac{qq'r^6}{d^7}$
6-fold co-ordination	$\frac{7}{3}\sqrt{\pi}\,\frac{qq'r^4}{d^5}$	$\frac{3}{2\sqrt{13}}\sqrt{\pi}\,\frac{qq'r^6}{d^7}$
4-fold co-ordination	$-\frac{28}{27}\sqrt{\pi}\,\frac{qq'r^4}{d^5}$	$\frac{16}{9\sqrt{13}}\sqrt{\pi}\,\frac{qq'r^6}{d^7}$

This potential energy, written in a slightly different form, is given by Low (1961) p.13, (with q' = + e, q = + Ze; N.B. There is an error in sign of his coefficient of $(Y_6^4 + Y_6^{-4})$, in the 4-fold and 8-fold co-ordination expressions).

A2.2.3 Number of harmonics occurring in the expression for the potential

It is found, as mentioned above, that the coefficients of most of the tesseral harmonics in the expansion of the potential are zero in the cubic cases considered. In general the potential function must reflect the point symmetry of the lattice site in question, that is, it must be invariant under the operations of the point group. The less symmetric the site, the more potential terms occur in the expansion. Prather (1961) p.10, lists the non-vanishing γ's for different point groups. The terms occurring depend very much on the axes chosen, and are in their simplest form when the axes are the symmetry axes

of the point group, as was taken for our examples.

There are two general rules which may be mentioned at this point. Firstly, if there is a centre of inversion at the ion site considered there will be no odd n terms in the potential; and secondly if the z axis is an m-fold axis of symmetry, the potential will contain terms Z_{nm}. For some high symmetry cases, there exist relations between the coefficients of the tesseral harmonics of the same n occurring in the potential, as we have already seen for the case of cubic fields.

It must be noted that not all the non-zero terms in the expansion of the potential will affect the energy levels of the magnetic ion, as their matrix elements may yet be zero.

As an example of the terms occurring in the expression for the crystalline potential, and giving non-zero matrix elements in general, we list below the terms up to n = 6 (see §A2.3.2) for some point groups relevant to work described in this thesis. (The V_n^m are defined at the end of §A2.3.3).

Cubic (ThO_2) V_4^0, V_4^4, V_6^0, V_6^4

C_{3h} (Ethyl Sulphates; some Rare-Earth Trichlorides) V_2^0, V_4^0, V_6^0, V_6^6, (V_6^{-6}).

D_2 (Garnets-rare earth site) V_2^0, V_2^2, V_4^0, V_4^2, V_4^4, V_6^0, V_6^2, V_6^4, V_6^6.

A2.3 Calculation of the matrix elements of the crystalline potential perturbing Hamiltonian

We now consider the evaluation of the matrix elements of the perturbing Hamiltonian between free ion states. The matrix

thus formed can then be diagonalised to find the energy levels and eigenfunctions of the ion in the crystalline field. If the classical potential energy of the magnetic ion in the crystalline electric field is, as in Equation (A2.2),

$$W_c = \sum_i q_i V(x_i, y_i, z_i)$$

the crystal field perturbing Hamiltonian operator, $\mathcal{H}_c$, is formed from this by applying the usual rules, $x \rightarrow x_{op}$, $y \rightarrow y_{op}$, etc. That is, the Hamiltonian operator is simply the classical potential energy.

$$\mathcal{H}_c = W_c = -|e| \sum_i V(x_i, y_i, z_i) \qquad (A2.14)$$

where we have put $q_i = -|e|$, and the summation is over the magnetic electrons. The free ion wavefunctions used will depend on the relative size of $\mathcal{H}_c$ to the intra-ionic interaction energies. For example, to a first approximation for the $(3d)^{n'}$ transition group ions in ionic compounds they will be characterised by $|L\ S\ L_z S_z\rangle$, as $\mathcal{H}_c$ [illegible] > Spin Orbit coupling; and in the $(4f)^{n'}$ rare earth group by $|L\ S\ J\ J_z\rangle$, as the Spin Orbit coupling is generally larger than $\mathcal{H}_c$. In order to calculate the matrix elements we may use one of two methods, these are described briefly in §A2.3.1 and §A2.3.3 below.

A2.3.1 Direct integration

This is the fundamental method and is clearly described in Bleaney and Stevens (1953) p.129. The free ion wavefunctions are expanded into determinental product states involving single electron wavefunctions ϕ_i on which the corresponding terms

$V(x_i,y_i,z_i)$ in $\mathcal{H}_c$ act. The matrix elements, expressed in polar co-ordinates, therefore reduce the sums of terms of the form $\int \phi^*(r_i,\theta_i,\phi_i) \times Y_n^m(r_i,\theta_i,\phi_i) \times \phi(r_i,\theta_i,\phi_i)d\tau$. As the radial part of the wavefunction f(r) is never accurately known, the radial integral, which separates out, is often taken as a parameter $\langle r^n \rangle = \int [f(r)]^2 r^n r^2 dr$. There have been several theoretical calculations of $\langle r^n \rangle$, (for example, for rare earth ions see Freeman and Watson 1962).

If $V(x_i,y_i,z_i)$ is written in terms of spherical harmonics, the matrix elements and several quite general rules can be found from their expansion, using Vector Coupling coefficients (see Edmonds 1957, p.37) and orthogonality properties. These rules have been discussed fully by Bleaney and Stevens (1953) p.126 and p.130, and will now be summarized. (More generally they follow from the Wigner-Eckart theorem, see Edmonds (1957) p.75, for example).

A2.3.2 Rules limiting the number of non zero matrix elements

As mentioned in §A2.2.3 the symmetry of the crystalline electric field limits the number of terms occurring in the expansion of the potential. The rules listed below indicate which of these give non zero matrix elements.

1) All terms of $n > 2l$, where l is the orbital quantum number of the single magnetic electrons, vanish. Thus we need only consider the expansion of the crystalline potential up to

4^{th} order for the $(3d)^{n'}$ group and 6^{th} order for the $(4f)^{n'}$ group, (n' = number of electrons in shell). Or if we use the operator equivalents method (§ A2.3.3) terms for which $n > 2L$, or $n > 2J$, vanish; where, for example, L and J are the coupled angular momentum for the (3d) group, or (4f) group, respectively.

ii) Operators of the form Z_{nm} have zero matrix elements between two states $\phi_{l'}$ and $\phi_{l''}$ unless $l' + l'' + n$ = even no. This means that within a given configuration, i.e. given l, the matrix elements of odd n terms vanish, but that they may couple different configurations.

iii) Operators of the form Z_{nm} have zero matrix elements between two states $\phi_{l'}^{m'}$ and $\phi_{l''}^{m''}$, unless $m + m' - m'' = 0$. In the coupled system, for example, this will mean that terms Z_{nm} link states of ΔJ_z, (or ΔL_z) = m.

A very useful check on all calculations may be made using the fact that number and types of the resulting energy levels can be found by group theoretical methods, but the eigenvalues and eigenfunctions cannot be found without full calculation in most cases.

There is a very important general theorem mentioned in Chapter 1, dealing with the energy levels of magnetic ions in a crystalline environment. Kramers (1930) theorem states that the energy levels of odd electron ions under electrostatic interaction of any nature are at least twofold degenerate. A

consequence of this theorem is that the matrices of $\mathcal{H}_c$ between states of an odd electron ion, always factorise into two similar matrices. (N.B. When Kramer's theorem does not apply Jahn and Teller (1937) have shown that the surroundings of a magnetic ion will distort and always tend to give non degenerate energy levels. Thus even electron ions tend to have singlet energy levels in crystals).

A2.3.3 Use of Stevens' "Operator equivalents" method

This is by far the most convenient method, within its limitations, for evaluating the matrix elements of the crystalline potential between coupled wavefunctions specified by one particular value of angular momentum J, (or L), and will be that used in all further discussions here. It is this method which has been used in the thesis. It eliminates the need to go back to single electron wavefunctions each time by the use of an "operator equivalent" to $\mathcal{H}_c$ consisting of angular momentum operators which act on the angular part of the wavefunction in the coupled system; this is really an application of the Wigner-Eckart theorem (see Edmonds 1957, p.75 for example). The method is described fully in Stevens (1952) and Bleaney and Stevens (1953) p.131. The rules for determining the operator equivalent to the Cartesian Hamiltonian given by Equation (A2.14)

$$\mathcal{H}_c = -\sum_i |e|\, V(x_i, y_i, z_i),$$

are given in Stevens (1952). If f(x,y,z) is a Cartesian function

of given order, then to find the operator equivalent to such terms as $\sum_i f(x_i,y_i,z_i)$ occurring in $\mathcal{H}_e$, one replaces x, y and z by J_x, J_y, and J_z respectively, always allowing for the non commutation of J_x, J_y and J_z. This is done by replacing products of x, y and z by an expression consisting of all the possible different combinations of J_x, J_y and J_z divided by the total number of combinations. In this way an operator is formed with the same transformation properties under rotation as the potential.

Some simple examples occurring in the garnet potential are,

$$\sum_i (3z_i^2 - r_i^2) \equiv \alpha_J \langle r^2 \rangle \left[3J_z^2 - J(J+1)\right] = \alpha_J \langle r^2 \rangle O_2^0$$

$$\sum_i (x_i^2 - y_i^2) \equiv \alpha_J \langle r^2 \rangle \left[J_x^2 - J_y^2\right] = \alpha_J \langle r^2 \rangle O_2^2$$

$$\sum_i (x_i^4 - 6x_i^2y_i^2 + y_i^4) \equiv \sum_i \left[\frac{(x_i + iy_i)^4 + (x_i - iy_i)^4}{2}\right]$$

$$\equiv \beta_J \langle r^4 \rangle \tfrac{1}{2} \left[J_+^4 + J_-^4\right] = \beta_J \langle r^4 \rangle O_4^4$$

where $J_\pm = J_x \pm iJ_y$ (A2.15).

When the non commutation effects cannot be immediately taken account of, the determination is more tedious (see Hutchings (1963) § 4.3.1).

We therefore have, for example, that the matrix elements of $\sum_i (3z_i^2 - r_i^2)$ between coupled states $|LSJJ_z\rangle$ are equal to those of $\alpha_J \langle r^2 \rangle O_2^0$ between the angular part of the coupled wavefunctions, i.e.

$$\langle LSJJ'_z | \sum_i (3z_i^2 - r_i^2) | LSJJ_z \rangle = \alpha_J \langle r^2 \rangle \langle LSJJ'_z | [3J_z^2 - J(J+1)] | LSJJ_z \rangle$$

The multiplicative factor α_J is a numerical constant depending on l (the orbital quantum number of the electrons in the unfilled shell), n' (the number of them), and J, (or L and S). The constant is denoted by β_J for fourth order terms, and γ_J for sixth order terms. These constants are originally determined by returning to the direct integration method of finding the matrix elements between single electron wavefunctions in a specific case. This method of determination is clearly described in Stevens (1952) p.211. (N.B. An alternative method is given by Elliott, Judd and Runciman (1957) using fractional percentage coefficients). Although Stevens paper relates mainly to matrix elements of rare earth ions' states characterised by the $|LSJJ_z\rangle$ it can be used for d-electron ions, or between states characterised by $|LSL_zS_z\rangle$, provided the correct numerical factors are used, in these cases the operator $\underline{J}$ above is replaced by $\underline{L}$. The multiplicative factors, for rare earth ions, are listed in Elliott and Stevens (1953a), and for 3d group ions (or for matrix elements between states characterised by L and S) can be found from a general formula given in Bleaney and Stevens (1953) p.132.

To illustrate the method in general we shall again consider the crystalline electric field Hamiltonian given by equation (A2.14),

$$\mathcal{H}_c = -|e| \sum_i V(x_i, y_i, z_i)$$

If the electrostatic potential V(x,y,z) is determined from a point charge model as in §A2.2 with the tesseral harmonics expressed in Cartesian co-ordinates, we have

$$V(x,y,z) = \sum_{n\alpha} r^n \gamma_{n\alpha} Z_{n\alpha} (x,y,z)$$

In order to make full use of operator equivalents whose matrix elements have been tabulated, we define Cartesian functions $f_{n\alpha}(x,y,z)$ which are related to the $Z_{n\alpha}(x,y,z)$ by $Z_{n\alpha} = (\text{const.})\ f_{n\alpha}/r^n$. For the Z^e_{nm} listed in Table A3.3, the f^e_{nm}/r^n are the functions in square brackets. It is these functions $f_{n\alpha}(x,y,z)$, (or rather $f^e_{nm}(x,y,z)$), so defined, which are directly related to the most commonly used operator equivalents O^m_n by the relation that the operator

$$\sum_i f^e_{nm}(x_i,y_i,z_i) \equiv \Theta_n \langle r^n \rangle O^m_n \qquad \text{(A2.16)}$$

where Θ_n is the multiplicative factor, $\Theta_2 = \alpha_J$

$\Theta_4 = \beta_J$

$\Theta_6 = \gamma_J$

The matrix elements of the O^m_n thus defined, between states of constant J, or L, have been tabulated in several papers. Some relevant O^m_n's are listed in Appendix III, Table A3.4.

Considering for simplicity the case of a crystal field with axes chosen such that $\gamma^e_{nm} = 0$, we re-express the potential energy of an electron in the crystalline potential V(x,y,z) (following the notation of Stevens, Elliott, and Judd) as

A2.16

$$-|e|\ V(x,y,z) = \sum_{nm} A_n^m\ r_{nm}^c\ (x,y,z) \qquad (A2.17)$$

where we have the connection between the coefficients;

$$A_n^m = \gamma_{nm}^c \times (-|e|)\times \text{(a numerical factor occurring in } Z_{nm}^c) \qquad (A2.18)$$

The numerical factor being that outside the square brackets for those Z_{nm}^c listed in Table A3.3. For example, in the case of cubic symmetry, using the notation of Equation (A2.17),

$$-|e|\ V(x_1,y_1,z_1) = A_4^0(35z_1^4 - 30\ r_1^2z_1^2 + r_1^4) + A_4^4(x_1^4 + y_1^4 - 6x_1^2y_1^2) +$$
$$+ A_6^0(231z_1^6 - 315z_1^4r_1^2 + 105z_1^2r_1^4 - 5r_1^6) +$$
$$+ A_6^4(11z_1^2 - r_1^2)(x_1^4 - 6x_1^2y_1^2 + y_1^4)$$

For a number of electrons, i, in the general potential $V(x,y,z)$ the operator is

$$\mathcal{H}_c = -|e| \sum_i V(x_i,y_i,z_i),$$

$$\text{or, } \mathcal{H}_c = \sum_i \sum_{nm} A_n^m\ r_{nm}^c\ (x_i,y_i,z_i) = \sum_{nm} \left[A_n^m \langle r^n \rangle\ \theta_n\right] O_n^m \qquad (A2.19)$$

where we have made use of Equations (A2.16) and (A2.17) above.

Note on notation

For the case of the rare earths, the quantities $A_n^m \langle r^n \rangle$ (or V_n^m in the notation of Elliott and Stevens, 1953b) are known as the "Crystal Field Parameters", and are usually determined by fitting $\mathcal{H}_c$ to experimental data. [N.B. V_n^m is sometimes also used to denote $\sum_i r_{nm}^c\ (x_i,y_i,z_i)$ (e.g. Stevens 1952, p.209).]

The operator equivalent Hamiltonian $\mathcal{H}_e$ is often written

$$\mathcal{H}_e = \sum_{nm} B_n^m O_n^m, \text{ (or } \mathcal{H}_e = \sum_{nm} B_n^m P_n^m),$$

where $B_n^m = A_n^m \langle r^n \rangle \theta_n$ (A2.20)

The B's rather than the A's will be used in §A2.4. (N.B. The A's and B's used by Bleaney and Stevens (1953) p.128-9 are different from those used here, but can easily be related to them).

Other notations commonly used are listed below (H. Watanabe, private communication).

$b_2^0 = 3B_2^0 = D$ $\qquad$ $b_6^6 = 1260B_6^6$

$b_2^2 = 3B_2^2 = 3E$ $\qquad$ $b_4^m = 60B_4^m$

$b_4^0 = 60B_4^0 = \frac{1}{3}F$ $\qquad$ $b_6^m = 1260B_6^m$

$b_6^0 = 1260B_6^0$

and, especially for cubic fields,

$b_4^0 = 60B_4^0 = \frac{1}{3}a = \frac{1}{4}c$

$b_6^0 = 1260B_6^0 = \frac{1}{4}d$

A2.4 Operator equivalents for cubic potentials

As an example we shall now determine the operator equivalent appropriate to the cubic crystal field potentials found in §A2.2.1. and §A2.2.2. Since these differ only in the coefficients for the three different co-ordinations, we need only consider how the functions transform into the appropriate operators.

A2.4.1 <u>For a cubic potential expressed in Cartesian co-ordinates</u>

If we put $q'_i = -|e|$ in the expression given in equation (A2.3) and Table A2.1,

$$\mathcal{H}_c = \sum_i \left\{ C_4\left[(x_i^4+y_i^4+z_i^4) - \tfrac{3}{5} r_i^4\right] + C_6\left[(x_i^6+y_i^6+z_i^6) + \tfrac{15}{4}(x_i^2y_i^4+x_i^2z_i^4 + y_i^2x_i^4+y_i^2z_i^4+z_i^2x_i^4+z_i^2y_i^4) - \tfrac{15}{14} r_i^6\right]\right\}$$

We rewrite the Cartesian functions in terms of the $f^c_{nm}(x_i,y_i,z_i)$. These then immediately go over into an operator equivalent in its usual form i.e. O_4^0, O_4^4, O_6^0 and O_6^4 as listed in Table A3.4. An example of the derivation of O_4^0 using Stevens' rules, is given in Hutchings (1963) § 4.3.1. Table A3.4 has been compiled from published papers.

Now
$$\left[(x^4+y^4+z^4) - \tfrac{3}{5} r^4\right] = \tfrac{1}{20}\left[(35z^4-30r^2z^2+3r^4) + 5(x^4+y^4-6x^2y^2)\right]$$
$$= \tfrac{1}{20}\left[(35z^4-30r^2z^2+3r^4) + 5\left(\frac{(x+iy)^4+(x-iy)^4}{2}\right)\right] \quad \text{(A2.21)}$$

So that the matrix elements of

$$\sum_i \left[x_i^4 + y_i^4 + z_i^4 - \tfrac{3}{5} r_i^4\right] \equiv \text{those of } \tfrac{1}{20}\beta_J \langle r^4\rangle \left[O_4^0 + 5O_4^4\right]$$

Similarly ... (A2.22)

$$\left[x^6+y^6+z^6+\tfrac{15}{4}(x^2y^4+x^2z^4+y^2x^4+y^2z^4+z^2x^4+z^2y^4) - \tfrac{15}{14} r^6\right]$$
$$= \tfrac{-1}{224}\left[(231z^6-315z^4r^2+105z^2r^4-5r^6) - 21(11z^2-r^2)\cdot\frac{(x+iy)^4+(x-iy)^4}{2}\right] \quad \text{(A2.23)}$$

∴ The matrix elements of

$$\sum_i \left[(x_i^6+y_i^6+z_i^6) + \frac{15}{4}(x_i^2y_i^4+x_i^2z_i^4+y_i^2x_i^4+y_i^2z_i^4+z_i^2x_i^4+z_i^2y_i^4) - \frac{15}{14} r_i^6\right] \qquad \text{A2.21}$$

$$= \text{those of } \frac{-1}{224}\gamma_J \langle r^6\rangle \left[O_6^0 - 210_6^4\right] \qquad \text{(A2.24)}$$

We therefore have that for a crystal field of cubic symmetry,

$$\mathcal{H}_e = \frac{C_4}{20}\beta_J \langle r^4\rangle \left[O_4^0 + 50_4^4\right] - \frac{D_6}{224}\gamma_J \langle r^6\rangle \left[O_6^0 - 210_6^4\right]$$

or

$$\mathcal{H}_e = B_4^0 \left[O_4^0 + 50_4^4\right] + B_6^0 \left[O_6^0 - 210_6^4\right] \qquad \text{(A2.25)}$$

Where, B_4^0 and B_6^0 are given in the table below for surrounding point charges of charge q, at distance d, in various co-ordinations about the magnetic ion site, and axes are chosen as in §A2.2.1. This is the same as the potential given, for example, in Baker, Bleaney, and Hayes (1958) p.150, and used in Chapters 4 & 12.

Table A2.3

	B_4^0	B_6^0
8-fold co-ordination	$+\frac{7}{18}\frac{\|e\|q}{d^5}\beta_J\langle r^4\rangle$	$-\frac{1}{9}\frac{\|e\|q}{d^7}\gamma_J\langle r^6\rangle$
6-fold co-ordination	$-\frac{7}{16}\frac{\|e\|q}{d^5}\beta_J\langle r^4\rangle$	$-\frac{1}{64}\frac{\|e\|q}{d^7}\gamma_J\langle r^6\rangle$
4-fold co-ordination	$+\frac{7}{36}\frac{\|e\|q}{d^5}\beta_J\langle r^4\rangle$	$-\frac{1}{18}\frac{\|e\|q}{d^7}\gamma_J\langle r^6\rangle$

We have put $q' = -|e|$ in the values listed in Table A2.1, the sign of the β_J, or γ_J, factors are consistent with this.

A2.4.2 <u>For a cubic potential expressed in spherical harmonics</u>

To illustrate how one rewrites, in terms of operator equivalents, the crystal field Hamiltonian operator when the potential is expressed in spherical or tesseral harmonics, we again consider the cubic case.

We first express the Hamiltonian in terms of tesseral harmonics $Z_{n\alpha}$. Using equation (A2.13), with $q' = -|e|$,

$$\mathcal{H}_c = -\sum_i \left\{ D_4' \left[Y_4^0 + \sqrt{\tfrac{5}{14}} \left(Y_4^4 + Y_4^{-4}\right)\right] + D_6' \left[Y_6^0 - \sqrt{\tfrac{7}{2}} \left(Y_6^4 + Y_6^{-4}\right)\right]\right\}$$

$$= -\sum_i \left\{ D_4' \left[Z_{40} + \sqrt{\tfrac{5}{7}}\, Z_{44}^c\right] + D_6' \left[Z_{60} - \sqrt{7}\, Z_{64}^c\right]\right\}$$

Let $D_4'' = D_4'/r^4$, and $D_6'' = D_6'/r^6$

Then $$\mathcal{H}_c = \sum_i \left\{ D_4'' \left[r^4 Z_{40} + \sqrt{\tfrac{5}{7}}\, r^4 Z_{44}^c\right] + D_6'' \left[r^6 Z_{60} - \sqrt{7}\, r^6 Z_{64}^c\right]\right\} \quad (A2.26)$$

We now write $r^4 Z_{4m}^c$ and $r^6 Z_{6m}^c$ in Cartesian co-ordinates, using the values of Z_{nm}^c from Table A3.3. The tesseral harmonics are directly proportional to the f_{nm}^c (x y z) which immediately go over into the operator form. Thus we get

$$\mathcal{H}_c = D_4'' \left[\tfrac{3}{16} \tfrac{1}{\sqrt{\pi}}\, \beta_J \langle r^4\rangle\, O_4^0 + \sqrt{\tfrac{5}{7}} \cdot \tfrac{3}{16} \sqrt{\tfrac{35}{\pi}}\, \beta_J \langle r^4\rangle\, O_4^4\right] +$$

$$+ D_6'' \left[\tfrac{1}{32} \sqrt{\tfrac{13}{\pi}}\, \gamma_J \langle r^6\rangle\, O_6^0 - \sqrt{7} \times \tfrac{21}{32} \sqrt{\tfrac{13}{7\pi}}\, \gamma_J \langle r^6\rangle\, O_6^6\right],$$

or

$$\mathcal{H}_c = \frac{3}{16\sqrt{\pi}}\, D_4''\, \beta_J \langle r^4\rangle \left[O_4^0 + 5 O_4^4\right] + \frac{1}{32} \sqrt{\frac{13}{\pi}}\, D_6''\, \gamma_J \langle r^6\rangle \left[O_6^0 - 21 O_6^6\right], \quad (A2.27)$$

and putting q' = -|e| in the values of D_4' and D_6' taken from Table A2.2, we arrive once more at the values of B_4^0 and B_6^0 listed in Table A2.3.

A2.4.4 Summary

We may summarize the different methods of calculating the point charge crystal field Hamiltonian, and its matrix elements, by the diagram below. The upper Cartesian method, is, however, far too tedious to be used in practice, and the general methods of §A2.2.2, §A2.3, and §A2.4, are used in Chapters 7 and 8, for the case of the garnets.

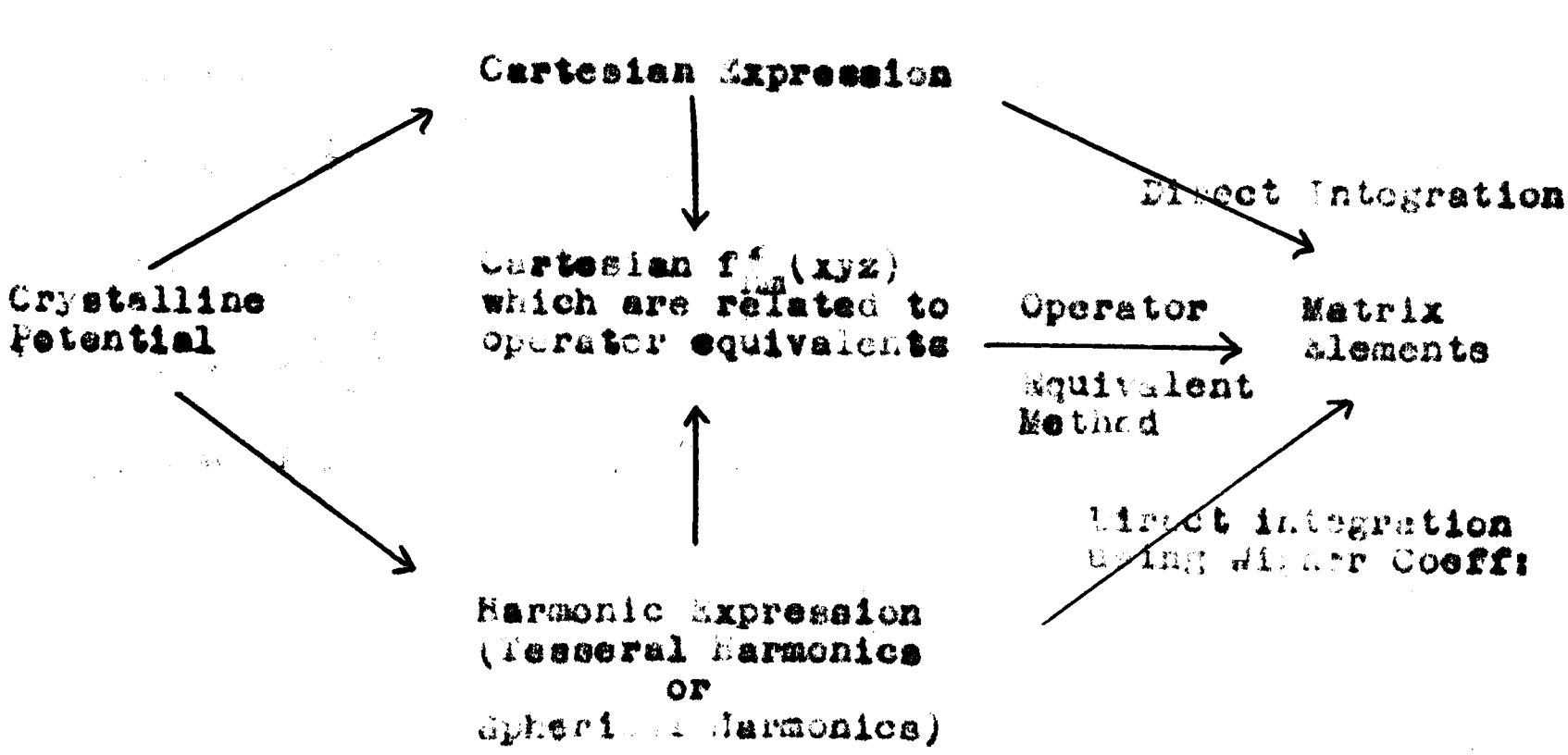


Figure A.2.3

APPENDIX III

Table A3.1

Some of the more commonly occurring Legendre functions (as defined by Equation (A2.5))

$$P_2^0(\cos\theta) = \tfrac{1}{2}(3\cos^2\theta - 1)$$

$$P_2^2(\cos\theta) = 3(1 - \cos^2\theta)$$

$$P_4^0(\cos\theta) = \tfrac{1}{8}(35\cos^4\theta - 30\cos^2\theta + 3)$$

$$P_4^2(\cos\theta) = \tfrac{15}{2}(1 - \cos^2\theta)(7\cos^2\theta - 1)$$

$$P_4^3(\cos\theta) = 105(1 - \cos^2\theta)^{3/2}\cos\theta$$

$$P_4^4(\cos\theta) = 105(1 - \cos^2\theta)^2$$

$$P_6^0(\cos\theta) = \tfrac{1}{16}(231\cos^6\theta - 315\cos^4\theta + 105\cos\theta - 5)$$

$$P_6^2(\cos\theta) = \tfrac{105}{8}(1 - \cos^2\theta)(33\cos^4\theta - 18\cos^2\theta + 1)$$

$$P_6^3(\cos\theta) = \tfrac{315}{2}(1 - \cos^2\theta)^{3/2}(11\cos^3\theta - 3\cos\theta)$$

$$P_6^4(\cos\theta) = \tfrac{945}{2}(1 - \cos^2\theta)^2(11\cos^2\theta - 1)$$

$$P_6^6(\cos\theta) = 10{,}395(1 - \cos^2\theta)^3$$

Table A3.2

Some of the more commonly occurring spherical harmonics.

(As defined by Equation (A2.5))

$$Y_2^0 = \frac{1}{4}\sqrt{\frac{5}{\pi}}\,(3\cos^2\theta - 1)$$

$$Y_2^{\pm 2} = \frac{1}{4}\sqrt{\frac{15}{2\pi}}\,\sin^2\theta\, e^{\pm 2i\phi}$$

$$Y_4^0 = \frac{3}{16}\sqrt{\frac{1}{\pi}}\,(35\cos^4\theta - 30\cos^2\theta + 3)$$

$$Y_4^{\pm 2} = \frac{3}{8}\sqrt{\frac{5}{2\pi}}\,\sin^2\theta\,(7\cos^2\theta - 1)\, e^{\pm 2i\phi}$$

$$Y_4^{\pm 3} = \mp\frac{3}{8}\sqrt{\frac{35}{\pi}}\,\sin^3\theta\cos\theta\, e^{\pm 3i\phi}$$

$$Y_4^{\pm 4} = \frac{3}{16}\sqrt{\frac{35}{2\pi}}\,\sin^4\theta\, e^{\pm 4i\phi}$$

$$Y_6^0 = \frac{1}{32}\sqrt{\frac{13}{\pi}}\,(231\cos^6\theta - 315\cos^4\theta + 105\cos^2\theta - 5)$$

$$Y_6^{\pm 2} = \frac{1}{64}\sqrt{\frac{2730}{2\pi}}\,\sin^2\theta\,(33\cos^4\theta - 18\cos^2\theta + 1)\, e^{\pm 2i\phi}$$

$$Y_6^{\pm 3} = \mp\frac{1}{32}\sqrt{\frac{2730}{2\pi}}\,\sin^3\theta\,(11\cos^3\theta - 3\cos\theta)\, e^{\pm 3i\phi}$$

$$Y_6^{\pm 4} = \frac{21}{32}\sqrt{\frac{13}{14\pi}}\,\sin^4\theta\,(11\cos^2\theta - 1)\, e^{\pm 4i\phi}$$

$$Y_6^{\pm 6} = \frac{231}{64}\sqrt{\frac{13}{231\pi}}\,\sin^6\theta\, e^{\pm 6i\phi}$$

Table A3.3

Some of the more commonly occurring tesseral harmonics expressed in Cartesian Co-ordinates. If required in polar co-ordinates, they can be found from Table A2.2, and Equation (A2.7).

$$z_{20} = \frac{1}{4}\sqrt{\frac{5}{\pi}}\left[(3z^2 - r^2)/r^2\right]$$

$$z^c_{22} = \frac{1}{4}\sqrt{\frac{15}{\pi}}\left[(x^2 - y^2)/r^2\right]$$

$$z_{40} = \frac{3}{16}\sqrt{\frac{1}{\pi}}\left[(35z^4 - 30z^2r^2 + 3r^4)/r^4\right]$$

$$z^c_{42} = \frac{3}{8}\sqrt{\frac{5}{\pi}}\left[(7z^2 - r^2)(x^2 - y^2)/r^4\right]$$

$$z^o_{43} = \frac{3}{8}\sqrt{\frac{70}{\pi}}\left[z(x^3 - 3xy^2)/r^4\right]$$

$$z^c_{44} = \frac{3}{16}\sqrt{\frac{35}{\pi}}\left[(x^4 - 6x^2y^2 + y^4)/r^4\right]$$

$$z_{60} = \frac{1}{32}\sqrt{\frac{13}{\pi}}\left[(231z^6 - 315z^4r^2 + 105z^2r^4 - 5r^6)/r^6\right]$$

$$z^c_{62} = \frac{1}{64}\sqrt{\frac{2730}{\pi}}\left[(16z^4 - 16(x^2 + y^2)z^2 + (x^2 + y^2)^2)(x^2 - y^2)/r^6\right]$$

$$z^c_{63} = \frac{1}{32}\sqrt{\frac{2730}{\pi}}\left[(11z^3 - 3zr^2)(x^3 - 3xy^2)/r^6\right]$$

$$z^c_{64} = \frac{21}{32}\sqrt{\frac{13}{7\pi}}\left[(11z^2 - r^2)(x^4 - 6x^2y^2 + y^4)/r^6\right]$$

$$z^o_{66} = \frac{231}{64}\sqrt{\frac{26}{231\pi}}\left[(x^6 - 15x^4y^2 + 15x^2y^4 - y^6)/r^6\right]$$

Table A3.4

List of operator equivalents to some commonly occurring functions, within a manifold of given J. The summation being over the co-ordinates of the magnetic electrons.

$$\sum(3z^2 - r^2) \equiv \alpha_J \langle r^2 \rangle \left[3J_z^2 - J(J+1)\right] = \alpha_J \langle r^2 \rangle \; O_2^0$$

$$\sum(x^2 - y^2) \equiv \alpha_J \langle r^2 \rangle \left[\frac{J_+^2 + J_-^2}{2}\right] \equiv \alpha_J \langle r^2 \rangle O_2^2$$

$$\sum(35z^4 - 30r^2z^2 + 3r^4) \equiv \beta_J \langle r^4 \rangle \left[35J_z^4 - 30J(J+1).J_x^2 + 25J_z^2 + \right.$$

$$\left. - 6J(J+1) + 3J^2(J+1)^2\right] = \beta_J \langle r^4 \rangle \; O_4^0$$

$$\sum(7z^2 - r^2)(x^2 - y^2) \equiv \beta_J \langle r^4 \rangle \tfrac{1}{4}\left[(7J_z^2 - J(J+1) - 5)(J_+^2 + J_-^2) + \right.$$

$$\left. + (J_+^2 + J_-^2) \times (7J_z^2 - J(J+1) - 5)\right] =$$

$$= \beta_J \langle r^4 \rangle \; O_4^2$$

$$\sum z(x^3 - 3xy^2) \equiv \beta_J \langle r^4 \rangle \tfrac{1}{4}\left[J_z(J_+^3 + J_-^3) + (J_+^3 + J_-^3)J_z\right] = \beta_J \langle r^4 \rangle \; O_4^3$$

$$\sum(x^4 - 6x^2y^2 + y^4) \equiv \beta_J \langle r^4 \rangle \tfrac{1}{8}(J_+^4 + J_-^4) = \beta_J \langle r^4 \rangle \; O_4^4$$

$$\sum(231z^6 - 315z^4r^2 + 105z^2r^4 - 5r^6) \equiv \gamma_J \langle r^6 \rangle \left[231J_z^6 - 315J(J+1)J_z^4 + 735J_z^4 + \right.$$

$$+ 105J^2(J+1)^2J_z^2 - 525J(J+1)J_z^2 + 294J_z^2 - 5J^3(J+1)^3 + 40J^2(J+1)^2 +$$

$$\left. - 60J(J+1)\right] = \gamma_J \langle r^6 \rangle \; O_6^0$$

$$\sum(16z^4 - 16(x^2+y^2)z^2 + (x^2+y^2)^2)(x^2 - y^2) \equiv \gamma_J \langle r^6 \rangle \tfrac{1}{4} \times$$

$$\left[\left\{33J_z^4 - \left[18J(J+1) + 123\right].J_z^2 + J^2(J+1)^2 + 10J(J+1) + 102\right\} \times \right.$$

$$\left. \times (J_+^2 + J_-^2) + (J_+^2 + J_-^2)\left\{33J_z^4 - \text{etc.}\right\}\right] = \gamma_J \langle r^6 \rangle \; O_6^2$$

$$\sum(11z^3 - 3zr^2)(x^3 - 3xy^2) \equiv \gamma_J \langle r^6 \rangle \tfrac{1}{4}\left[(11J_z^3 - 3J(J+1)J_z - 59J_z)(J_+^3 + J_-^3) + \right.$$

$$\left. (J_+^3 + J_-^3)(11J_z^3 - 3J(J+1)J_z - 59J_z)\right] = \gamma_J \langle r^6 \rangle \; O_6^3$$

$$\sum(11z^2 - r^2)(x^4-6x^2y^2+y^4) = \gamma_J\langle r^6\rangle \tfrac{1}{4}\Big[(11J_z^2-J(J+1)-38)(J_+^4+J_-^4) + (J_+^4+J_-^4)(11J_z^2-J(J+1)-38)\Big] = \gamma_J\langle r^6\rangle O_6^4$$

$$\sum(x^6-15x^4y^2+15x^2y^4-y^6) = \gamma_J\langle r^6\rangle \tfrac{1}{4}\left[J_+^6+J_-^6\right] = \gamma_J\langle r^6\rangle O_6^6$$

APPENDIX IV

Computer Programmes

This appendix contains an account of the computer programmes written in Autocode for the Oxford University Mercury Computer and used for the work described in the thesis. The programmes are not given in full, but flow diagrams and subroutines are given when necessary. Some discussion is also given in the main text. The Library programmes referred to are from the Oxford University Computer Library.

IVA Programme CL119 "Garnet Spectra"

For given principal g values as data, this programme calculates, from Equations (3.3), g_{eff} and g^2_{eff} at 5° intervals for each of the four lines of the garnet (110) spectrum. Time ~ 15 secs.

IVB Programme CL143 "Nd Garnet"

This programme calculates the principal g values of the split and admixed Γ_8 state of Nd^{3+} (in a cubic field) using Equations (4.16). The cubic wavefunction coefficients a_1, a_2, a_3, b_1, and b_2, are fed in as data. Time ~ 1 min.

IVC Programme CL145a "C.E.F."

This programme calculates the coefficients, $\alpha_{n\nu}$, occurring in the expression (Equation (7.1)) for the potential at a point near the origin due to a general array of point charges. The co-ordinates of the origin, the position and magnitude of contributing charges, and the lattice constant. are fed in as

data. The reference co-ordinate system can be varied by using the appropriate steering Chapter 0. The $\alpha_{n\alpha}$, closely related to $\gamma_{n\alpha}$, are calculated from an equation similar to (A2.10) by straightforward summation within a loop, and printed to six significant figures. The calculation is performed in cylindrical co-ordinates. Time ~ 10 secs. per charge.

IVD Programme CL145b "C. E. F. Full Sum"

This programme is written specifically for the garnet structure, though it could also be used for any regular cubic lattice. It calculates, with respect to axes (x',y',z') of Figure 7.2b, the nine relevant values of β_n^m defined by Equation (7.2) (and proportional to γ_{nm}^a and A_n^m). A term proportional to γ_{22}^a, which should vanish by symmetry is also calculated. The summation, using Equation (A2.10), is over all ions within a given radius from the origin, and the contribution from ions in different shells, together with the total contribution, is printed as described in §7.3.2. In order to avoid using the auxiliary store (drum), the programme can only deal with about 40 ions in the unit cell at a time, and the contributions to the β_n^m from the c, a, d, and h sites (split into three groups) must be found separately. The co-ordinates of the three groups of the 96 h sites are written, with respect to unit cell axes, into Chapters 1, 2 and 3, the c, a, and d sites co-ordinates are fed in as data. Flow parameters enable the contribution

from each type of site to be determined for only the second order, or all, the coefficients β_n^m. The result is printed to six significant figures.

The data required are:- (a) The number of unit cells to be summed over.

(b) Flow parameters

(c) Origin; lattice constant; charge on ions; and oxygen parameters - or co-ordinates of c, a, and d sites.

Care was taken to ensure that all the ions within the outermost shell were taken into account. A flow diagram is given in Figure A4D - 1, and to illustrate the calculation a section of Chapter 4 is given in Table A4D.1. Time ~ 1½ hours per garnet lattice.

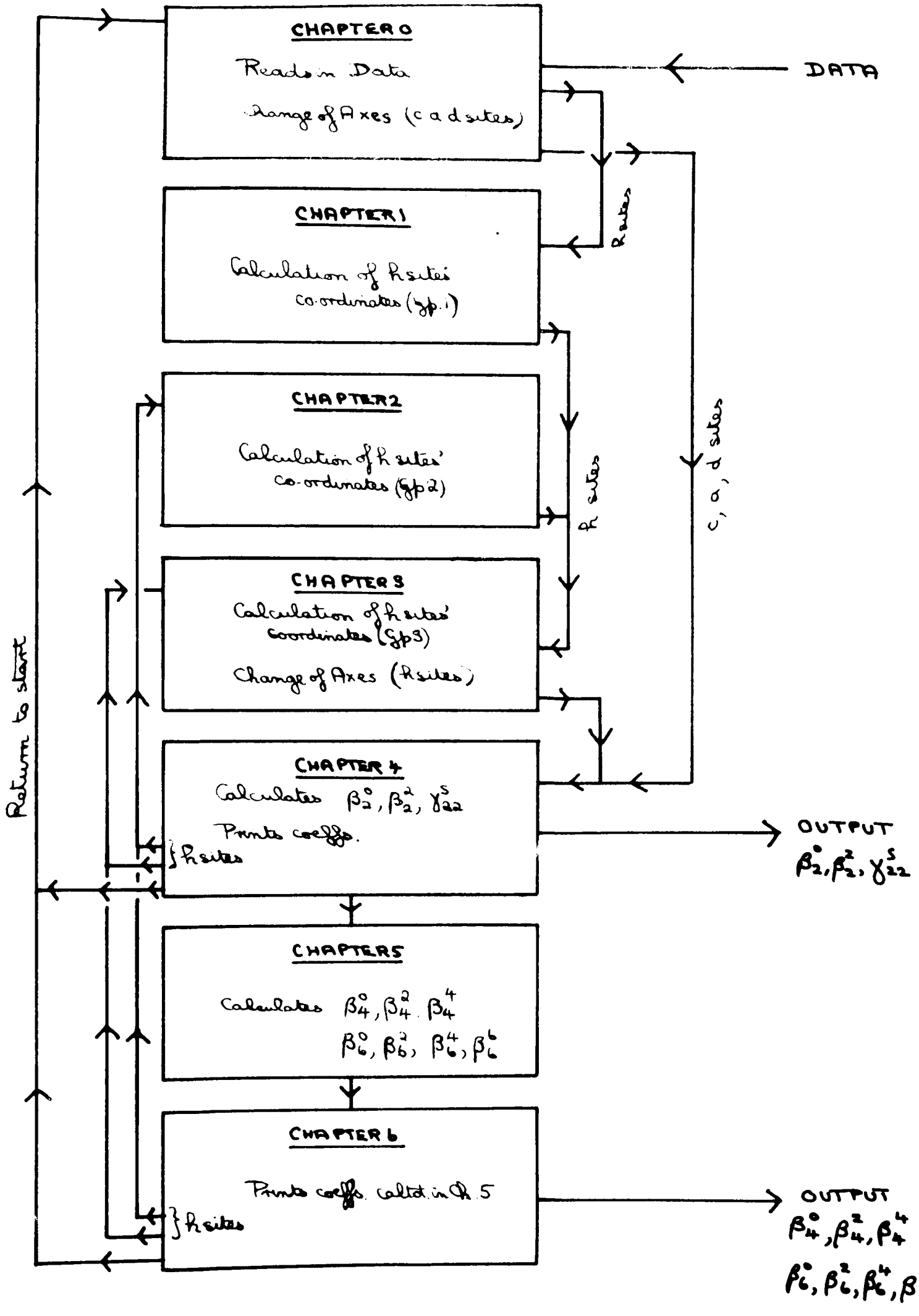
IVE Programme CL171a "Straight Diag"

This programme consists of a steering chapter, and J. S. Rollett's "Library Programme 517" for the diagonalisation of real symmetric matrices. Individual matrix elements are fed in as data, and the programme prints the eigenvalues and eigenvectors. Time - as for Library Programme 517.

N.B. A slight variation of this programme (CL171b), with the matrix of the J = 5/2 state of Yb^{3+} (Table 8.3) written in, was used in conjunction with the programme described in Appendix IVF.

CL145b CEF FULL SUM

FIGURE A4D-1



```
  CHAPTER 4
  VARIABLES1

1 )Bo=AoVo
  H=TAo
  K=4T
→ P=o(1)K
  E(P+1)=o
  F(P+1)=o
  G(P+1)=o
  REPEAT
→ I=1(1)N
  R=-T
→ L=R(1)T
→ M=R(1)T
→ Q=R(1)T
  AI=XI+LBo+MBo
  BI=YI+QAo
  CI=ZI+LBo-MBo
  Z=CICI
  WI=AIAI+BIBI+Z
  JUMP7,0.01>WI
  WI=XSQRT(WI)
  W=WIWI
  A=3Z-W
  C=WWWI
  Bn=1/C
  E=ABn
  A=AIAI-BIBI
  F=ABn
  G=AIBIBn
→ P=o(1)K
  C=H-0.25PAo
  JUMP2,C>WI
  E(P+1)=E(P+1)+E
  F(P+1)=F(P+1)+F
  G(P+1)=G(P+1)+G
  P=K
2 )REPEAT
7 )REPEAT
  REPEAT
  REPEAT
  620,3
  580,0
  REPEAT
  NEWLINE
```

TABLE A4D.1

- Sets variables to zero
- Selects ion in unit cell
- Puts it into each unit cell within T of origin
- Avoids ion at origin
- Calculates $\int_{nm}^{c} / r^{2n+1}$ for each ion
- Puts it into appropiate shell, adds contributions

IVF Programme CL172a "Yb 5/2 Fit"

This programme is very similar to that described in Appendix IVG, but fits only the C.E.F. parameters V_2^0, V_2^2 and V_4^0 to date for the $J = 5/2$ state of Yb^{3+} in YGG. It uses M. J. D. Powell's subroutine for the minimisation of a function of several variables (C.P.N. 50). The function being defined by Equation (8.5) and being determined from the eigenvalues and eigenvectors of the matrix given in Table 8.3. (It does not have the facility of diagonalising the matrix without fitting; for this use was made of the programme CL171b, mentioned in Appendix IVE). The data required are:-

(a) Three, or five, pieces of experimental data (with either a sign given to the g values or their modulus taken), weighting factors.

(b) Starting values of the three C.E.F. parameters, accuracy to which they are to be fitted.

(c) Flow parameters.

(N.B. The ratios (of Table 8.2) were fixed, as they were written into the matrix of Table 8.3).

IVG Programme CL172b "Yb ^2F Full Fit"

This programme fits the terms V_2^0, V_2^2, V_4^0 and V_6^0, occurring in the crystal field Hamiltonian of Equation (8.7), to experimental values for the splittings and g values listed in Table 8.1. It uses M. J. D. Powell's subroutine (C.P.N. 50) for the

minimisation of a function of several variables. The function, defined by Equation (6.3), is determined from the eigenvalues and eigenvectors of the complete matrix given in Table 6.4. The matrix is diagonalised using Library Programme 517.

A flow diagram of the programme is given in Figure A4.1. The fitting routine (C.P.N. 50) is in Chapters 1 and 2, and requires a subroutine for the determination of F at the end of each chapter. Owing to the length of this subroutine it had to be written in a separate Chapter 3. C.P.N. 50 calculates $\frac{\partial F}{\partial V_n^m}$ etc. by repeated calculation of F for slightly different values of V_n^m, and it is only necessary to specify the starting values of the parameters, accuracy required, and a subroutine for F.

Flow parameters enable F to be determined from the theoretical g values as calculated, or from their moduli. F may depend on only Δ_1, Δ_2, g_5 (5/2) and g_5 (7/2); or on all the g values. The programme may also be used, by-passing chapters 1, 2, and 3, for the straightforward diagonalisation of the matrix in Table 6.4 and calculation of the g values.

The data required are:-

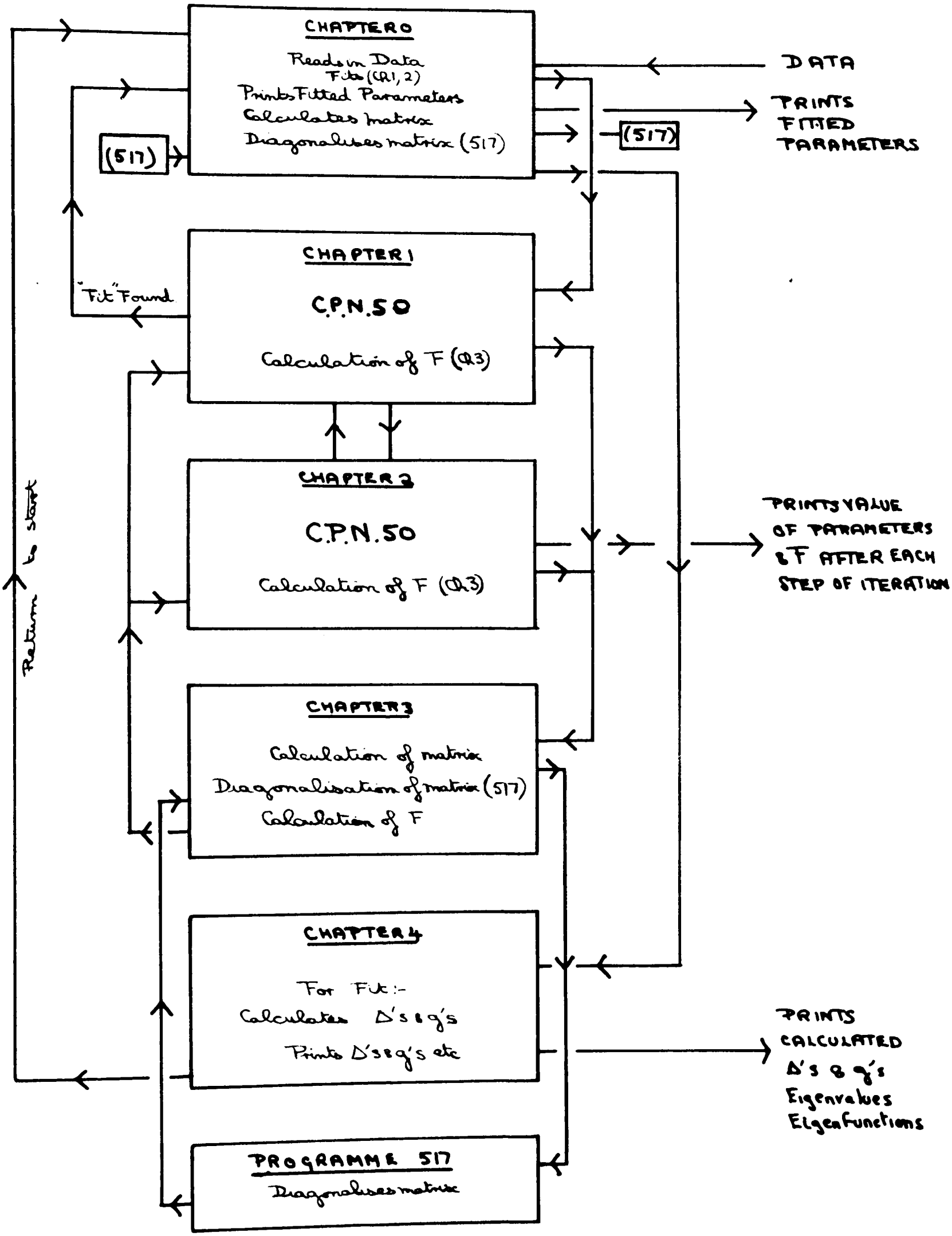
(a) Four, or eight, pieces of experimental data (with correct sign of g values, or their modulus), weighting factors.

(b) Starting values for the four C.P.N. parameters, accuracy to which they are to be fitted.

(c) Values of λ, and the ratios of parameters ξ_0, ζ_0, ζ_0, Ω, and (H).

CL 172b Yb ^{2}F FULL FIT

FIGURE A4G·1



(d) Flow parameters

The programme may print the value of F, and of the parameters V_n^m, after each step of the iteration. After printing the "fitted" V_n^m, it prints the eigenvalues, eigenvectors, splittings and g values of the fitted Hamiltonian. Time ~ 1 hour per fit. (The time is mainly taken up in diagonalising the 7 x 7 matrix (~ 25 secs) this could be reduced by use of slightly different fitting routine and specifying analytic expressions for $\frac{\partial F}{\partial V_n^m}$ as well as for F, but would involve some extremely lengthy algebra incorporated into the programme).

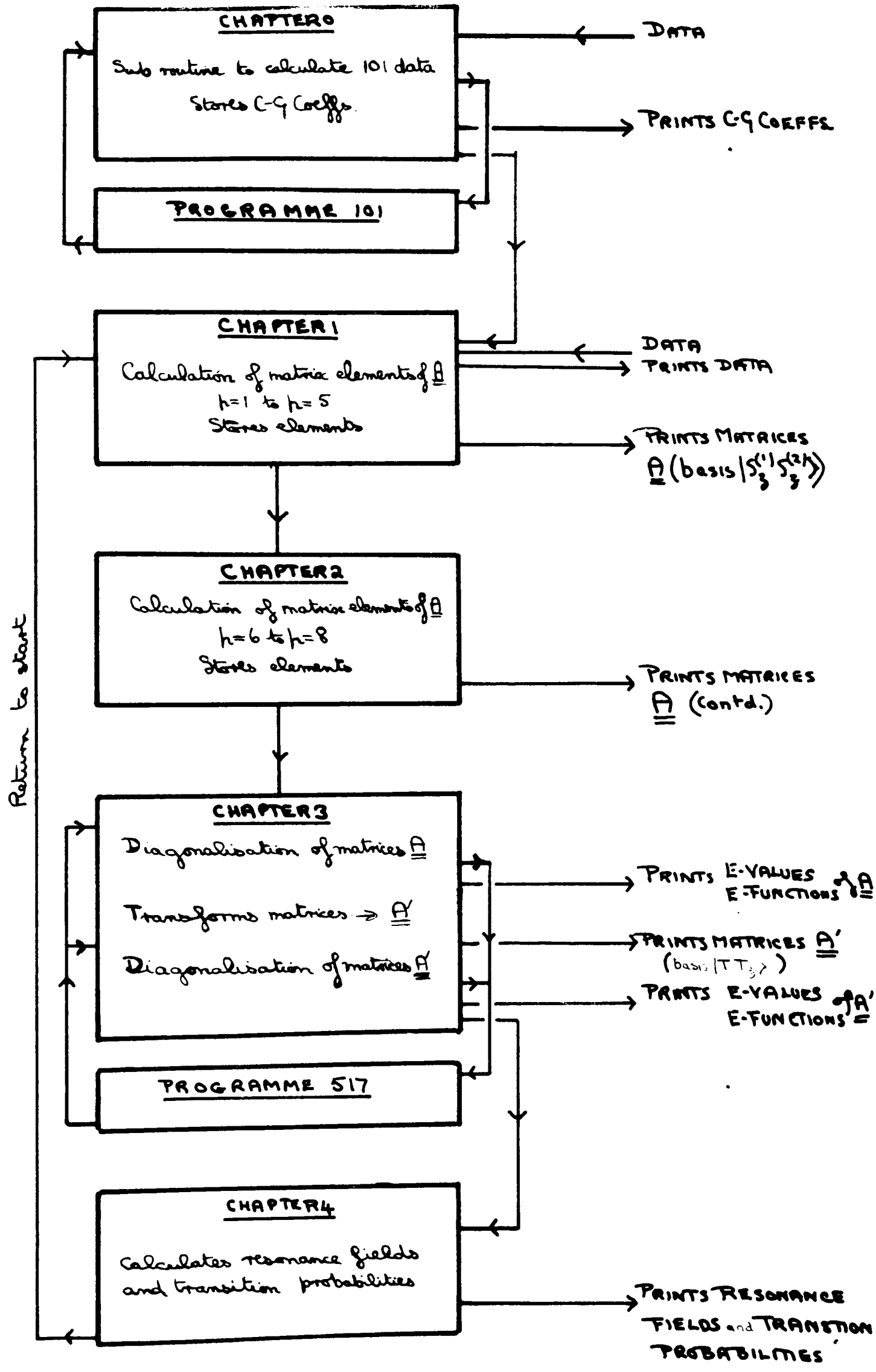
IVH Programme C.L. 1716. "$GdCl_3$ Pair Lines"

This programme calculates the eigenvalues and eigenfunctions of the Hamiltonian, $\mathcal{H}_p$, of Equation (11.2) in terms of a basis of states $|S^{(1)}S^{(2)}S_z^{(1)}S_z^{(2)}\rangle$, or $|S^{(1)}S^{(2)}T T_z\rangle$. The matrices of $\mathcal{H}_p$ in these two representations may also be printed before diagonalisation. The transition probabilities and fields for resonance are calculated.

Figure A4.H.1 shows a flow diagram of the programme. Dr. B. F. Mayer's Library programme 101 is used to calculate the 204 Clebsch-Gordan coefficients required for the transformation between the bases. A series of loops in Chapter 1 calculates the input data necessary for this pgogramme, that is the six values of $(2S^{(1)}, 2S^{(2)}, 2T, 2S_z^{(1)} 2S_z^{(2)}, 2T_z)$

CL171c $GdCl_3$ PAIR LINES

FIGURE A4H·1



for each coefficient $(s^{(1)}s^{(1)}_{z}s^{(2)}s^{(2)}_{z} \mid s^{(1)}s^{(2)}TT_{z})$. Programme 517 is used to diagonalise the eight matrices, and autocode matrix instructions are used to perform the matrix operations.

The matrices given in Appendix VA (referred to a basis of states $|s^{(1)}_{z}s^{(2)}_{z}\rangle$), are written into the programme in Chapters 1 and 2, and the diagonalisations and transformations are performed in Chapter 3.

The calculation of the resonance fields and transition probabilities is performed in Chapter 4 using an extensive system of loops. This section of the programme is reproduced in Table A4.H.1. The calculation is performed in a $|TT_{z}\rangle$ representation, and uses the fact that the eight matrices (given in Appendix VB) factorise into sub matrices whose basis consists of states of odd or even T. [N.B. It was found that the eigenvalues of each of the eight matrices, if listed in increasing order of magnitude, have eigenfunctions consisting of states with T alternately odd and even. This, and the fact that in the cases considered the symmetry of the first eigenstates of the matrices was always one of two alternatives, simplified the problem.]. The programme finds the difference between energy levels whose eigenfunctions have the same symmetry (odd or even T) ?, and calculates the resonance field from equation (11.3). Any negative fields given by the programme must be considered positive. The relative transition

probability is calculated from Equation (11.4). N.B. Although $G = g\mu_B$ is included in the matrices, it must be set equal to zero if the resonant fields are to be calculated.

The data required are:- (a) Flow parameters (enabling different information to be printed.)

(b) Values of J_{ex}, H, α, b_2^0, b_4^0, b_6^0 (The programme prints these to check, together with values of B, G and J).

(c) The value of $\tilde{\nu}$ in cm^{-1}.

Time ~ 5 mins. per set of data.

TABLE A4H.1

```
      P=0
1)    P=P+1
      NEWLINE
      NEWLINE
      JUMP6,P>8
      JUMP15,0.00001>B21
      0)=3)
      JUMP16
15)   0)=4)
      620,3
16)   L=0
      I=P(-1)1
      L=I+L
      REPEAT
      J=0
      I=P(-1)1
      J=II+J
      REPEAT
      S=J-PP
      M=8-P
      PSA
      N=1(1)P
      JUMP(0)
3)    K=2
      0)=4)
      JUMP5
4)    K=1
      0)=3)
5)    I=L+N-P
      A=AI
      R=K(2)20
      I=P+1
      JUMP2,R>I
      I=L+R
      B=AI
      X=A-B
      JUMP17,0.00001>B21
      F=0.5P-0.5N
      F=XFRPT(F)
      F=10F
      JUMP11,F>2
      I=I
      JUMP12
17)   F=0.5N
      F=XFRPT(F)
      F=10F
      620,3
      JUMP11,2>F
      I=I
      JUMP12
11)   I=2
12)   E=0
```

Calculates Energy level differences

```
      Q=I(2)20
      JUMP9,Q>P
      T=S+NP-P+Q
      C1=BT
      T=J+RP-P+R+Q-1
      C2=BT
      D=C1C2
      T=8-Q
      C=TT+T-MM+M
      C=XSQRT(C)
      D=CD
      E=E+D
      JUMP10
    9)Q=20
   10)REPEAT
      E=EE
      PRINT(P)1,0
      PRINT(N)1,0
      SPACE
      T=P+1
      PRINT(T)1,0
      PRINT(R)1,0
      SPACE
      G=Y0-X
      H1=10757.8G
      G=Y0+X
      H2=10757.8G
      PRINT(H1)5,2
      PRINT(H2)5,2
      SPACE
      PRINT(E)3,4
      NEWLINE
      JUMP8
    2)R=20
    8)REPEAT
      REPEAT
      JUMP1
      PSA
      HOOT
      HOOT
    6)JUMP31,Vo>Zn
      END
   31)ACROSS19/1
      PSA
      XSQRT
      PSA
      CLOSE
```

Calculates Transition Probability

Calculates Fields for Resonance

APPENDIX VA

Matrices of the Hamiltonian of Equation (11.2)

$$\mathcal{H}_F = G(S_z^{(1)}+S_z^{(2)})+J(S_+^{(1)}S_-^{(2)}+S_-^{(1)}S_+^{(2)})+ DS_z^{(1)}S_z^{(2)}+\mathcal{H}_c^{(1)}+\mathcal{H}_c^{(2)}$$

written with respect to a basis of states $|S^{(1)}S^{(2)}S_z^{(1)}S_z^{(2)}\rangle$

$G = g\mu_B H_z$; $J = \frac{1}{2}(J_{ex} + \alpha)$; $D = (J_{ex} - 2\alpha)$; $\alpha = \frac{g^2\mu^2}{r^3}$

$$\mathcal{H}_c^{(1)} = \frac{b_2^0}{3} O_2^{0(1)} + \frac{b_4^0}{60} O_4^{0(1)} + \frac{b_6^0}{1260} O_6^{0(1)}$$

	$\lvert 7/2, 7/2\rangle$
$\langle 7/2, 7/2 \rvert$	$+7G$ $+\frac{49}{4}D$ $+14b_2^0$ $+14b_4^0$ $+25b_6^0$

$h=1$

	$\lvert 7/2, 5/2\rangle$	$\lvert 5/2, 7/2\rangle$
$\langle 7/2, 5/2 \rvert$	$+6G$ $+\frac{35}{4}D$ $+8b_2^0$ $-6b_4^0$ $-4b_6^0$	$+7J$
$\langle 5/2, 7/2 \rvert$	$+7J$	$+6G$ $+\frac{35}{4}D$ $+8b_2^0$ $-6b_4^0$ $-4b_6^0$

$h=2$

	$\lvert 7/2, 3/2\rangle$	$\lvert 5/2, 5/2\rangle$	$\lvert 3/2, 7/2\rangle$
$\langle 7/2, 3/2 \rvert$	$+5G$ $+\frac{21}{4}D$ $+4b_2^0$ $+4b_4^0$ $+10b_6^0$	$+J\sqrt{84}$	0
$\langle 5/2, 5/2 \rvert$	$+J\sqrt{84}$	$+5G$ $+\frac{35}{4}D$ $+2b_2^0$ $-26b_4^0$ $-10b_6^0$	$+J\sqrt{84}$
$\langle 3/2, 7/2 \rvert$		$+J\sqrt{84}$	$+5G$ $+\frac{21}{4}D$ $+4b_2^0$ $+4b_4^0$ $+10b_6^0$

$h=3$

$n=4$

	$\lvert 7/2, 1/2\rangle$	$\lvert 5/2, 3/2\rangle$	$\lvert 3/2, 5/2\rangle$	$\lvert 1/2, 7/2\rangle$
$\langle 7/2, 1/2 \rvert$	$+4G$ $+\frac{7}{4}D$ $+26_2^\circ$ $+16b_4^\circ$ -46_6°	$+J\sqrt{105}$	0	0
$\langle 5/2, 3/2 \rvert$	$+J\sqrt{105}$	$+4G$ $+\frac{15}{4}D$ -21_2° $-16b_4^\circ$ $+46_6^\circ$	$+12J$	0
$\langle 3/2, 5/2 \rvert$	0	$+12J$	$+4G$ $+\frac{15}{4}D$ -26_2° $-16b_4^\circ$ $+46_6^\circ$	$+J\sqrt{105}$
$\langle 1/2, 7/2 \rvert$			$+J\sqrt{105}$	$+4G$ $+\frac{7}{4}D$ $+26_2^\circ$ $+16b_4^\circ$ -46_6°

$n=5$

	$\lvert 7/2, -1/2\rangle$	$\lvert 5/2, 1/2\rangle$	$\lvert 3/2, 3/2\rangle$	$\lvert 1/2, 5/2\rangle$	$\lvert -1/2, 7/2\rangle$
$\langle 7/2, -1/2 \rvert$	$+3G$ $-\frac{7}{4}D$ $+21_2^\circ$ $+11b_4^\circ$ -46_6°	$+4\sqrt{7}J$	0	0	0
$\langle 5/2, 1/2 \rvert$	$+4\sqrt{7}J$	$+3G$ $+\frac{5}{4}D$ -46_2° -46_4° $-19b_6^\circ$	$+6\sqrt{5}J$	0	0
$\langle 3/2, 3/2 \rvert$	0	$+6\sqrt{5}J$	$+3G$ $+\frac{9}{4}D$ -61_2° -66_4° $+18b_6^\circ$	$+6\sqrt{5}J$	0
$\langle 1/2, 5/2 \rvert$	0	0	$+6\sqrt{5}J$	$+3G$ $+\frac{5}{4}D$ -46_2° $-41b_4^\circ$ $-10b_6^\circ$	$+4\sqrt{7}J$
$\langle -1/2, 7/2 \rvert$	0	0	0	$+4\sqrt{7}J$	$+3G$ $-\frac{7}{4}D$ $+26_2^\circ$ $+16b_4^\circ$ $-14b_6^\circ$

	$\lvert 7/2,-3/2\rangle$	$\lvert 5/2,-1/2\rangle$	$\lvert 3/2,1/2\rangle$	$\lvert 1/2,3/2\rangle$	$\lvert -1/2,5/2\rangle$	$\lvert -3/2,7/2\rangle$
$\langle 7/2,-3/2\rvert$	$+2G$ $-\frac{21}{4}D$ $+4b_2^0$ $+4b_4^0$ $+10b_6^0$	$+\sqrt{105}J$	0	0	0	0
$\langle 5/2,-1/2\rvert$	$+\sqrt{105}J$	$+2G$ $-\frac{5}{4}D$ $-4b_2^0$ $-4b_4^0$ $-10b_6^0$	$+8\sqrt{3}J$	0	0	0
$\langle 3/2,1/2\rvert$	0	$+8\sqrt{3}J$	$+2G$ $+\frac{3}{4}D$ $-8b_2^0$ $+1b_4^0$ $+1b_6^0$	$+16J$	0	0
$\langle 1/2,3/2\rvert$	0	0	$+16J$	$+2G$ $+\frac{9}{4}D$ $-8b_2^0$ $+6b_4^0$ $+4b_6^0$	$+8\sqrt{3}J$	0
$\langle -1/2,5/2\rvert$	0	0	0	$+8\sqrt{3}J$	$+2G$ $-\frac{5}{4}D$ $-4b_2^0$ $-4b_4^0$ $-10b_6^0$	$+\sqrt{105}J$
$\langle -3/2,7/2\rvert$	0	0	0	0	$+\sqrt{105}J$	$+2G$ $-\frac{21}{4}D$ $+4b_2^0$ $+4b_4^0$ $+10b_6^0$

$h=6$

A54

	$\lvert 7/2,-5/2\rangle$	$\lvert 5/2,-3/2\rangle$	$\lvert 3/2,-1/2\rangle$	$\lvert 1/2,1/2\rangle$	$\lvert -1/2,3/2\rangle$	$\lvert -3/2,5/2\rangle$	$\lvert -5/2,7/2\rangle$
$\langle 7/2,-5/2\rvert$	$+G$ $-\frac{35}{4}D$ $+8b_2^0$ $-6b_4^0$ $-4b_6^0$	$+\sqrt{84}\,J$	0	0	0	0	0
$\langle 5/2,-3/2\rvert$	$+\sqrt{84}\,J$	$+G$ $-\frac{15}{4}D$ $-2b_2^0$ $-16b_4^0$ $+4b_6^0$	$+6\sqrt{5}\,J$	0	0	0	0
$\langle 3/2,-1/2\rvert$	0	$+6\sqrt{5}\,J$	$+G$ $-\frac{3}{4}D$ $-8b_2^0$ $+6b_4^0$ $+4b_6^0$	$+4\sqrt{15}\,J$	0	0	0
$\langle 1/2,1/2\rvert$	0	0	$+4\sqrt{15}\,J$	$+G$ $+D$ $-10b_2^0$ $+12b_4^0$ $-10b_6^0$	$+11\sqrt{15}\,J$	0	0
$\langle -1/2,3/2\rvert$	0	0	0	$+4\sqrt{15}\,J$	$+G$ $-\frac{3}{4}D$ $-2b_2^0$ $+6b_4^0$ $+4b_6^0$	$+\sqrt{5}\,J$	0
$\langle -3/2,5/2\rvert$	0	0	0	0	$+6\sqrt{5}\,J$	$+G$ $-\frac{15}{4}D$ $-2b_2^0$ $+16b_4^0$ $+4b_6^0$	$+\sqrt{84}\,J$
$\langle -5/2,7/2\rvert$	0	0	0	0	0	$+\sqrt{84}\,J$	$+G$ $-\frac{35}{4}D$ $+8b_2^0$ $+6b_4^0$ $-4b_6^0$

$h=7$

AS-5

	$\lvert \frac{7}{2}, -\frac{7}{2} \rangle$	$\lvert \frac{5}{2}, -\frac{5}{2} \rangle$	$\lvert \frac{3}{2}, -\frac{3}{2} \rangle$	$\lvert \frac{1}{2}, -\frac{1}{2} \rangle$	$\lvert -\frac{1}{2}, \frac{1}{2} \rangle$	$\lvert -\frac{3}{2}, \frac{3}{2} \rangle$	$\lvert -\frac{5}{2}, \frac{5}{2} \rangle$	$\lvert -\frac{7}{2}, \frac{7}{2} \rangle$
$\langle \frac{7}{2}, -\frac{7}{2} \rvert$	$-\frac{49}{4}D$ $+146\frac{\circ}{2}$ $+146\frac{\circ}{4}$ $+26\frac{\circ}{6}$	$+7J$	0	0	0	0	0	0
$\langle \frac{5}{2}, -\frac{5}{2} \rvert$	$+7J$	$-\frac{25}{4}D$ $+26\frac{\circ}{2}$ $-26\frac{\circ}{4}$ $-10\frac{\circ}{6}$	$+12J$	0	0	0	0	0
$\langle \frac{3}{2}, -\frac{3}{2} \rvert$	0	$+12J$	$-\frac{9}{4}D$ $-6\frac{\circ}{2}$ $-66\frac{\circ}{4}$ $+18\frac{\circ}{6}$	$+15J$	0	0	0	0
$\langle \frac{1}{2}, -\frac{1}{2} \rvert$	0	0	$+15J$	$-\frac{D}{4}$ $-10\frac{\circ}{2}$ $+12\frac{\circ}{4}$ $-10\frac{\circ}{6}$	$+16J$	0	0	0
$\langle -\frac{1}{2}, \frac{1}{2} \rvert$	0	0	0	$+16J$	$-\frac{D}{4}$ $-10\frac{\circ}{2}$ $+10\frac{\circ}{4}$ $-10\frac{\circ}{6}$	$+15J$	0	0
$\langle -\frac{3}{2}, \frac{3}{2} \rvert$	0	0	0	0	$+15J$	$-\frac{9}{4}D$ $-6\frac{\circ}{2}$ $-66\frac{\circ}{4}$ $+18\frac{\circ}{6}$	$+12J$	0
$\langle -\frac{5}{2}, \frac{5}{2} \rvert$	0	0	0	0	$+12J$	$-\frac{25}{4}D$ $+26\frac{\circ}{2}$ $-26\frac{\circ}{4}$ $-10\frac{\circ}{6}$	$+7J$	
$\langle -\frac{7}{2}, \frac{7}{2} \rvert$	0	0	0	0	0	$+7J$	$-\frac{49}{4}D$ $+14\frac{\circ}{2}$ $+14\frac{\circ}{4}$ $+26\frac{\circ}{6}$	

A5.6

8 of 8

APPENDIX VB

Matrices of the Hamiltonian of Equation (11.1)

$$\mathcal{H}_p = G(S_z^{(1)}+S_z^{(2)})+J_{ex}\,\underline{S}^{(1)}\cdot\underline{S}^{(2)}+\alpha(\underline{S}^{(1)}\cdot\underline{S}^{(2)}-3S_z^{(1)}S_z^{(2)})+\mathcal{H}_c^{(1)}+\mathcal{H}_c^{(2)}$$

written with respect to a basis of states $|S^{(1)}S^{(2)}\,T\,T_z\rangle$

$$G = g\mu_B H_z;\quad \alpha = \frac{g^2\mu^2}{r^3};\quad \mathcal{H}_c^{(1)} = \frac{b_2^0}{3}O_2^{0(1)} + \frac{b_4^0}{60}O_4^{0(1)} + \frac{b_6^0}{1260}O_6^{0(1)}$$

$h=1$

$\langle 7,7 \vert$	$\vert 7,7\rangle$
	$+7G$ -24.5α $+12.25J_{exc}$ $+14b_2^\circ$ $+14b_4^\circ$ $+2b_6^\circ$

$h=2$

$\langle 7,6 \vert$	$\vert 7,6\rangle$	$\vert 6,6\rangle$
	$+6G$ -14α $+12.25J_{exc}$ $+8b_2^\circ$ $-6b_4^\circ$ $-4b_6^\circ$	0
$\langle 6,6 \vert$	0	$+6G$ -21α $+5.25J_{exc}$ $+8b_2^\circ$ $-6b_4^\circ$ $-4b_6^\circ$

$h=3$

$\langle 7,5 \vert$	$\vert 7,5\rangle$	$\vert 6,5\rangle$	$\vert 5,5\rangle$
	$+5G$ -5.1154α $+12.25J_{exc}$ $+2.9231b_2^\circ$ $-12.1538b_4^\circ$ $-0.7692b_6^\circ$	0	$+1.4956\alpha$ $+0.9970b_2^\circ$ $+14.9556b_4^\circ$ $+9.9704b_6^\circ$
$\langle 6,5 \vert$	0	$+5G$ -10.5α $+5.25J_{exc}$ $+4b_2^\circ$ $+4b_4^\circ$ $+10b_6^\circ$	0
$\langle 5,5 \vert$	$+1.4956\alpha$ $+0.9970b_2^\circ$ $+14.9556b_4^\circ$ $+9.9704b_6^\circ$	0	$+5G$ -17.885α $-0.75J_{exc}$ $+3.0769b_2^\circ$ $-9.8462b_4^\circ$ $+0.7692b_6^\circ$

A5.8

	|7,4⟩	|6,4⟩	|5,4⟩	|4,4⟩
⟨7,4|	+4G +2.1538α +12.25 J_{ex} -1.2308 b_2^0 -9.8462 b_4^0 +2.4615 b_6^0	0	+2.3647α +1.5765 b_2^0 +12.6116 b_4^0 -3.1529 b_6^0	0
⟨6,4|	0	+4G -1.9091α +5.25 J_{ex} +0.7273 b_2^0 +5.8182 b_4^0 -1.4545 b_6^0	0	+2.7946α +1.8631 b_2^0 +14.9047 b_4^0 -3.7262 b_6^0
⟨5,4|	+2.3647α +1.5765 b_2^0 +12.6116 b_4^0 -3.1529 b_6^0	0	+4G -7.1538α -0.75 J_{ex} +1.2308 b_2^0 +9.8462 b_4^0 -2.4615 b_6^0	0
⟨4,4|	0	+2.7946α +1.8631 b_2^0 +14.9047 b_4^0 -3.7262 b_6^0	0	+4G -15.0907α -5.75 J_{ex} -0.7273 b_2^0 -5.8182 b_4^0 +1.4545 b_6^0

h=4

	|7,3⟩	|6,3⟩	|5,3⟩	|4,3⟩	|3,3⟩
⟨7,3|	+3G +7.8077α +12.25 J_{ex} -4.4615 b_2^0 -3.4825 b_4^0 +2.7552 b_6^0	0	+3.0249α +2.0166 b_2^0 +5.1536 b_4^0 -8.0664 b_6^0	0	+1.7051 b_4^0 +10.9614 b_6^0
⟨6,3|	0	+3G +4.7727α +5.25 J_{ex} -1.8182 b_2^0 +3.2727 b_4^0 -7.8182 b_6^0	0	+4.3294α +2.8863 b_2^0 +9.6209 b_4^0 +2.8863 b_6^0	
⟨5,3|	+3.0249α +2.0166 b_2^0 +5.1536 b_4^0 -8.0664 b_6^0	0	+3G +1.1923α -0.75 J_{ex} -0.2051 b_2^0 +9.8462 b_4^0 +1.4872 b_6^0	0	+4.3845α +2.0990 b_2^0 +8.3624 b_4^0 -5.4634 b_6^0
⟨4,3|	0	+4.3294α +2.8863 b_2^0 +9.6209 b_4^0 +2.8863 b_6^0	0	+3G -3.7727α -5.75 J_{ex} -0.1818 b_2^0 +8.7273 b_4^0 -6.1818 b_6^0	0
⟨3,3|	+1.7051 b_4^0 +10.9614 b_6^0	0	+4.3485α +2.8990 b_2^0 +8.3624 b_4^0 -5.4634 b_6^0	0	+3G -12.5α -9.75 J_{ex} -3.3333 b_2^0 -0.3636 b_4^0 -0.2424 b_6^0

h=5

$k=6$

	$\|7,2\rangle$	$\|6,2\rangle$	$\|5,2\rangle$	$\|4,2\rangle$	$\|3,2\rangle$	$\|2,2\rangle$
$\langle 7,2 \|$	$+2G$ $+11.8446\,\alpha$ $+13.25\,T_{ex}$ $-6.7692\,b_2^0$ $+3.5105\,b_{1\pi}^0$ $+0.6993\,b_{1\pi}^0$	0	$+3.4929\,\alpha$ $+2.3286\,b_2^0$ $-3.10448\,b_{1\pi}^0$ $-3.4929\,b_{1\pi}^0$	$+2G$ $+4.3117\,\alpha$ $-5.75\,T_{ex}$ $+0.2079\,b_2^0$ $+4.5714\,b_{1\pi}^0$ $+8\,b_{1\pi}^0$	$+2G$ $+4.4495\,b_{1\pi}^0$ $+7.6377\,b_{1\pi}^0$	0
$\langle 6,2 \|$	0	$+2G$ $+9.5454\,\alpha$ $+5.25\,T_{ex}$ $-3.6344\,b_2^0$ $-0.6667\,b_{1\pi}^0$ $-4\,b_{1\pi}^0$	$+5.3997\,\alpha$ $+3.5998\,b_2^0$ $0.b_{1\pi}^0$ $+3.8234\,b_{1\pi}^0$	$+2G$ $+4.3117\,\alpha$ $-5.75\,T_{ex}$ $+0.2079\,b_2^0$ $+4.5714\,b_{1\pi}^0$ $+8\,b_{1\pi}^0$	$+2G$ $0.\alpha$ $-9.75\,T_{ex}$ $0.b_2^0$ $+0.8465\,b_{1\pi}^0$ $+1.1545\,b_{1\pi}^0$	0
$\langle 5,2 \|$	$+3.4929\,\alpha$ $+2.3286\,b_2^0$ $-3.1044\,b_{1\pi}^0$ $-3.4929\,b_{1\pi}^0$	0	$+2G$ $+7.1538\,\alpha$ $-0.75\,T_{ex}$ $-1.2308\,b_2^0$ $+1.6410\,b_{1\pi}^0$ $+1.8462\,b_{1\pi}^0$	0	$+6.5327\,\alpha$ $+4.3485\,b_{1\pi}^0$ $+2.7875\,b_{1\pi}^0$ $+4.1923\,b_{1\pi}^0$	0
$\langle 4,2 \|$	$+2.9533\,b_{1\pi}^0$ $+5.0429\,b_{1\pi}^0$	0	$+6.5327\,\alpha$ $+4.3485\,b_2^0$ $+2.7875\,b_{1\pi}^0$ $+8.1923\,b_{1\pi}^0$	0	$+2G$ $0.\alpha$ $-9.75\,T_{ex}$ $0.b_2^0$ $+0.8465\,b_{1\pi}^0$ $+1.1545\,b_{1\pi}^0$	0
$\langle 3,2 \|$	0	$+4.4495\,b_{1\pi}^0$ $+7.6377\,b_{1\pi}^0$	0	$+4.3117\,\alpha$ $+3.2378\,b_2^0$ $-1.1558\,b_{1\pi}^0$ $+1.3848\,b_{1\pi}^0$	0	$+2G$ $-9.8571\,\alpha$ $-12.75\,T_{ex}$ $-4.571\,b_2^0$ $+3.0952\,b_{1\pi}^0$ $0.\,b_2^0$

$h=7$

	$\langle 1,1 \rangle$	$\langle 2,1 \rangle$	$\langle 3,1 \rangle$	$\langle 4,1 \rangle$	$\langle 5,1 \rangle$	$\langle 6,1 \rangle$	$\langle 7,1 \rangle$
$\langle 1,1 \rangle$	$+3.679\,56_{6}^{6}$	0	$+3.813\,7_{44}^{0}$ $-4.3\,1^{0}\,5_{6}^{6}$	0	$+3.773\,7_{44}$ $-7.223\,3_{44}^{0}$ $+3.952_{44}\,6_{6}^{6}$	$+6.037\,1_{44}$ $-8.0\,49_{44}\,6_{44}^{0}$ $-1.1\,49\,9\,6_{6}^{6}$	$+G$ $+14.247\,3_{44}$ $+13.\,1\,5\,T_{\infty}$ $-8.153\,8\,6_{4}^{0}$ $+8.\,6\,53\,6_{44}^{0}$ $-1.749\,2\,6_{6}^{6}$
$\langle 2,1 \rangle$	0	$+7.035\,3_{44}^{0}$ $-1.\,20\,6\,0\,6_{6}^{6}$	0	$+8.\,9\,8\,9\,8_{44}$ $+5.\,9\,9\,3\,2\,6_{4}^{0}$ $+0.\,27\,3\,4_{44}^{0}$ $-3.\,8\,13\,9\,6_{6}^{6}$	$+G$ $+4.\,9\,2\,6_{44}$ $-13.\,7\,5\,T_{\infty}$ $+3.\,28\,5\,7\,6_{4}^{0}$ $-8.\,3\,9\,10\,6_{44}^{0}$ $0.\,6_{6}^{6}$	$+G$ $+13.\,4\,0\,9\,1_{44}$ $-4.\,7\,3\,7\,3_{44}^{0}$ $+5.\,3\,5\,T_{\infty}$ $-3.\,8\,7\,8\,8_{44}^{0}$ $+3.\,6\,3\,4_{44}^{0}$ $-1.\,1\,4\,9\,7_{6}^{6}$	$+7.\,0\,3\,5\,3_{44}^{0}$ $-1.\,20\,6\,0_{6}^{6}$	0
$\langle 3,1 \rangle$	$+3.813\,7_{44}^{0}$ $-4.\,3\,1^{0}\,5_{6}^{6}$	0	$+7.\,7\,9\,6\,1_{44}$ $+5.\,19\,7_{44}^{0}$ $-3.\,6\,6_{44}^{0}\,8_{44}$ $0.\,6_{6}^{6}$	0	$+G$ $+7.\,5_{44}$ $-9.\,7\,5\,T_{\infty}$ $+2\,6_{44}^{0}$ $-0.\,12\,1\,2_{44}^{0}$ $-3.\,6\,3\,6_{44}^{0}\,6_{6}^{6}$	0	$+9.\,2\,11\,8_{44}$ $+6.\,1\,4\,1\,2\,6_{4}^{0}$ $-8.\,1\,8\,8\,3\,6_{44}^{0}$ $0.\,6_{6}^{6}$
$\langle 4,1 \rangle$	0	$+6.\,0\,3\,7\,1_{44}$ $+4.\,0\,3\,4\,7\,6_{4}^{0}$ $-8.\,0\,4\,9\,4_{44}\,6_{44}^{0}$ $-1.\,1\,4\,9\,9\,6_{6}^{6}$	0	$+G$ $+9.\,1\,6\,2\,3_{44}$ $-5.\,7\,5\,T_{\infty}$ $+0.\,4\,4\,1\,6\,6_{44}^{0}$ $-3.\,7\,4\,0\,3\,6_{44}^{0}$ $+0.\,3\,6\,3\,6\,6_{6}^{6}$	0	$+8.\,9\,2\,9\,8_{44}$ $+5.\,9\,9\,3\,2\,6_{4}^{0}$ $+0.\,3\,7\,3\,4_{44}\,6_{44}^{0}$ $-3.\,8\,13\,7\,6_{6}^{6}$	0
$\langle 5,1 \rangle$	$+3.\,7\,7\,3\,7_{44}$ $+2.\,5\,1\,5\,2\,6_{4}^{0}$ $-9.\,2\,2\,3\,3\,6_{44}^{0}$ $+3.\,9\,5\,3\,4_{44}\,6_{6}^{6}$	0	$+G$ $+10.\,73\,0\,8_{44}$ $-0.\,7\,5\,T_{\infty}$ $-1.\,8\,4\,6\,3\,6_{4}^{0}$ $-6.\,5\,6\,4\,1\,6_{44}^{0}$ $-0.\,6\,1\,5\,4\,6_{6}^{6}$	0	$+7.\,7\,9\,6\,1_{44}$ $+5.\,19\,7\,6_{4}^{0}$ $-3.\,6\,6\,4\,3_{44}\,6_{44}^{0}$ $0.\,6_{6}^{6}$	0	$+9.\,3\,0\,9\,5\,6_{44}^{0}$ $-4.\,3\,7\,6\,7\,6_{6}^{6}$
$\langle 6,1 \rangle$	0	$+12.\,4\,0\,9\,1_{44}$ $+5.\,3\,5\,T_{\infty}$ $-4.\,7\,3\,7\,3_{44}^{0}$ $-3.\,8\,7\,8\,8_{44}^{0}$ $+3.\,6\,3\,4_{44}^{0}\,6_{6}^{6}$	$+6.\,0\,3\,7\,1_{44}$ $+4.\,0\,3\,4\,7\,6_{4}^{0}$ $-8.\,0\,4\,9\,4_{44}\,6_{44}^{0}$ $-1.\,1\,4\,9\,7\,6_{6}^{6}$	0	$+7.\,0\,3\,5\,3_{44}^{0}$ $-1.\,20\,6\,0\,6_{6}^{6}$	0	$+3.\,6\,7\,9\,5_{6}^{6}$
$\langle 7,1 \rangle$	$+G$ $+14.\,2\,6\,1\,3_{44}$ $+13.\,1\,5\,T_{\infty}$ $-8.\,1\,5\,3\,8\,6_{4}^{0}$ $+8.\,6\,5\,3\,6_{44}^{0}$ $-1.\,7\,4\,9\,2\,6_{6}^{6}$	0	$+13.\,7\,7\,3\,7_{44}$ $+2.\,5\,1\,5\,2\,6_{4}^{0}$ $-1.\,2\,2\,3\,2\,6_{44}^{0}$ $+3.\,9\,5\,3\,4_{44}\,6_{6}^{6}$	0	$+3.\,8\,1\,3\,7_{44}$ $-4.\,8\,4\,5\,5\,6_{6}^{6}$	0	$+3.\,6\,7\,9\,5_{6}^{6}$

AS·11

	۱۶٫۰	۱۵٫۰	۱۴٫۰	۱۳٫۰	۱۲٫۰	۱۱٫۰	۱۰٫۰
<۶٫۰۱	۰ +۱۵.۰۶۶ ₭ +۱۲.۵۲ ₸₀₀ −۴.۰۱۶۸ ₺₀ ۱۰.۶۶۱۴ ₺₀ −۲.۶۶۶ ₺₀	۰ +۳.۴۷۹۶ ₭ +۲.۶۶۶۳ ₺₀ −۱۱.۴۶۴۶ ₺₀ +۶.۳۶۱۵ ₺₀	۰ +۲.۶۶۶۳ ₺₀ −۱۱.۴۶۴۶ ₺₀ +۶.۳۶۱۵ ₺₀	۰ +۴.۱۱۴۲ ₺₀ −۹.۶۶۶۳ ₺₀	۰ +۷.۹۶۲۳ ₺₀ −۴.۶۶۶۳ ₺₀	۰ +۱۱.۲۴۲۱ ₭ +۶.۲۴۹۰ ₺₀ −۳.۶۶۶۴ ₺₀	۰ +۱۳.۶۶۶۶ ₭ +۱۲.۶۶۶۶ ₺₀ −۴.۶۶۶۶ ₺₀
<۶٫۰۱	۰ +۱۳.۶۷۳۶ ₭ +۶.۲۴۹۰ ₺₀ −۵.۰۶۰۹ ₺₀ +۷.۰۶۶۷ ₺₀	۰ +۱۳.۶۷۳۶ ₭ +۶.۲۴۹۰ ₺₀ −۵.۰۶۰۹ ₺₀ +۷.۰۶۶۷ ₺₀	۰ +۴.۱۶۶۰ ₺₀ −۱۱.۱۰۹۳ ₺₀ −۳.۳۳۶ ₺₀	۰ +۷.۹۶۲۳ ₺₀ −۶.۳۸۱۶ ₺₀	۰ +۱۱.۴۹۲۱ ₺₀		
<۵٫۰۱	۰ +۳.۸۶۵۶ ₭ +۲.۵۶۶۳ ₺₀ −۱۱.۴۵۴۵ ₺₀ +۷.۳۷۶ ₺₀	۰ +۱۱.۹۲۳۱ ₭ −۰.۶۵۳ ₸₀₀ −۳.۰۵۱۳ ₺₀ −۹.۹۱۰۶۲ ₺₀ −۳.۰۵۱۳ ₺₀	۰ +۴.۸۶۶۳ ₺₀ −۷.۳۶۱۴ ₺₀ −۷.۰۳۶۴ ₺₀	۰ +۱۳.۰۱۶۵ ₺₀ +۸ ₺₀ ۰.۶۱۴ ₺₀	۰ +۱۳.۶۶۶۶ ₭ −۱۴.۶۶۶۳ ₸₀₀ +۸ ₺₀ ۰.۶۱۴ ₺₀	۰ +۱۳.۶۶۶۶ ₭ +۹.۱۶۵۳ ₺₀ ۰.۶۱۴ ₺₀ ۰.۶۱۴ ₺₀	۰ +۱۳.۶۶۶۶ ₭ −۱۶.۶۶۳ ₸₀₀ ۰.۶۱۴ ₺₀ ۰.۶۱۴ ₺₀
<۴٫۰۱	۰ +۱۳.۶۶۶۶ ₭ +۷.۶۶۶۳ ₺₀ −۱۱.۴۶۴۶ ₺₀ +۶.۳۶۱۵ ₺₀	۰ +۱۳.۶۶۶۶ ₭ +۷.۶۶۶۳ ₺₀ −۱۱.۴۶۴۶ ₺₀ +۶.۳۶۱۵ ₺₀	۰ +۱۰.۶۶۹۳ ₭ −۵.۶۶۳ ₸₀₀ ۰.۶۱۹۶ ₺₀ −۷.۴۶۰۵۶ ₺₀ −۷.۲۶۳۷ ₺₀	۰ +۱۲.۰۱۶۵ ₺₀ +۶.۶۶۶۱۴ ₺₀	۰ +۱۳.۶۶۶۶ ₭ +۱۲.۶۶۶۶ ₺₀ −۴.۶۶۶۶ ₺₀	۰ +۱۳.۶۶۶۶ ₭ +۹.۱۶۵۳ ₺₀ ۰.۶۱۴ ₺₀ ۰.۶۱۴ ₺₀	۰ +۱۳.۶۶۶۶ ₭ −۱۶.۶۶۳ ₸₀₀ ۰.۶۱۴ ₺₀ ۰.۶۱۴ ₺₀

REFERENCES

Ayant, Y., and Thomas, J., 1960, C.R.Acad. Sci. Paris, 250, 2688.

1962[a], J.Phys. Soc. Japan, 17, Supp. B-1, 448.

See also Thomas, J., 1962[b], Thesis, Grenoble.

Bagguley, D. M. S., and Owen, J., 1957, Repts. Prog. Phys. 20, 304.

Baker, J. M., and Bleaney, B., 1955, Proc. Conf. Low Temp. Phys. Paris.

Baker, J. M., Bleaney, B., and Hayes, W., 1958, Proc. Roy. Soc., A247, 141.

Ball, M., Garton, G., Leask, M. J. M., and Wolf, W. P., 1960, Proc. 7th Int. Conf. Low Temp. Physics, Toronto.

Ball, M., Hutchings, M.T., Leask, M.J.M., and Wolf, W.P., 1962, Proc. 8th Int. Low Temp. Conf., London, (to be published).

Bertaut, F., and Ferrat, F., 1956, C.R. Acad. Sci. Paris, 242, 382.

Bleaney, B., 1959, Proc. Phys. Soc., 73, 939.

Bleaney, B., 1961, Proc. Phys. Soc., 77, 113.

Bleaney, B., Elliott, R.J., and Scovil, H.E.D., 1951, Proc. Phys. Soc., A64, 933.

Bleaney, B., and Stevens, K.W.H., 1953, Repts. Prog. Phys. 16, 108.

Bleaney, B., Scovil, H.E.D., and Trenam, R.S., 1954, Proc. Roy. Soc. A223, 15.

Boakes, D., Garton, G., Ryan, D., and Wolf, W.P., 1959, Proc. Phys. Soc., 74, 663.

Bowers, K.D., and Owen, J., 1955, Repts. Prog. Phys. 18, 304.

Brown, M.R., Coles, B.A., Owen, J., and Stevenson, R.W.H., 1961, Phys. Rev. Letters, 7, 246.

Carson, J.W., and White, R.L., 1960, J.Appl. Phys. 31, 53S.

Coles, B.A., 1959, D.Phil. Thesis, Oxford.

Condon, E.U., and Shortley, G.H., 1951, "The Theory of Atomic Spectra", (Cambridge: Cambridge University Press).

Cooke, A.H., Edmonds, D.T., McKim, F.R., and Wolf, W.P., 1959a, Proc. Roy. Soc., A252, 246.

Cooke, A.H., Edmonds, D.T., Finn, C., and Wolf, W.P., 1959b, Proc. Phys. Soc., 74, 791.

Dieke, G.H., 1962, Bull. Am. Phys. Soc. II, 7, 209.

Dillon, J.F., and Nielsen, J.W., 1960, Phys. Rev., 120, 105.

Dillon, J.F., and Walker, L.R., 1961, Phys. Rev. 124, 1401.

Edmonds, A.R., 1957, "Angular Momentum in Quantum Mechanics (Princeton: Princeton University Press).

Elliott, J.P., Judd, B.R., and Runciman, W.A., 1957, Proc. Roy. Soc., A240, 509.

Elliott, R.J., and Stevens, K.W.H., 1952, Proc. Roy. Soc. A215, 437.

1953a, ibid. A218, 553.

1953b, ibid. A219, 387.

Euler, F., and Bruce, J., 1962, Proc. 20th Pittsburgh Diffraction Conference, (to be published).

Freeman, A.J., and Watson, R.E., 1962, Phys. Rev., 127, 2058.

Garton, G., Lenak, M.J.M., Wolf, W.P., and Wyatt, A.F.G., 1962, Proc. 8th Conf. Magnetism and Magnetic Materials, J. Appl. Phys. (to be published).

Geller, S., and Gilleo, M.A., 1957, J.Phys. Chem. Solids, 3, 30.

Geschwind, S., 1961, Phys. Rev., 121, 363.

Griffith, J.S., 1961, "The Theory of Transition-Metal Ions" (Cambridge: Cambridge University Press).

Griffiths, J.H.E., Owen, J., Park, J.G., and Partridge, M.F., 1959, Proc. Roy. Soc. A250, 84.

Hayes, W., and Twidell, J.W., 1961, J.Chem. Phys., 35, 1521.

Heine, V., 1960, "Group Theory in Quantum Mechanics, (London: Pergamon Press).

Herpin, A., Kochler, W.C., and Meriel, P., 1960, C.R. Acad. Sci. 251, 1359.

Hutchings, M.T., 1963, U.S.A.F. Contract no. AF61(052)-125, Technical Note 13. (Unpublished).

Hutchings, M.T., and Ray, B.R., 1963, Proc. Phys. Soc., 81, 663.

Hutchison, C.A., Judd, B.R., and Pope, D.F.D., 1957, Proc. Phys. Soc. B70, 514.

Hutchison, C.A., and Wang, E., 1958, J.Chem. Phys., 29, 754.

Ingram, D.J.E., 1955, "Spectroscopy at Radio and Microwave Frequencies", (London: Butterworths Scientific Publications).

International Tables for X-ray Crystallography, 1952, (Birmingham: Kynoch Press).

Jahn, H.A., and Teller, E., 1937, Proc. Roy. Soc., A.161, 220.

Jahnke, E., and Emde, F., 1945, "Tables of Functions", 4th Edition (New York: Dover Publications).

Judd, B., 1959, Molecular Physics, 2, 407.

Kittel, C., 1960, Phys. Rev., 117, 681.

Koster, G.F., 1962, Quarterly progress report, No. 45, M.I.T. (Unpublished).

Kramers, H.A., 1930, Proc. Acad. Sci., Amsterdam., 33, 959.

Lea, K.R., Leask, M.J.M., and Wolf, W.P., 1962, J.Phys. Chem. Solids, 23, 1381.

Leask, M.J.M., 1960, D.Phil. Thesis, Oxford.

Leask, M.J.M., Orbach, R., Powell, M.J.D., and Wolf, W.P., 1963, Proc. Roy. Soc. A272, 371.

Llewellyn, P.M., 1956, D.Phil. Thesis, Oxford.

Llewellyn, P.M., 1957, Journ. Sci. Inst., 34, 236.

Low, W., 1960, "Paramagnetic Resonance in Solids", (New York and London: Academic Press).

Low, W., and Shaltiel, D., 1958, Phys. Chem. Solids, 6, 315.

Mandl, F., 1957, "Quantum Mechanics" (London: Butterworths Scientific publications).

Hutchings, M.T., 1963, U.K.A.E.A. Contract no. AF61(052)-125. Technical Note 13. (Unpublished).

Hutchings, M.T., and Ray, D.K., 1963, Proc. Phys. Soc., 81, 663.

Hutchison, C.A., Judd, B.R., and Pope, D.F.D., 1957, Proc. Phys. Soc. B70, 514.

Hutchison, C.A., and Wang, E., 1958, J.Chem. Phys., 29, 754.

Ingram, D.J.E., 1955, "Spectroscopy at Radio and Microwave Frequencies", (London: Butterworths Scientific Publications).

International Tables for X-ray Crystallography, 1952, (Birmingham: Kynoch Press).

Jahn, H.A., and Teller, E., 1937, Proc. Roy. Soc., A.161, 220.

Jahnke, E., and Emde, F., 1945, "Tables of Functions", 4th Edition (New York: Dover Publications).

Judd, B., 1959, Molecular Physics, 2, 407.

Kittel, C., 1960, Phys. Rev., 117, 681.

Koster, G.F., 1962, Quarterly progress report, No. 45, M.I.T. (Unpublished).

Kramers, H.A., 1930, Proc. Acad. Sci., Amsterdam., 33, 959.

Lea, K.R., Leask, M.J.M., and Wolf, W.P., 1962, J.Phys. Chem. Solids, 23, 1381.

Leask, M.J.M., 1960, D.Phil. Thesis, Oxford.

Leask, M.J.M., Orbach, R., Powell, M.J.P., and Wolf, W.P., 1963, Proc. Roy. Soc. A272, 371.

Llewellyn, P.M., 1956, D.Phil. Thesis, Oxford.

Llewellyn, P.M., 1957, Journ. Sci. Inst., 34, 236.

Low, W., 1960, "Paramagnetic Resonance in Solids", (New York and London: Academic Press).

Low, W., and Shaltiel, D., 1958, Phys. Chem. Solids, 6, 315.

Mandl, F., 1957, "Quantum Mechanics" (London: Butterworths Scientific publications).

Margenau, H., and Murphy, G.M., 1956, "The Mathematics of Physics and Chemistry", 2nd. Edition (Princeton; D. Van Nostrand Co. Inc.).

Margolis, J.S., 1961, J. Chem. Phys., 35, 1367.

Nielsen, J.W., 1960, J.App. Phys. 31, 51 (S).

Orton, J.W., 1959, Reps. Prog. Phys., 22, 204.

Overmeyer, J., Geiss, K.A., Preiser, M.J., Calhoun, B.A., 1962, I.B.M. Research Paper, RC-705. (Unpublished).

1962, Proc. Conf. Paramag. Res., Jerusalem.

Owen, J., 1961, J. App. Phys., Supp. 32, 213S.

Owen, J., 1962, J. App. Phys., Supp. 33, 355.

Pake, G.E., 1962, "Paramagnetic Resonance", (Benjamin: New York).

Pappalardo, R., and Wood, D.L., 1960, J. Chem. Phys. 33, 1734.

Park, J.G., 1957, D.Phil. Thesis, Oxford.

Pauthenet, R., 1958, Ann. Chim. Phys., 3, 424.

Powell, M.J.D., 1962, The Computer Journal, 5, 147.

Prather, J.L., 1961, "Atomic Energy Levels in Crystals" (N.B.S. Monograph No. 19.).

Pryce, M.H.L., 1950, Proc. Phys. Soc. A63, 25.

Pryce, M.H.L., 1959, Phys. Rev. Letters, 3, 375.

Ray, D.K., 1963, U.S.A.F. Contract no. AF 61(052)-125, Technical Note 14. (Unpublished).

Rimai, L., and De Mars, G.A., 1962, J. App. Phys. Supp. 33, 1254.

Robinson, F.N.H., 1959, Journ. Sci. Insts., 36, 481.

Ryan, D., 1960, B.Sc., Thesis, Oxford.

(See also:- Ball et al., 1961, U.S.A.F. Contract no. AF61(052)-125, Technical Note 5 (Unpublished).
Boakes et al., 1959, Proc. Phys. Soc., 74, 663.
Ball et al., 1961, J. App. Phys., 32, 2673.)

Scovil, H.E.D., 1951, D.Phil. Thesis, Oxford.

Statz, H., Rimai, L., Weber, M.J., de Mars, G.A., and Koster, G.F., 1961, J. Appl. Phys., 32, 2168.

Stevens, K.W.H., 1952, Proc. Phys. Soc., A65, 209.

Templeton, D.H., and Carter, G.F., 1954, J. Phys. Chem. 58, 940.

Thomas, J., 1962, Thesis Grenoble.

Tinkham, M., and Sievers, A.J., 1962, Proc. 8th Conference Magnetism and Magnetic Materials, J. Appl. Phys. (to be published).

Van Vleck, J.H., 1932, "The Theory of Electric and Magnetic Susceptibilities". (Oxford: Oxford University Press).

Van Vleck, J.H., 1962, J. Phys. Soc., Japan, 17, Supp. B-1, 352.

White, J.A., 1962, J. Phys. Chem. Solids, 23, 1787.

Wickersheim, K.A., 1961, Phys. Rev., 122, 1376.

Wickersheim, K.A., and White, R.L., 1962, Phys. Rev. Letters, 8, 483.

Wolf, W.P., 1957, Phys. Rev., 108, 1152.

Wolf, W.P., 1959, Proc. Phys. Soc., 74, 665.

Wolf, W.P., 1961a, Repts. Prog. in Phys., 24, 212.

Wolf, W.P., 1961b, Am. J. App. Phys., 32, 742.

Wolf, W.P., Ball, M., Hutchings, M.T., Leask, M.J.M., and Wyatt, A.F.G., 1962a, J. Phys. Soc., Japan, 17, Supp. B-1, 443.

Wolf, W.P., Leask, M.J.M., Mangum, B., and Wyatt, A.F.G., 1962b, J. Phys. Soc. Japan, 17, Supp B-1, 487.

Wyatt, A.F.G., 1963, D.Phil. Thesis, Oxford.

Wycoff, 1960, "Crystal Structures", (New York: Interscience Publishers Inc.).

Zachariasen, W.H., 1948, J.Chem. Phys., 16, 254.